

University of Central Florida

STARS

Electronic Theses and Dissertations

2010

An Uncertainty Quantification Of The Variation Of Internal Heat Transfer Coefficients And The Effect On Airfoil Life

Jan H. Marsh

University of Central Florida



Part of the [Aerospace Engineering Commons](#)

Find similar works at: <https://stars.library.ucf.edu/etd>

University of Central Florida Libraries <http://library.ucf.edu>

This Masters Thesis (Open Access) is brought to you for free and open access by STARS. It has been accepted for inclusion in Electronic Theses and Dissertations by an authorized administrator of STARS. For more information, please contact STARS@ucf.edu.

STARS Citation

Marsh, Jan H., "An Uncertainty Quantification Of The Variation Of Internal Heat Transfer Coefficients And The Effect On Airfoil Life" (2010). *Electronic Theses and Dissertations*. 1642.

<https://stars.library.ucf.edu/etd/1642>

AN UNCERTAINTY QUANTIFICATION OF THE VARIATION OF INTERNAL HEAT
TRANSFER COEFFICIENTS AND THE EFFECT ON AIRFOIL LIFE

by

JAN H. MARSH
B.S. University of Central Florida, 2008

A thesis submitted in partial fulfillment of the requirements
for the degree of Master of Science in Aerospace Engineering
in the Department of Mechanical, Materials, and Aerospace Engineering
in the College of Engineering and Computer Science
at the University of Central Florida
Orlando, Florida

Fall Term
2010

© 2010 Jan H. Marsh

ABSTRACT

Uncertainty in accurately knowing applied internal heat transfer coefficients inside of a cooling passage can lead to variability in predicting low cycle fatigue life of a turbine vane or blade. Under-predicting a life value for a turbine part can have disastrous effects on the engine as a whole, and can negate efforts in innovative design for advanced cooling techniques for turbine components. Quantification of this fatigue life uncertainty utilizing a computational framework is the primary objective of this thesis.

Through the use of probabilistic design methodologies a process is developed to simulate uncertainties of internal heat transfer coefficient, which are then applied to the aft section of a non-rotating turbine blade component, internally cooled through a multi-pass serpentine channel. While keeping all other parameters constant internal heat transfer coefficients are varied according to a prescribed uncertainty range throughout the passages. The effect on the low cycle fatigue life of the airfoil is then evaluated at three discrete locations: near the base of the airfoil, towards the tip, and at mid-span. A generic low cycle fatigue life prediction model is used for these evaluations.

Even though the probabilistic design process uses independent random numbers to simulate the variation, in reality, heat transfer coefficients at points located closely together should be correlated. For this reason, an autocorrelation function is implemented. By changing the value of this function the strength of the correlation of

neighboring internal heat transfer coefficients to each other over a certain distance can be controlled. In order to test the effect that this correlation strength has on the low cycle fatigue life calculation, low and high values are chosen and analyzed.

The magnitude of the prescribed uncertainty range of the internal heat transfer coefficient variation is varied to further study the effects on life. Investigated values include 5%, 10% and 20% for the straight ribbed passages and 10%, 20%, and 40% for both the tip and hub turns. As expected there is a significant dependence of low cycle fatigue life to the variation in internal heat transfer coefficients. For the 20/40% case, variations in life as high as 50-60% are recorded, furthermore a trend is observed showing that as the magnitude of the uncertainty range of internal heat transfer coefficients narrows so does the range of the low cycle fatigue life uncertainty.

To my parents for always being there, guiding me in the right direction and ceaselessly pushing me towards my full potential, even if it's farther than I want to be pushed at times.

Thank you for everything you've done for me.

ACKNOWLEDGMENTS

Firstly, I would like to thank all of my committee members for helping me through the entire process. Special thanks to Dr. Kapat, my committee chair and advisor. Without your help and guidance this would not have been possible. You have not only been a great teacher, but through your passion and determination have inspired me to not simply take on this task, but to take my entire academic career to the next level.

Furthermore, I would like acknowledge the Siemens Energy Inc. and UCF collaboration. Hopefully this close collaboration continues for many years, providing others such great opportunities. Special thanks to Dr. Brunelli, my co-chair, without your help and insight this work would not have been possible.

Additionally, a very special thanks goes to Brian, Paul, Sameer, and Chirag. Without all of your expertise and assistance this would have been a much more painful process.

Finally, thank you to all of my friends and family for supporting me through not only this work, but everything life throws at me. Special thanks to Billy for not only all of the direct contributions, but more importantly for always being there. We manage to laugh our way through both the good and bad times of yet another chapter of life.

TABLE OF CONTENTS

LIST OF FIGURES	x
LIST OF TABLES	xiv
LIST OF ABBREVIATIONS	xv
CHAPTER I INTRODUCTION	1
1.1 Gas Turbine Background	1
1.2 Internal Convective Cooling Overview	6
1.3 Objectives	8
CHAPTER II LITERATURE REVIEW	10
2.1 Internal Heat Transfer	10
2.2 Low Cycle Fatigue Life	27
2.3 Probabilistic Design	32
CHAPTER III PROBLEM DEFINITION	36
3.1 Challenges	37
3.1.1 Modeling	37
3.1.1.a Provided Geometric Information	38
3.1.1.b Provided Boundary Conditions	43
3.1.2 Probabilistic Design	46

3.1.2.a Number of Variables.....	47
3.1.2.b Computational Power	48
3.1.2.c Correlation of Random Variables	49
3.2 Test Matrix and Predictions	51
CHAPTER IV MODELING.....	53
4.1 CAD Modeling.....	53
4.2 FEA modeling.....	58
4.2.1 Initial model Creation.....	58
4.2.2 Boundary Condition Application	61
4.2.3 Mesh Optimization.....	62
4.3 Internal Flow Network	67
4.4 Material Model.....	68
CHAPTER V METHODOLOGY	70
5.1 Probabilistic Design	70
5.1.1 Approach	72
5.1.2 Validation - Distribution	74
5.1.3 Validation - Correlation Coefficient	82
5.2 Finite Element Analysis	85

5.2.1 Advection Network	85
5.2.2 Automation	91
5.3 Low Cycle Fatigue Life Calculation	92
CHAPTER VI RESULTS	96
CHAPTER VII DISCUSSION	102
7.1 Discussion of Results	102
7.2 Future Work	106
CHAPTER VIII CONCLUSION	108
APPENDIX A: ANSYS BOUDNARY CONDITION APPLICATION MACRO	109
APPENDIX B: MATLAB CODE	113
APPENDIX C: VALIDATION PLOTS FOR ALL POINTS OF RUN 1	119
APPENDIX D: ANSYS MACRO	150
APPENDIX E: AIRFOIL COORDINATES	155
REFERENCES	160

LIST OF FIGURES

Figure 1-1: Generic, Ideal Brayton Cycle (adapted from Moran and Shapiro, 2004).....	1
Figure 1-2: Inlet Temperature vs. Power Output, (Sautner et. al., 1992)	2
Figure 1-3: Performance map of a simple cycle gas turbine (Boyce, 2006)	3
Figure 1-4: Cooling Improvements over time (Clifford, 1985)	4
Figure 1-5: Blade Cooling Techniques (Gladden and Simoneau, 1988).....	5
Figure 1-6: Simplified Serpentine Cooling Circuit	7
Figure 2-1: Radial Cooling Holes; The early stages of internal cooling (Downs and Landis, 2009)	11
Figure 2-2: Modern gas turbine blade with common cooling techniques (Han, 2004) ...	12
Figure 2-3: Relation of Cycle efficiency and Mass flow	13
Figure 2-4: Loss Coefficient Profiles at different Coolant Flows (Otomo et al., 1997)	15
Figure 2-5: Rib-roughened duct illustration (Han, 2004).....	17
Figure 2-6: Comparison of Conceptual Secondary Flows (Han, 2004)	19
Figure 2-7: Comparison of Higher Order Flows due to Ribs and Rotation (Azad et al., 2001)	20
Figure 2-8: Expected Higher Level Flow Patterns in a Two-Pass Duct (Kim et al., 2006) .	21
Figure 2-9: Velocity Vectors in a Two-Pass Rotating and Non-Rotating Duct (Kim et al., 2006)	22
Figure 2-10: General Stress Equation of a Plate (Manson, 1954).....	28
Figure 2-11: Coffin-Manson Equation (Dowling, 1999)	29

Figure 2-12: Generalized Strain Amplitude Vs Life Curve (Dowling, 1999)	29
Figure 2-13: Decreasing LCF Material Properties with Temperature	30
Figure 2-14: Crack Initiation vs. Fracture	31
Figure 2-15: Modified Marrow Approach Equation (Dowling, 1999)	31
Figure 3-1: GE NASA E ³ Blade 1 External Coordinates Sample (Timko, 1990)	39
Figure 3-2: GE NASA E ³ Blade 1 Airfoil Side View (Halila, 1982)	41
Figure 3-3: GE NASA E ³ Blade 1 Cross Section at unknown radius (Halila, 1982)	42
Figure 3-4: GE NASA E ³ Blade 1 Cooling Hole Definition (Timko, 1990)	42
Figure 3-5: GE NASA E ³ Blade 1 Additional Section Design Data (Timko, 1990)	43
Figure 3-6: GE NASA E ³ Blade 1 Heat Transfer Coefficients at unknown radius (Halila, 1982)	44
Figure 3-7: GE NASA E ³ Vane 1 Temperature Profile (Timko, 1990)	45
Figure 3-8: Generated Blade 1 Temperature Profile	45
Figure 3-9: Correlation Equations (Deserno, 2002)	50
Figure 3-10: Randomly generated correlated and uncorrelated data points	51
Figure 4-1: Pro-E Generated Airfoil External Geometry	54
Figure 4-2: Gridded Side View	55
Figure 4-3: Pro-E Generated Core Geometry	56
Figure 4-4: Combined Core and Airfoil	57
Figure 4-5: Meshed Airfoil – 1st Cut Exterior View	60
Figure 4-6: Meshed Airfoil – 1st Cut Internal Details	60

Figure 4-7: Thermal Results – Rev 12	63
Figure 4-8: Thermal Results – Rev 13	63
Figure 4-9: Structural Results – Rev 12	64
Figure 4-10: Structural Results – Rev 13	64
Figure 4-11: Cut Planes	65
Figure 4-12: Final FEA Model – Rev 15	66
Figure 5-1: Isight Model	71
Figure 5-2: Validation for Test Case Point 1	76
Figure 5-3: Validation for Test Case Point 15	77
Figure 5-4: Validation for Test Case Point 9	78
Figure 5-5: Validation for Actual Case Point 1	80
Figure 5-6: Validation for Actual Case Point 9	81
Figure 5-7: Correlation Coefficient Equations (Deserno, 2002)	82
Figure 5-8: Correlation Length	84
Figure 5-9: CAD Generated line network.....	86
Figure 5-10: Channel Distributions at Various Node Numbers	87
Figure 5-11: Fluid/Solid Model Interaction.....	89
Figure 5-12: Generalized Lifting Procedure	93
Figure 5-13: Low Life Node Location	94
Figure 5-14: Temperature, Stress, and Life Variations	95
Figure 6-1: Results for Run 1	97

Figure 6-2: Results for Run 2	98
Figure 6-3: Results for Run 3	99
Figure 6-4: Results for Run 4	100
Figure 6-5: Results for Run 5	101
Figure 7-1: LCF Variation Comparison of Runs 1,2, and 3	104
Figure 7-2: LCF Variation Comparison of Runs 1 and 4	104
Figure 7-3: LCF Variation Comparison of Runs 1 and 5	105

LIST OF TABLES

Table 3-1: External Coordinates Excel File Sample	40
Table 3-2: Test Matrix	52
Table 4-1: Baseline Internal HTC's ($\text{mW}/\text{mm}^2\text{-}^\circ\text{C}$)	68
Table 5-1: Correlation Coefficient Verification	83
Table 5-2: Provided Flow Rates in kg/s	89
Table 6-1: Input parameter and Run #'s	96

LIST OF ABBREVIATIONS

D	Diameter
L	Length
P	Pressure
R	Gas constant
T	Temperature
U	Velocity
m	Mass flow rate
q	Heat Transfer
G1C	Total Compressor Flow
E	Elastic Modulus

Greek

τ	Autocorrelation Value
σ	Standard Deviation
μ	Mean
α	Coefficient of expansion

Subscripts

av	Average
0	Initial

CHAPTER I INTRODUCTION

1.1 Gas Turbine Background

Gas turbines come in various shapes and sizes, however the purpose remains the same, namely to generate power (be it thrust for aero-engines, or shaft-power for power generation turbines) through the ingestion, compression, combustion and expansion of air. On a thermodynamic level gas turbines can be represented by an ideal Brayton Cycle for power generation such as the one shown in the diagram below.

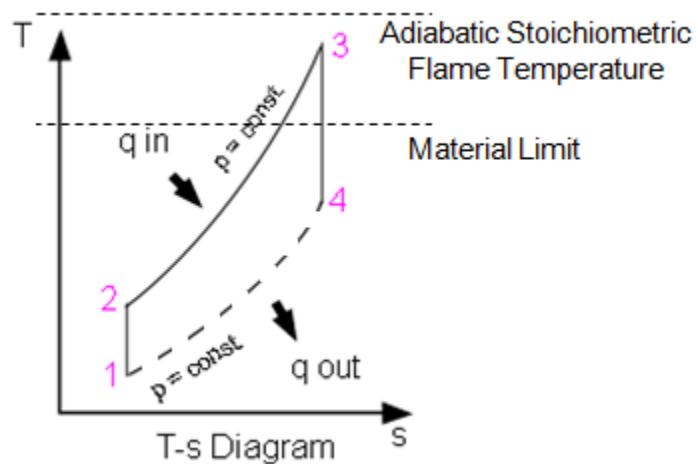


Figure 1-1: Generic, Ideal Brayton Cycle (adapted from Moran and Shapiro, 2004)

Air enters an “ideal” gas turbine at stage 1, gets compressed as it travels through the compressor to reach stage 2, at which point the air is mixed with an available fuel and undergoes combustion which brings the gas to point 3 on the T-s Diagram. The gas then

expands through the turbine to get to stage 4 producing work, finally the air returns back to ambient conditions in the exhaust diffuser.

The major driving force behind both the power output and efficiency of gas turbines is the temperature at the inlet of the turbine, which is directly controlled by the firing temperature in the combustor. “For every 100 °F (55.5 °C) increase in [firing] temperature, the work output [of the turbine] increases by approximately 10% and gives about a 1-1/2% increase in efficiency” (Boyce, 2006). This effect is clearly visible in the following two figures.

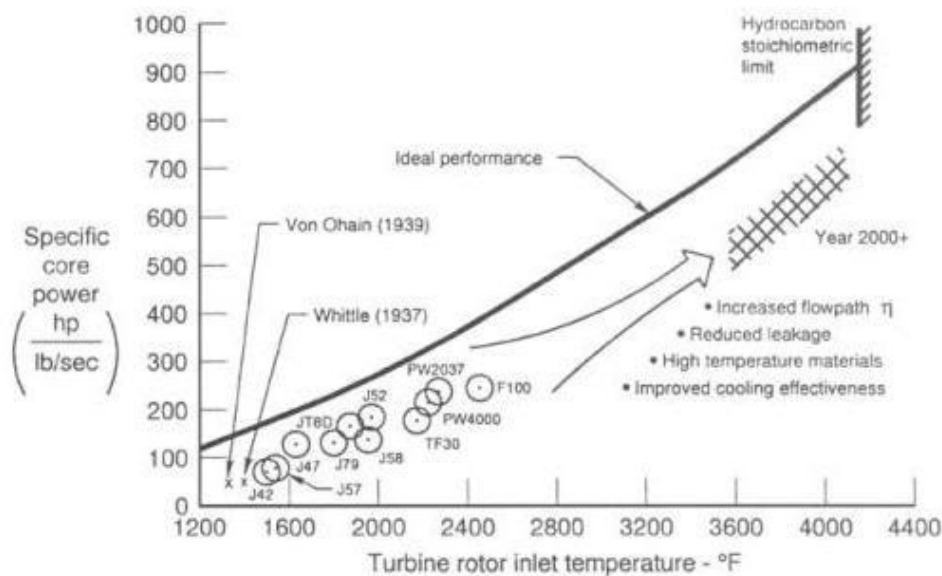


Figure 1-2: Inlet Temperature vs. Power Output, (Sautner et. al., 1992)

Even though the maximum attainable combustion temperature, the adiabatic flame temperature, is on the order of 2000-3000 °C (Ricklick, 2009), it is not feasible to operate at those temperatures due to material limits. There have been countless

advances in material science, but even so the melting temperature of most modern super alloys used for turbine components is still only around 1500 °C.

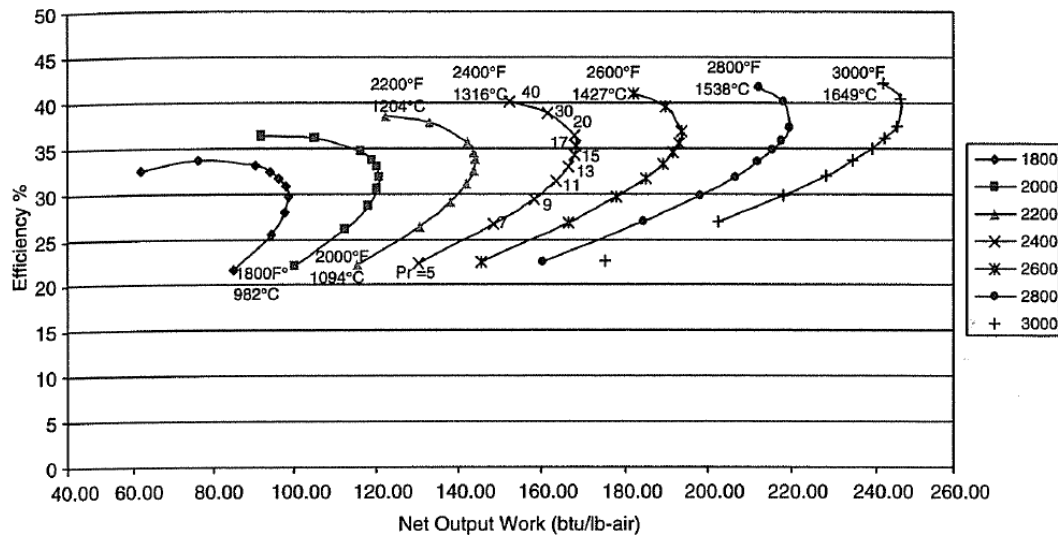


Figure 1-3: Performance map of a simple cycle gas turbine (Boyce, 2006)

However to meet environmental and economic challenges turbine efficiencies must be pushed above this limited posed by material properties, which can only be done through cooling the components.

According to Mustapha et. al. (2003) combustor exit temperatures are in the region of 3000 °F (1650 °C) today and a growth to 3800 °F (2100 °C) is expected. These are well above the melting point of the alloys available for blades and vanes, so that cooling is essential. Much like material science has made leaps and bounds forward, so has cooling technology improved in order to better protect components from thermally driven breakdown and fatigue.

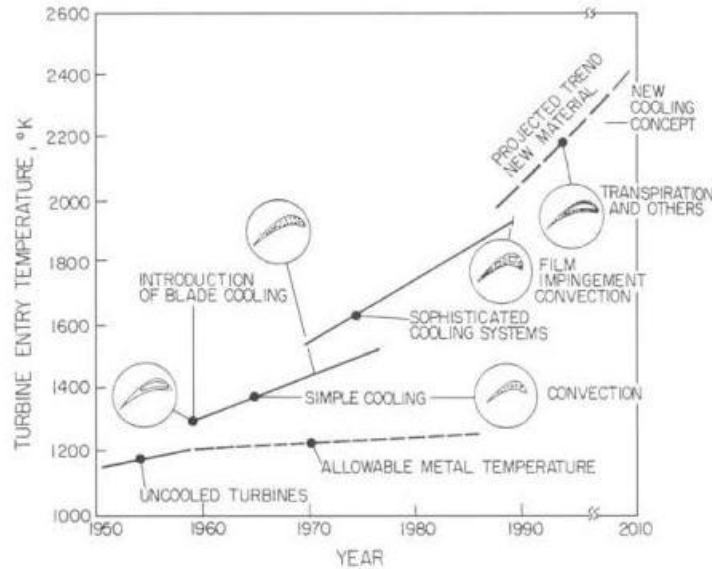


Figure 1-4: Cooling Improvements over time (Clifford, 1985)

Improvements in cooling technology directly increases the magnitude of the turbine inlet temperature, a summary of the effects of recent developments can be seen in the previous figure. There are many different ways to help protect gas turbine components from excessive gas path temperatures, such techniques range from the addition of low conductivity thermal barrier coatings (TBC) to reduce heat pickup, addition of film cooling holes to produce a cooler layer around the components, as well as internal convection, or impingement cooling to remove heat from the components. Most commonly a combination of some or all of these cooling techniques is employed, as can be seen in the blade below. It is important to note that whenever the word “cool” is used that it is a relative term, in that air used for cooling purposes is only a few hundred degrees cooler than the main flow. However this is still sufficient, according to Han and

Ekkad (2000), to lower the effective temperature experience by the components significantly, lowering the overall thermal stress experienced by the part.

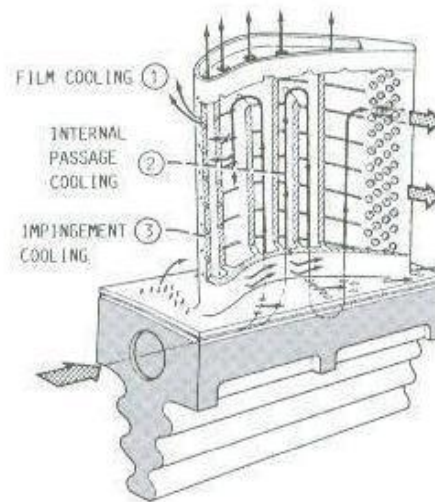


Figure 1-5: Blade Cooling Techniques (Gladden and Simoneau, 1988)

Naturally there is a drawback to cooling components, in that any air used for cooling is bled from the compressor before combustion, meaning that less air is available for power, or thrust generation. Therefore it is not only important to increase the cooling effectiveness as much as possible, which has been one of the goals of researches ever since cooling has been added to components, but to also find a good balance between air used for power generation and air used for cooling purposes. The previous image shows how cooling schemes are designed to take as much advantage of coolant air as possible. Air from the compressor enters the blade and is used for internal convection and impingement cooling to remove as much heat as possible, before being ejected out of film cooling holes to reduce the effective gas path temperature felt by the

blade. This dual use of coolant allows the turbine to run closer to peak performance temperatures while simultaneously reducing the amount of air “wasted” on cooling. As such, there is a constant drive to increase the amount of cooling done with less and less air usage.

1.2 Internal Convective Cooling Overview

Internal convective cooling is both one of the simplest form of cooling, along with one of the most important and widely used. Coolant gas passes through a channel placed relatively close to gas path and removes heat from the component by transferring it from the walls of the airfoil to the fluid. By arranging the coolant channels into multiple pass serpentine coolant channels the amount of heat removed can be optimized before ejecting the spent cooling air into the main stream flow via film cooling holes, or leading/trailing edge ejection. A simplified model of this kind of serpentine layout can be seen in the following illustration. The amount of heat that can be transferred out of the airfoil, and as such the cooling efficiency is directly related to the magnitude of the heat transfer coefficient (HTC) produced in the channels.

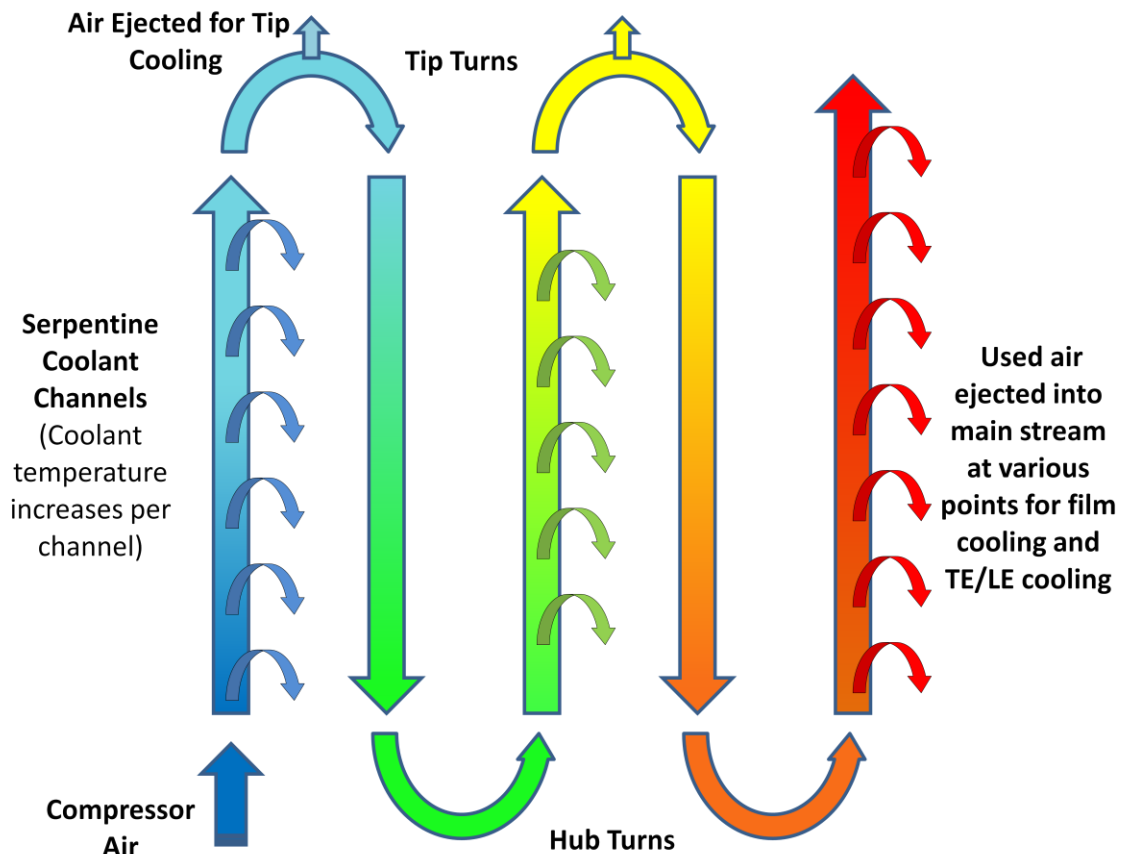


Figure 1-6: Simplified Serpentine Cooling Circuit

As mentioned above the magnitude of the internal HTC is the driving force behind the amount of heat that is removed by convective cooling. There are several options available to enhance heat transfer associated with internal flows; enhancement may be achieved by increasing the convective coefficient directly or by increasing the convective surface area (Incropera et. al., 2002). Initially smooth channels were turbulated with small horizontal trip strips, but currently the choices for augmenting internal HTCs are nearly limitless. Trip strips now come in all shapes, sizes, and orientations, such as for example relatively simple 45° angled ribs, more complicated wedge shapes, or even split V-shaped ribs. Other more complex structures can be found inside passages as well,

such as arrays of dimples or patches of surface roughness that both increase the convective surface area and also set up fairly complicated secondary and tertiary flow fields which further benefit heat transfer.

However, as more and more obstructions are added to coolant channels to increase HTC's, the pressure drop across that channel increases as well, which drives up the amount of pumping power required to pass air through the channel. This can either increase the required supply pressure which may not always be available, or lower the flow rates and velocities through the channels. Therefore, much like there is correlation between the benefit gained from using air for cooling purposes in the engine as a whole and power loss, there is a delicate balance between internal heat transfer augmentation and an increase in pressure drop.

1.3 Objectives

Throughout an entire HTC augmented serpentine passage there are numerous areas where the prediction of heat transfer and friction factor data is made nearly impossible due to the complex flow created by periodic rib-roughness elements such as separation, reattachment, and recirculation (Han et. al., 2000). The problem is further advanced due to the creation of various vortices in any turns that the flow is required to

take. Any time one of these features is encountered variation is introduced into the results, and even though countless research is being published regarding internal flows, HTC augmentation and the effect on friction factors, there is very little emphasis placed on the effect that any of these variations have. Naturally there are other sources of variation as well, such as experimental inaccuracies, or even manufacturing inconsistencies, for example the rounding of rib corners due to gradual wearing of the core die (Han et. al., 2000). The potential sources of variation are nearly limitless, and as such the primary objective of this work is to quantify, through an interdisciplinary probabilistic design approach, the effect that these variations have on the overall component life.

CHAPTER II LITERATURE REVIEW

Due to the interdisciplinary aspect of this work literature regarding internal heat transfer, fatigue life as well as probabilistic design needs to be reviewed. Since the focus however is on internal heat transfer and its effects, this topic will be covered in a much more in-depth fashion.

2.1 Internal Heat Transfer

Internal Heat Transfer has taken huge steps forward over the past 50 years. Downs (2009), Bunker (2007) and Han (2004) have all published papers covering the history of turbine blade cooling improvements which draw their origins from the simple radially cooled blade shown on the next page to the complicated cooling schemes of today. However even though the technology level has vastly increased since then, the basic principle remains the same.

According to Downs (2009) turbine blades on a fundamental level act like heat exchanges, making them subject to the basic thermodynamic laws and principles, such as heat balance. Since the mass flow of the hot gas is much larger than that of the coolant it is treated as a constant temperature source.

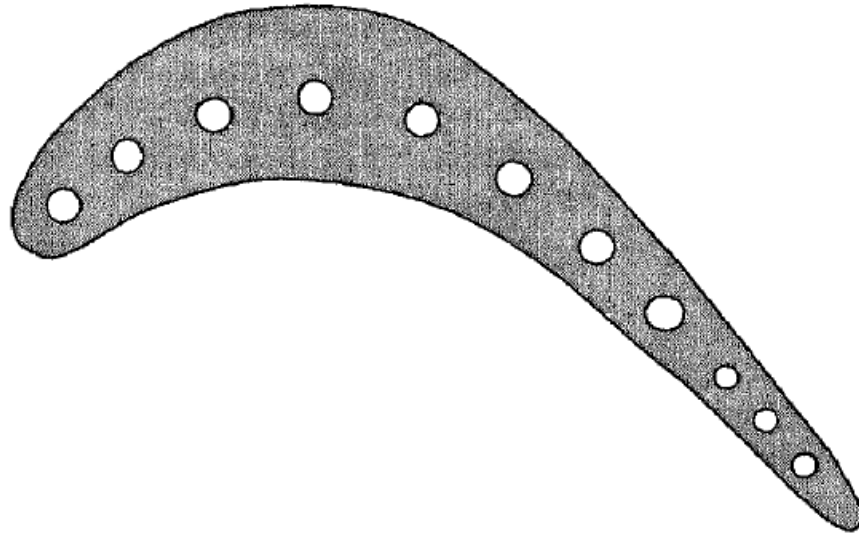


Figure 2-1: Radial Cooling Holes; The early stages of internal cooling (Downs and Landis, 2009)

Therefore instead of reducing the temperature of the main stream gas, as would be the case in a traditional heat exchanger, the turbine blade is instead cooled and its temperature is held below material limits. As turbine inlet temperatures increase, so does the heat transferred to the turbine blades (Han, 2004) and other components. In order to deal with this increased heat load internal channels in modern gas turbine blades, like the one shown in the image on the following page, have adopted multi pass coolant channels with HTC enhancement features, which allows the fluid to pick up more heat from the component than would be possible with only a single radial pass.

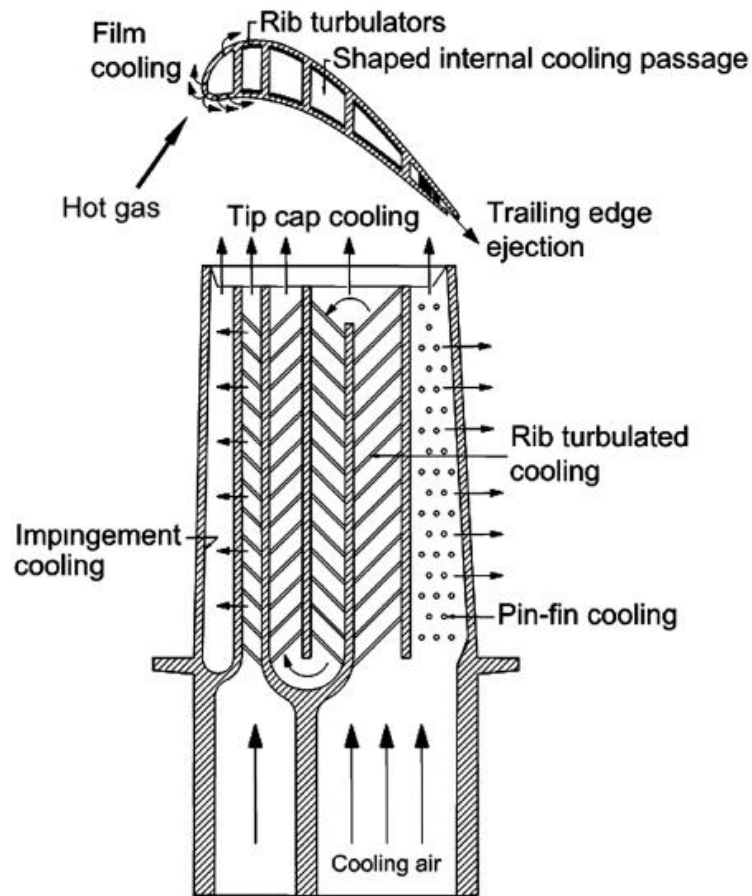


Figure 2-2: Modern gas turbine blade with common cooling techniques (Han, 2004)

It is innovations like these that have allowed cooling advances to contribute approximately 11°C per year to engine firing temperatures whereas material advances have only provided roughly 4°C annually (Boyce, 2006). This alone emphasizes the importance of component cooling. Iacovides (2007) provides further support by stating that “the improvements of overall thermal efficiency directly attributed to internal blade cooling arguably outstrip those achieved in any other area of jet-engine research.” The importance placed on internal component cooling will undoubtedly remain the

same in the future even though the rate of technological improvement in the area has reached somewhat of a plateau in the past 10 years (Bunker, 2007).

As was mentioned previously, even though component cooling allows the turbine to run hotter and more efficient, cooling also produces drawbacks. Since air used for cooling purposes is taken from the compressor before combustion, there is only a finite amount of air available to be used as coolant, due to the fact that any air leeched from the compressor in this fashion produces multiple losses, all of which negatively impact turbine efficiency and performance. This is shown pictorially in the following sketch.

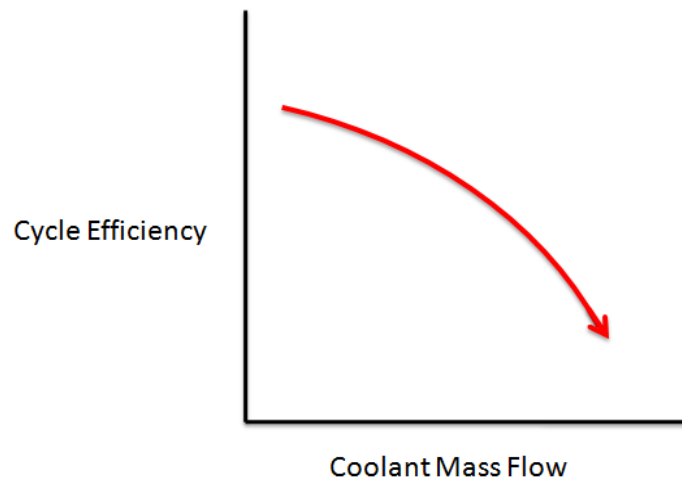


Figure 2-3: Relation of Cycle efficiency and Mass flow

The obvious loss that is associated with component cooling is the fact that any air extracted from the compressor does not reach the combustor to be combusted and used for power generation. An extremely large portion of the gas turbines total work output is required to operate the compressor. Thus, any non-combusted air represents

a direct energy drain to the system as a whole, since the gas turbine has already invested energy to compress the air, but will now no longer see a direct return on this investment. To quantify this immense loss, work done to remove the required amount of heat from a single turbine blade could provide power for 14 average homes (Moustapha, 2003). Other direct losses are due to any kind of conditioning that needs to be applied to the coolant fluid, be it air or steam. For example, in some row one blades cold, high pressure coolant air is desired. However, since high pressure air is bled from the aft sections of the compressor, it is warmer than the front stage air due to heat up caused by rapid compression. In this case it must first go through a cooler to reduce the temperature, before being used for cooling purposes. Meaning that more work needs to be expended to provide the turbine with the coolant needed to operate at conditions required for a certain performance. Naturally, in both of these cases, as the amount of required coolant increases the work loss associated with it also rises.

In addition to these “direct” losses there are a number of indirect ones associated with component cooling. According to Boyce (2006) the primary cause of efficiency losses in an axial-flow turbine is the build-up of a boundary layer on the blade. Furthermore Boyce (2006) states that the losses associated with a boundary layer are viscous losses, mixing losses, and trailing edge losses. Since spent cooling air eventually ends up being ejected out of the blade as film, it actually causes the boundary layer to reenergize. This interaction of the cooling film with the surface boundary layers could cause an increase of the boundary layer growth and an increase of the secondary flows,

and vortices (Moustapha, et al. 2003). This directly affects the magnitudes of all of the losses described previously, due to the positive correlation that exists between boundary layer growth and the negative effects produced by it. Another major indirect loss associated with cooling is aerodynamic loss, which is caused by increased friction induced through the mixing of ejected cooling air and the main stream (Han et. al. 2000). Furthermore there is a pressure loss associated with film ejection. As shown in the figure below, which was determined experimentally, there is an increase in the total pressure loss coefficient as the coolant flow rate increases. This can once again be linked to the boundary layer problem, in that there is a profile loss originating from a drop in stagnation pressure due to the boundary-layer build-up, which is directly caused by a reduction of momentum in the viscous fluid (Boyce, 2006).

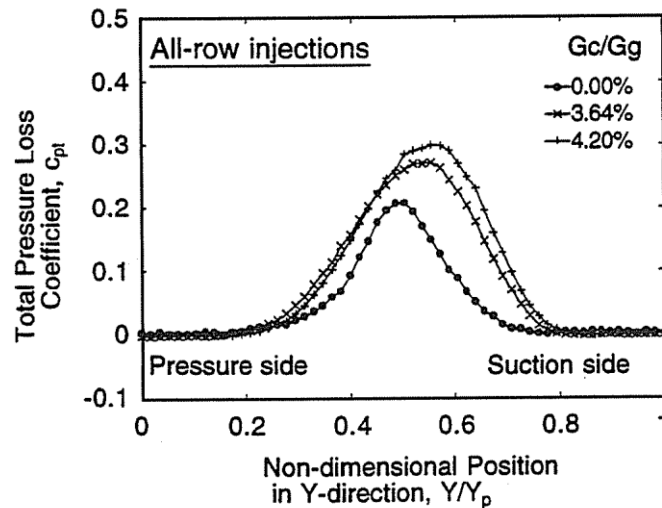


Figure 2-4: Loss Coefficient Profiles at different Coolant Flows (Otomo et al., 1997)

Much like for the direct losses described previously, the magnitude of the efficiency loss produced by the secondary losses increases with an increasing cooling flow. Therefore, in order to meet today's extremely high turbine efficiency goals, it is imperative to achieve the most cooling with as little cooling air as possible. As such, much of the research invested into internal cooling is aimed at raising the cooling efficiency as much as possible.

The standard internal cooling enhancement feature is the rib roughened duct, which relies on small strips, placed perpendicular to the coolant flow in order to literally trip the flow. This "tripping" of the flow promotes turbulent mixing, and thus increase the overall heat transfer coefficient of the passage. Any features inserted into a channel to promote heat transfer also increases the pressure drop in the channel, making it more difficult to force fluid through the passage, as such there is a constant struggle between increasing a passages HTC values without overinflating the associated pressure drop. But, since these rib turbulators only disturb the near-wall flow for the purpose of heat transfer enhancement the pressure drop caused by them is considered affordable for internal cooling designs (Han, 2004). As shown in the following figure, the important parameters when dealing with rib-roughened channels are the height of the rib (e), the pitch between adjacent ribs (p) and the height of the channel that the ribs are inserted in (H). The last parameter shown in the figure (α) is the angle of the rib relative to the coolant flow, in addition to this a sketch of the secondary flows is provided, which is instrumental in providing heat transfer augmentation.

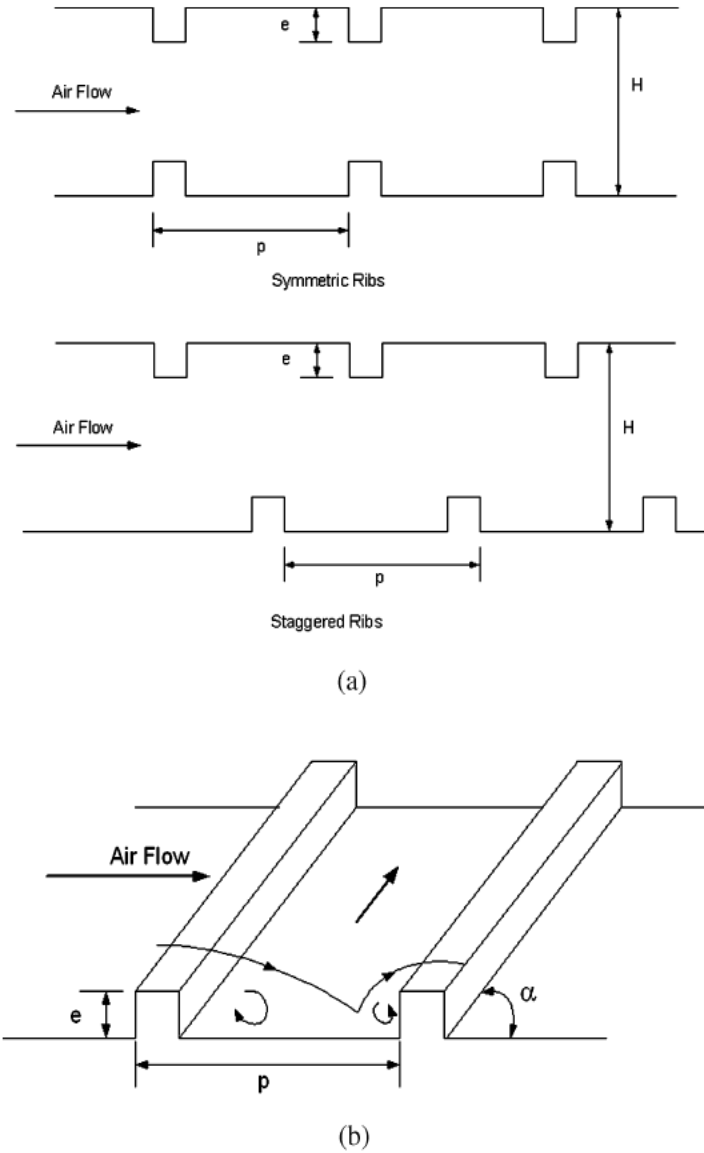


Figure 2-5: Rib-roughened duct illustration (Han, 2004)

J.C. Han and his team have performed extensive research on rib roughened channels. Han et al. (1978, 1985, 1988, 1989, 1991) and Han (1988) all deal with the basics of rib roughened channels. The overall focus was to understand the relationship between the augmentation factor in regards to heat transfer provided by various different rib-roughened duct setups, relative to the corresponding friction factor. Test

were conducted at Reynolds numbers of between 10,000 to roughly 80,000, which is much below the value that can be reached in actual power generation turbines. It was shown that generally speaking both heat transfer augmentation and pressure drop increases with increasing Reynolds number, rib height to channel height ration (e/H), as well as decreasing pitch. Rib-roughened channels provide an addition benefit in regards to heat transfer through the fin-effect, meaning that it is possible to physically transfer more heat out of a rib-roughened channel due to the increased surface area provided by the trip strips. This is especially noticeable on large ribs placed close together, which are desirable to use if pressure drop is not a real concern in the cooling design (Han, 2004).

Since it has been recognized that much of the heat transfer benefit comes from the secondary flows produced by the ribs, whereas the pressure drop is largely a function of the flow blockage, research has been conducted on different, more efficient rib layouts. Alternative rib layouts could include V-shaped, angled ribs, as well as inverted V-shaped ribs. Once again work performed by Han et al. in 1992, and 1993 has shown that these V-shaped ribs provide better heat transfer performance than traditional angled ribs with the same pressure drop. This is largely due to the more complex secondary flow network which is generated. The following from Han (2004) image provides a conceptual view of the secondary vortices produced by traditional 45 degree ribs, V-shaped ribs and inverted V-shaped ribs. It is important to note that this is for a non-rotating, straight, single-pass channel. Once turns and rotational forces are

added, both the experimental design and numerical analysis difficulty as well as uncertainty increase immensely.

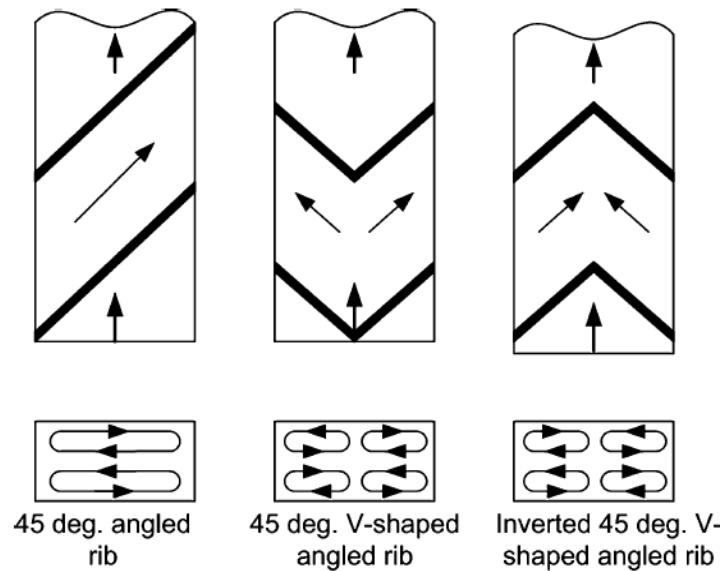
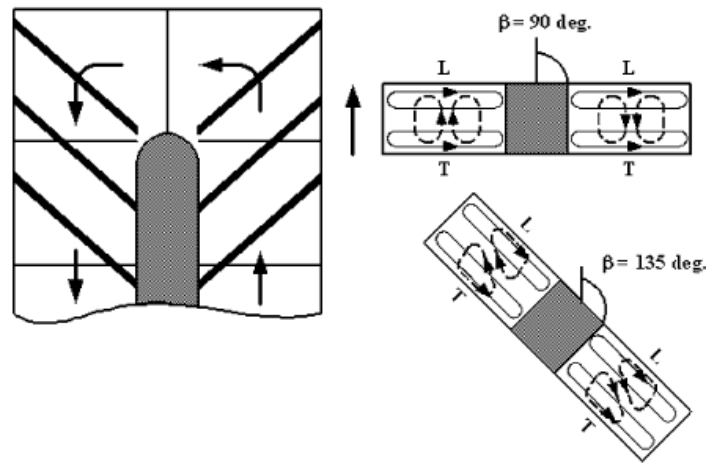


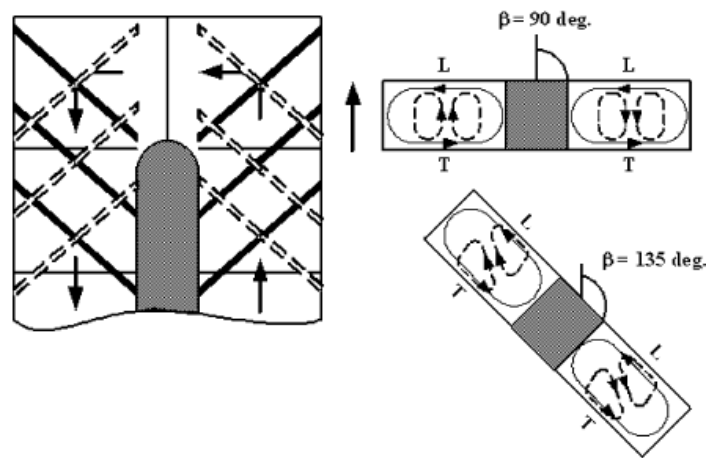
Figure 2-6: Comparison of Conceptual Secondary Flows (Han, 2004)

In recent years there has been an increase in research performed both experimentally and numerically, which include both rotation and tip turns. Through the addition of Coriolis and centrifugal forces which arise due to rotation there are now no longer just secondary flows created by the ribs, but also tertiary and even higher order flows. Work done by Azad et al. (2001) shows a conceptual view of this complicated flow and vortex structure applied to a two pass rectangular channel with a 45 degree criss-crossed rib structure at two different orientations; the diagram of which is provided on the following page. The dashed lines represent the vortices induced by rotation, whereas the solid ones are those produced by the ribs. A similar study was performed by Al-Hadhami et al. (2002), however instead of using criss-crossed 45 degree ribs a

parallel and crossed 45 degree V-shaped rib pattern was analyzed. Naturally the vortices produced by rotation remained the same, but instead of applying the 45 degree rib secondary flow pattern, the V-shaped one was applied, which further complicated the flow structure.



Parallel 45 Deg. Angled Ribs



Crossed 45 Deg. Angled Ribs

Figure 2-7: Comparison of Higher Order Flows due to Ribs and Rotation (Azad et al., 2001)

In addition to the higher order flows that have been presented above, there are a number of vortices and flow irregularities that are results of the fluid turning through U-bends. According to Kim et al. (2006) fluid flowing past the turning region produces a pair of counter rotating “dean vortices.” These are produced due to the curvature forcing flow from the middle of the duct to the outer wall.

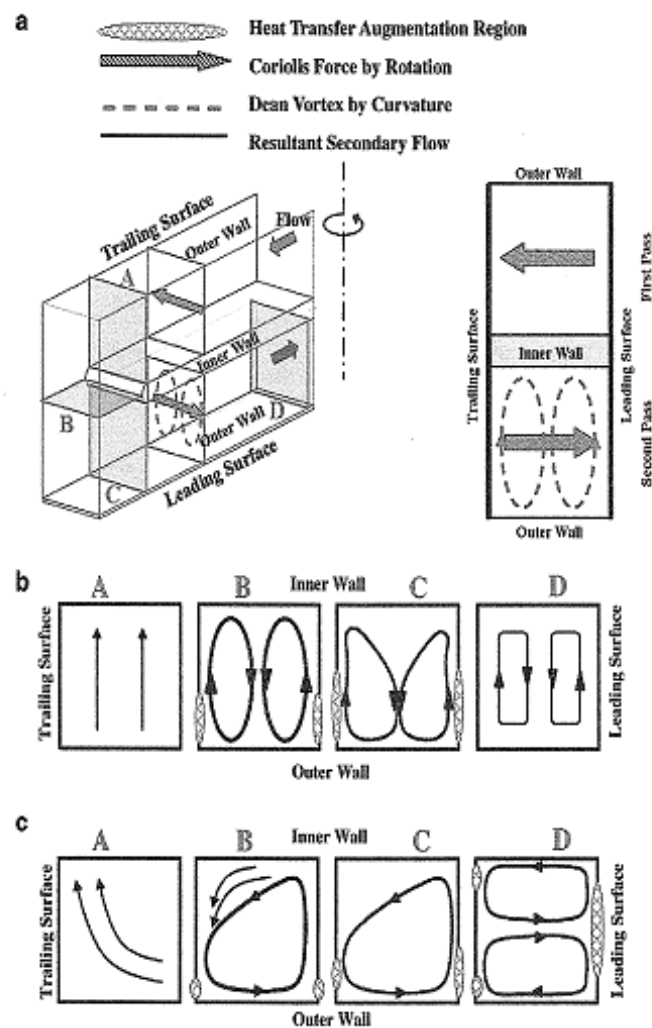


Figure 2-8: Expected Higher Level Flow Patterns in a Two-Pass Duct (Kim et al., 2006)

This mixing enhances heat transfer in the region quite considerably in that the core fluid is generally cooler than the fluid around the outer wall. There are other locally occurring flow patterns caused by the turn, such as for example the zone of separation directly following the turn, which creates a separation bubble on the near side of the divider wall (Kim et al., 2006).

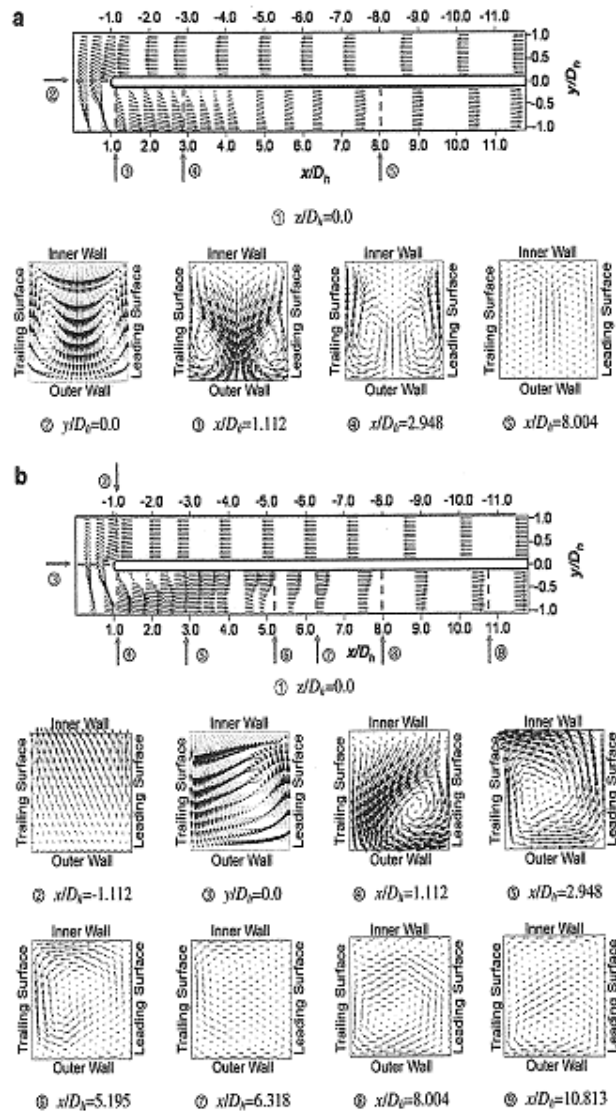


Figure 2-9: Velocity Vectors in a Two-Pass Rotating and Non-Rotating Duct (Kim et al., 2006)

All of these flow characteristics are included in figure 2-8, which provides a clear and concise overview and comparison of the expected flow behavior due to 180 degree turns with and without rotation. The expected flow behavior has been shown to agree with other studies of various authors such as Murata and Mochizuki (1999), Lin et al. (2001) and Al-Qahtani et al. (2002) (Kim et al., 2006). In addition to the expected flow schematic, a numerical simulation of the flow in a square duct with 90 degree ribs was conducted. The results of which are shown on the previous page. This once again shows a comparison between both a rotating and non-rotating case. The most important feature that is highlighted in the image is the fact that as the rotational forces are applied, the trailing edge vortex is weakened by the Coriolis forces leaving an asymmetric vortex in place of the counter-rotating pair.

Now that some of the basic correlations, and higher order flow fields have been described it is pertinent to look at other research performed on the topic. The effects of nearly any parameter imaginable on internal cooling have been extensively researched by numerous teams both numerically and experimentally. In addition to two superb overviews of the developments in internal cooling written by Han (2004) as well as Downs and Landis (2009) respectively, which have been referenced previously, an overview of some additional key works, the findings and overall conclusions are provided here. Firstly, since the work done by Kim et. al. (2006) has already been extensively delved into, the main focus of their work was to understand the effects of channel aspect ratio on heat/mass transfer in rotating cooling passages. After analyzing

ducts with constant ribs and hydraulic diameters at three different aspect ratios ($W/H = 0.5, 1.0, \text{ and } 2.0$) it was found that although the heat transfer coefficient increases as the duct aspect ratio does, the effects of duct turning and rotation become less significant at higher aspect ratios (Kim et al., 2006). The results obtained matched the trends generated previously by Han et al. (1992). This work was aimed at understanding the effects that duct aspect ratios have on local heat transfer coefficients. Aspect ratios of 0.25, 0.5, 1.0, 2.0 and 4.0 were studied.

Taking a step away from research involving rotation and 180 degree turns, Aliaga et al., (1994) investigated the effects that rib pitch ratios have on the distance required for the flow to reattach to the channel wall and found that this “reattachment distance” is independent of both the rib pitch ratio as well as the Reynolds number. In recent years more and more research has been done regarding “broken” rib patterns, which have been shown to reduce the friction factors while still maintaining relatively high heat transfer augmentations. The term “broken” rib pattern originates from the fact that discrete ribs are added to a channel wall rather than continuous ones, which causes the ribs to appear to be broken in various places. Work has been done to this regard by Cho et al. (2000, and 2003a). The first paper investigated the effect of discrete rib patterns on local heat transfer, whereas the second was aimed at directly at the effects of gap positioning. Chandra and Han (1989) as well as Mochizuki et al. (1999) have both studied the effects that sharp turns have on flows in ducts with various rib angles (60 or 90 degree).

It is a well known fact that rotation alters the expected heat transfer rates due largely to the fact that a temperature asymmetry is created. This alteration in the heat transfer phenomena is explained by Kim et. al. (2006) to be the result of Coriolis and centrifugal forces creating a temperature discrepancy between the leading and trailing surfaces of the duct. Both Taslim et al. (1991) and Park et al. (1998) have conducted experimental research in order to determine the effects that rib blockage ratios and rotation have on heat transfer asymmetry. It was concluded that the Coriolis forces have a greater effect on smooth ducts than on ribbed ones. This could partially be due to the fact that the secondary flows created by the rib patterns interfere with those created by rotation. In addition to the above mentioned experimental research, numerical analysis was also performed by Lin et al. (2001) and Al-Qahtani et al. (2002) to study the flow and heat transfer in two-pass rotating channels, which was then compared to non-rotating conditions and shown to match the experimental data. Finally Hwang and Lai (2000) and Chang and Morris (2003) reported the effects of the centrifugal force, which is shown to depress heat transfer on the leading edge of the ducts while enhancing that of the trailing edge surface after the turn. This phenomenon was previously studied by Parsons et al. (1994) and Zhang et al. (1995) who had the same findings as the previous two papers, but in addition they concluded that before the turn the leading edge heat transfer is enhanced relative to that of the trailing edge wall.

Even though all of the papers presented above only cover a small fraction of all work done on internal cooling, it serves as a good overview of what kind of research is

being done in the field today. The end result of all this effort is the creation of trends and correlations used for turbine design. Due to the fact that currently more importance has been placed on uniform temperature distributions in order to reduce thermal stress, there has recently been a shift away from channel averaged approaches towards local values. This was captured by Iacovides and Launder (2007) who state that modern experimental and computation research strategies provide full-coverage data of surface temperatures and local heat transfer coefficients. They go on to state that this is revealing a good deal of local non-uniformity in Nusselt number, which is further increased by rotation and that these non-uniformities should be taken into account when dealing with stress calculations of turbine components. There is however a major difficulty in obtaining accurate localized heat transfer data in turns and after features of internal cooling channels, which is a direct result of the complex flow fields present in these locations. As such a large variance exists there; this can have a large impact on the overall component life. Naturally there are other sources of variation induced throughout the total length of an internal cooling channel, such as parameter inaccuracies, rotation, or other sources. For example, a work by Willett and Bergles (2000) pointed out that channel orientation induces a significant variation in the heat transfer coefficient in rotating single pass ducts. According to data provided by Chyu et al. (2009) a threefold increase in the internal heat transfer coefficient alone reduces metal temperature by approximately 470K. Even though variation could have a very large impact on the component, virtually no research (of the papers presented above, or

in general) has been focused on the topic. One of the very few papers found combining heat transfer and the effects of variation was a work done by Williams (2009), which was based on a probabilistic study to determine the influence of parameter uncertainty on thermal radiation heat transfer.

As such it is the primary goal of this paper to introduce interdisciplinary, probabilistic internal heat transfer design, by providing an uncertainty quantification of the effects that variation of internal cooling heat transfer coefficients have directly on the life of the component. Following are two short overviews of fatigue life and probabilistic design in order to provide the reader with sufficient background information in the fields.

2.2 Low Cycle Fatigue Life

The following section will provide a brief overview of the history of low cycle fatigue lifing. Please note that this is not meant to serve as a complete literature review, but merely to provide the reader with a baseline knowledge of the topic, such as a brief history, some of the most prevalent equations, and a quick overview of the direction currently being taken.

The beginnings of low cycle fatigue work started in the 1950's. L.F. Coffin (1954) and S.S. Manson (1954), two of the most influential people in the field, independently published papers titled "A study on the effects of cyclic thermal stresses on a ductile metal" and "Behavior of materials under conditions of thermal stress" respectively. Both papers were focused around plastic strain, and the effect of thermal cyclic stresses. These papers led to the generation of stress equations, such as the following one produced by S.S. Manson (1954) for general stress of a plate. Please note that in this case σ refers to stress and μ represents the Poisson's Ratio.

$$\sigma^* = \frac{\sigma(1 - \mu)}{E\alpha T_0}$$

Figure 2-10: General Stress Equation of a Plate (Manson, 1954)

This work was further built upon by S.S. Manson in 1960 and Coffin in 1979 with the creation of the mainstay of the low cycle fatigue world, the Coffin - Manson Equation. Although the equation was first created by Manson, it was furthered and popularized by Coffin's later work, and as such the equation shown below retains both authors' names. It accounts for strain induced to materials under cyclic loading usually with the presence of plastic deformation, and its effects, which usually originates in micro cracks and eventually fracture.

$$\varepsilon_a = \frac{\sigma'_f}{E} (2N_f)^b + \varepsilon'_f (2N_f)^c$$

Figure 2-11: Coffin-Manson Equation (Dowling, 1999)

This equations shows that the total strain amplitude is a combination of the elastic stress amplitude (the first term of the equation) and the plastic one (the second term). The values for σ'_f , ε'_f , b and c are material dependent properties which are generated through material testing and are generally plotted on strain versus life curves like the one shown in figure 2-12 on the following page. These material properties are temperature dependant, usually decreasing with increasing temperature, shown in figure 2-13 below.

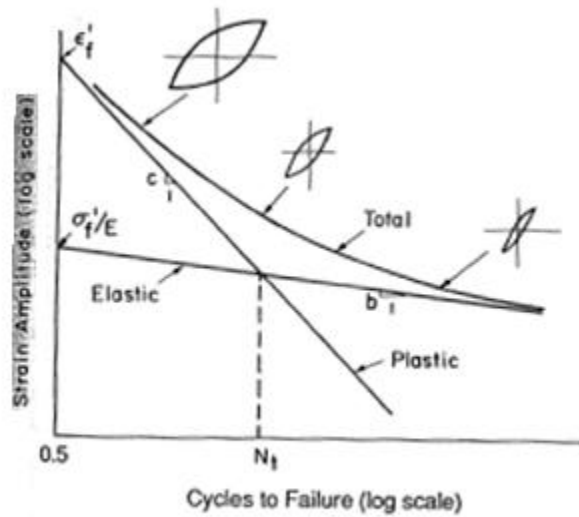


Figure 2-12: Generalized Strain Amplitude Vs Life Curve (Dowling, 1999)

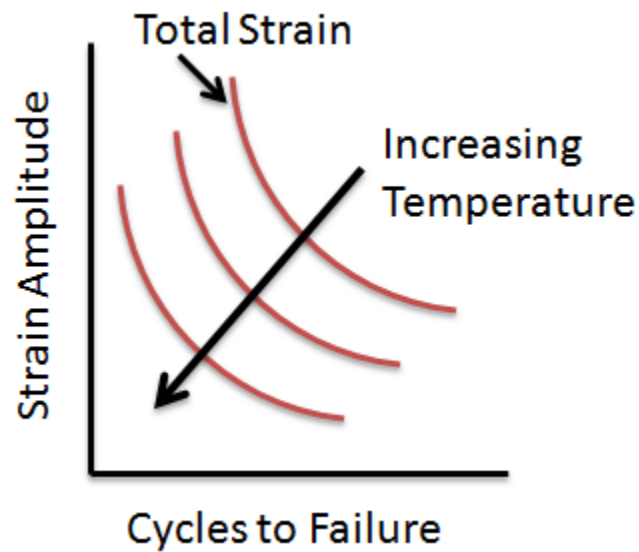


Figure 2-13: Decreasing LCF Material Properties with Temperature

This is extremely important in the gas turbine world as engines are started and stopped often. One start and stop is known as one cycle, and results in high cyclic loading as parts expand during heat up and shrink upon cooling, which will eventually lead to low cycle fatigue failure in components. Low cycle fatigue failure in this case does not mean catastrophic failure as one might expect, but rather refers to crack initiation, which depending on the loading on the component may or may not propagate to cause ultimate, catastrophic failure, or fracture of the component. However if the strain amplitude is high enough it is possible for catastrophic LCF failure to occur immediately, which is shown below on the simplified total strain amplitude versus cycles to failure plot.

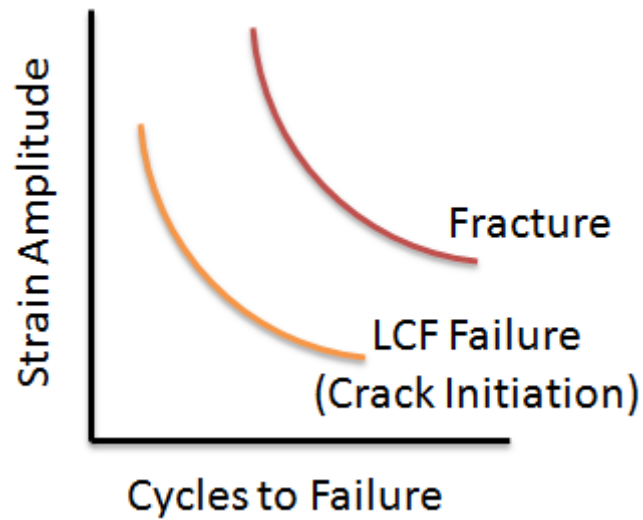


Figure 2-14: Crack Initiation vs. Fracture

Some offshoot equations have been developed from the Coffin-Manson relationship over time, such as for example the modified Marrow approach shown below. The general purpose and function of the equation remains the same, however some minor changes were made such as for example according to Dowling (1999) “the mean stress dependence has been removed from the second (plastic) strain term.”

$$\varepsilon_a = \frac{\sigma'_f}{E} \left(1 - \frac{\sigma_m}{\sigma'_f} \right) (2N_f)^b + \varepsilon'_f (2N_f)^c$$

Figure 2-15: Modified Marrow Approach Equation (Dowling, 1999)

A move has recently been made towards investigating the effects of multi-axial stresses on low cycle fatigue calculations. A very good review paper is provided by Brown and Miller (1982), which sums of the last two decades of progress in the

assessment of low cycle fatigue life. It states that very little has been done with regards to multiaxial LCF life over the last twenty years. Chen (1996, 1999) has done quite extensive testing of multiaxial loading on different steels under non-proportional loading, which generated new equation with more damage parameters to better predict the effects of non-proportional, multiaxial loading. However the equations provided above are what is currently used for calculating low cycle fatigue life.

2.3 Probabilistic Design

Although the idea of probabilistic design has been around for an extremely long time its applicability was dependant on secondary inventions, notably the computer. Through advancements in computational power, statistical approaches have become a more common sight in the engineering world, especially in the area of design. According to Siddall (1983), “statistical techniques have been used in engineering in areas such as quality control, reliability and the control and interpretation of research experiments, but there has been very little application of probability theory in the central role of the engineer – design.” He goes on to state that even though design engineers have always depended on probability in their design work, up until the popularization of the digital computer, most of this work was based on intuition and feelings in the form of simple

safety factors rather than more formal probabilistic techniques. Even though Siddalls book was published in 1983, it is important to note that the trend has continued through to today. As computers become more and more powerful, probabilistic design has infiltrated more and more areas of the scientific community. With this being the case, it has become time for probabilistic design to be absorbed by the heat transfer community.

The growing impact that statistical methods are having on today's world cannot be more clearly described than by cooperate Americas rapidly emerging "six sigma" culture. According to a paper by Koch (2002), probabilistic design to address uncertainty and variability has been approached from many angles by different communities. Recently "six sigma" quality concepts have arisen from the manufacturing area, and the term "Design for Six Sigma (DFSS)" has been coined, and is the current push in industry. Koch further goes on to develop a probabilistic design model which focuses heavily on the application of uncertainty to design methods and optimization. The importance of uncertainty is summed up by stating that "optimization without including uncertainty leads to design that cannot be called "optimal", but instead are potentially high risk solutions that likely have a high probability of failing in use." This high importance on uncertainty is mirrored in other works, and is nearly ignored in today's heat transfer design, which still rely heavily on the use of high factors of safety rather than statistical analysis, and as such the quantification of uncertainty arising from internal heat transfer

coefficients is not only important, but also a good first step in wholly ushering probabilistic design into heat transfer engineering.

Some of the more prevalent probabilistic methods used today include the Monte Carlo method, propagation of error, design of experiments, the method of moments as well as statistical interference. Since this project aims at modeling uncertainty in an output through a random generation of variability in the input the main focus will be on the Monte Carlo Method, and a brief history will be provided. It was decided to employ the Monte Carlo Method largely due to the fact that according to Hammersly and Handscomb (1964) a Monte Carlo Method focuses on characterizing the statistical nature of a response by randomly simulating an input provided stochastic properties for at least one variable, which in essence is exactly what will be required of this project. Even though advances have been made in the field, mostly through the addition of more advanced, efficient, and faster converging methods all built around the basic Monte Carlo Method, the fundamentals of the approach have not changed much since the '40's. A paper published by Metropolis and Ulam in 1949 first introduced the Monte Carlo Method as a method "dealing with a class of problems in mathematical physics", that is "essentially a statistical approach to the study of differential equations, or more generally, of integro-differential equations that occur in various branches of the natural sciences." Metropolis published a paper over two decades later in 1987 covering the history of the Monte Carlo Method, which credits the method to "the creation of the world's first computer (the ENIAC)" and "Stan's [Stanislaw Ulam] interest in random

processes.” The paper also contains a “further reading” section which provides a handful of good papers detailing the creation of the method which has been touched upon here.

As was mentioned earlier, this section was not meant to provide a complete in depth look into the probabilistic design world, but to merely provide the reader with a basic understanding and a very brief history.

CHAPTER III PROBLEM DEFINITION

It was decided to work with the General Electric version of the NASA Energy Efficient Engine (E³) blade 1. This blade is a perfect choice, since it is a public domain airfoil, which not only contains the required multi-pass serpentine cooling, but has also been used extensively in other research. The availability of other test data will be especially beneficial when it comes to a validation effort, as either part of this work, or future ones. However even though the airfoil has been in the public domain for an extended period of time, finding a previously created model proved to be quite challenging, as such it was decided to generate a model from the available information and make it available to the public for future use and refinement.

The main purpose of the following section is to highlight some of the major difficulties that needed to be overcome long before any analysis work could even be attempted. Most of the challenges arose during the model creation process, which had to be overcome since no three dimensional model was available for use. In fact, the creation of readily available three dimensional FEA and CAD models for a public domain airfoil is a secondary benefit of this project in that future research done using this component will not need to go through the model recreation steps as was done here. In addition to pointing out and discussing these challenges this chapter will also contain some initial predictions of anticipated results as well as the test matrix.

3.1 Challenges

Even though a majority of the problems are on the modeling side, there were also a number of challenges that needed to be overcome with the setup of the probabilistic design process. This being the case the following section is broken down into two parts, the first to discuss the modeling challenges including lack of both geometric and boundary condition information, and the second to address the probabilistic design hurdles.

3.1.1 Modeling

Most of the challenges related to modeling the airfoil arose due to the fact that only a limited amount of information was available on the component that was chosen, the General Electric version of the NASA E3 (Energy Efficient Engine) row one turbine blade. This was especially challenging since there were no actual models available for the component, meaning that a new one had to be created from the limited information contained within the provided reports. In addition to this lack of geometric detail, the provided information with regards to boundary conditions is also somewhat lackluster. This further complicates the matter of not only accurately recreating the model, but also regenerating any kind of temperature or stress data. However, this should not greatly

affect the project, since the major focus is to study the effect of internal heat transfer coefficient variation not on recreating previously generated data.

3.1.1.a Provided Geometric Information

Even though the original NASA report by Halila (1982) contains very little by way of actual empirical data regarding any form of geometry, the secondary design report by Timko (1990) contains external coordinates for the airfoil at three cuts. This information is provided in tabular form by Timko. This provided a very good starting point, in that at least the un-cored airfoil could be accurately recreated. However, as far as actually modeling the rest of the airfoil is concerned, this was the only direct data that was available, meaning that the entire core of the airfoil had to be modeled using various two dimensional images found in the reports. One of these image was a side view of the airfoil (figure 3-2) whereas the other was a cross sectional view at an undisclosed radius (figure 3-3). Although these images could be used as somewhat of a guideline the fact that it is never stated if the side-view is an uncurled camber-line view, or just a straight cut side view, and that the cross sectional view is not referenced to a particular radius, makes it very difficult to accurately model a core off of. The major impact that this has on the project as a whole is that some assumptions will need to be made in order to

complete the modeling task, which is acceptable given the lack of detailed information.

A sample of both the provided coordinates from Timko (1990) as well as the same data

in the corresponding excel file are shown here. The generated excel files are provided in

their entirety in Appendix E. It is important to note that the information provided is

given at a 10x scale.

PRESSURE SURFACE COORDINATE					
PT.	X	Y	PT.	X	Y
42	0.350044	0.899838	83	0.883318	-7.071395
43	0.585823	0.895710	84	0.839255	-7.078383
44	0.781202	0.876018	85	0.814348	-7.082100
45	0.983781	0.812918	86	0.789178	-7.093258
46	1.212380	0.811258	87	0.764141	-7.108598
47	1.427939	0.091182	88	0.739878	-7.107850
48	1.643518	1.852815	89	0.718211	-7.080322
49	1.859097	1.890003	90	0.694180	-7.053371
50	2.074676	1.905824	91	0.673909	-7.038411
51	2.290255	0.890871	92	0.655813	-7.020909
52	2.505834	0.873274	93	0.640152	-7.001158
53	2.721413	0.923698	94	0.624888	-6.920848
54	2.936992	-0.048482	95	0.609581	-6.840478
55	3.152570	-0.438287	96	0.474278	-6.780098
56	3.368149	-0.842570	97	0.418371	-6.679577
57	3.583728	-1.274374	98	0.303668	-6.599045
58	3.799307	-1.728078	99	0.308380	-6.518458
59	4.014886	-2.184884	100	0.682781	-6.203458
60	4.230465	-2.657625	101	4.827882	-5.895220
61	4.446044	-3.142337	102	4.681823	-5.571448
62	4.661623	-3.640008	103	4.448044	-5.237887
63	4.877202	-4.147542	104	4.230485	-4.893578
64	5.092781	-4.652558	105	4.014886	-4.554459
65	5.308360	-5.160181	106	3.799307	-4.288324
66	5.418148	-5.450898	107	3.583728	-4.096348
67	5.527936	-5.722041	108	3.368149	-3.893778
68	5.637724	-6.001918	109	3.152570	-3.690319
69	5.751091	-6.289182	110	2.936992	-3.588880
70	5.865208	-6.545957	111	2.721413	-3.141272
71	5.979326	-6.823128	112	2.505834	-2.990098
72	6.093545	-7.142889	113	2.290255	-2.742158
73	6.207764	-7.471858	114	2.074676	-2.561884
74	6.321983	-7.897006	115	1.859097	-2.303143
75	6.436202	-8.328032	116	1.643518	-2.233014
76	6.550421	-8.748024	117	1.427939	-2.081308
77	6.670414	-9.175381	118	1.212380	-1.840858
78	6.858719	-9.688817	119	0.983781	-1.808811
79	6.946178	-7.613171	120	0.781202	-1.803253
80	6.927847	-7.051822	121	0.585823	-1.582582
81	6.807828	-7.047848	122	0.350044	-1.452951
82	6.888258	-7.060801			

Stage 1 Blade Airfoil Coordinates (10X), inches

Radius = 12.731 inches

Figure 3-1: GE NASA E³ Blade 1 External Coordinates Sample (Timko, 1990)

Table 3-1: External Coordinates Excel File Sample

Radius 12.731 inches		Radius 12.731 inches		Radius 12.731 inches	
x	y	x	y	x	y
0.350044	2.999538	5.731591	-6.209482	5.474278	-6.760055
0.565623	2.85571	5.892398	-6.545557	5.418971	-6.679577
0.781202	2.696068	5.973206	-6.823128	5.363668	-6.599045
0.993781	2.512958	5.980948	-6.847085	5.30836	-6.518458
1.21236	2.311299	5.985454	-6.871856	5.092781	-6.203495
1.427939	2.091152	5.986646	-6.897006	4.877202	-5.88572
1.643518	1.852515	5.984302	-6.922092	4.661623	-5.571445
1.859097	1.590063	5.978059	-6.946674	4.446044	-5.257657
2.074676	1.305524	5.970414	-6.970321	4.230465	-4.952578
2.290255	0.999871	5.956719	-6.992617	4.014289	-4.654459
2.505834	0.672754	5.944178	-7.013171	3.799307	-4.368324
2.721413	0.323088	5.927047	-7.031622	3.583728	-4.096248
2.930992	-0.046462	5.907628	-7.047646	3.368149	-3.835775
3.15257	-0.438297	5.886258	-7.060961	3.15257	-3.590719
3.368149	-0.84757	5.863318	-7.071335	2.936992	-3.35808
3.583728	-1.274374	5.839205	-7.078583	2.721413	-3.141272
3.799307	-1.720078	5.814346	-7.08258	2.505834	-2.936096
4.014886	-2.184684	5.789176	-7.083255	2.290255	-2.742198
4.230465	-2.657628	5.764141	-7.080596	2.074676	-2.561894
4.446044	-3.142337	5.739676	-7.07465	1.859097	-2.393143
4.661623	-3.640508	5.716211	-7.065322	1.643518	-2.233014
4.877202	-4.147542	5.69416	-7.053371	1.427939	-2.081508
5.092781	-4.652588	5.673909	-7.038411	1.21236	-1.940656
5.30336	-5.180191	5.655813	-7.020905	0.986781	-1.808611
5.419168	-5.450656	5.640192	-7.001159	0.781202	-1.693253
5.523975	-5.722041	5.584886	-6.920846	0.565623	-1.564582
5.640783	-5.984918	5.529581	-6.840478	0.350044	-1.452951

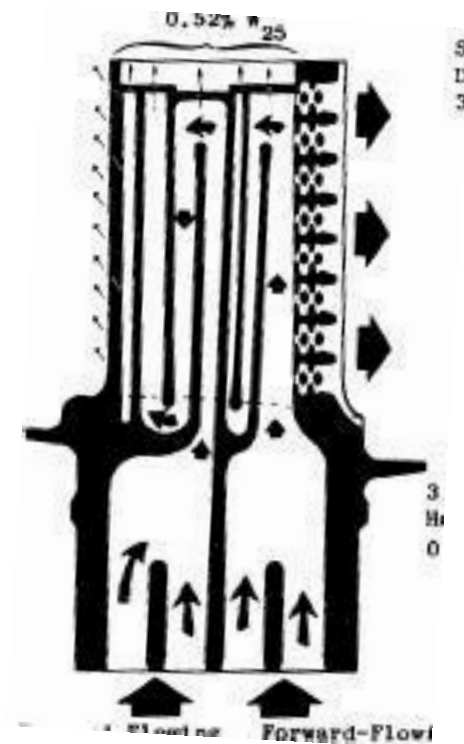


Figure 3-2: GE NASA E³ Blade 1 Airfoil Side View (Halila, 1982)

One of the positives however, is that between the two views that are provided, all of the internal details are shown, meaning that the general location of any kind of ejection holes, be it tip, pressure side, or leading edge are provided. Also it is possible to get an understanding of the relative sizes of different passages to each other, along with the rough location of the internal ribs. Some additional, more detailed information is provided in the following figure, which contains data on all of the cooling holes, such as number of holes, diameter, and type of hole. Even though this information is not critical to the analysis being currently performed, since film cooling will not be taken into account, it might be useful for further studies in the future.

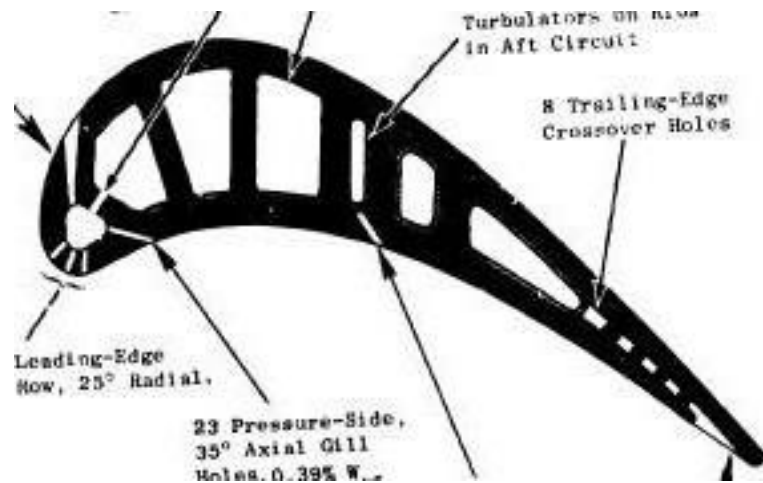


Figure 3-3: GE NASA E³ Blade 1 Cross Section at unknown radius (Halila, 1982)

It is however extremely important to know the relative flow rates (which are provided in figures in the reports themselves) so that the right amount of flow can be subtracted from the main channel flow for cooling air heatup calculation purposes.

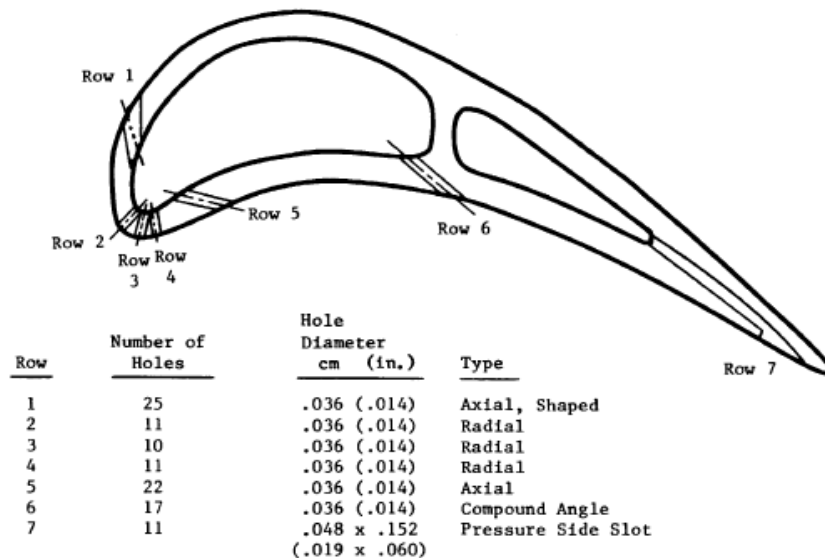


Figure 3-4: GE NASA E³ Blade 1 Cooling Hole Definition (Timko, 1990)

Even though the information is not essential to creating a model of the airfoil, the table below contains some useful information which will be needed later on, such as the blade count. Although the provided geometric information is not as complete as was hoped, the details gained should be more than adequate to generate a good approximation of both the airfoil as well as the the core and all internal details.

	<u>Hub</u>	<u>Pitch</u>	<u>Tip</u>
Number	<hr/> 76 <hr/>		
Radius, cm (in.)	32.337 (12.731)	34.468 (13.570)	36.601 (14.410)
Axial Width, cm (in.)	2.87 (1.13)	2.87 (1.13)	2.87 (1.13)
Trailing Edge Thickness, cm (in.)	0.0965 (0.038)	0.0965 (0.038)	0.0965 (0.038)
Uncovered Turning, degrees	13.0	13.0	13.0
Trailing Edge Wedge Angle, degrees	12.5	12.5	12.5

Figure 3-5: GE NASA E³ Blade 1 Additional Section Design Data (Timko, 1990)

3.1.1.b Provided Boundary Conditions

Much like was the case with the geometric data, there was also a lack of available boundary condition information. The only charts provided in any of the reports that were found regarding the NASA E3 engine consist of one showing the gas path temperature profile for the row one vane, and another depicting gas side heat transfer

coefficients for the row one blade. Both of these graphics are provided below for reference.

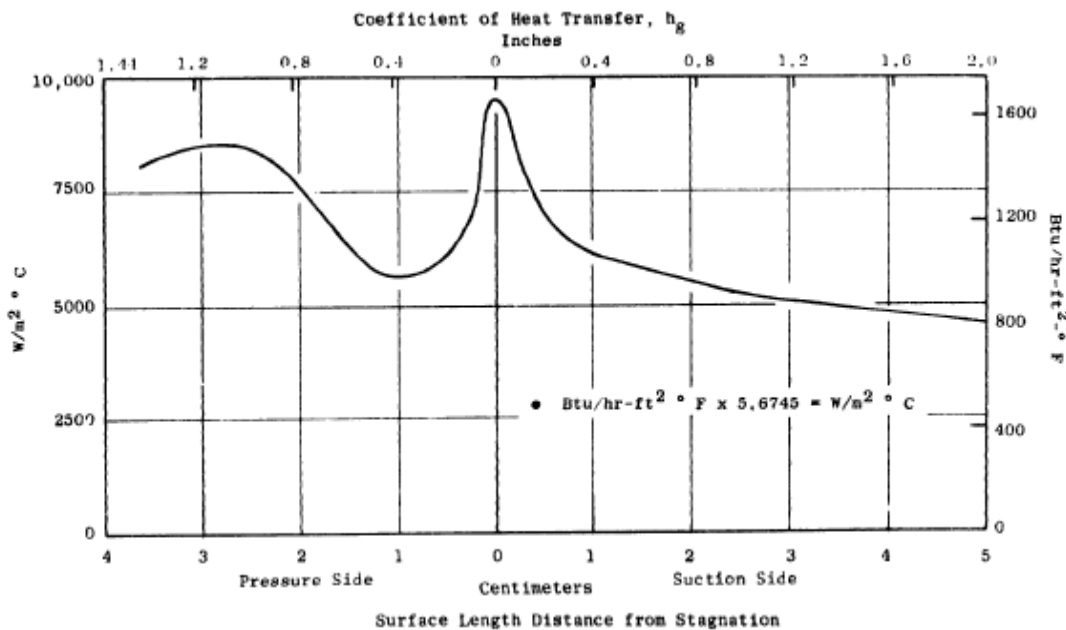


Figure 3-6: GE NASA E³ Blade 1 Heat Transfer Coefficients at unknown radius (Halila, 1982)

Since no gas path profile was provided for the blade, the vane profile had to be used, but was adjusted to a peak temperature of 1421°C. The recreated gas path temperature profile that will be applied to the model is shown in figure 3-8. On the contrary to the radial temperature profile, the heat transfer coefficient chart is only representative of one radial height. With no additional information provided it had to be assumed that the same coefficients will be applicable at all sections. Further assumptions will be required for heat transfer coefficient values at the tip of the blade, since no data whatsoever is provided for that area.

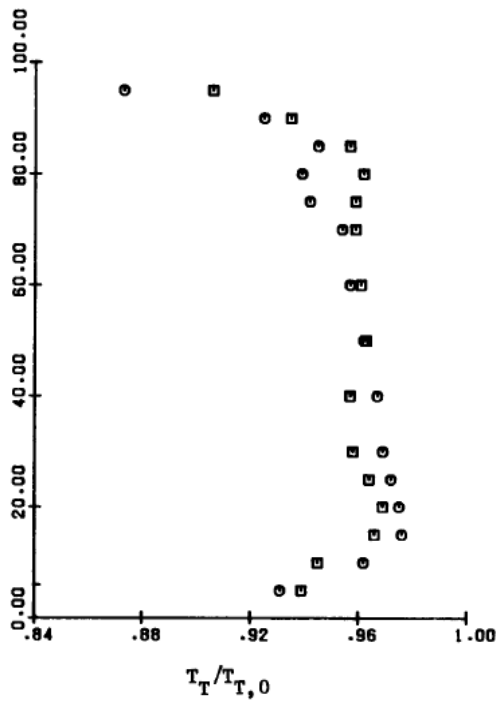


Figure 3-7: GE NASA E³ Vane 1 Temperature Profile (Timko, 1990)

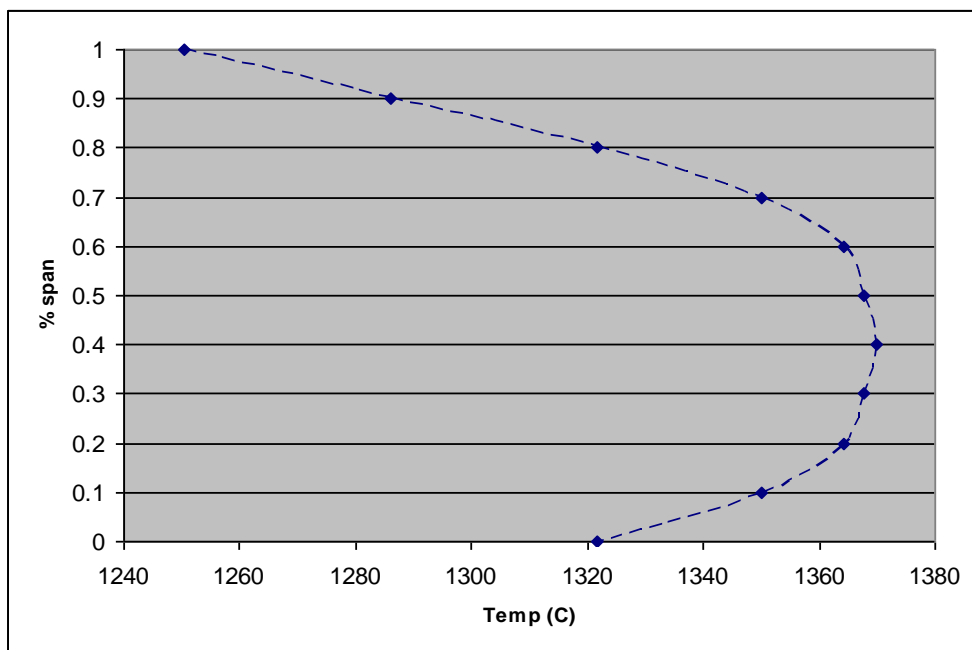


Figure 3-8: Generated Blade 1 Temperature Profile

This will not have any significant impact on the study however, since the metal temperature calculations in the tip will be skewed already due to the neglecting of any tip ejection, which has a significant impact on tip temperatures. As such the extreme top of the blade will already be ignored for any lifing purposes, meaning that any additional assumptions made there will not have a negative effect on the analysis as a whole

Even though this does not directly affect the current phase of the project, since as of now, only the thermal side of the analysis is considered, the complete lack of direct pressure data will need to be addressed in the future. In conclusion, even though the provided boundary condition information is not as complete as one would have hoped, it is sufficient for this study with the use of only two assumptions, namely heat transfer conditions at the tip, and an application of the same gas path heat transfer coefficient conditions independent of radial height.

3.1.2 Probabilistic Design

In addition to the challenges that were faced by the modeling of the component in order to do the analysis, there are a number of problems that came up on the probabilistic side of the equation. The most notable of which is the fact that to properly represent the variation of heat transfer coefficients inside of a three pass serpentine

channel, a large number of random variables are needed, and as the number of variables increases, so does the number of runs required to complete a probabilistic model with good resolution. This is further complicated by the fact that the computation resources available for this project are not infinite, be it in number of available software licenses, or even with raw computing power. Finally the fact that heat transfer coefficients within a channel are not unrelated to each other provides yet another challenge which will need to be addressed.

3.1.2.a Number of Variables

From a heat transfer standpoint the more random variables that can be used to modify heat transfer coefficients the better. From a probabilistic design point of view it is advantageous to try and limit this number as much as possible. This being the case it, was decided to model the uncertainty of HTC's with thirty independent, normally distributed random points, which will allow each passage to be subdivided into ten sections with independently chosen variations. Since thirty variables is still a lot in the probabilistic world, it will not be possible to achieve high resolution probability curves. In general, low cycle fatigue lifing models prefer to have very high resolution, especially towards the low tail of the curve. But since this work is focused on merely quantifying

the effect that uncertainty in measured and applied heat transfer coefficients has on the variation in LCF life, that kind of detail is not required. Thus, in order to allow for a good number of random variables to be used for uncertainty modeling it was decided to not run any full, sophisticated, probabilistic methods such as Latin Hypercube Sampling (LHS) or Most Probable Point (MPP). Although these are advanced Monte Carlo methods, they will still require an extremely large number of runs with thirty random variables. However, this project will instead rely on very low run, or minimalistic, Monte Carlo approaches to generate low resolution probabilistic curves. This will still show general trends and allow for good uncertainty quantifications.

3.1.2.b Computational Power

By deciding to stick with a low run Monte Carlo method this problem of raw computing power is addressed, however, in addition to this there is also a software license issue which will dictate how much analysis work can be performed. In order to go through a single analysis loop, three separate software packages are required, all of which have only limited licenses. This problem is avoided largely by limiting any analysis effort to the weekend or night time, but even so, the effect on computational time needs to be taken into account. Therefore, it can be seen that here, as is the case with

most probabilistic projects, both raw analysis time and computational resources provide two of the major chokepoints, which need to be circumvented by careful planning and allocating a sufficient amount of time to complete all runs.

3.1.2.c Correlation of Random Variables

An entirely different problem that was encountered is that in reality there is a correlation between heat transfer coefficients within a certain neighborhood. This means that it is physically impossible to have extremely large changes in magnitude of HTC's over a certain distance in a channel. Normally this would not have to be taken into consideration, since most flow solvers used to generate internal heat transfer data calculate heat transfer coefficients from the given geometrical conditions and fluid properties, which in a relatively unchanging channel will not vary much (with the exception of heat pickup or pressure changes due to pumping). Naturally this phenomenon is altered in the presence of internal cooling features such as ribs. But, since the data that is being generated to model the variation within the heat transfer coefficients is uncorrelated normal Gaussian distributed data, it needs to in some way be altered to represent this correlation.

This problem was addressed in a paper by Markus Deserno (2002), which provides both an autocorrelation function (shown below) that transforms randomly generated, uncorrelated, Gaussian normally distributed data into randomly generated, correlated, Gaussian normally distributed data, as well as the mathematical proof of the theory. By altering the value of tau it is possible to change the degree of correlation of the modified generated data. As the value approaches zero the data become more and more uncorrelated, whereas a value of infinity would imply perfectly correlated data (all generated data points have the same value).

$$r_0 := g_0 \quad ; \quad r_{n+1} := f r_n + \sqrt{1 - f^2} g_{n+1}.$$
$$f := e^{-1/\tau}.$$

Figure 3-9: Correlation Equations (Deserno, 2002)

In order to visualize this effect, the following graph provides an example of uncorrelated and correlated randomly generated data at different values of tau. By employing this autocorrelation function it will be possible to generate the correlated data that is required for the analysis effort.

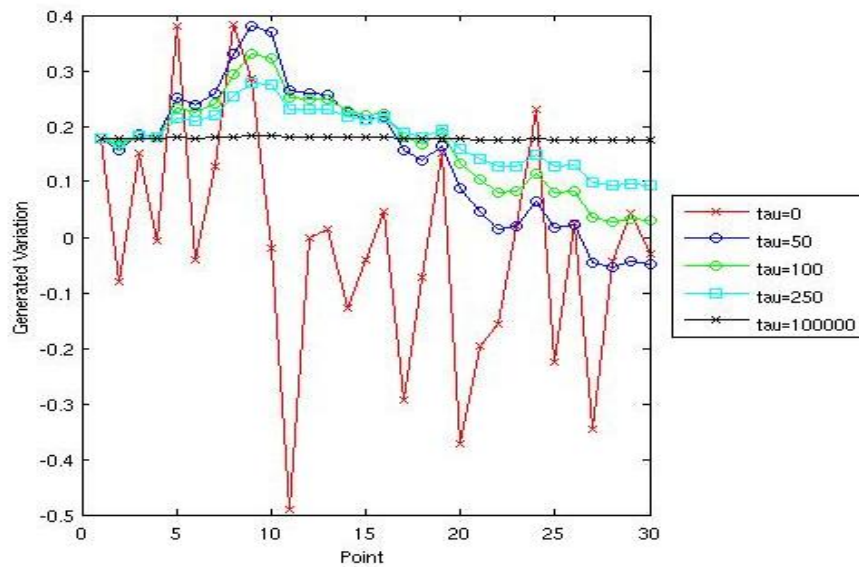


Figure 3-10: Randomly generated correlated and uncorrelated data points

3.2 Test Matrix and Predictions

Before any form of analysis was performed, a test matrix was created. As was demonstrated in the previous chapter, there is a larger uncertainty associated with turns in a duct versus the straight sections, as such for each case that will be tested, there are two values provided for the prescribed uncertainty range, the first corresponding to the straight passage, whereas the second, larger number is used for the hub and tip turn.

With this matrix also came some preliminary predictions of the results. These predictions were not generated from any empirical evidence, but rather were simply

based on knowledge in the heat transfer field and “gut feelings” of what kind of outcomes might be expected and as such carry no weight in the actual analysis effort.

Table 3-2: Test Matrix

		Run #1	Run #2	Run #3	Run #4	Run #5
Uncertainty Band	5% / 10%			X		
	10% / 20%		X			
	20% / 40%	X			X	X
Tau Value	0				X	
	50	X	X	X		X
Gas Path Temperature	Baseline	X	X	X	X	
	-100 C					X

Naturally, one expects there to be an effect on the output based on variation of input parameters, in this case meaning that with a forced uncertainty in heat transfer coefficients also comes a variation in LCF life. One would also expect the variation of the output to be related in magnitude to the variation in the input, meaning that as the prescribed uncertainty range of the HTC's is reduced from 20/40 down to the 5/10 case, there should also be a reduction in the magnitude of the LCF life variation. Furthermore, it is expected that with a reduction of gas path temperature, there should also be a reduction of LCF life variation, since generally speaking materials have more forgiving LCF properties at lower temperatures. Also, it is expected that at cooler gas path temperatures, the average life should be significantly increased. As far as the effect that the presence of a correlation function has on the analysis, no preliminary prediction is made mostly due to the fact this has not previously been studied, and as such any prediction provided would merely be an uneducated guess.

CHAPTER IV MODELING

The model creation process consists of two major components, first a three dimensional CAD model needed to be constructed, which was later meshed and turned into the usable finite element model. In addition to this some minor steps had to be taken, such as the creation of an internal flow network to generate baseline internal boundary conditions, as well as to select an appropriate material model to use for the analysis.

4.1 CAD Modeling

As was mentioned in the previous section, since all of the required data for the exterior of the airfoil was readily available, modeling it was fairly straight forward. The three tables containing all of the coordinates were manually typed into Microsoft Excel, which was then read into Pro-E. This created three planes of points that were then connected with splines in order to produce slices of the airfoil at each of the three radial heights. These sections were then lofted together, combining them into a single three dimensional airfoil. Since the root is of no real importance for this study, it was represented by a rectangular block, created to simply house the root section of the internal flow network and serve as an endwall for the airfoil. Furthermore, a temporary

squealer tip was added to the model by cutting away some of the material from the tip. This will be updated on the actual model once the core is generated and subtracted from the currently solid airfoil. The complete model of the external airfoil and the root can be seen in the following image.

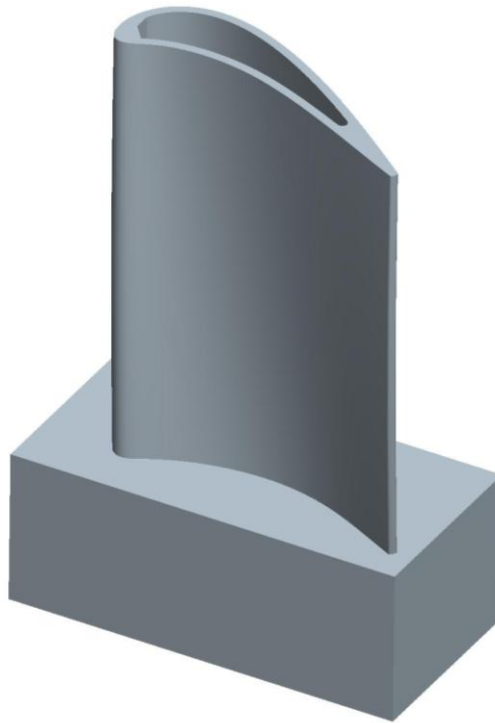


Figure 4-1: Pro-E Generated Airfoil External Geometry

Correctly creating the core for this airfoil was by far the most challenging part of the modeling process. Since no actual dimensions, short of the restrictions provided by the exterior of the airfoil, were provided, they had to be obtained by other means. This was creatively done through applying a constantly spaced horizontal and vertical grid to the two dimensional plots that were able to be accessed, and then using the known

exterior dimensions such as vertical extend to “back calculate” the missing information. Naturally this approach is not completely accurate, especially since curvature is involved, however in the absence of actual data it was deemed acceptable. The two dimensional section with an applied grid is shown in the following image.

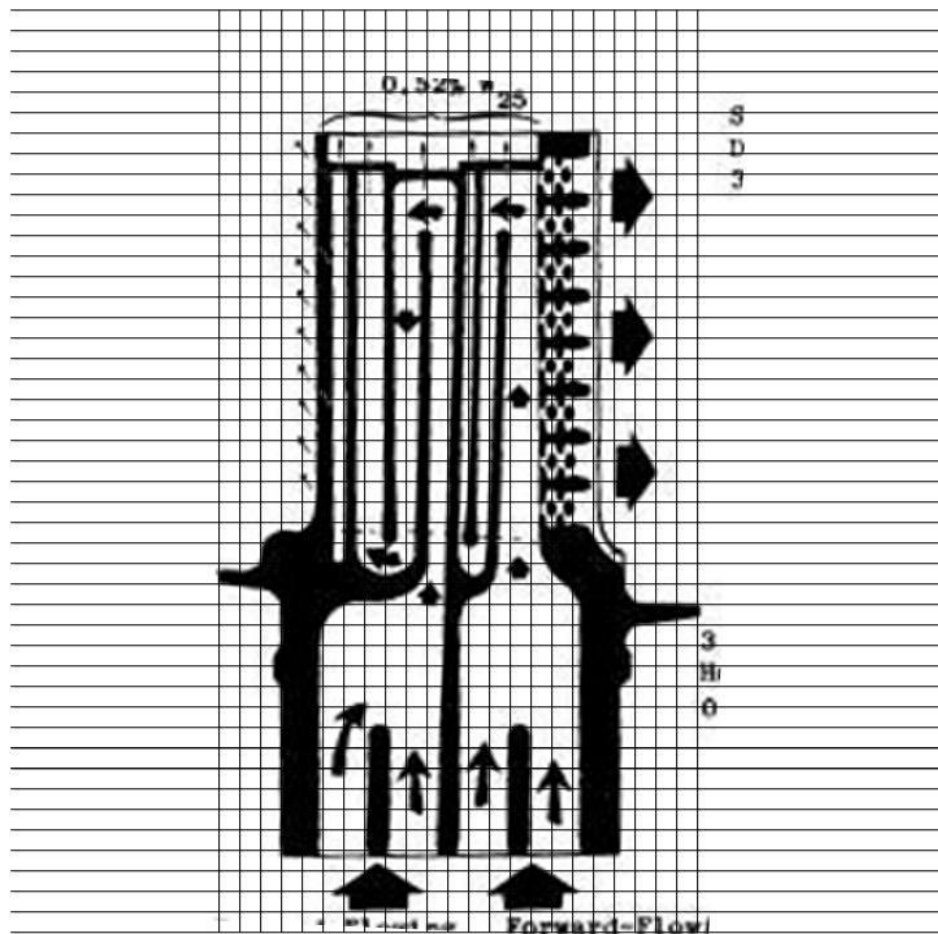


Figure 4-2: Gridded Side View

Since the trailing edge section of an airfoil more closely resembles a straight line than does the leading edge, it was decided to start from the aft end and work towards the front. This allowed for nearly the entire aft serpentine to be constructed fairly accurately, whereas the forward passes required some iterative work in order to

achieve desirable results. Extra care was taken to properly place all ribs, and to try and include some fillets on the core as a structural analysis will need to be completed in order to generate life data. The sizing and location of fillets was based on “best practices” since no data of any kind was available. Note that the tip section was also included in the core, which allowed for the creation of an accurate squealer tip. The generated core model, including the coolant feed passages and tip section, can be seen in its entirety in the figure below.

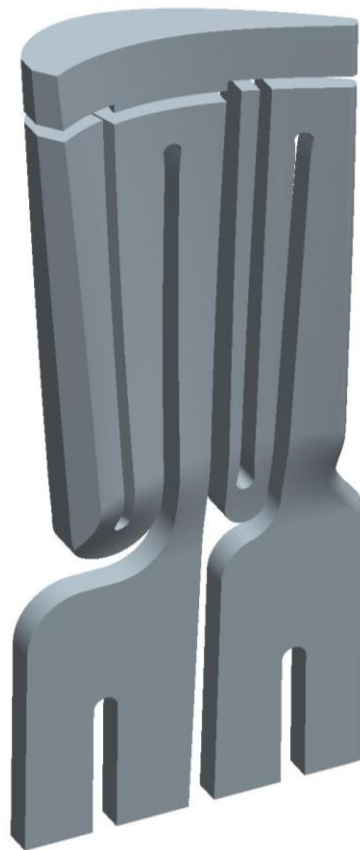


Figure 4-3: Pro-E Generated Core Geometry

Once both the external and internal models were created, the core was simply placed inside the solid airfoil and subtracted. This produced the final model that was needed for the finite element analysis. Once the final model was created it was possible to create various cross sectional views in order to attempt to match the cross sectional drawing provided in the NASA reports even though there was no radial height provided. Since the exterior of the airfoil was generated from data directly it was possible to match airfoil shapes to ensure that the correct radial heights were being compared. The generated model did not match perfectly on the first try, but with a few simple iterations of core dimensions it was possible to create an airfoil model that matched closely. This final model is shown below with a cross sectional cut-plane activated, in order to see the internal passages of the component.

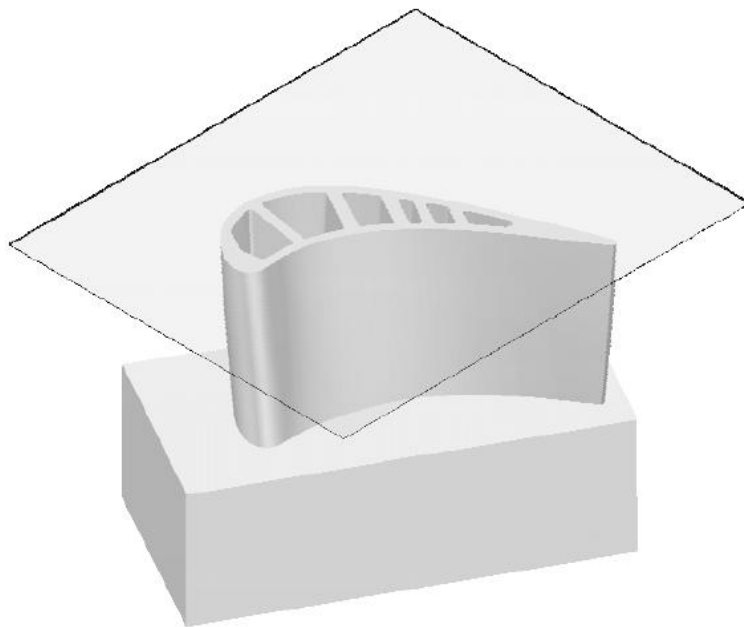


Figure 4-4: Combined Core and Airfoil

4.2 FEA modeling

Creating a functioning finite element model consisted of three major steps, first the CAD model needed to be meshed, and the boundary conditions applied. Following this, mesh sensitivity studies had to be performed. These studies can be quite time consuming, but are extremely important in that they ensure that the applied mesh is fine enough to accurately predict both temperatures and stresses. Since the creation of the model was not the main purpose of this project, but merely a step required for the completion, the level of detail provided is sufficient enough for an advanced ANSYS user to recreate the component, meaning that all the necessary steps are provided, however the direct commands or menu options are not.

4.2.1 Initial model Creation

Before importing any geometries, element types were setup and material models imported from the Siemens Energy Inc. materials database. Elements that were used include: Mesh200, Solid87 and two types of Surf152's. Once all of this front end work was completed, the final version of the CAD geometry was imported as an iges file. All initial meshing was done with very coarse grids (an edge length of between .5 to 1

mm). Using the predefined Mesh200 element type area meshes were generated on all internal and external surfaces, any delicate areas such as fillets that produced mesh error were simply re-meshed with finer settings. Components were created from these area meshes for later purposes. The area meshes were then volume meshed using the Solid87 element type. This solid 3D ten node tetrahedral thermal element is very well suited for irregular meshes such as the one produced by this model. It is not necessary to go back and delete any of the area meshes, as Mesh200 element types are ignored by the solver. In addition to generating a volume mesh, surface meshes needed to be applied to all surfaces exposed to either the gas path, or any internal cooling. To later be able to easily distinguish between intern and external surface elements, a different element type was used for both cases even though SURF152 was selected for both. Using the previously created components all of the required areas (namely all internal passages, tip, airfoil, endwall, and root sections) were selected and surface meshed. It is important to point out here that even though all surface meshing was done by selecting the desired component and then applying the surface mesh, this will not create a separate component for the surface elements only. Thus, in order to simplify later steps once the surface mesh was completed, all generated SURF152 elements were selected and grouped into their own component. Much like the Mesh200 elements, SURF152 elements don't drastically effect the solve time since they share nodes with the volume mesh. However, they greatly simplify the application of boundary conditions to the model. The images on the following page show details of the first cut of the FEA model

before any boundary conditions or mesh refinement was applied. Once the thermal model was completed, an element transform (thermal to structural) was performed in order to obtain a structural model.

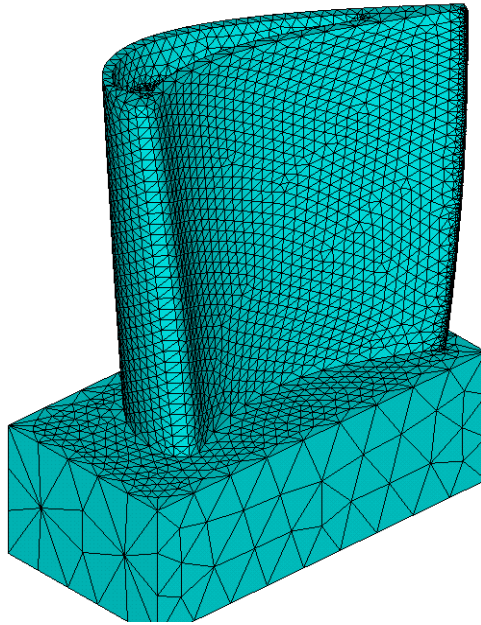


Figure 4-5: Meshed Airfoil – 1st Cut Exterior View

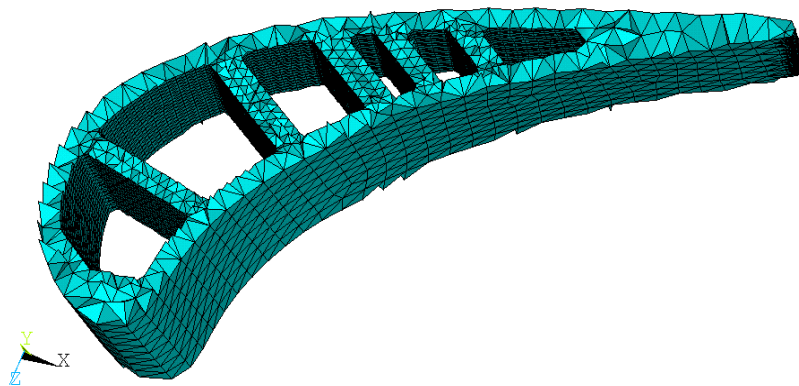


Figure 4-6: Meshed Airfoil – 1st Cut Internal Details

4.2.2 Boundary Condition Application

Since anytime the mesh is altered, it is necessary to reapply any boundary conditions that were previous applied, it was decided to do all boundary condition application through a macro. The macro itself is provided in appendix A, and should be pretty self explanatory. In essence, the following steps are repeated for all components. First, dimension and create a table with all of the required values for both temperatures and HTC's, then simply select the desired component and apply the table. It should be noted here, that in order for the generated macro to work properly, the components that need to be selected are those containing surface elements, not the initial area components. It was previously discussed how any required boundary conditions were obtained, so those procedures will not be provided again here. However, since the airfoil heat transfer coefficients differed between the suction and pressure sides of the airfoil it was required to divide the airfoil along the camberline and make components of from the surface elements of either side.

4.2.3 Mesh Optimization

As was mentioned previously, the most tedious and time consuming process behind generate a FEA model is the mesh optimization which is done through a number of mesh sensitivity studies. Originally it was thought that an element length of around .5 to 1mm would be too fine, and require coarsening up in order to reduce run time. However due to the fact that the model being meshed is an aero-blade which is approximately 10-20 times smaller than the average industrial gas turbine blade this proved to not be the case. The process behind mesh optimization is pretty simple. Decrease the mesh size, apply boundary conditions, and solve the model until any changes in stresses and temperatures are less than either one degree Celsius and between one to five mega Pascal's. Once this point is reached the previous mesh size is used for the remainder of the experiment. Usually only a few iterations are required. However, since the initial mesh that was applied was incredibly coarse a total of thirteen different mesh sizes were investigated, until convergence was reached. The resulting temperature and stress contour plots are in the following four images. Even though the structural models are considered to be converged even if they differ from each other by five Pascal's, whereas the thermals need to be within one Kelvin, it is much easier to achieve convergence on thermal models. This is mostly due to the fact that structural meshes in general are more refined than thermal ones, meaning that the thermal mesh converges long before the structural one does. It is possible to bring the structural mesh convergence to one Pascal, however the resulting element count is generally excessive.

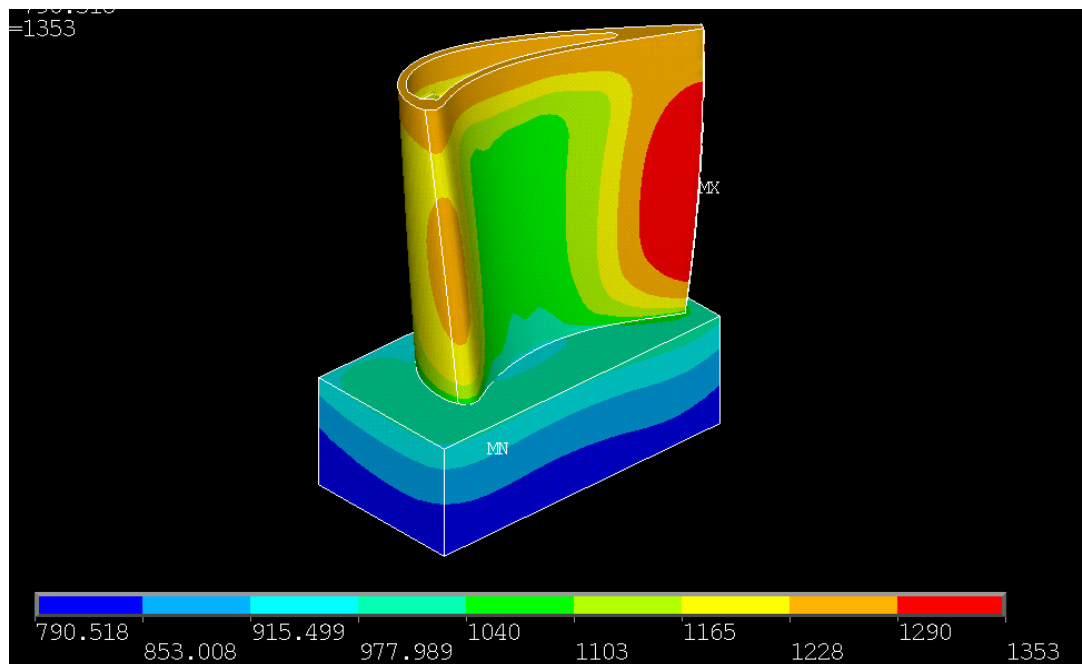


Figure 4-7: Thermal Results – Rev 12

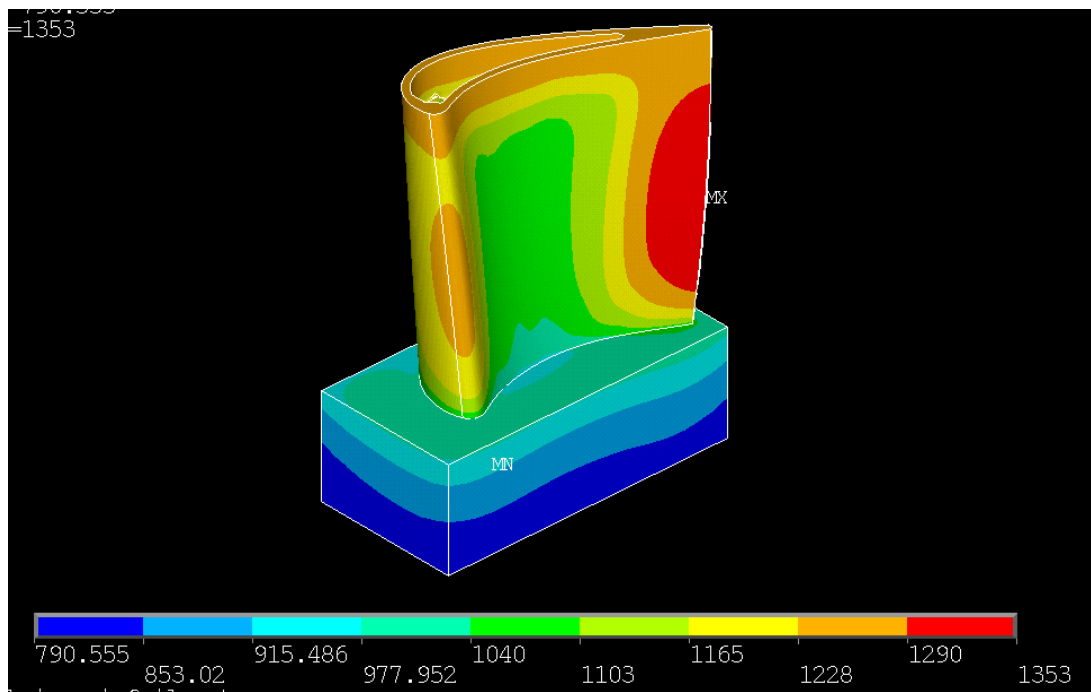


Figure 4-8: Thermal Results – Rev 13

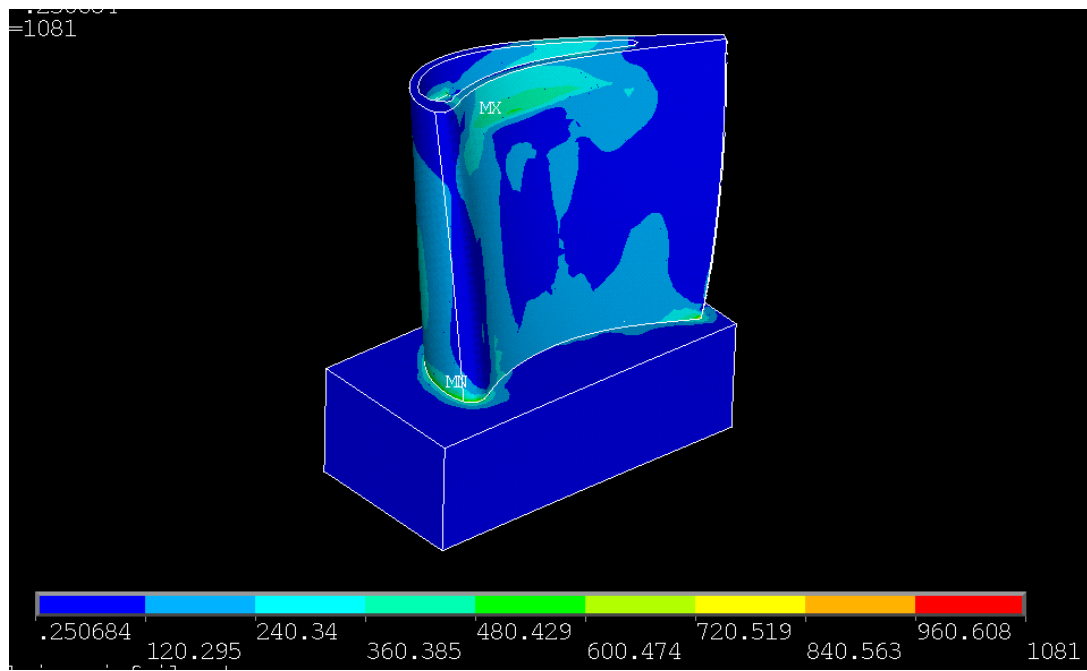


Figure 4-9: Structural Results – Rev 12

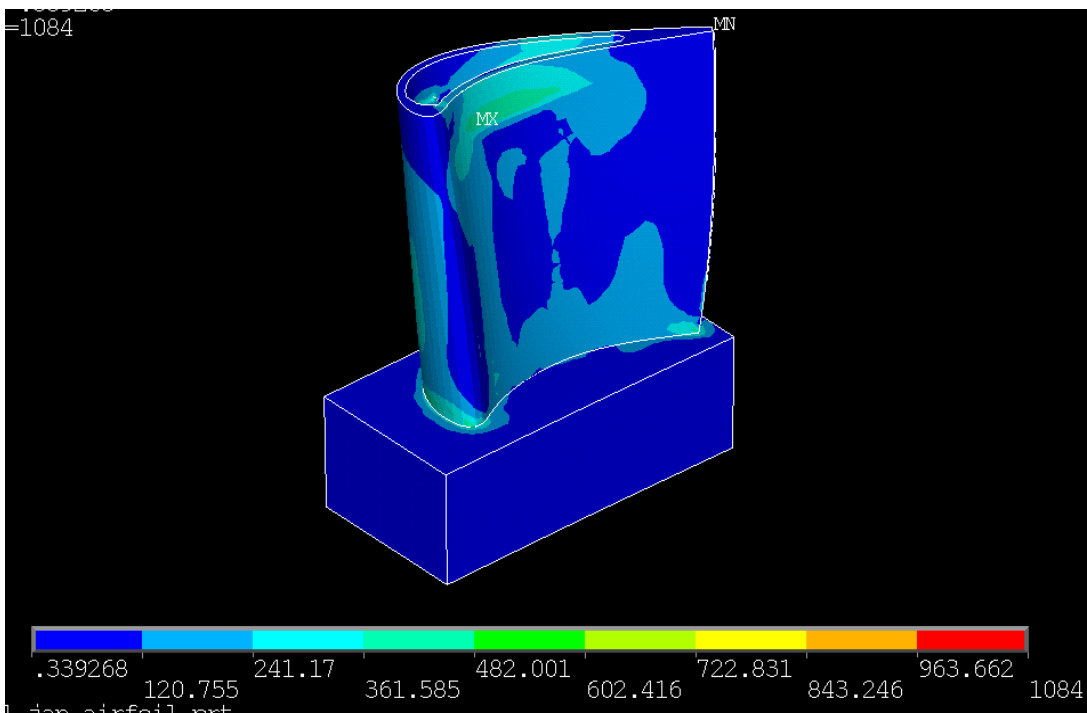


Figure 4-10: Structural Results – Rev 13

This proved to be a problem either way, in that the model for rev 13 took nearly two hours to complete a full thermal/structural run, which was unacceptable for an optimization task. Two options presented themselves in order to reduce the solve time, either reduce the mesh quality or only analyze a portion of the model. In order to preserve the mesh quality and as such the accuracy of any generated results it was decided to only analyze the aft serpentine of the blade at this time using adiabatic boundaries at any cuts. The model was further cut to remove some sections of the blade that were not being used for the analysis, such as the squealer tip, as well as a good portion of the trailing edge and root. The result is a model with good mesh quality containing 339372 nodes and 210614 elements which solves in approximately 45 minutes using a single CPU. The final model (rev 15) is shown in figure 4-12. The cuts made to the model are graphically shown in the figure shown here.

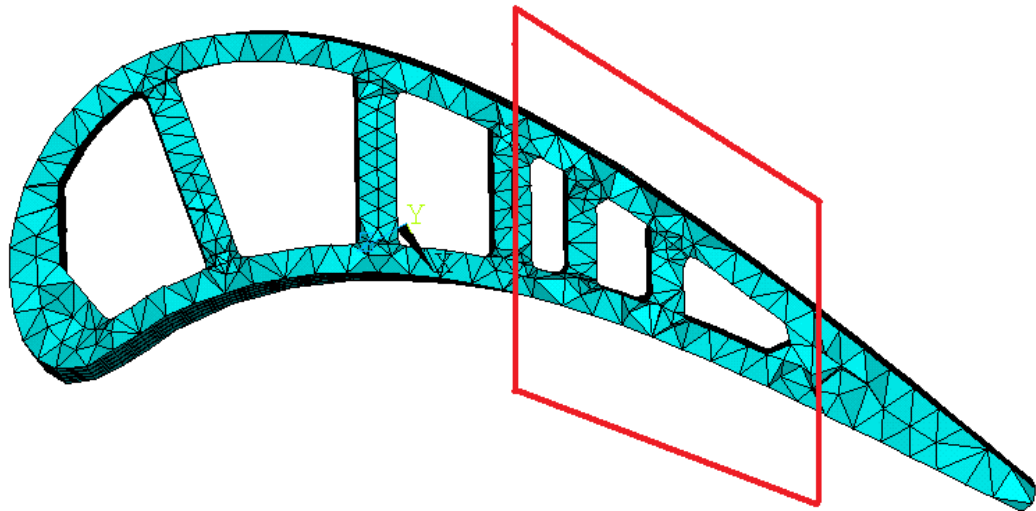


Figure 4-11: Cut Planes

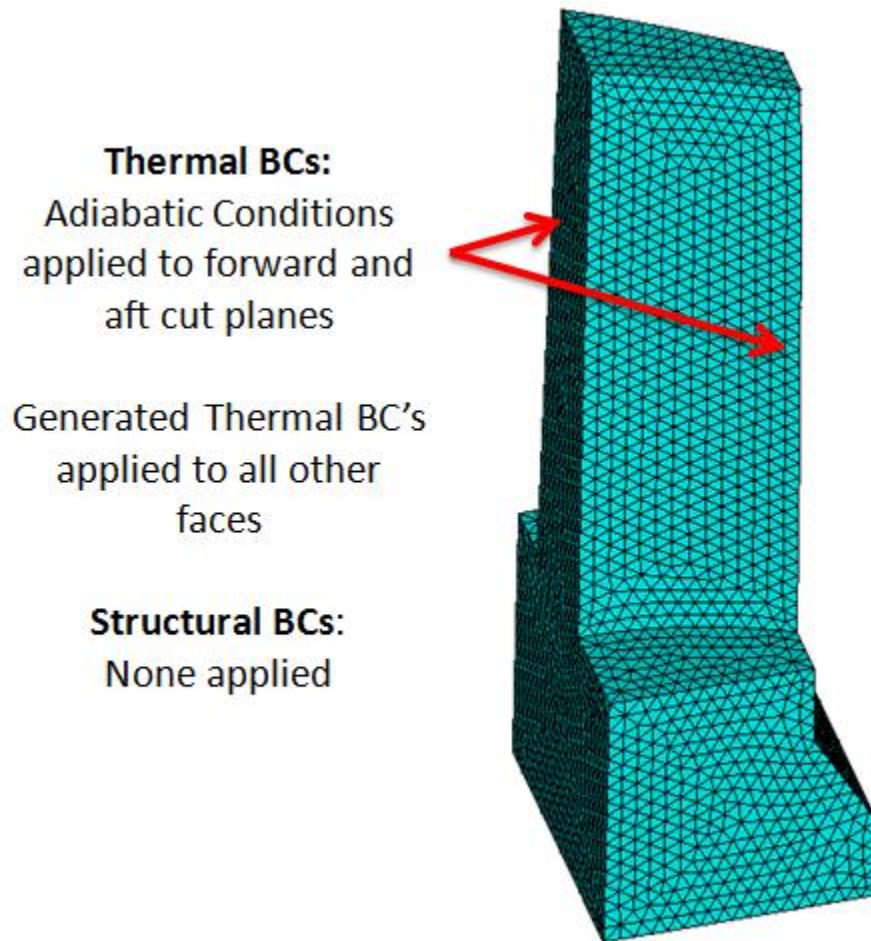


Figure 4-12: Final FEA Model – Rev 15

It is important to note that by using only a portion of the model, and only thermally constraining the cut faces it is possible for the model to expand more easily than it could in the presence of the rest of the model. This will lower any stresses experienced by the part due to thermal growth which will lead to inflated life predications. Although this is not an ideal case, it has been deemed acceptable for the current study since it is simply not feasible to run the entire model due to limited computational power.

4.3 Internal Flow Network

In order to generate baseline internal heat transfer coefficients a simple flow network was created. This was done using a Siemens Energy Inc. proprietary one dimensional flow solver, meaning that no details on the actual flow solver can be provided with the exception that it is based on generic compressible/incompressible flow equations found in virtually any heat transfer and fluid dynamics text book. However, the process that was used will be provided, and can be freely recreated using public domain flow solvers. Channels were created with a flow area equal to the cross sectional areas of the six cooling passages, with dummy channels added in to mimic any form of ejection holes, such as the pressure side, leading edge, trailing edge, or the tip. Supply temperatures and pressures were then applied to the flow network. Since no other pressure values were provided, an iterative process was used to alter the sink pressures for any ejection point, until the flow rates matches relatively close to those provided in the reports. Finally the flow solver was run and heat transfer coefficients extracted in tabular form. All of the generated values are provided in table 4-1, which were manually mapped to the ANSYS model and used as the baseline condition.

Table 4-1: Baseline Internal HTC's (mW/mm²-°C)

	Passges					
	1	2	3	4	5	6
Location (Hub)			1.5			1.5
			1.7			1.7
	2.1775	3.7965	1.9	3.2135	3.5295	1.9
	2.201	3.733	3.3245	3.1565	3.549	3.3245
	2.226	3.671	3.3385	3.1015	3.567	3.442
	2.251	3.6095	3.353	3.051	3.581	3.5685
	2.2765	3.548	3.368	2.999	3.593	3.7085
	2.303	3.4865	3.3835	2.949	3.6025	3.8585
	2.3295	3.423	3.3985	2.9025	3.608	4.0165
	2.3575	3.3565	3.413	2.855	3.6075	4.186
	2.3865	3.2805	3.4275	2.809	3.5965	4.372
	2.416	3.1715	3.43	2.767	3.54	4.5675

Note that passages three and six contain two more values than all of the other channels, this is due to the fact that these are the feed channels, meaning that they are extended all the way through the root whereas the others are not.

4.4 Material Model

According to the NASA report by Halila (1982) the component is made from cast René 150. However, the Siemens Energy Inc. materials library did not include this alloy, and since manually entering material information into ANSYS is not only tedious, but also an easy source of error, it was decided to find a material in the library which was close to René 150 in either physical properties, chemical composition, or both. The alloy

that was found which matched closely in both thermal and mechanical properties is considered a Siemens Energy Inc. proprietary material and as such details can not be provided. Properties of cast René 150 are not provided here but are readily available online.

CHAPTER V METHODOLOGY

The following sections will provide an in-depth look into the methodologies that were used in order to achieve solutions. Attention will more heavily be focused on the generation of the probabilistic design codes which provided the driver for the whole analysis, namely the prescribed variation of the internal HTC's, as well as on some more advanced ANSYS methods which allowed for all of the analysis to be completed in a single automated loop without any iterating. Finally a brief overview of the employed LCF lifing techniques will be provided.

5.1 Probabilistic Design

As has been mentioned previously, this project was designed as an interdisciplinary project combining conventional heat transfer work with a probabilistic design aspect. Even though all analysis runs were driven by Isight, the “brains” of the probabilistic process were generated using a Matlab code. As such not much detail is spent on discussing the final Isight model, or on how to regenerate it, with the exception of showing an image of the loop which is shown on the following page. Note that in order to reduce the number of Isight license used (since there were only a very

limited few to use) it was decided to use parallel computing. This allowed for four iterations of an analysis to be conducted in a single iteration of the Isight loop, and between 200 – 600 runs to be completed for each set of input parameters. The remainder of the section however, will focus on the details of the probabilistic design code, such as its creation, a discussion of errors that were found, as well as an overview of required verification processes which showed that the probabilistic code still generated the outputs that it should have been producing.

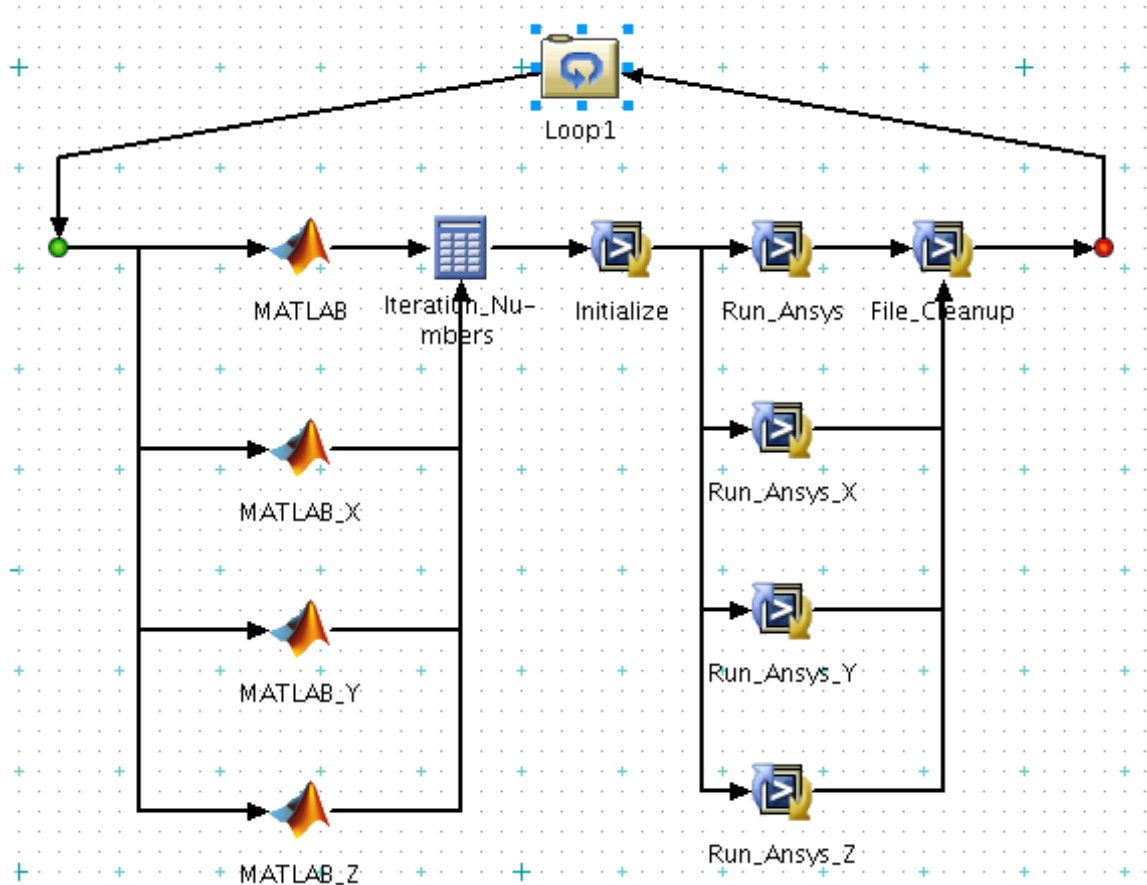


Figure 5-1: Isight Model

5.1.1 Approach

The Matlab code that was created in order to generate the random variables needed for the analysis effort is provided in its entirety in appendix B. It is assumed that the reader is somewhat familiar with Matlab, and as such it is not described exactly how each command was executed to generate the code. In addition to any descriptions provided here the code itself is well commented, facilitating an easy understanding of what is being done. The code is broken down into three main sections, the first being the actual random number generation, the second being the transformation of the generated values into correlated variation data, which is finally written into an input file readable by ANSYS.

Generation of random numbers was done using a built in function within Matlab, the “normrnd” function, which generates random Gaussian normally distributed data with mean μ and standard deviation σ . Before any real values were assigned the random number generator was tested, and shown to indeed produce what was expected. However, when Isight was used to create a number of sample input files, they were all identical. This is due to the fact that random number generators within Matlab default to using the same seed of numbers, so that even though any numbers that are output are in fact random and normally distributed, if the code is closed and reopened (which is done in every iteration of Isight) the seed is not reset, meaning that it starts

over and the same numbers are generated. This was solved by simply inserting a command that reseeded the random number generator every time.

At this point the correlation function discussed previously was inserted into the code, in addition with the inputs required to generate the conditions for the first analysis case. Note that two values of variation are provided, since as was discovered in the literature search, any turn region is also a region of much higher uncertainty. Thus, in order to model this increased uncertainty, the generated values for variations in the turns (points 9-12 for the tip and points 19-22 for the hub) were simply doubled. This is not the most optimum way to produce this shift in variation, however after repeated discussions it was decided to be sufficient for this phase of the project. As was mentioned in the beginning of this section, two errors were made while generating the Matlab code (it was later found out that one caused the other), the first of which was introduced with the selection of the input parameters. Neither of these errors were noticed until all analysis had been completed, however through validation steps undertaken “post mortem” it was shown that the impact was negligible, and as such the experiment did not need to be rerun. However, while the inputs were being provided for the random number generator, the standard deviation was set to match the maximum prescribed variation. This has a significant impact, in that instead of having 95% of all generated values fall within the prescribed variation band only 65% of values fell into the range.

It was noticed that after applying and plotting the autocorrelation function that a good number of points fell outside of the range. However, this was not immediately attributed to an error, but instead was taken as a byproduct of the correlation function. To prevent this a type of truncation function was implemented which checked each correlated random number that was generated, and if it fell outside the prescribed range would require the code to regenerate all thirty values, until they all fell within the range. This was later identified as the second error, in that instead of inputting truly random Gaussian normal distributed data into ANSYS, it was instead provided with truncated random Gaussian normal distributed data, which once again was verified and shown to have a negligible effect.

Finally all thirty generated points were written into a single input file which was used by ANSYS to modify the baseline heat transfer coefficients.

5.1.2 Validation - Distribution

In order to verify that even though the above mentioned mistakes were made, all generated data is without a doubt useable, two things needed to be shown. Firstly, it had to be verified that if provided with the correct inputs that the Matlab code produced the correct outputs, and finally that for all generated variation values, at every

point of every set of input parameters, the applied distribution is normally distributed, with a mean of one and a standard deviation of very close to the desired output. Due to the truncation that was performed it is impossible to generate a distribution that, using the ASCII standard 95% confidence interval, will produce a standard deviation of exactly the value that was provided as an input. Instead a value of slightly less than that is expected. If both of these conditions are met, then it can be confidently stated that although errors were made, their effect is minimal.

Showing that if the correct values are used in the random number generator the correct output is produced is relatively straight forward. After disabling the truncation function, a set of 999 input files was created and statistically analyzed for different input parameters. In all cases it was shown that the outputs were normally distributed, and showed means and standard deviations equal to those provided initially to the code. It was not possible to present the information for all cases, however three sample points are shown on the following pages. These files were generated from data points that were created using standard deviation of 0.1, a mean of 1, and a tau value of 50. Points one and fifteen are taken from within the straight passages, meaning that they should reproduce both the mean of 1 and the standard deviation of 0.1. Point nine however falls into a tip turn region, and as such the generated data should show a mean of very close to 0.2. The generated data matched the inputs not only in the three sample points shown here, but in all of the test cases that were generated. As such it can be said that the first part of the distribution validation has been successfully completed.

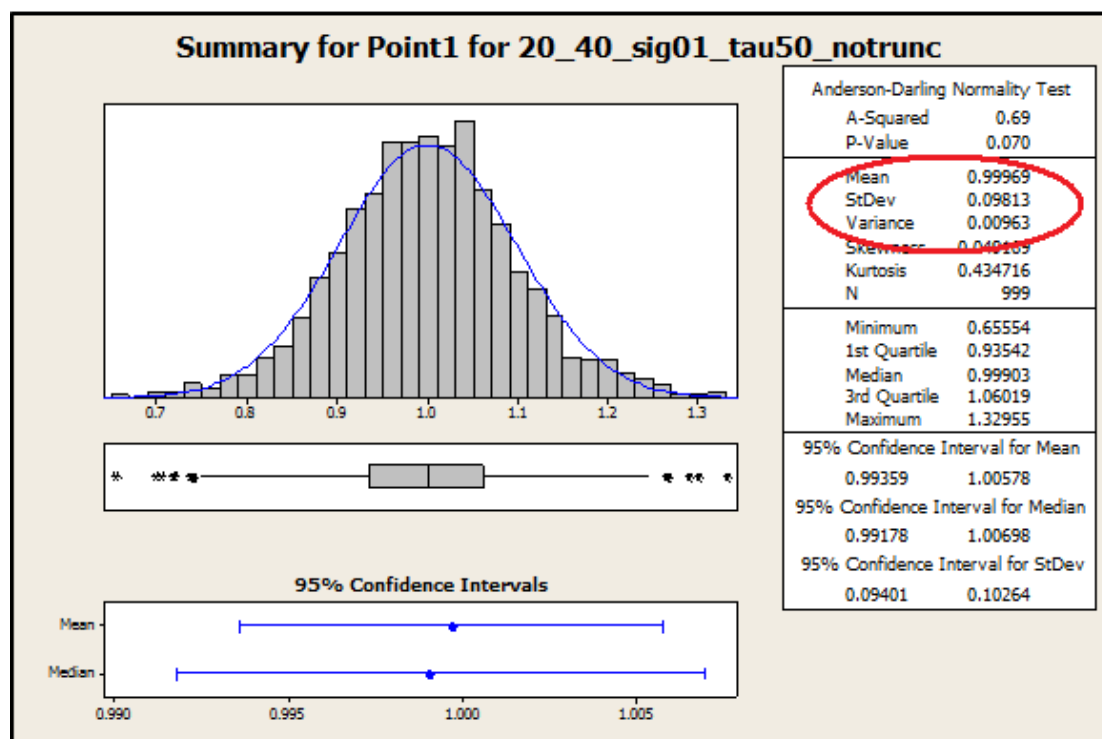
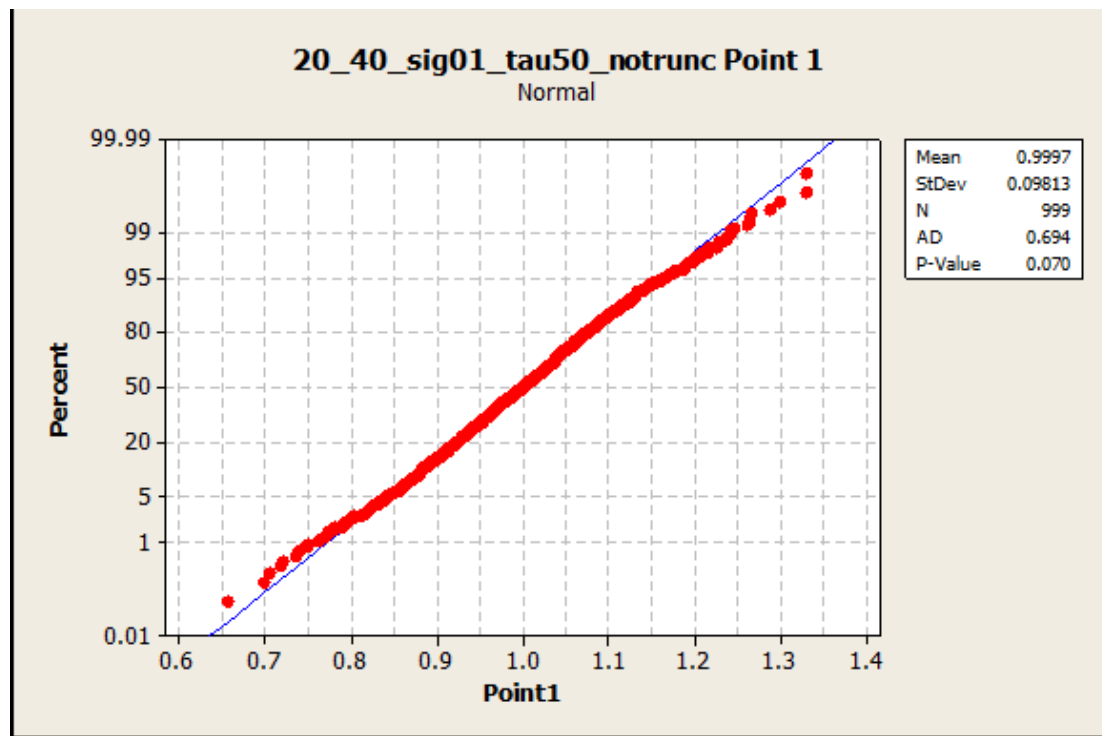


Figure 5-2: Validation for Test Case Point 1

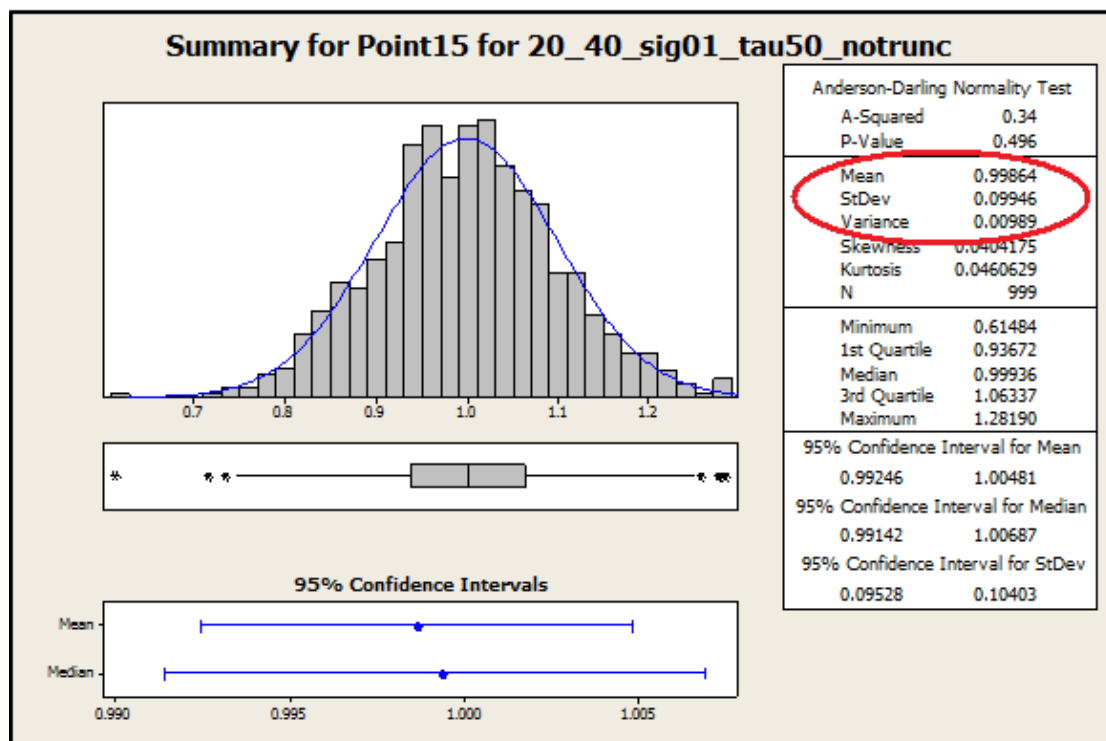
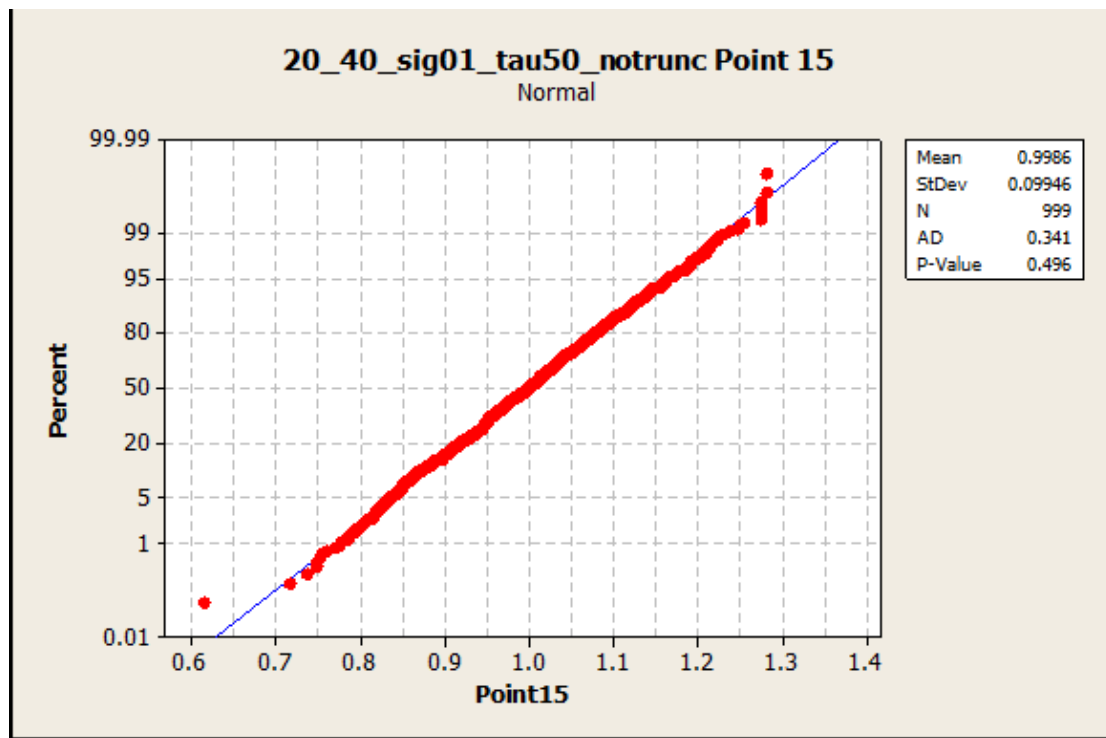


Figure 5-3: Validation for Test Case Point 15

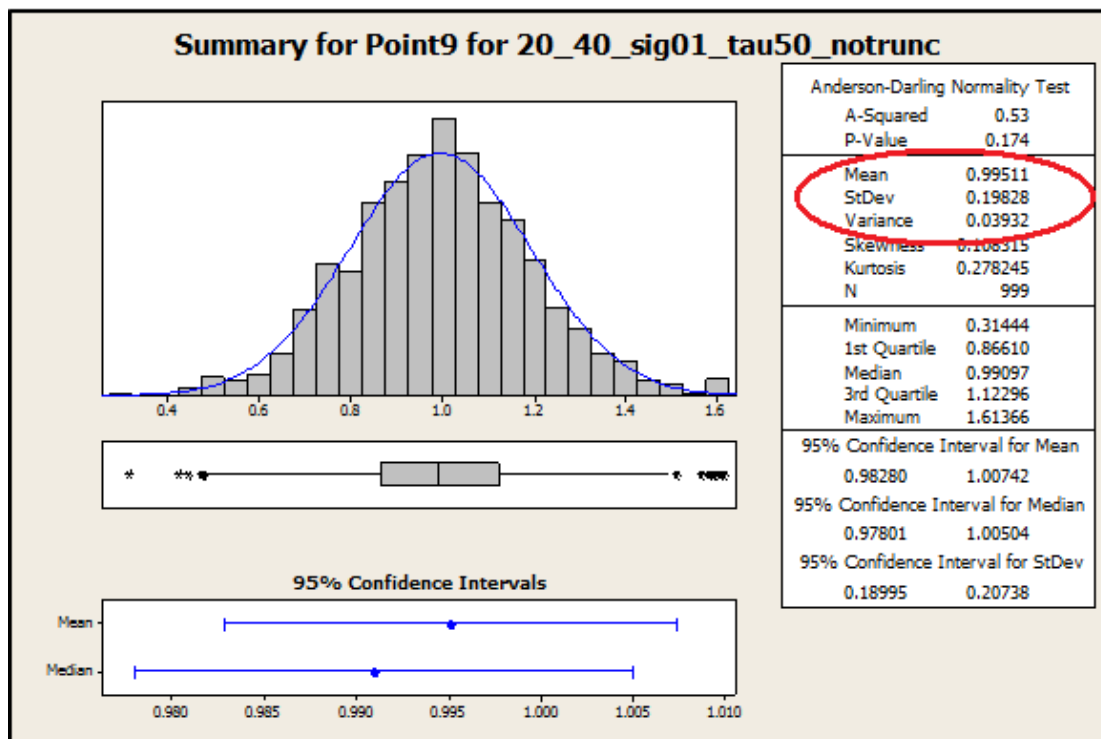
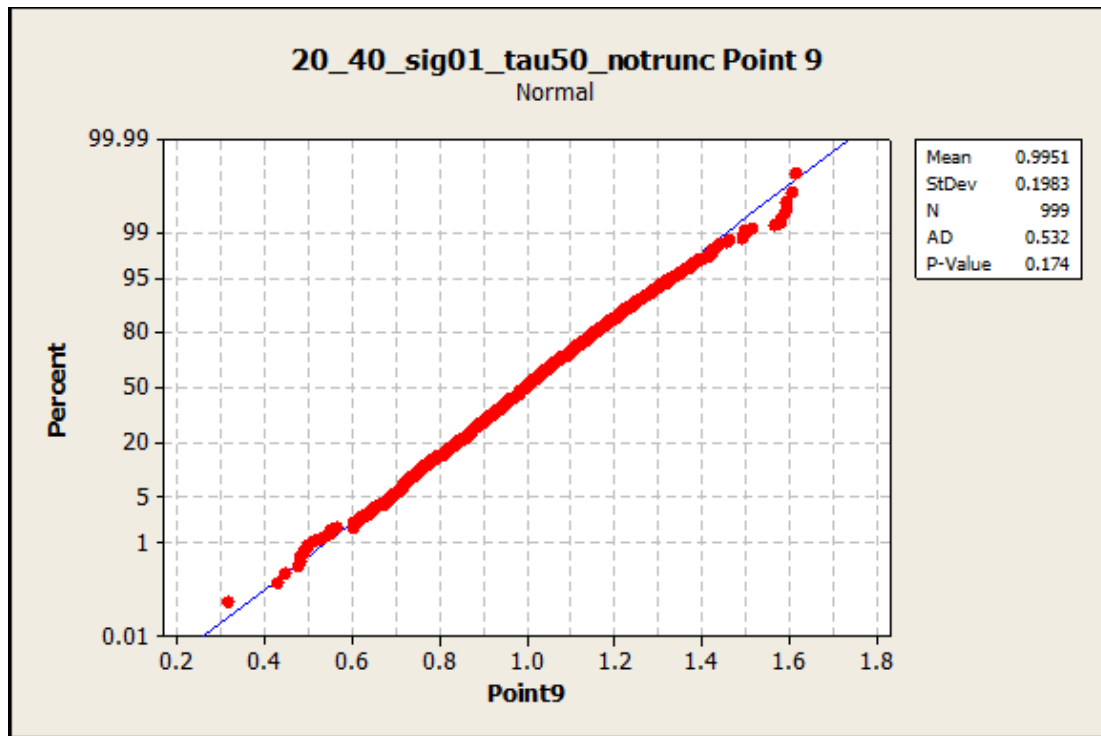


Figure 5-4: Validation for Test Case Point 9

In order to provide the required proof that for all of the previously generated data, which used both incorrect values for sigma, as well as truncation the same process had to be implemented for every generated set of data points. The results should again show a mean of one, and in this case a sigma value of less than half of the input sigma. Even though the analysis was performed for all data points, it is not feasible to show every generated plot here, as this would require a separate document of equal or greater length than this one. Appendix C however provides the statistical result plots for all thirty points that were generated using a sigma of 0.2, tau of 50, and truncation. Two of these plots are provided here as well to demonstrate that the expected values were in fact generated.

Since both required checks have been performed, and acceptable results have been provided, it can be confidently said that the impact on the overall analysis is minimal. For future work however, the correct values and procedures will be implemented. It is important to note however, that all prescribed uncertainty bands are not provided at the ASCI standard confidence interval of 95%. Instead, they are provided as they were before for the remainder of this experiment (for example 10/20%). However, since all values fall within the prescribed band these values are provided at a 100% confidence interval.

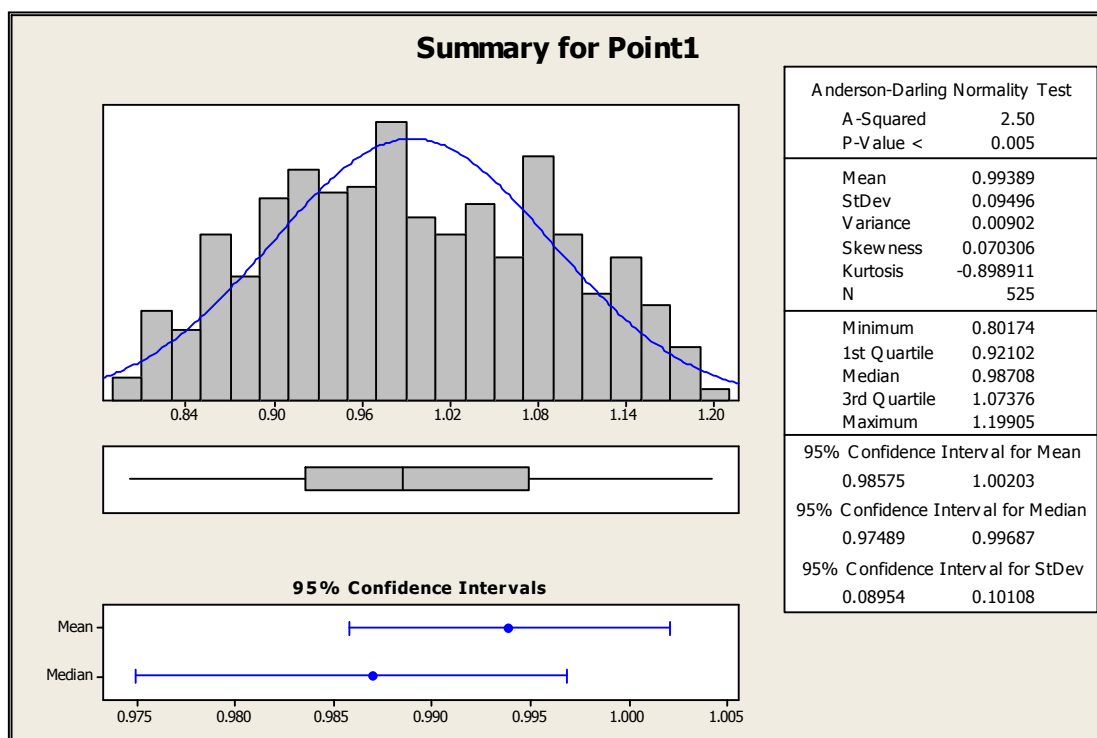
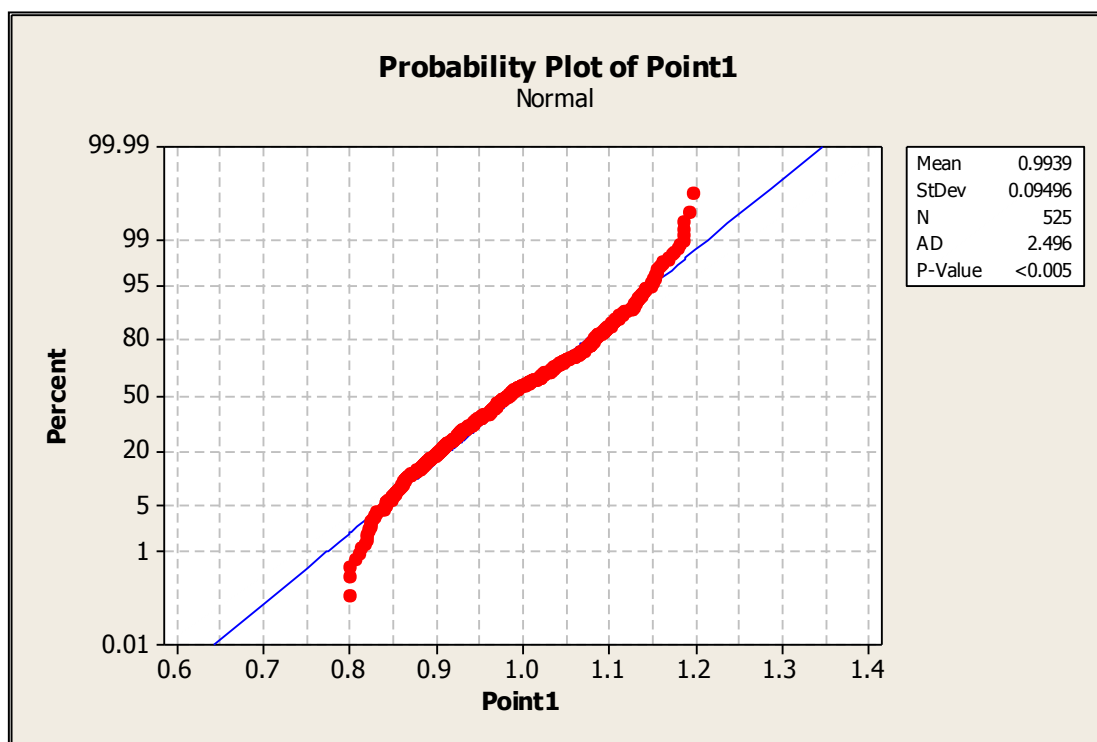


Figure 5-5: Validation for Actual Case Point 1

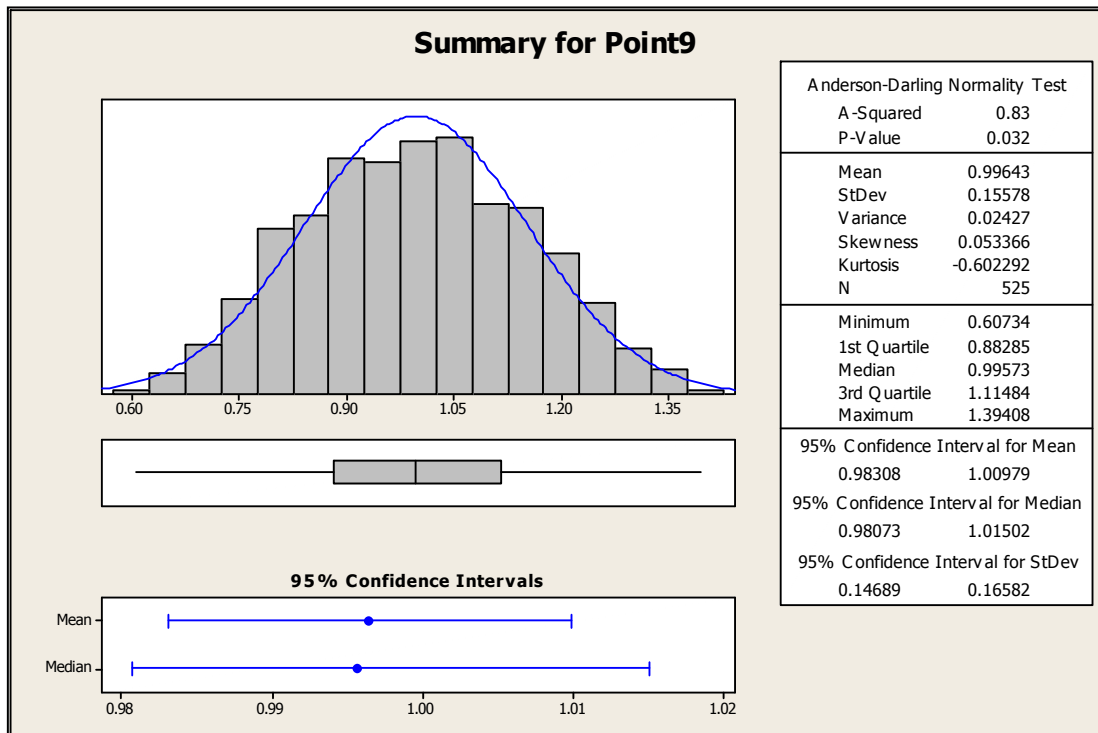
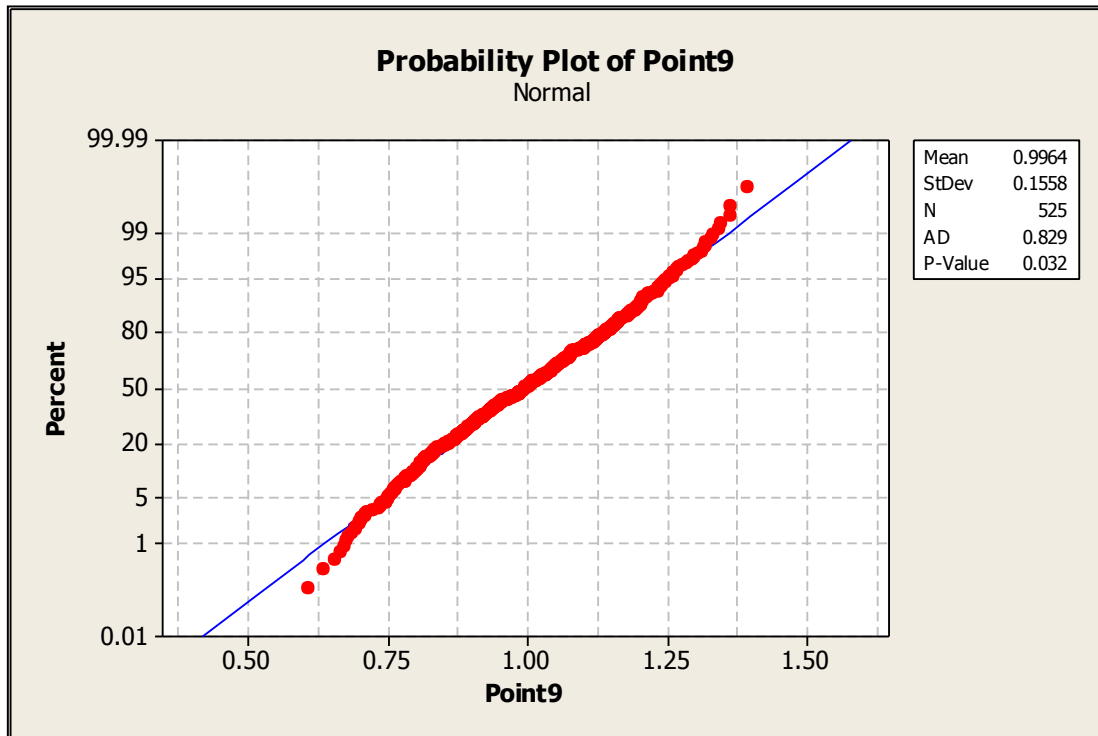


Figure 5-6: Validation for Actual Case Point 9

5.1.3 Validation - Correlation Coefficient

In order to consider the generated results to be fully validated, it was decided to double check that the correlation coefficient that was provided to the correlation function was reflected in the generated random numbers. Since all of the generated data was already tabulated for previous validations, this step was completed by solving the two equations provided by Deserno (2002) for values of $n = 0, 1, 2, 3, \dots, 7$. This will provide the correlation coefficients for all points in the first upward passage, using point one as the origin. The first equation will produce the input correlation coefficient, which should match that of the output (calculated by the second equation) for all values of n .

$$c(n; m) \equiv c(n) = f^n = e^{-n/\tau}.$$
$$c(n; m) := \frac{\langle r_m r_{m+n} \rangle - \langle r_m \rangle \langle r_{m+n} \rangle}{\langle (r_m - \langle r_m \rangle)^2 \rangle^{1/2} \langle (r_{m+n} - \langle r_{m+n} \rangle)^2 \rangle^{1/2}}.$$

Figure 5-7: Correlation Coefficient Equations (Deserno, 2002)

Once all of the values were calculated they were compared to each other by calculating the percent error, which was less than 3% for all cases, which is shown in the table on the following page. This being the case it can be concluded that the correlation coefficient for the input indeed matches the output, hence completely validating the code.

Table 5-1: Correlation Coefficient Verification

Correlation Coefficient Verification			
	Input	Output	% Error
c(1;1)	1	1	0.00%
c(2;1)	0.974595	0.980199	0.58%
c(3;1)	0.95107	0.960789	1.02%
c(4;1)	0.93095	0.941765	1.16%
c(5;1)	0.915447	0.923116	0.84%
c(6;1)	0.880585	0.904837	2.75%
c(7;1)	0.863486	0.88692	2.71%

A τ value of 50 was chosen to model the correlation for this experiment, after calculation confirmed that this value corresponds to a correlation length of 50% of the straight passages. In order to calculate the correlation length, the correlation coefficients calculated for the generated data were plotted for values of $n = 0, 1, 2, \dots, 7$, which corresponds to an entire passage in the blade, with the two tip sections removed as they are not correlated to the rest of the passage. A curve was fitted to the generated data points and integrated in order to calculate the area under the curve (in this case the area was 5.14). A square of unit height and equal area is then graphed on the curve, and the intersection point between the line and the square is taken as the correlation length, in this case it corresponds to $n = 5.14$ or roughly 5, or 50% of the blade height. This is shown graphically in the following image.

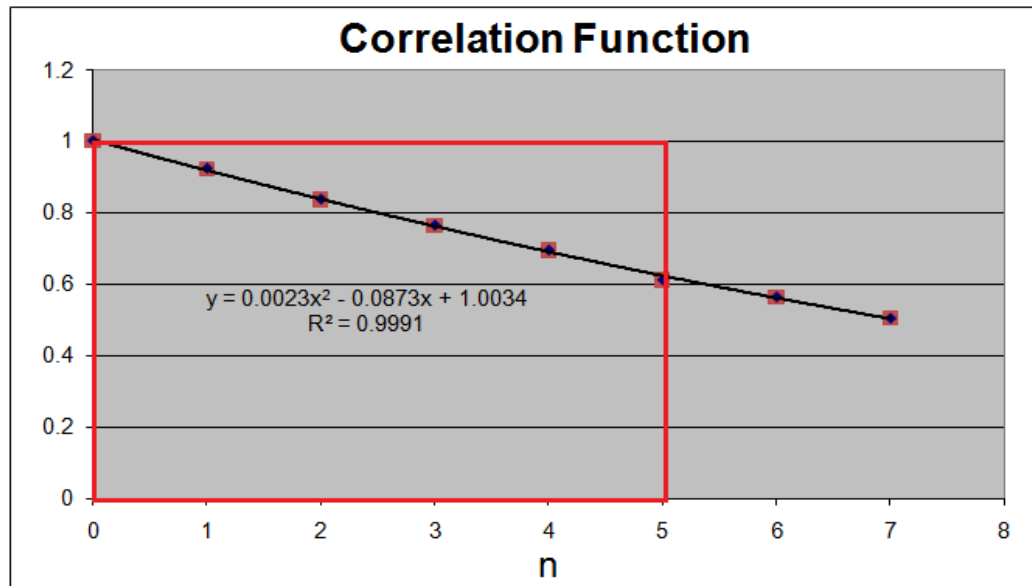


Figure 5-8: Correlation Length

Most of the experiments were conducted using a τ value of 50 as one of the input parameters, however one was also run with a τ value of zero, in order to get a basic understanding of the effect that this input parameter has on the overall variation. It is important to note that in reality τ should not be related to the blade height, but rather to geometric conditions of the channel, such as channel width, height, or the presence and size of any internal features. Finding out exactly how the value of τ should be determined and what factors make up the equation should be looked at and defined in detail, but is not the focus of the current study. This will be further mentioned and addressed in the future works section provided later.

5.2 Finite Element Analysis

Since the entire analysis effort revolves around a large number of runs with simulated variation of internal HTC's, it is essential that everything done within ANSYS is not only automated but also does not require any iterating, in order to reduce the run time as much as possible. The automation itself was done through the use of various macros. Since varying HTC's throughout the entire passage also leads to a change in coolant temperature, which can have a significant impact on upstream cooling effectiveness, it is important to capture this effect. Usually this would be done outside of ANSYS through the help of either one dimensional flow solvers, or three dimensional computational fluid dynamics approaches. However in this case fluid temperature heat-up is accounted for using an advection network within ANSYS itself.

5.2.1 Advection Network

Instead of depending on external software packages to calculate internal conditions such as fluid temperature it was decided to use an internal advection network. The major benefit is that any kind of third party program requires iterations to be done between ANSYS and the program in order to correctly match the conditions within the passage to that of the fluid, which adds run time. Normally this would not be

too large of a concern, but since this work uses a probabilistic approach, an incredibly large number of runs are performed, meaning that even a little bit of time added per run ends up as a huge drain on computational resources.

Using the previously generated Pro-E CAD models of the airfoil and core, lines were drawn that follow the centerline of all of the coolant passages. Additionally lines were added at any locations where any kind of flow extraction is being done, be it for film cooling, trailing edge ejection, leading edge impingement, or even tip cooling. The resultant network of lines can be seen in the following image.

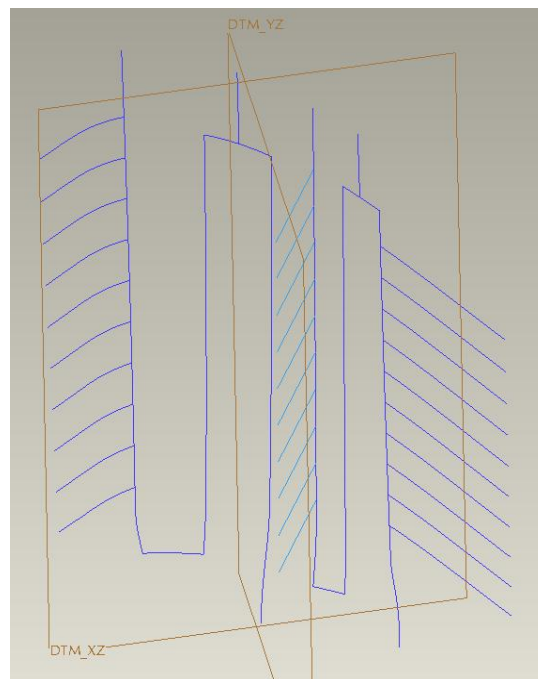


Figure 5-9: CAD Generated line network

This file was then imported into ANSYS, and since it was drawn within the original airfoil and core on the same coordinate system within Pro-E, it is now automatically placed inside of the coolant passage in the FEA model. Using Fluid116 elements the newly

imported features is line meshed. Through the element size it is possible to control at how many different locations the fluid temperatures are re-evaluated, and also how much of the passage is “attributed” to each node. For example part (a) of the following figure only contains a two element, or three node fluid network, this means that the half of the heat of the passage is transferred to the fluid at node 2, and the other half at node 3 (node 1 is used to initiate the fluid temperature and is therefore not included). In contrast (b) shows the same channel and fluid network however in this case four elements are used, which doubles the number of nodes that can be connected to the channel, meaning that each node only picks up an amount of heat equivalent to 25% of the channel.

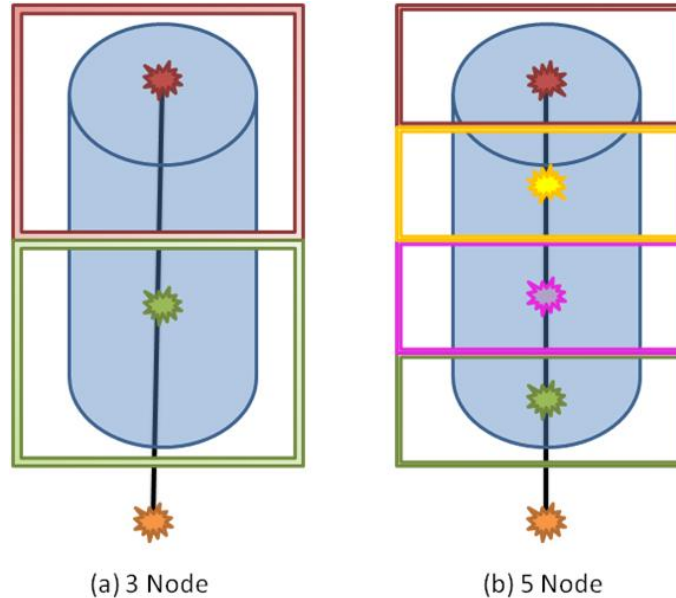


Figure 5-10: Channel Distributions at Various Node Numbers

This allows for more resolution when tracking the fluid temperature, as well as provides more accurate upstream heat transfer conditions. In the case of this thesis, each vertical

channel was split up roughly ten times (more for the first pass, since it is a longer section due to the root), which allowed for very reasonable fluid temperature modeling.

In order for the meshed fluid network to be able to communicate with the solid model and transfer heat out of the component the nodes of the fluid network need to be directly linked to the surface nodes of the internal channels. This was done by creating a separate surface element type, which is still a SURF152 element. This element type has the extra node key option enabled. Much like the name implies, it literally forces the surface elements to take on an additional node. The extra node in this case comes from the fluid network which links the two. The following command within ANSYS selects a certain radial height worth of surface elements and maps the corresponding fluid node in that area to them:

```
ESEL, S, TYPE,,152  
ESEL, R, LOC, Y, min location, max location  
EMODIF, ALL, -9, line-element-number
```

This procedure was repeated until all of the surface elements of the internal channels are mapped to the closest fluid node. The following image is a sample cut from the model showing how the connections between a fluid node and the solid model look using the extra node option.

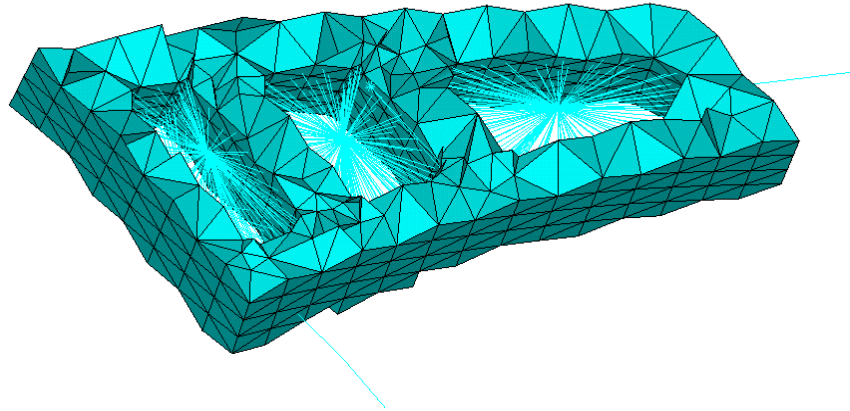


Figure 5-11: Fluid/Solid Model Interaction

Once the entire fluid network is linked to the solid model an initial temperature needs to be provided to the first node in the network, and flow rates must be applied to all of the elements. The inlet temperature was taken directly from the NASA reports and was set to 577 degree Celsius. Flow rates had to first be converted from %G1C which is provided in the reports to actual kg/s values. These values are shown in the following chart, and were generated by taking the given percentage of total compressor flow for the entire turbine stage and dividing by the blade count.

Table 5-2: Provided Flow Rates in kg/s

%G1C	Flow (kg/s)
3.3	0.02150
AFT	
1.67	0.01088
FWD	
1.63	0.01062

Ejected Flow (kg/s)		
	Total	Per Blade
PS	0.00241	0.00024
Tip-TE	0.00195	0.00098
LE	0.00919	0.00092
Tip-LE	0.00143	0.00072

Finally, since the fluid is air, all appropriate properties, such as specific heat, were entered into ANSYS. Even though the analysis performed does not include any effects of film cooling, or trailing edge ejection it is still important to model those channels as part of the advection network. By doing so, it is possible to directly take into account any flow being debited from the main coolant passage and being used for other purposes. However, since none of these elements are linked to the solid model in any way, they will not perform any heat transfer function.

It is important to note, that even though the advection network will continually update the coolant temperature according to the amount of heat removed downstream, it cannot alter the heat transfer coefficients in any way, as these are directly applied to the solid model. However, this was not deemed to be a major concern, due to the fact that any changes in HTC's resulting in fluid temperature, or velocity changes are minimal compared to the effect that the fluid temperature directly has on the heat flux. But as was mentioned before, accounting for these minor changes would require the use of an iterative process which although it would produce more accurate results, is not feasible in the current application. In its current state, although the initial setup of the advection network was rather time consuming, nothing needs to be changed per iteration, making automation of the process that much easier.

5.2.2 Automation

As was mentioned previously, automating ANSYS simply required the writing of a couple of macros. The first, a Unix ANSYS launch command embedded in a C-shell allows Isight to launch ANSYS. In this case ANSYS was run locally on individual work stations, with the allocation of two processors per job, and four jobs run in parallel. By using two processors per run, the solve time is reduced by approximately $1/3$, without the use of an additional ANSYS licenses. While launching ANSYS in batch mode, a driver macro is also required as an input, this provides a list of commands to be executed. The macro is provided in appendix D. Note that only the ANSYS commands shown, even though the macro was also used to call out and interface with the lifing software. Since this is Siemens Energy Inc. proprietary information the details and scripting cannot be provided.

The macro itself is not too complicated, since the model was well setup initially and very little modification is required per run. First the working directory is set to the current directory that the particular job was launched from. This allows jobs to be run in parallel without accidentally overwriting each other. Following this, the thermal model data base is resumed while the generated input file is read into ANSYS and stored as thirty different variables. Next, all of the internal HTC's tables are edited using tabular equation editing as well as the variables from the input file. Upon completion, the thermal model is solved. Finally the database file for the structural model is resumed;

the thermal results are read in, which applies all body temperatures generated in the thermal solution to the structural model. The final step is to solve the structural model, and select the nodes and elements to be used for lifing purposes. In this case three cuts were used located at the following radial heights: 333.82 mm to 335.88 mm, 343.09 mm to 345.15 mm, and 353.3 mm to 355.3 mm.

5.3 Low Cycle Fatigue Life Calculation

As was mentioned previously the software used to perform all of the low cycle fatigue lifing for this project was developed by Siemens Energy Inc. and is proprietary information. This being the case no details can be provided, with the exception that the software is based upon the equations from “Mechanical Behavior of Materials” by Norman E. Dowling, which have been shown and discussed in section 2.2.

However, even though the specifics of the code cannot be delved into, an overview of the generalized process is shown in the diagram below. After the cuts at the three desired sections are made von Mises stress and temperature data is exported into the lifing system along with all of the previously mentioned material data. Temperature data is needed for all nodes, as all of the material data being imported into the lifing software is heavily temperature dependant.

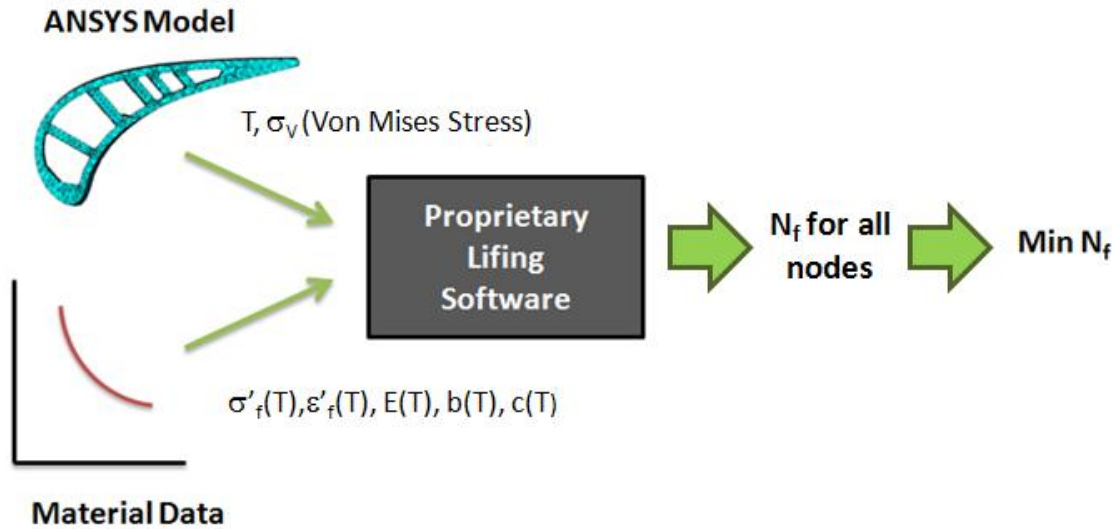


Figure 5-12: Generalized Lifting Procedure

Using the above mentioned equations this data is transformed into LCF life data per node, and the lowest value is selected by ANSYS and output in a text file. Since the input value is a stress and lifting calculations are done with regards to strain, it is necessary to transform the stress data into strain values using material specific elastic-plastic curves and Hooke's Law.

Once all the runs were completed, every data point from run 3 was collected, the low life node located and plotted on the following figure. This shows that for every iteration that was run, the low life node did not change, but instead is located at the point farthest away from the coolant channel.

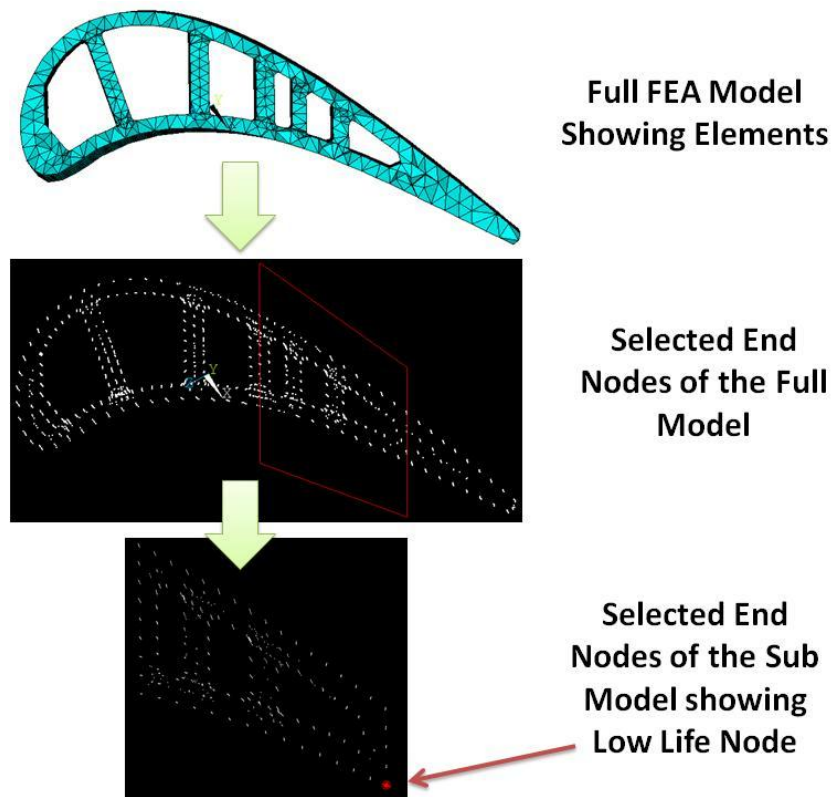


Figure 5-13: Low Life Node Location

In addition to plotting the low life node, all stress, temperature, and life values were extracted for run three and plotted as scatter plots in order to provide a graphical representation of the data. All of the data points were taken for the low life node at mid-span shown above. It should be immediately obvious that the changes in stress and temperature are relatively low, ten and one percent respectively, however this leads to very large changes in LCF life. As one would expect it is not possible to pinpoint which of the two inputs, temperature or stress, are the prime driver for life, as both values required for the life calculations.

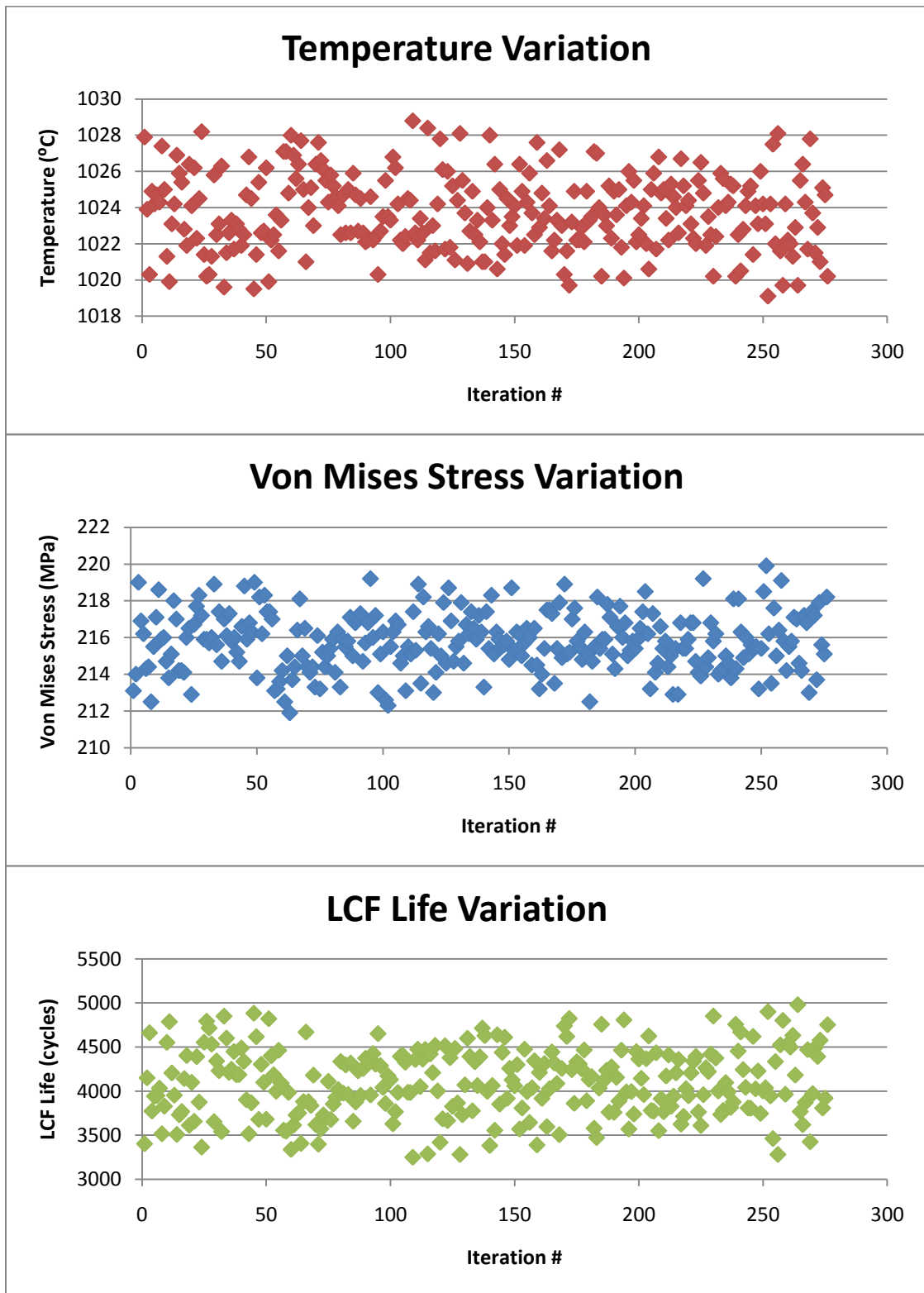


Figure 5-14: Temperature, Stress, and Life Variations

CHAPTER VI RESULTS

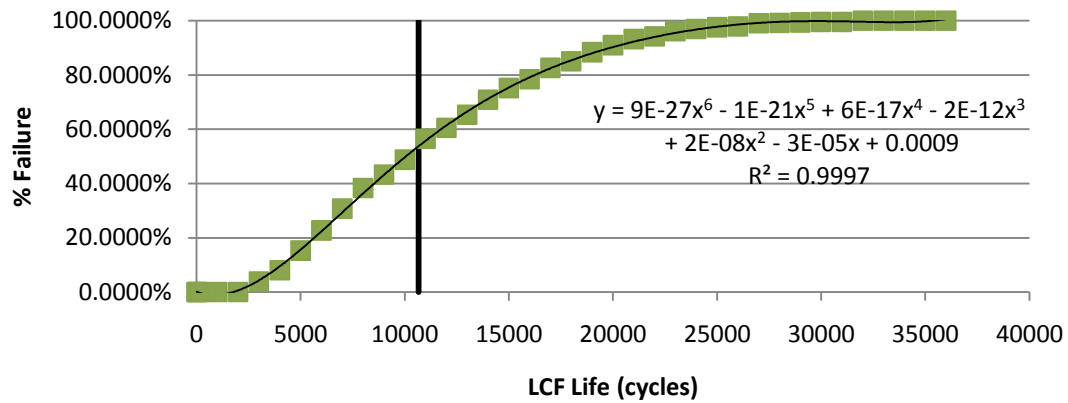
Throughout the analysis process thousands of output files were created and automatically placed in a predetermined folder structure. These values were then combined into different excel files based on their run number. Each run number was generated using different input parameters, which are provided in the table below.

Table 6-1: Input parameter and Run #'s

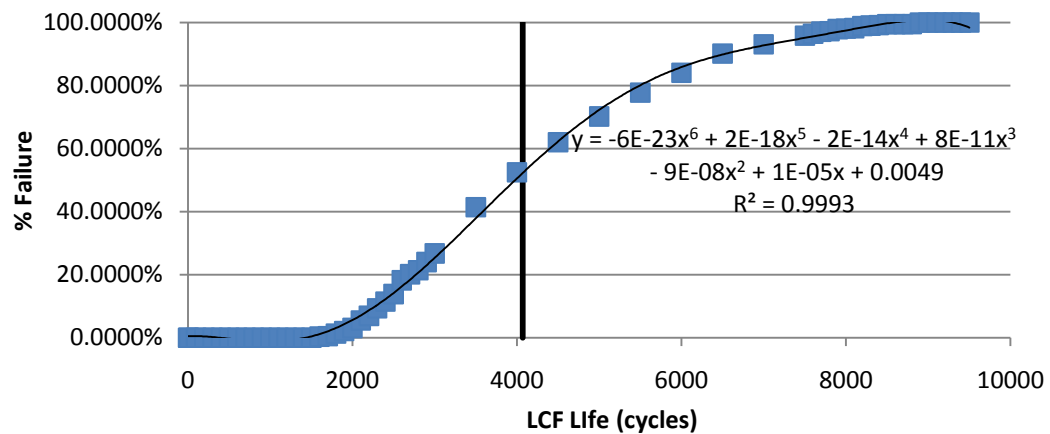
	Run 1	Run 2	Run 3	Run 4	Run 5
Variation Range	20/40%	10/20%	5/10%	20/40%	20/40%
Tau	50	50	50	0	50
Sigma	0.2	0.2	0.2	0.1	0.2
Truncation	yes	yes	yes	no	yes
Temperature	base	base	base	base	-100

Since the raw, or even tabulated data does not provide much information, only a graphical representation of all results is provided, by means of a probability plot. It was mentioned previously that for each analysis iteration that was performed, three different life values were calculated, one towards the tip of the blade, one near the hub and one at midspan. As such there are three plots generated, and provided for every run. The black bars in the graphs indicate the deterministic value that would be provided as a life value had a probabilistic approach not been taken. Note that the purpose of this section is to merely provide the results, a discussion thereof will be provided in the next chapter, followed by a few concluding remarks.

Run 1 Tip LCF Non Rotating



Run 1 Mid-Span LCF Non Rotating



Run 1 Hub LCF Non Rotating

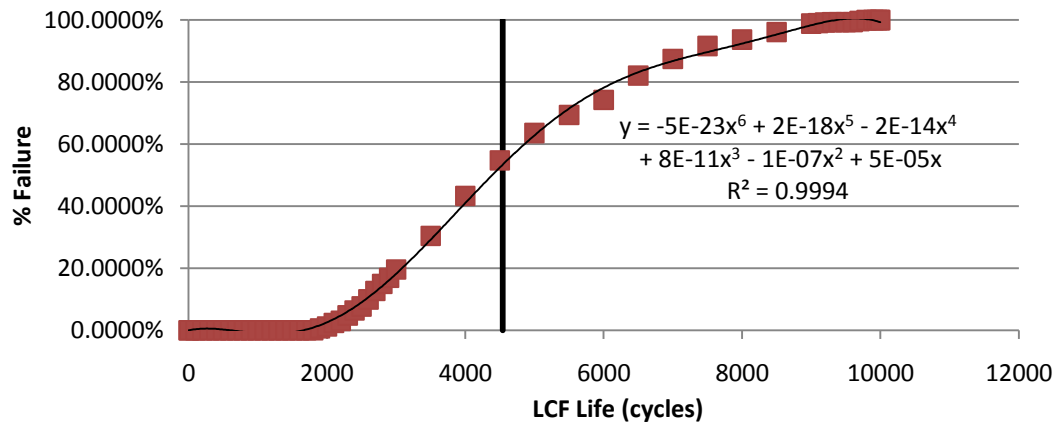
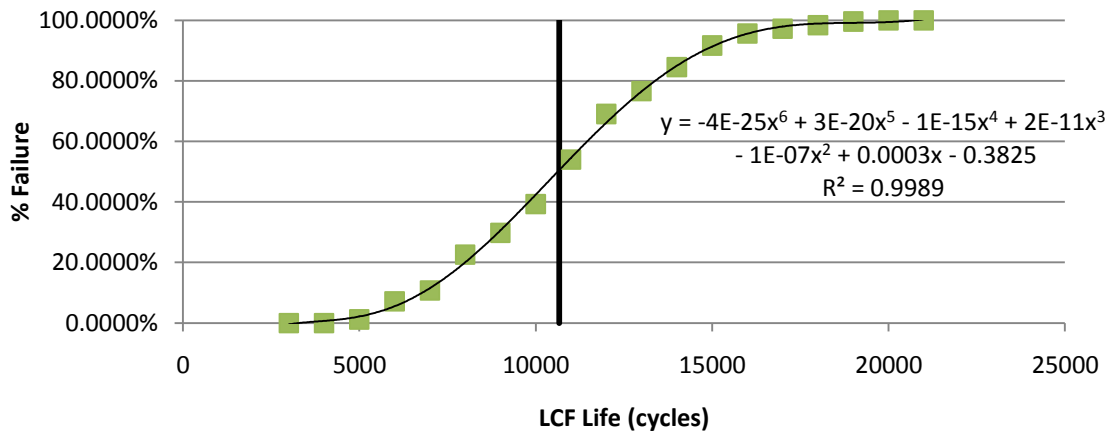
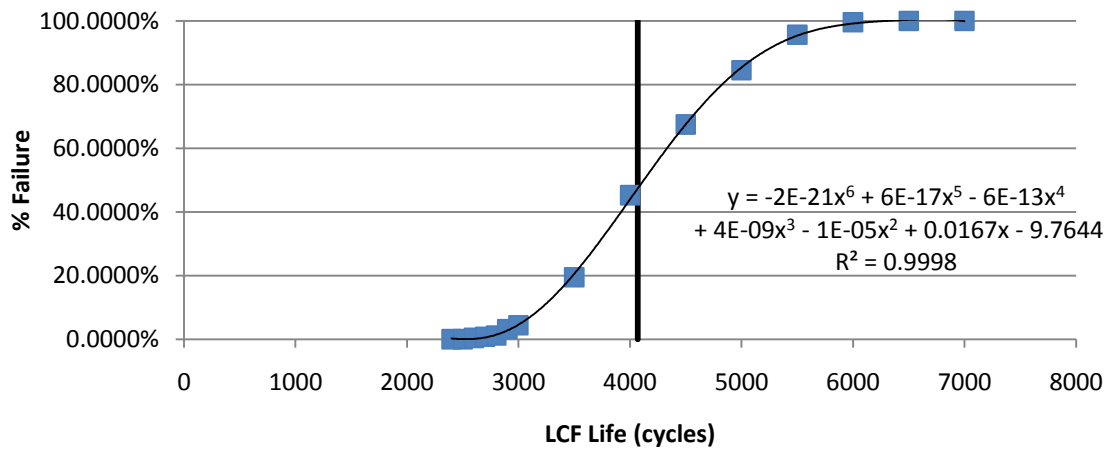


Figure 6-1: Results for Run 1

Run 2 Tip LCF Non Rotating



Run 2 Mid-Span LCF Non Rotating



Run 2 Hub LCF Non Rotating

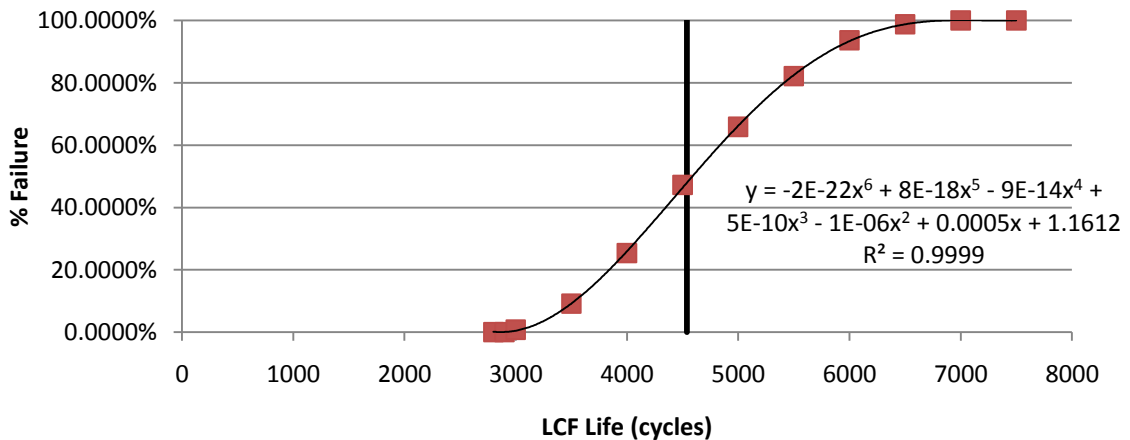


Figure 6-2: Results for Run 2

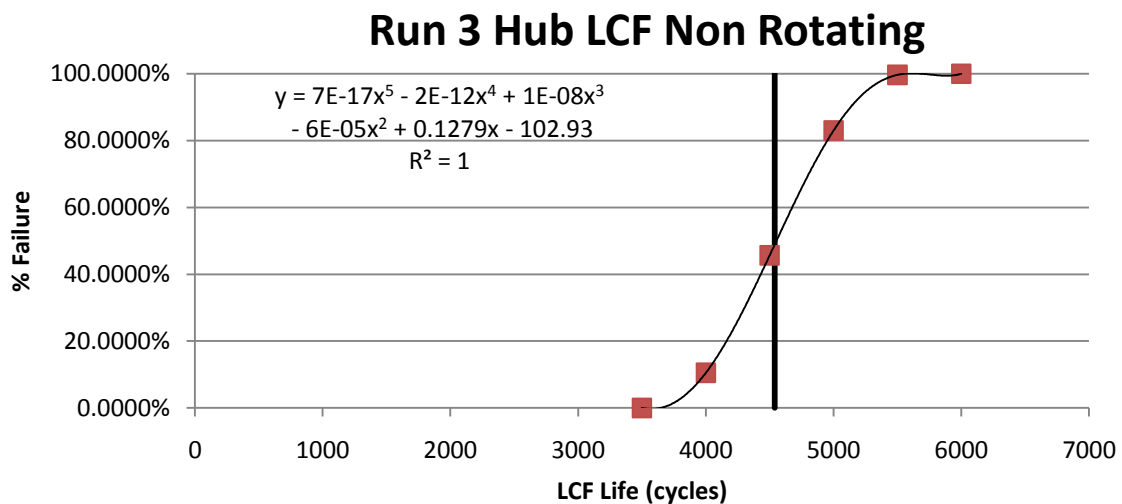
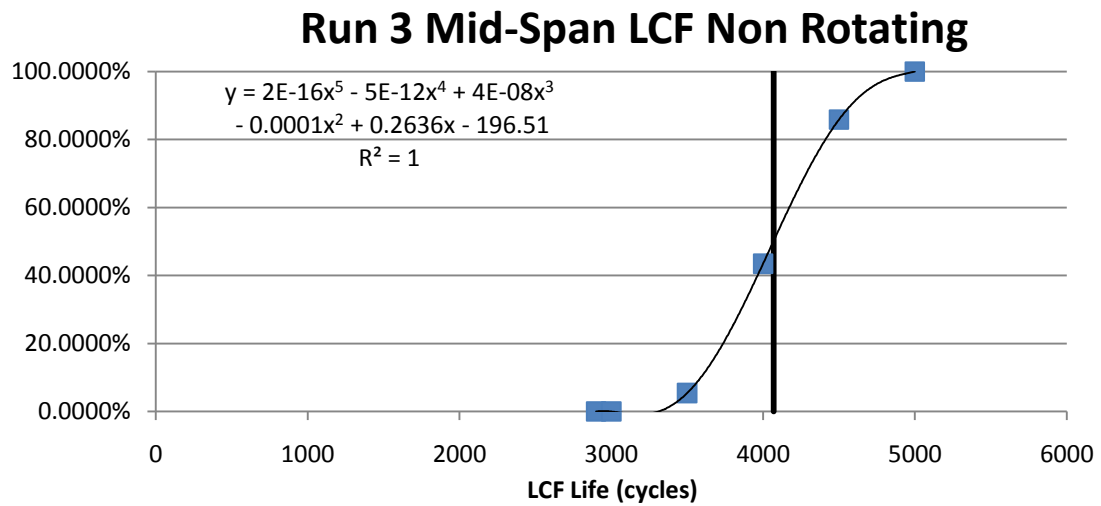
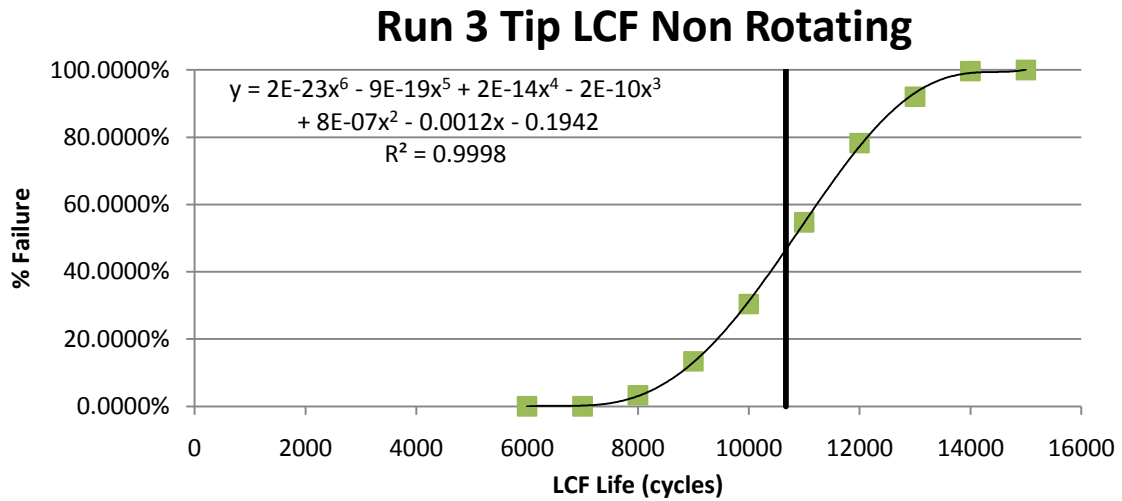


Figure 6-3: Results for Run 3

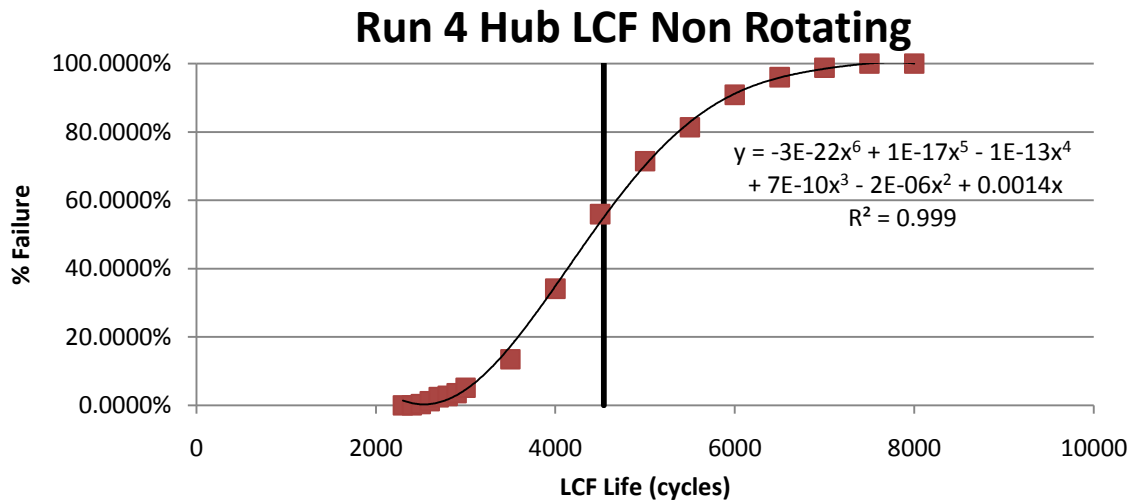
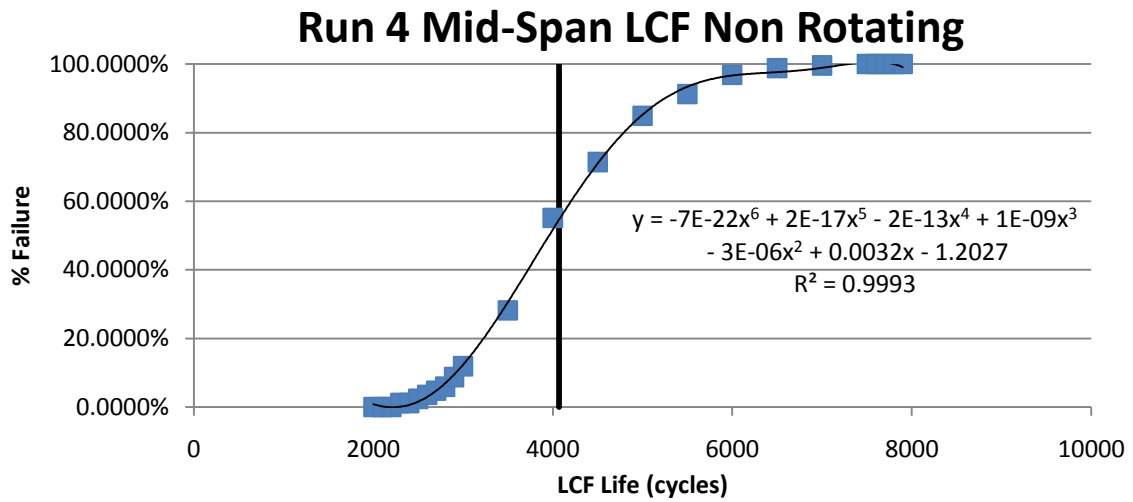
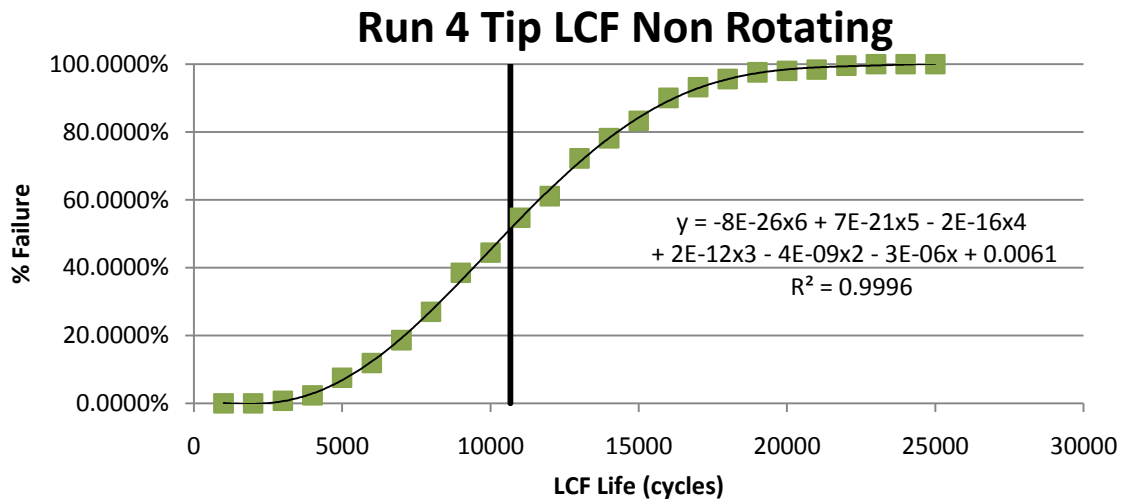


Figure 6-4: Results for Run 4

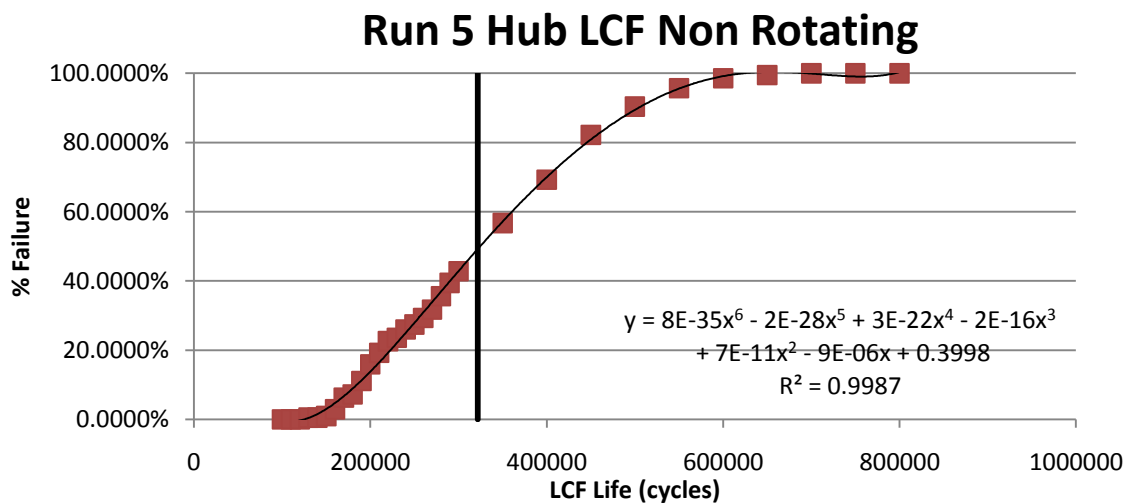
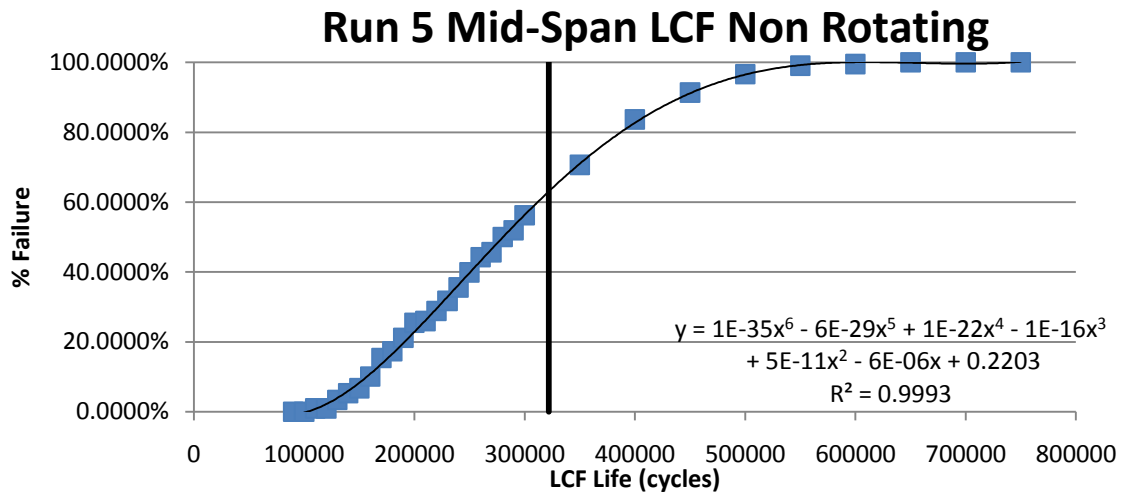
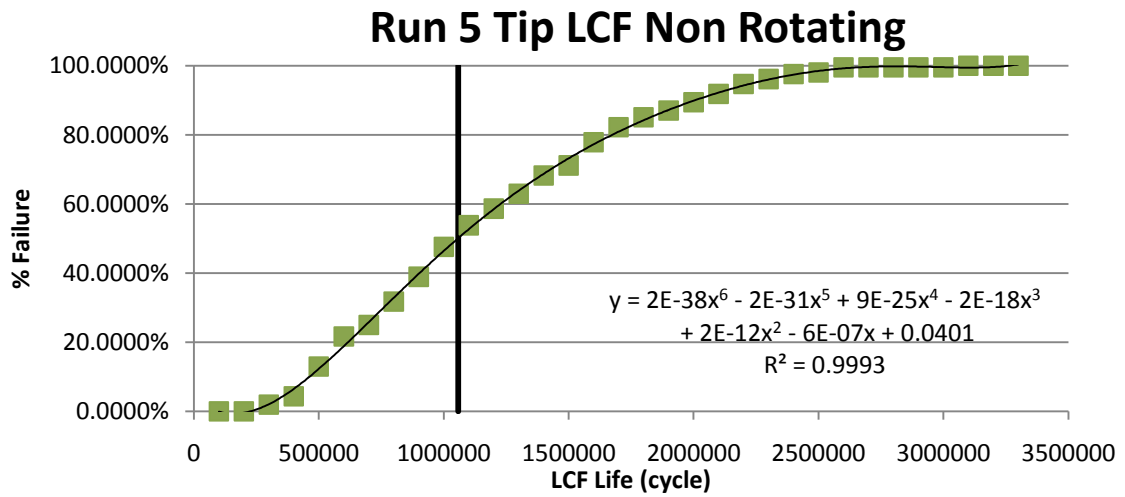


Figure 6-5: Results for Run 5

CHAPTER VII DISCUSSION

7.1 Discussion of Results

The very first comment that needs to be made regarding all of the generated data is that all predicted LCF lives seem extremely high for a turbine component. It should be recalled however that every analysis was done for non-rotating components, with no pressures mapped onto the structural components. This means that neither pressure, nor centrifugal loading is applied, so that the only force acting on the component is from the thermal side, effectively reducing the total stress. With a reduction in stress naturally comes an increase in life. Even though the life predictions are inaccurate to actual components in magnitude, all observed trends should hold true. Take for example the mid-span results of run four. The mean life is approximately 4000 hours, and the minimum value is as low as 2000 hours, meaning that even if a life of 4000 hours is quoted by the analysis work, approximately 1% of all parts will have failed before the 2000 hour mark is reached. If in reality, however the mean life is only predicted to be 1600 hours, it can be deducted that roughly 1% of all parts will have failed by 800 hours. Another trend that was quite obvious is that the LCF life at the tip was shown to be significantly higher than at the other locations on the blade. This could be due to any number of reasons. Most probably however, this is caused by the fact

that the applied gas path temperature at the tip is much lower than the rest of the airfoil, which in the absence of any other forces provides the only driver for stress.

In general, when analyzing probability plots with regards to low cycle fatigue life, the upper tail of the curve will be ignored, as the impact it has is far less important. This is largely due to the fact that there is no resulting catastrophic failure if a turbine blade survives for 10,000 hours instead of the estimated 5,000 hours. One would actually want a solution with even higher resolution in the low tail than is provided by any of the results above. However, due to computational and timing limitations, it was not feasible to produce the extra runs that would have been required. When a percent change in life is quoted due to a certain heat transfer variation it is with regards to the mean and low life components, not the high ones. Even though it was expected to see an imposed variation of life caused by HTC uncertainties, the magnitude of the effect was shown to be much more significant than previously considered. For example the 20/40% prescribed uncertainty run produced life variations at the mid span of over 50%, the 10/20% case at the same location produces a variation of approximately 38%, whereas a 5/10% uncertainty leads to a life shift of 25%. This is also shown graphically in the image on the following page. The trend repeats itself for the hub and tip sections as well, however, the tips show an increased variation of nearly 1.5 times, which can be attributed to the fact that a larger variation is assigned there.

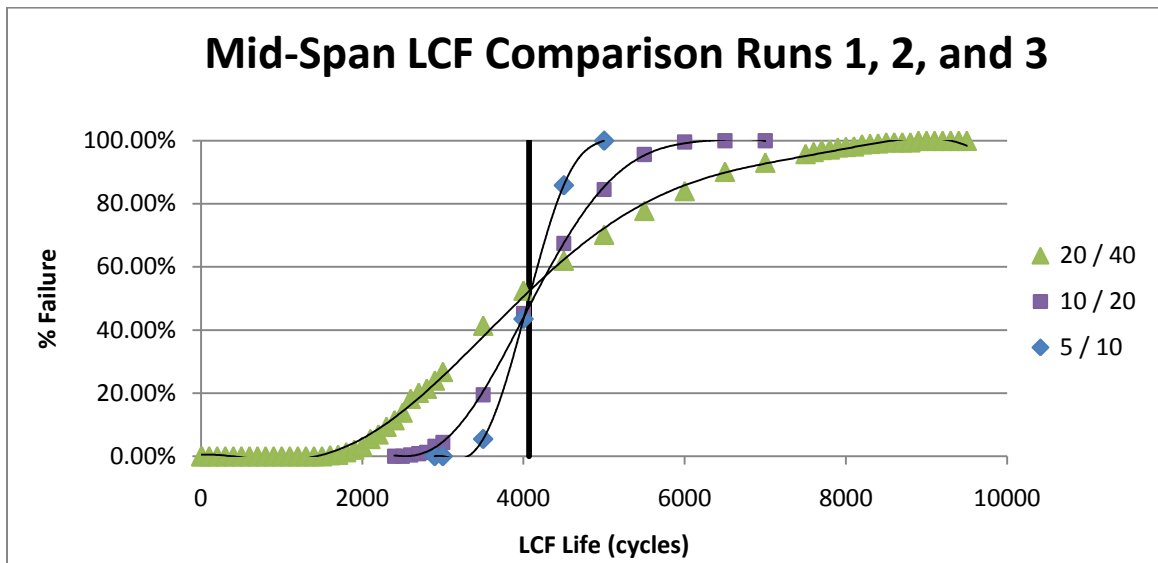


Figure 7-1: LCF Variation Comparison of Runs 1,2, and 3

Due to the fact that there is no real difference in the LCF life variation between runs one and four, it would suggest that the presence or absence of a correlation function has no effect.

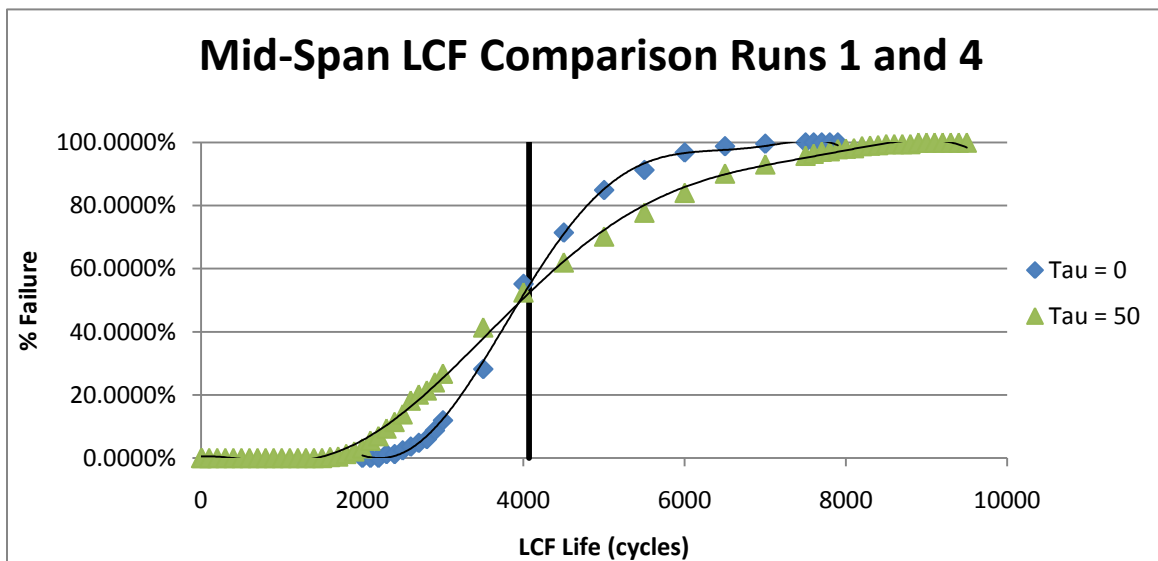


Figure 7-2: LCF Variation Comparison of Runs 1 and 4

However, as can be seen by the previous figure, there is a shift in the probability curve, with increasing τ the probability curve becomes flatter, which is expected due to the fact that if fully correlated data is inputted there will be no HTC variation leading to no change in LCF variation. It is however, not fully possible to draw a conclusion of the effect of correlation length from this study. It is promising that the results generated by runs one and four match so well, as this serves as another proof that any problems regarding the Matlab code have been adequately resolved.

Finally when comparing runs one and five to determine the effect of temperature, it is obvious to see that a 100 degree Celsius reduction in gas path temperatures has lead to a change in life on the order of magnitudes.

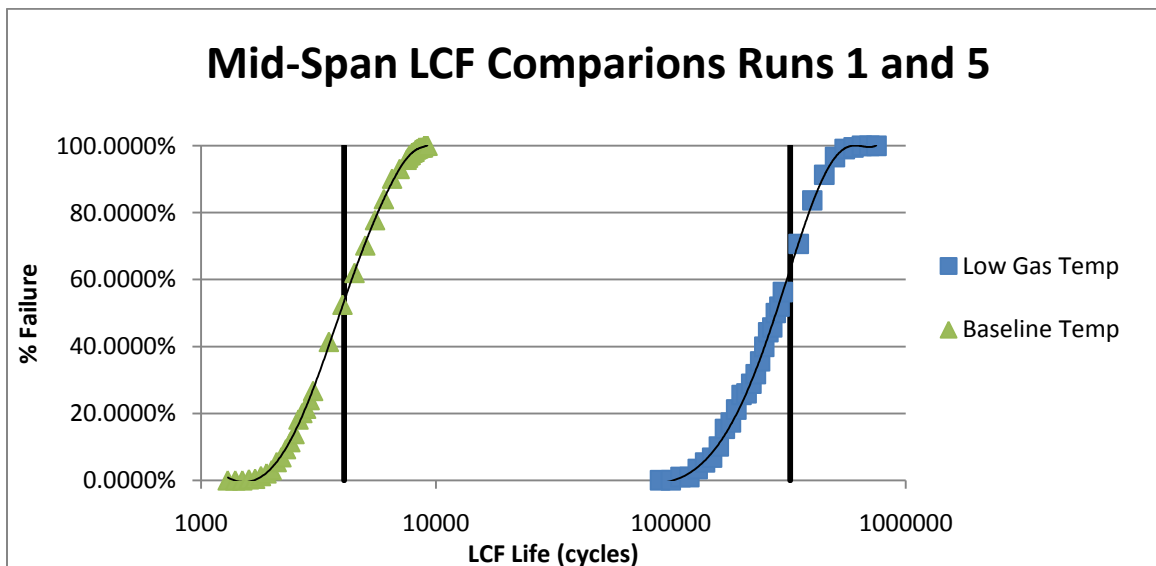


Figure 7-3: LCF Variation Comparison of Runs 1 and 5

However, the results do not indicate the percentage of fluctuations has changed much (only by a few percentage points). This could be due to the fact that the blade model is taking into account the effect of a thermal barrier coating, so that a change of 100 degrees on the gas path does not produce nearly the same effect on the metal itself. Nevertheless, as this was only a side study, the outcome is not vital to the project as a whole.

After delving into the presented results, it becomes clear that uncertainties in heat transfer coefficients have a large effect on the life as a whole, especially on a non-rotating component.

7.2 Future Work

As this project was merely meant to introduce the theory of probabilistic heat transfer, there remains a lot of work to be done in the future to further build on this study. Most importantly it would be interesting to see what kind of effects would be seen on a rotating blade, so that both CF and pressure loading can play their part. As was mentioned earlier, studies should be conducted in order to not only better understand the effect that the correlation length has on the results, but also on how to define and generate the correlation length based cooling channel geometry and internal features. Furthermore, the effect of the interface between straight passages and turns

have on the correlation function of the entire blade should also be of interest. Steps should also be taken to include a more sophisticated random number generator, so that multiple regions of variation can be modeled correctly, instead of simply scaling an output.

A major region of further uncertainty could come from the external boundary conditions, meaning that it would be interesting to run similar uncertainty quantifications for those variables. Eventually the two could be combined since many blades, such as this one, rely extensively on film cooling to generate acceptable external conditions. Therefore it would be interesting to see how changes in internal HTC's not only directly affect metal temperatures, but to also measure the influence of secondary effects cause by changes in film temperature. In addition to this an investigation of the effects of structural uncertainties, such as wall thickness variation due to casting and machining tolerances, could also prove to be a very interesting study.

As such the ultimate goal is to build on this study, not only by running all of the above studies individually, but to tie them all together and probabilistically design a blade that accounts for the effects of all uncertainties.

CHAPTER VIII CONCLUSION

In conclusion, it has been shown that there is a significant impact on the overall low cycle fatigue life of the airfoil caused by variations or uncertainties with measurements as well as applications of internal heat transfer coefficients. Variation measurements as high as 50-60% have been recorded. This should highlight the importance of reducing uncertainty as much as possible, in order to minimize variations in the output. A trend is clearly visible in the data connecting a decrease in internal heat transfer coefficient uncertainty to a decrease in airfoil life variation at all three measured locations. As such it can be stated that the primary goal of the project has been achieved, which was to quantify the effect that any form of uncertainty in internal heat transfer coefficients could have on the variation of low cycle fatigue of the airfoil as a whole.

APPENDIX A: ANSYS BOUNDARY CONDITION APPLICATION MACRO

allsel,all
csys,0

/prep7

*dim,t_side1,table,11,1,1,y
*SET,t_side1(1,0),317.5,327.66,331.47,335.28,339.09,342.9,346.71,350.52,354.33,358.1
4,368.3

*SET,t_side1(1),1321.53,1349.95,1364.16,1367.713,1369.844,1367.713,1364.16,1349.9
5,1321.53,1286.005,1250.48

*dim,h_side1,table,12,1,1,z
*SET,h_side1(1,0),-15.24,-12.7,-10.16,-7.62,-5.08,-2.54,0,1.778, 3.556,5.558,7.366,9.144
*SET,h_side1(1),8.0,8.5,8.6,8.5,7.6,7.0,6.250,5.5,5.6,6.250,7.0,8.5

cmsel,s,e_PS
nsle,s,1
sf,all,conv,%H_SIDE1%,%T_SIDE1%

*dim,h_side2,table,12,1,1,z
*SET,h_side2(1,0),-15.24,-12.7,-10.16,-7.62,-5.08,-2.54,0,1.778,3.556,5.558,7.366,9.144
*SET,h_side2(1),4.6,4.7,4.850,5.0,5.2,5.4,5.6,5.8,6.0,6.250,7.0,8.5

cmsel,s,e_SS
nsle,s,1
sf,all,conv,%H_SIDE2%,%T_SIDE1%

cmsel,s,e_endwall
nsle,s,1
sf, all, conv, 3.5, 1334.53

cmsel,s,e_root_box
nsle,s,1
sf, all, conv, 1.2, 673.1

*dim,t_side3,table,13,1,1,y
*SET,t_side3(1,0),304.8,314.96,319.024,323.088,327.406,331.47,335.534,339.852,343.9
16,347.98,352.298,356.362,360.68
*SET,t_side3(1),673.1,673.1,674.4,675.6,676.9,678.1,679.4,680.6,681.9,683.1,684.3,685
.6,685.6

*dim,h_side3,table,12,1,1,y
*SET,h_side3(1,0),304.8,309.88,314.96,320.04,325.12,330.2,335.28,340.36,345.44,350.
52,355.6,360.68,

*SET,h_side3(1),1.500,1.700,1.900,3.3245,3.442,3.5685,3.7085,3.8585,4.0165,4.186,4.372,4.5675

cmsel,s,e_six
nsle,s,1
sf,all,conv,%H_SIDE3%

*dim,t_side4,table,13,1,1,y
*SET,t_side4(1,0),304.8,314.96,319.024,323.088,327.406,331.47,335.534,339.852,343.916,347.98,352.298,356.362,360.68
*SET,t_side4(1),673.1,673.1,673.7,674.2,674.7,675.2,675.7,676.2,676.7,677.2,677.7,678.2,678.2

*dim,h_side4,table,12,1,1,y
*SET,h_side4(1,0),304.8,309.88,314.96,320.04,325.12,330.2,335.28,340.36,345.44,350.52,355.6,360.68,
*SET,h_side4(1),1.500,1.700,1.900,3.3245,3.3385,3.353,3.368,3.3835,3.3985,3.413,3.4275,3.443

cmsel,s,e_three
nsle,s,1
sf,all,conv,%H_SIDE4%,%T_SIDE4%

*dim,t_side5,table,12,1,1,y
*SET,t_side5(1,0),314.96,319.024,323.088,327.406,331.47,335.534,339.852,343.916,347.98,352.298,356.362,360.68
*SET,t_side5(1),694.9,694.9,694,693.1,692.2,691.3,690.3,689.4,688.5,687.5,686.6,685.6

*dim,h_side5,table,10,1,1,y
*SET,h_side5(1,0),314.96,320.04,325.12,330.2,335.28,340.36,345.44,350.52,355.6,360.68,
*SET,h_side5(1),3.2135,3.1565,3.1015,3.051,2.999,2.949,2.9025,2.855,2.809,2.767

cmsel,s,e_five
nsle,s,1
sf,all,conv,%H_SIDE5%

*dim,t_side6,table,12,1,1,y
*SET,t_side6(1,0),314.96,319.024,323.088,327.406,331.47,335.534,339.852,343.916,347.98,352.298,356.362,360.68
*SET,t_side6(1),694.9,695.8,696.7,697.6,698.5,699.3,700.2,701,701.8,702.6,703.3,703.3

*dim,h_side6,table,10,1,1,y
*SET,h_side6(1,0),314.96,320.04,325.12,330.2,335.28,340.36,345.44,350.52,355.6,360.68,

```

68,
*SET,h_side6(1),3.5295,3.549,3.567,3.581,3.593,3.6025,3.608,3.6075,3.5965,3.540

cmsel,s,e_four
nsle,s,1
sf,all,conv,%H_SIDE6%

*dim,t_side7,table,12,1,1,y
*SET,t_side7(1,0),314.96,319.024,323.088,327.406,331.47,335.534,339.852,343.916,34
7.98,352.298,356.362,360.68
*SET,t_side7(1),682.3,682.3,681.9,681.5,681.1,680.7,680.2,679.8,679.4,679,678.6,678.2

*dim,h_side7,table,10,1,1,y
*SET,h_side7(1,0),314.96,320.04,325.12,330.2,335.28,340.36,345.44,350.52,355.6,360.
68,
*SET,h_side7(1),2.1775,2.201,2.226,2.251,2.2765,2.303,2.3295,2.3575,2.3865,2.416

cmsel,s,e_two
nsle,s,1
sf,all,conv,%H_SIDE7%,%T_SIDE7%

*dim,t_side8,table,12,1,1,y
*SET,t_side8(1,0),314.96,319.024,323.088,327.406,331.47,335.534,339.852,343.916,34
7.98,352.298,356.362,360.68
*SET,t_side8(1),682.2,682.2,683.2,683.7,684.2,684.6,685.1,685.5,686,686.4,686.8,686.8

*dim,h_side8,table,10,1,1,y
*SET,h_side8(1,0),314.96,320.04,325.12,330.2,335.28,340.36,345.44,350.52,355.6,360.
68,
*SET,h_side8(1),3.7965,3.733,3.671,3.6095,3.548,3.4865,3.423,3.3565,3.2805,3.1715

cmsel,s,e_one
nsle,s,1
sf,all,conv,%H_SIDE8%,%T_SIDE8%

allsel, all

```


APPENDIX B: MATLAB CODE

```

clc;
clear;

RandStream.setDefaultStream ...
    (RandStream('mt19937ar','seed',sum(100*clock)));

%Set Parameters: Max -> number of points,
%      Tau -> correlation length
%      maxvar -> maximum allowed variance (2x for turns)

Max=30;
Tau=50;
maxvar=.20;

converge=1;

while converge<31;

%Generate Normally Distributed random numbers with Mean=0 and Var=maxvar

G=normrnd(0,maxvar,Max,1);

%Exponential correlation function

f=exp(-1/Tau);

%Initialization

R(1,1)=G(1,1);

SumG(1,1)=G(1,1);
SumR(1,1)=SumG(1,1);

converge=1;

%Generate the correlated random numbers (R)

for i=2:1:Max
    R(i,1)=(f*R(i-1,1))+((1-(f^2))^0.5)*(G(i,1));
    SumG(i,1)=SumG(i-1,1)+G(i,1);
    SumR(i,1)=SumR(i-1,1)+R(i,1);
end

```

%X and Y are two different ways to generate the variance increase in
 %the turns. X uses 2G to plug into R (not used in this case) and Y
 %uses twice the output R

%U and Q just setup the bounds of the maximum variance

```

for i=1:1:8
    X(i,1)=R(i,1);
    Y(i,1)=R(i,1);
    U(i,1)=maxvar;
    Q(i,1)=-maxvar;
end

for i=9:1:12
    X(i,1)=(f*R(i-1,1))+((1-(f^2))^0.5)*(2*(G(i,1)));
    U(i,1)=2*maxvar;
    Q(i,1)=-2*maxvar;
end

for i=9:1:12
    Y(i,1)=2*(R(i,1));
end

for i=13:1:18
    X(i,1)=R(i,1);
    Y(i,1)=R(i,1);
    U(i,1)=maxvar;
    Q(i,1)=-maxvar;
end

for i=19:1:22
    X(i,1)=(f*R(i-1,1))+((1-(f^2))^0.5)*(2*(G(i,1)));
    U(i,1)=2*maxvar;
    Q(i,1)=-2*maxvar;
end

for i=19:1:22
    Y(i,1)=2*(R(i,1));
end

for i=23:1:30

```

```

X(i,1)=R(i,1);
Y(i,1)=R(i,1);
U(i,1)=maxvar;
Q(i,1)=-maxvar;
end

```

```

%if any of the values of Y are outside of the range setup by U and Q this
%will force the while loop to continue and reselected the uncorrelated
%random numbers to try again. This will repeat until all values of Y fall
%within the specified range

```

```

for i=1:1:30
if abs(Y(i,1))>U(i,1);
    converge=converge+0;
else converge=converge+1;
end
end

```

```

end

```

```

%Input the Original HTC's

```

```

OrigHTC(1,1)=3324;
OrigHTC(2,1)=3324;
OrigHTC(3,1)=3338;
OrigHTC(4,1)=3353;
OrigHTC(5,1)=3368;
OrigHTC(6,1)=3383;
OrigHTC(7,1)=3398;
OrigHTC(8,1)=3413;
OrigHTC(9,1)=3427;
OrigHTC(10,1)=3443;
OrigHTC(11,1)=3796;
OrigHTC(12,1)=3733;
OrigHTC(13,1)=3671;
OrigHTC(14,1)=3609;
OrigHTC(15,1)=3548;
OrigHTC(16,1)=3486;
OrigHTC(17,1)=3423;
OrigHTC(18,1)=3356;
OrigHTC(19,1)=3280;
OrigHTC(20,1)=3171;

```

```

OrigHTC(21,1)=2416;
OrigHTC(22,1)=2386;
OrigHTC(23,1)=2357;
OrigHTC(24,1)=2329;
OrigHTC(25,1)=2303;
OrigHTC(26,1)=2276;
OrigHTC(27,1)=2251;
OrigHTC(28,1)=2226;
OrigHTC(29,1)=2201;
OrigHTC(30,1)=2177;

```

```

%Modify the original HTCS by the generated variation

```

```

for i=1:1:30
    HTCVar(i,1)=1+Y(i,1);
    NewHTC(i,1)=OrigHTC(i,1)*HTCVar(i,1);
end

```

```

%Generate the plots
% SUBPLOT(2,1,1),
% plot(G,'r')
% hold on
% plot(R)
% hold on
% plot(Y,'go-')
% hold on
% plot(U,'c')
% hold on
% plot(Q,'c')
% hold off
%
% legend('rndm #', 'corr rndm #', 'modif corr rndm #', 'max var', 'location', 'EastOutside')
% xlabel('Point')
% ylabel('Generated Variation')
%
%
% SUBPLOT(2,1,2),
% plot(HTCVar,'rx-')
% % hold on
% % plot(NewHTC,'bo-')
% % hold off
% legend('Baseline HTC', 'Modified HTC', 'location', 'EastOutside')

```

```

% xlabel('Point')
% ylabel('HTC')

% Open input file for writing

Input = fopen('Input_isight.inp','w');

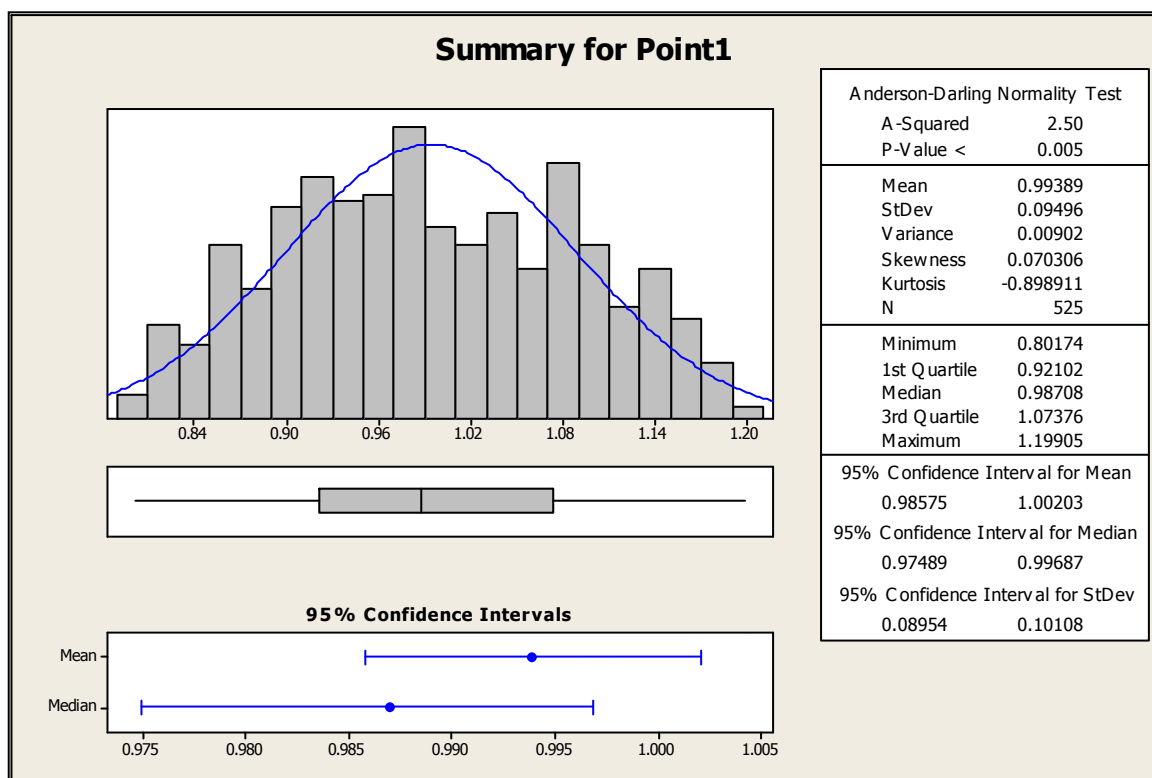
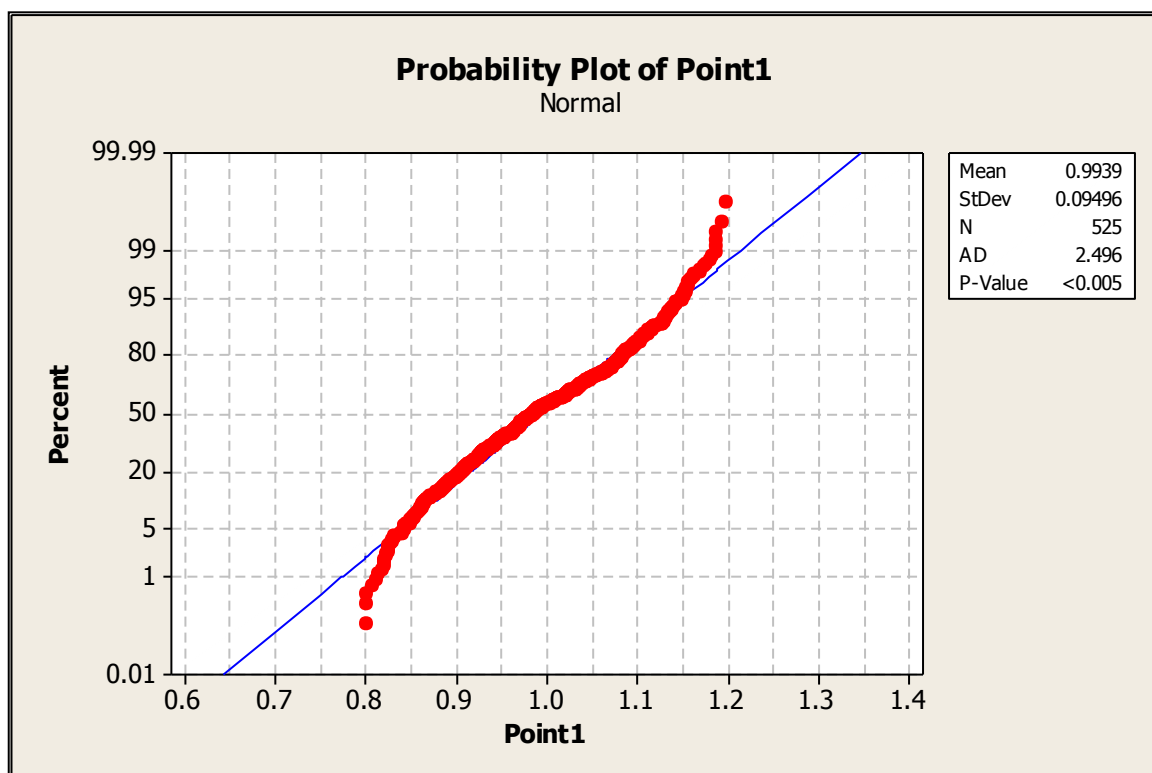
% Write data to input file

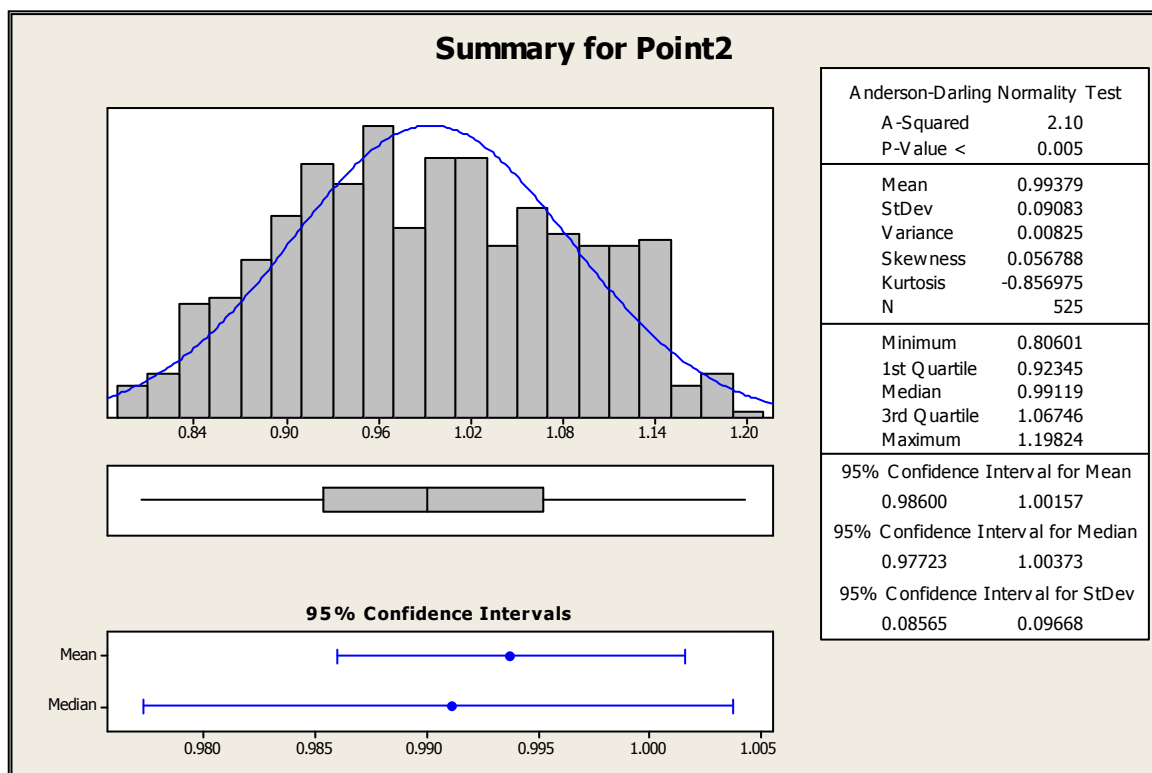
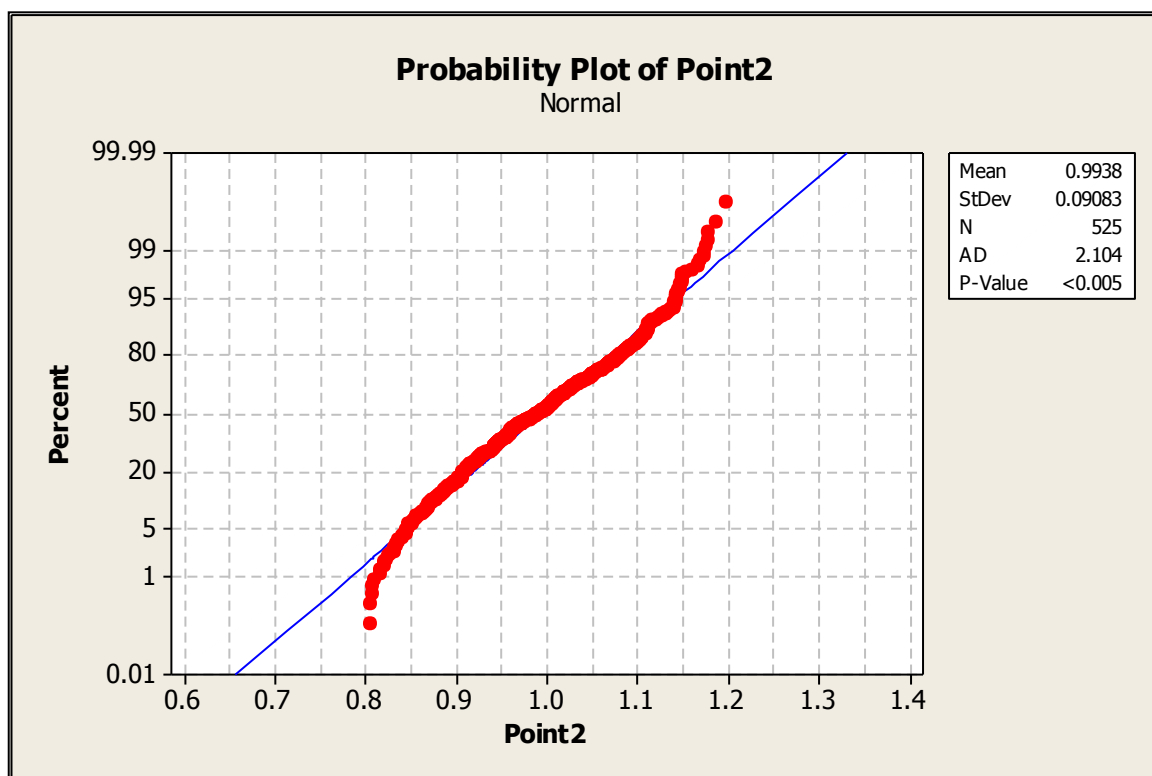
fprintf(Input, 'fact_one=%f\n',HTCVar(1,1));
fprintf(Input, 'fact_two=%f\n',HTCVar(2,1));
fprintf(Input, 'fact_three=%f\n',HTCVar(3,1));
fprintf(Input, 'fact_four=%f\n',HTCVar(4,1));
fprintf(Input, 'fact_five=%f\n',HTCVar(5,1));
fprintf(Input, 'fact_six=%f\n',HTCVar(6,1));
fprintf(Input, 'fact_seven=%f\n',HTCVar(7,1));
fprintf(Input, 'fact_eight=%f\n',HTCVar(8,1));
fprintf(Input, 'fact_nine=%f\n',HTCVar(9,1));
fprintf(Input, 'fact_ten=%f\n',HTCVar(10,1));
fprintf(Input, 'fact_eleven=%f\n',HTCVar(11,1));
fprintf(Input, 'fact_twelve=%f\n',HTCVar(12,1));
fprintf(Input, 'fact_thirteen=%f\n',HTCVar(13,1));
fprintf(Input, 'fact_fourteen=%f\n',HTCVar(14,1));
fprintf(Input, 'fact_fifteen=%f\n',HTCVar(15,1));
fprintf(Input, 'fact_sixteen=%f\n',HTCVar(16,1));
fprintf(Input, 'fact_seventeen=%f\n',HTCVar(17,1));
fprintf(Input, 'fact_eighteen=%f\n',HTCVar(18,1));
fprintf(Input, 'fact_nineteen=%f\n',HTCVar(19,1));
fprintf(Input, 'fact_twenty=%f\n',HTCVar(20,1));
fprintf(Input, 'fact_twentyone=%f\n',HTCVar(21,1));
fprintf(Input, 'fact_twentytwo=%f\n',HTCVar(22,1));
fprintf(Input, 'fact_twentythree=%f\n',HTCVar(23,1));
fprintf(Input, 'fact_twentyfour=%f\n',HTCVar(24,1));
fprintf(Input, 'fact_twentyfive=%f\n',HTCVar(25,1));
fprintf(Input, 'fact_twentysix=%f\n',HTCVar(26,1));
fprintf(Input, 'fact_twentyseven=%f\n',HTCVar(27,1));
fprintf(Input, 'fact_twentyeight=%f\n',HTCVar(28,1));
fprintf(Input, 'fact_twentynine=%f\n',HTCVar(29,1));
fprintf(Input, 'fact_thirty=%f\n',HTCVar(30,1));

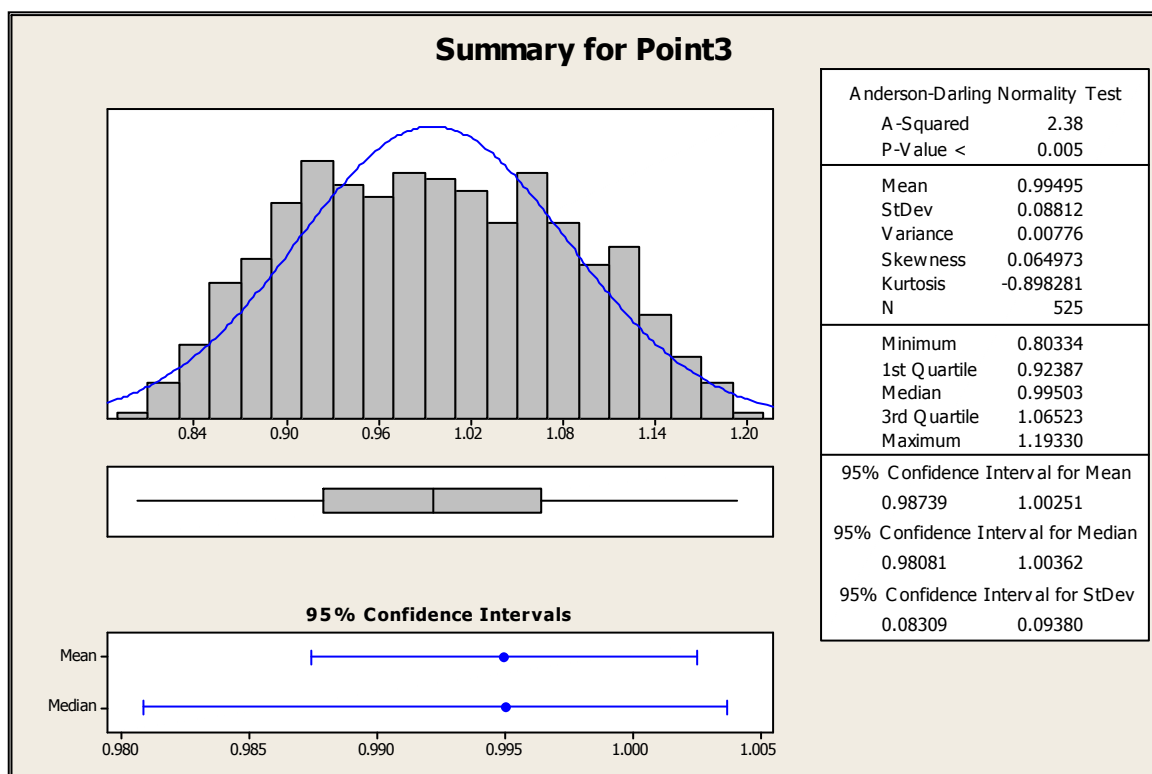
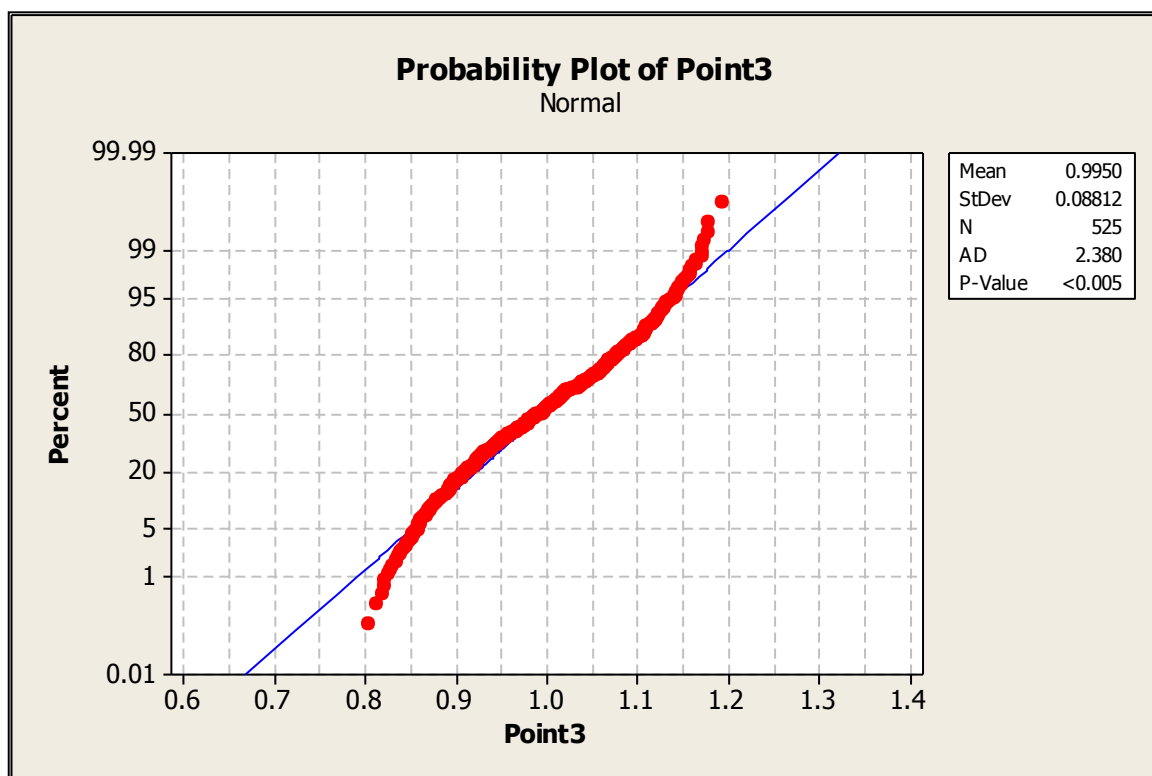
% Close input file
fclose(Input)

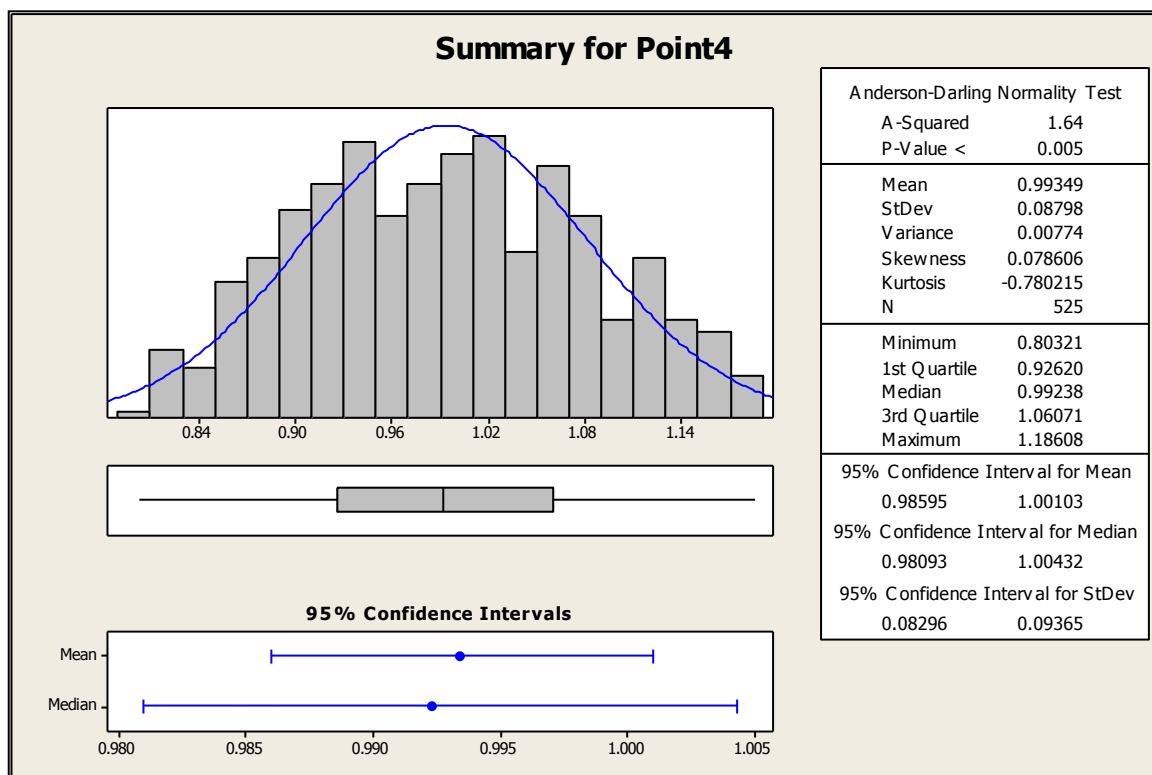
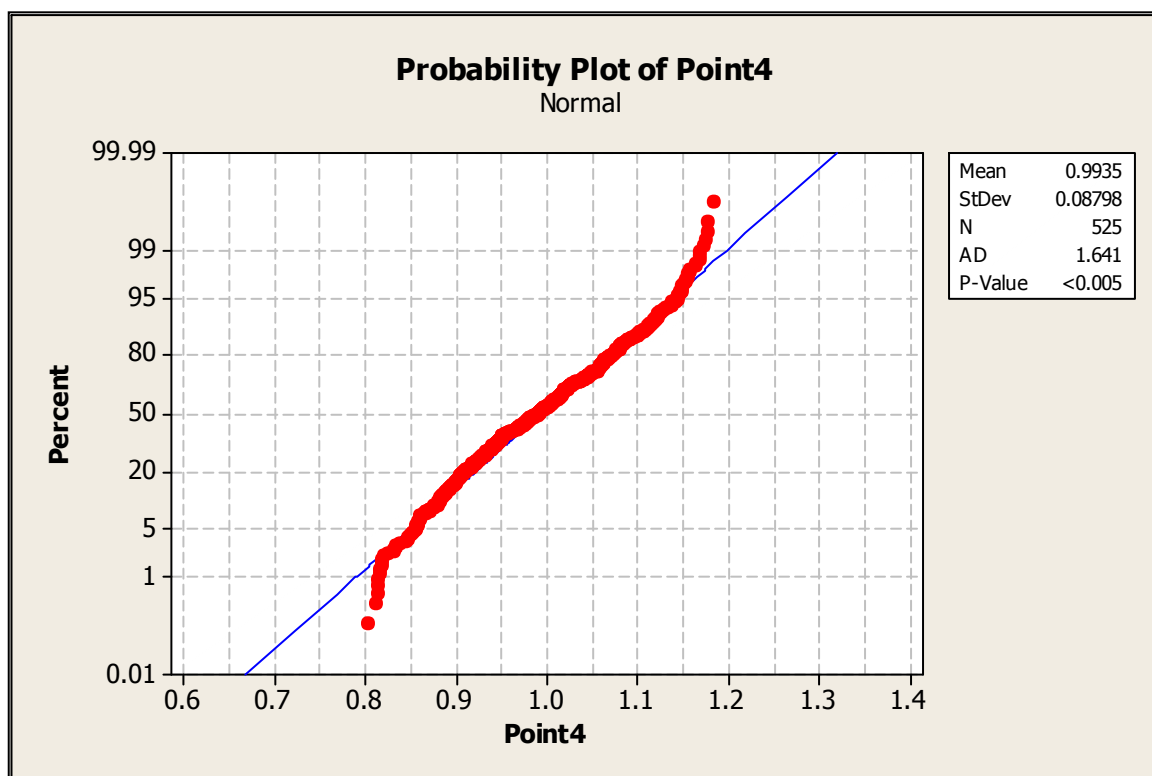
```

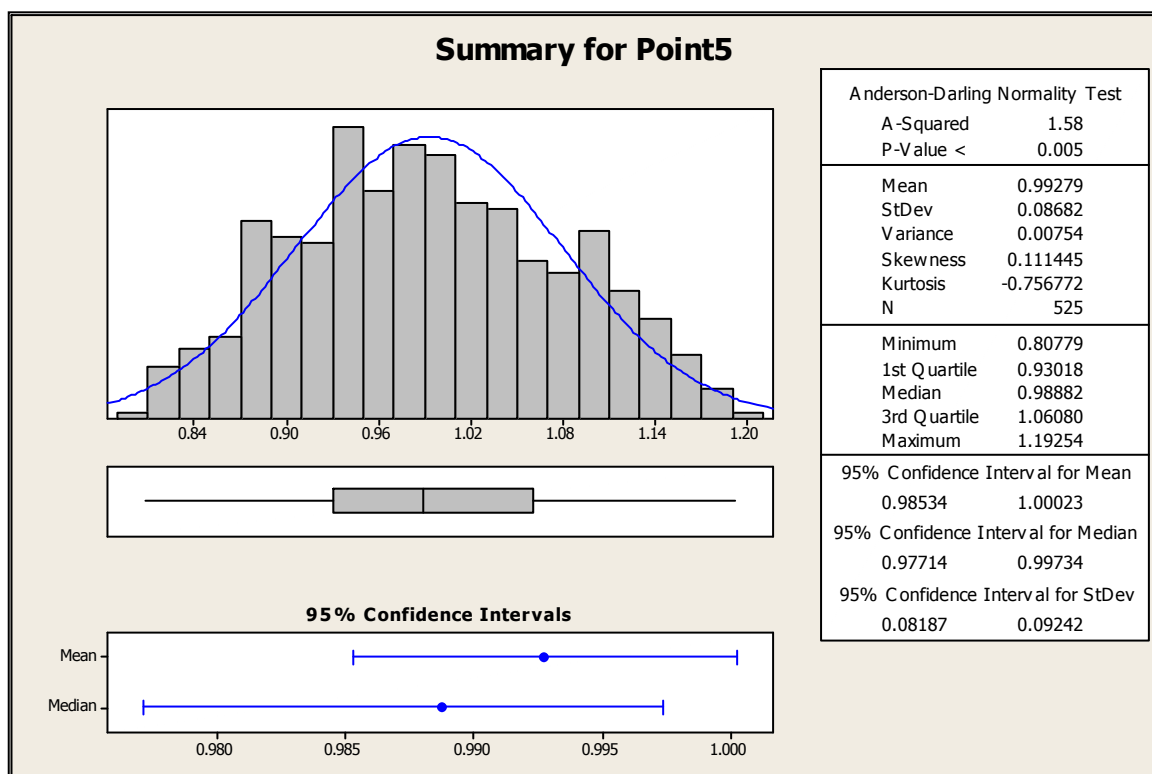
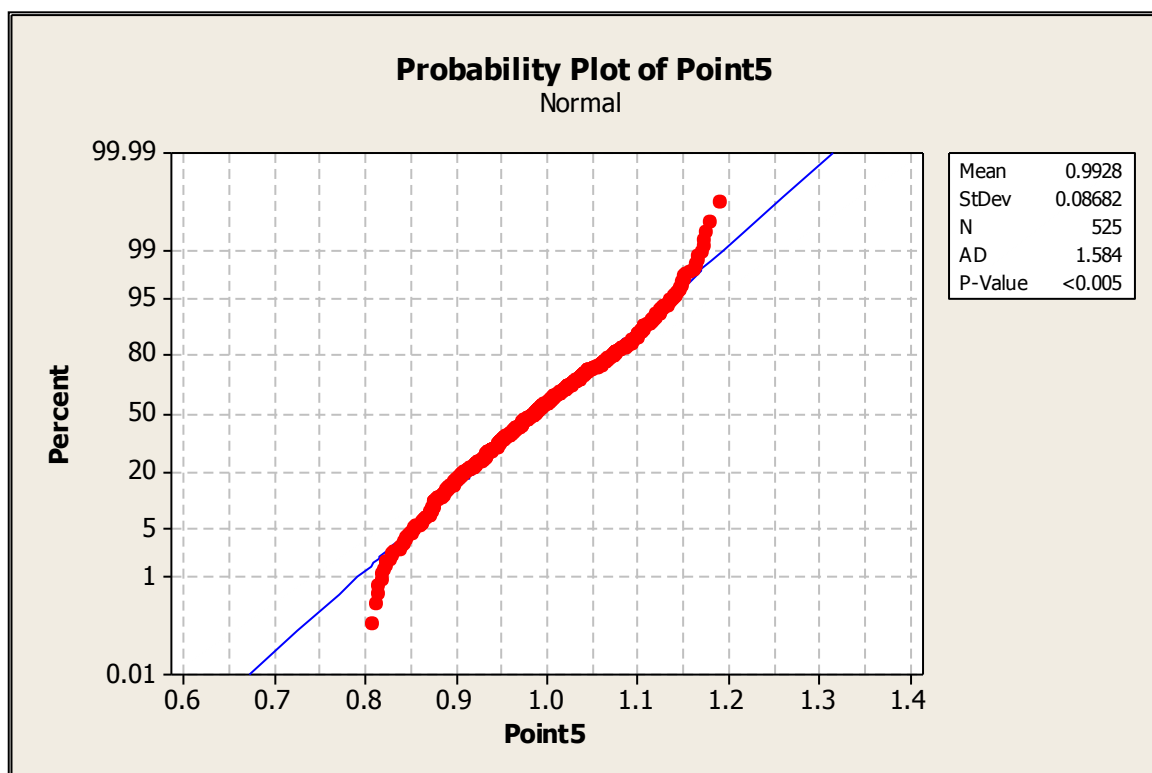
APPENDIX C: VALIDATION PLOTS FOR ALL POINTS OF RUN 1

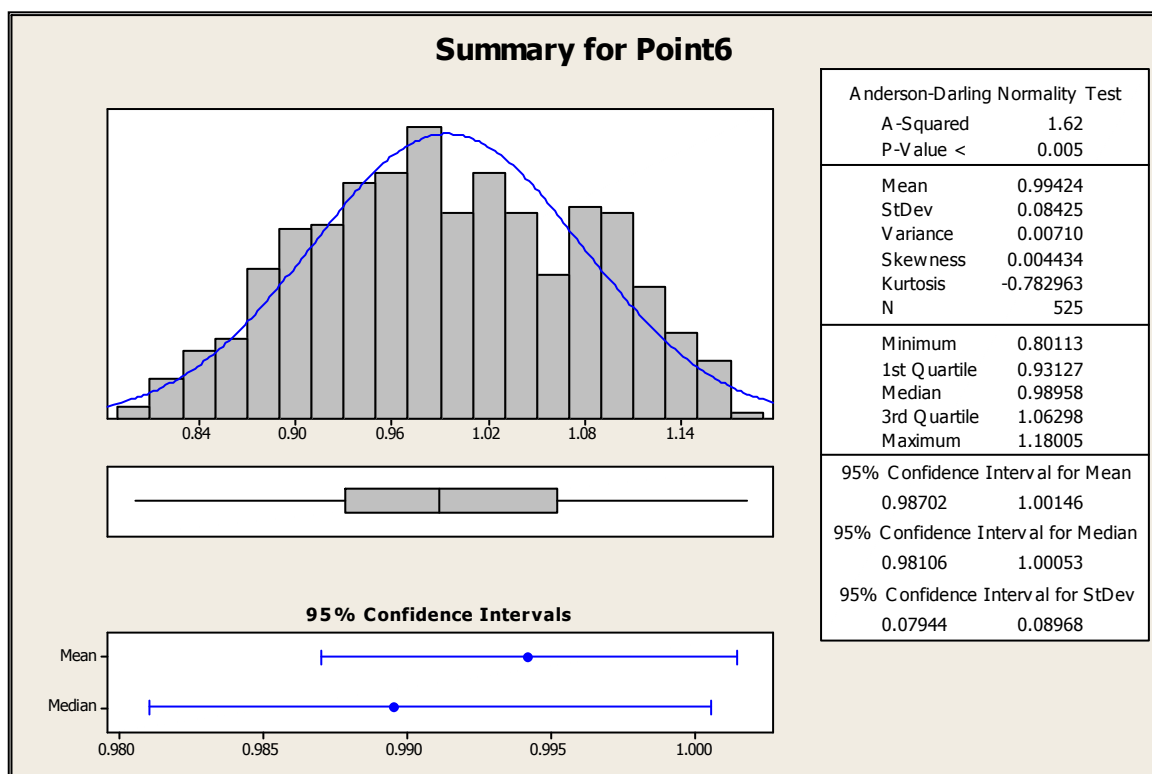
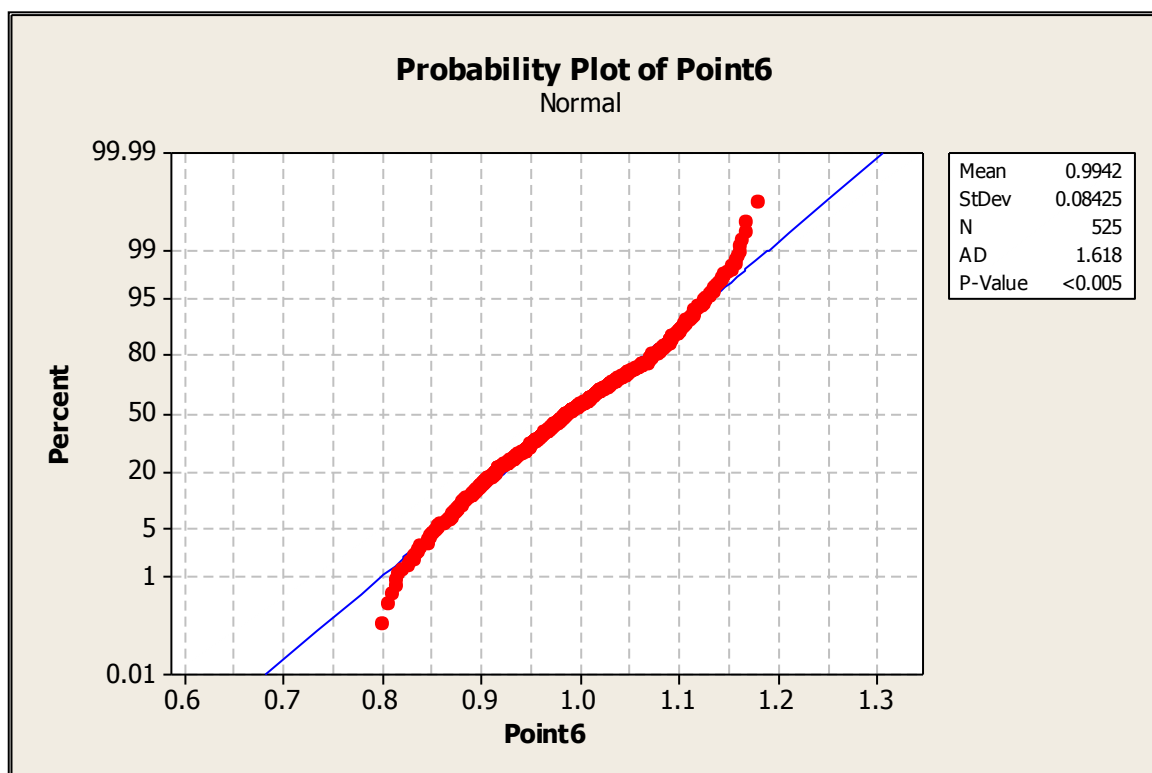


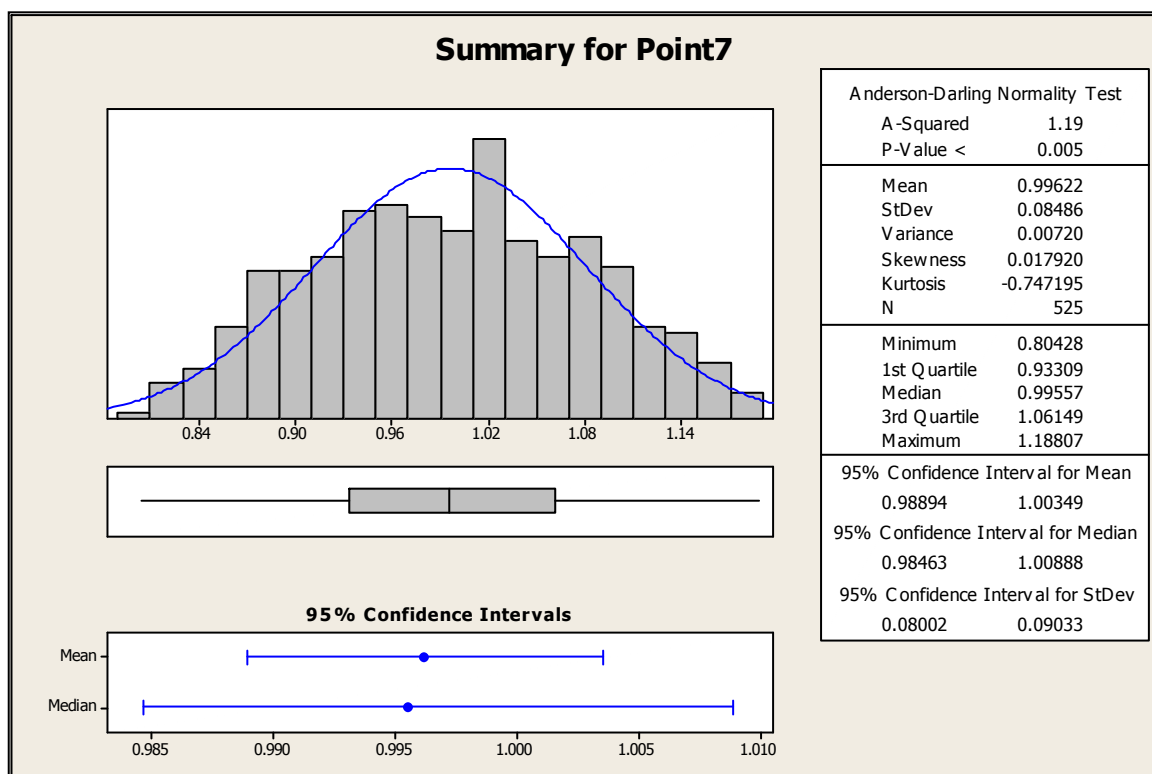
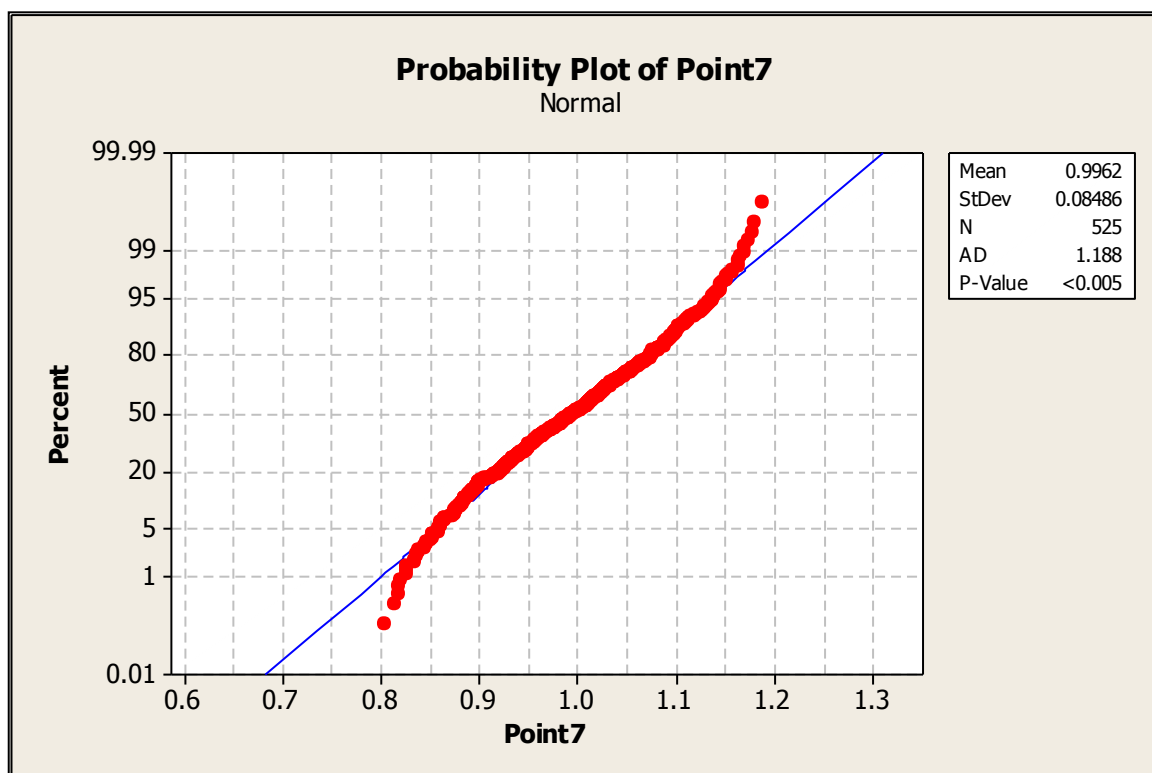


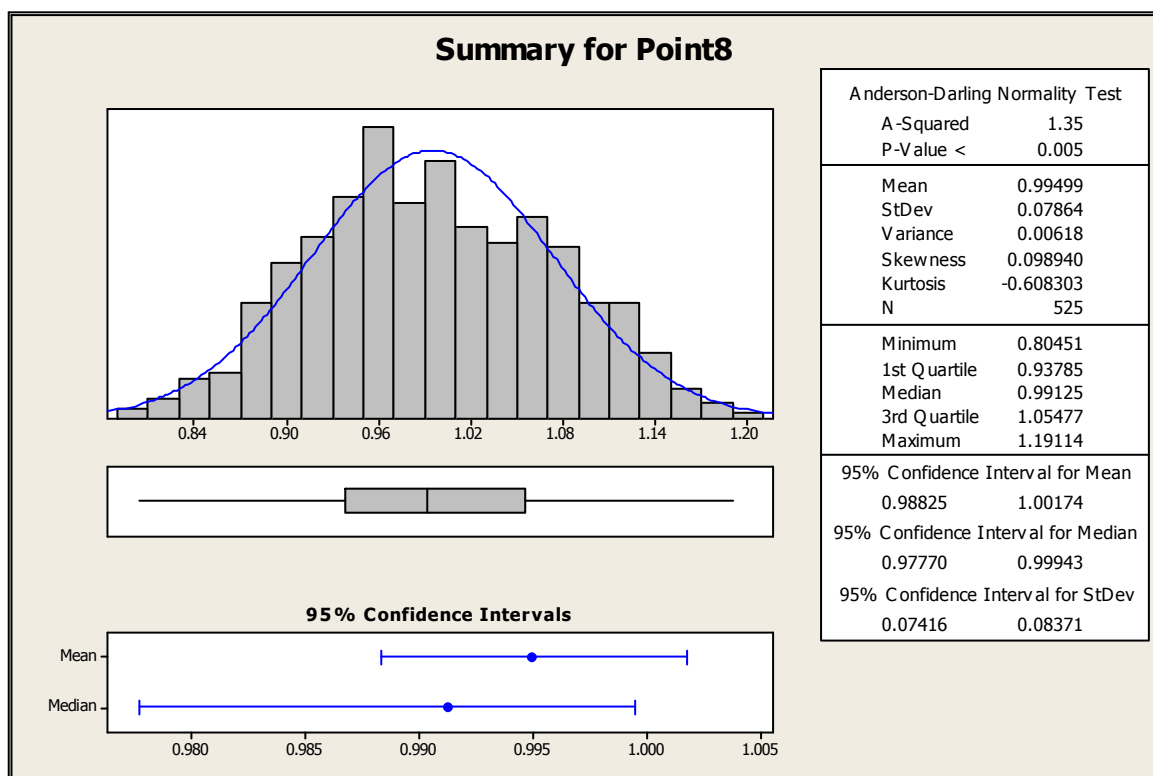
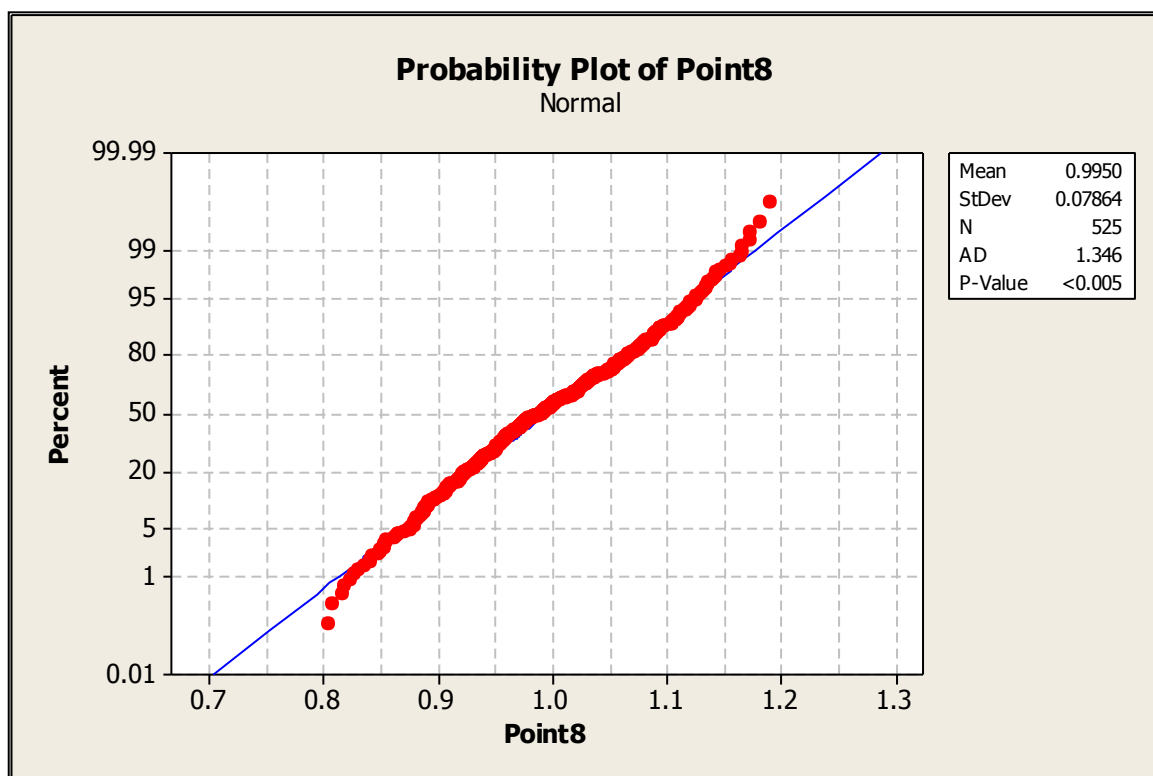


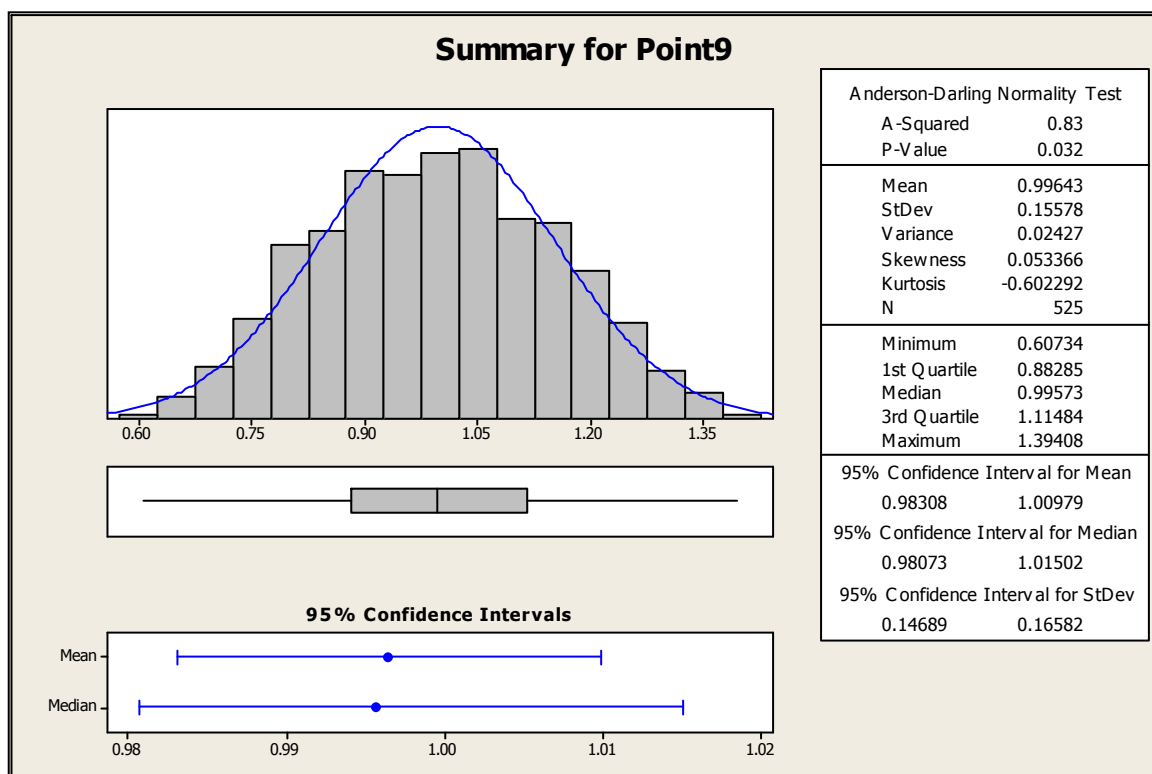
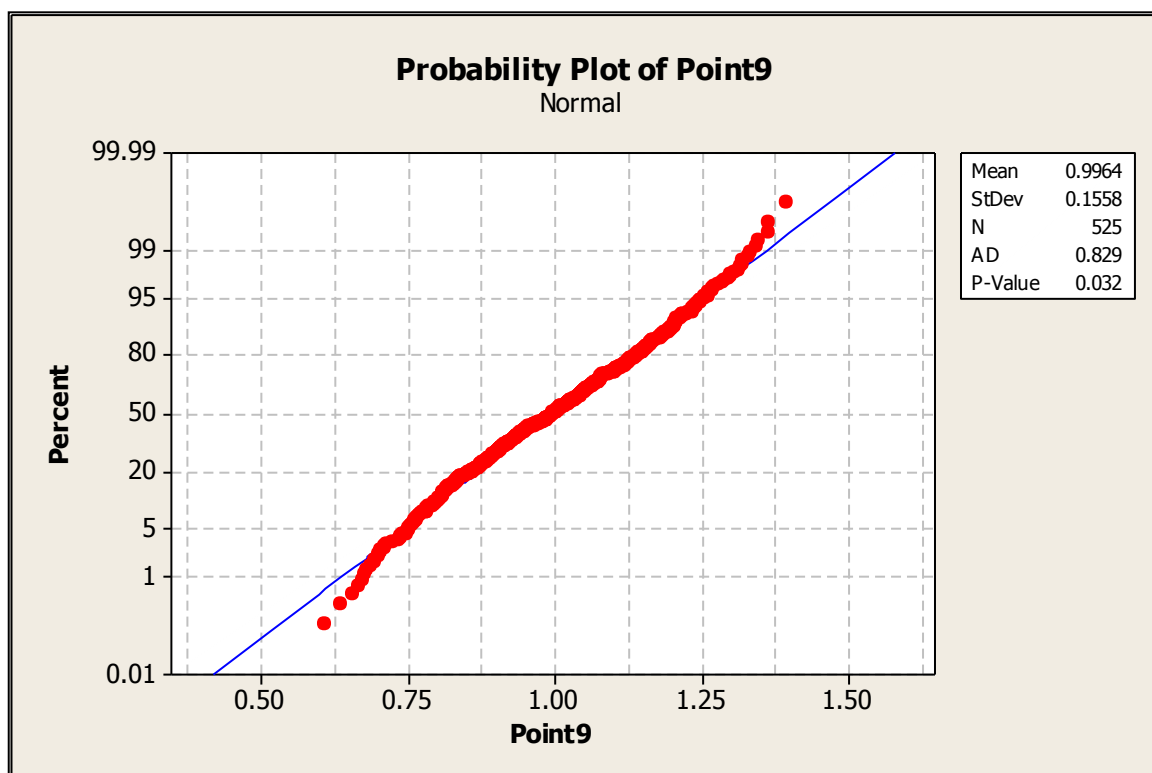


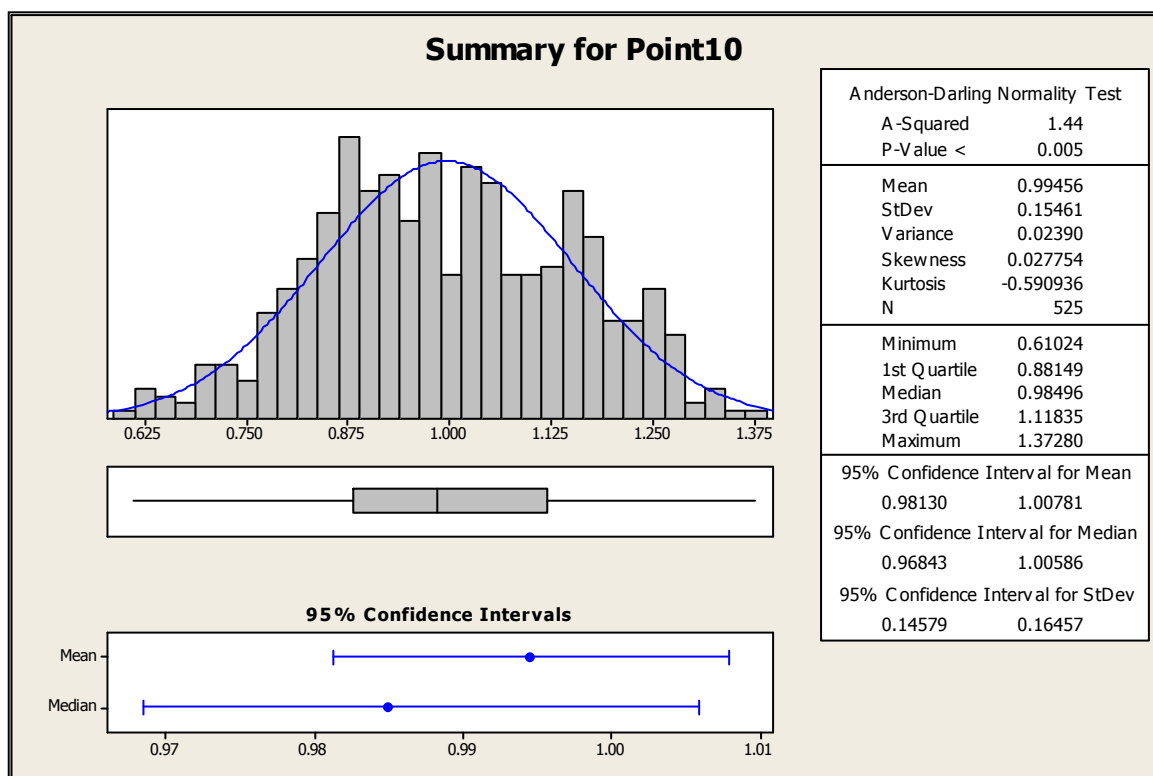
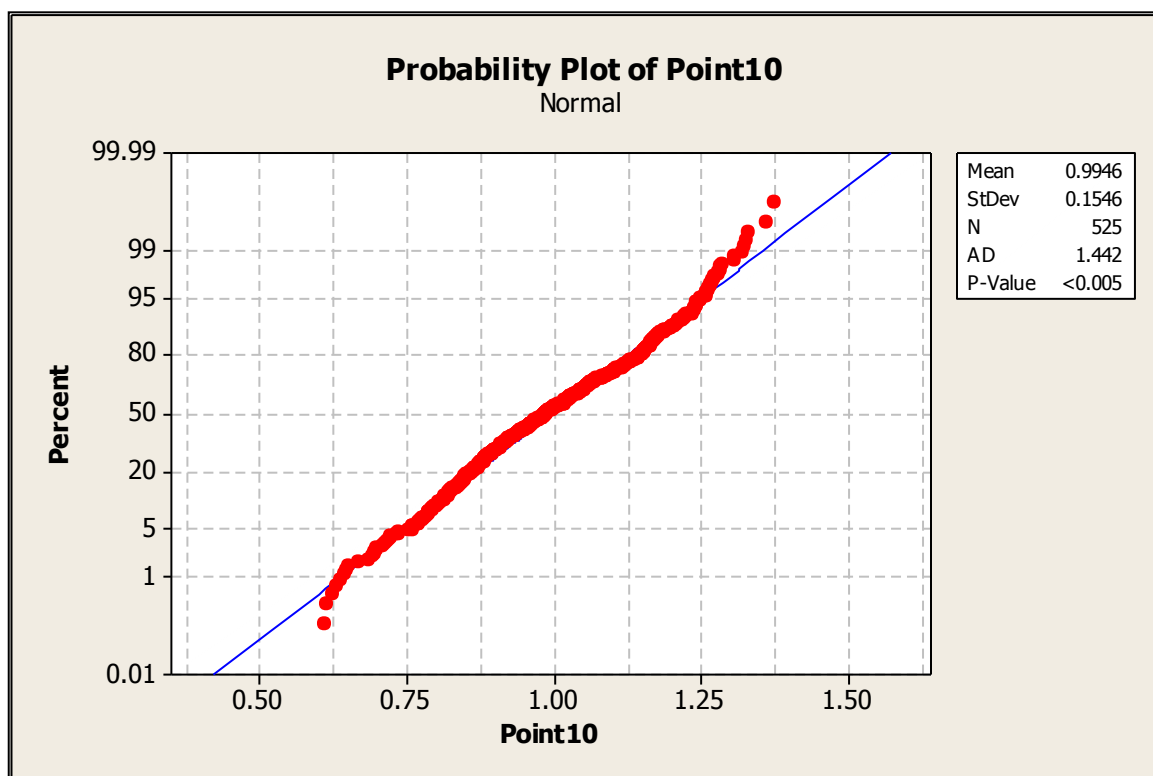


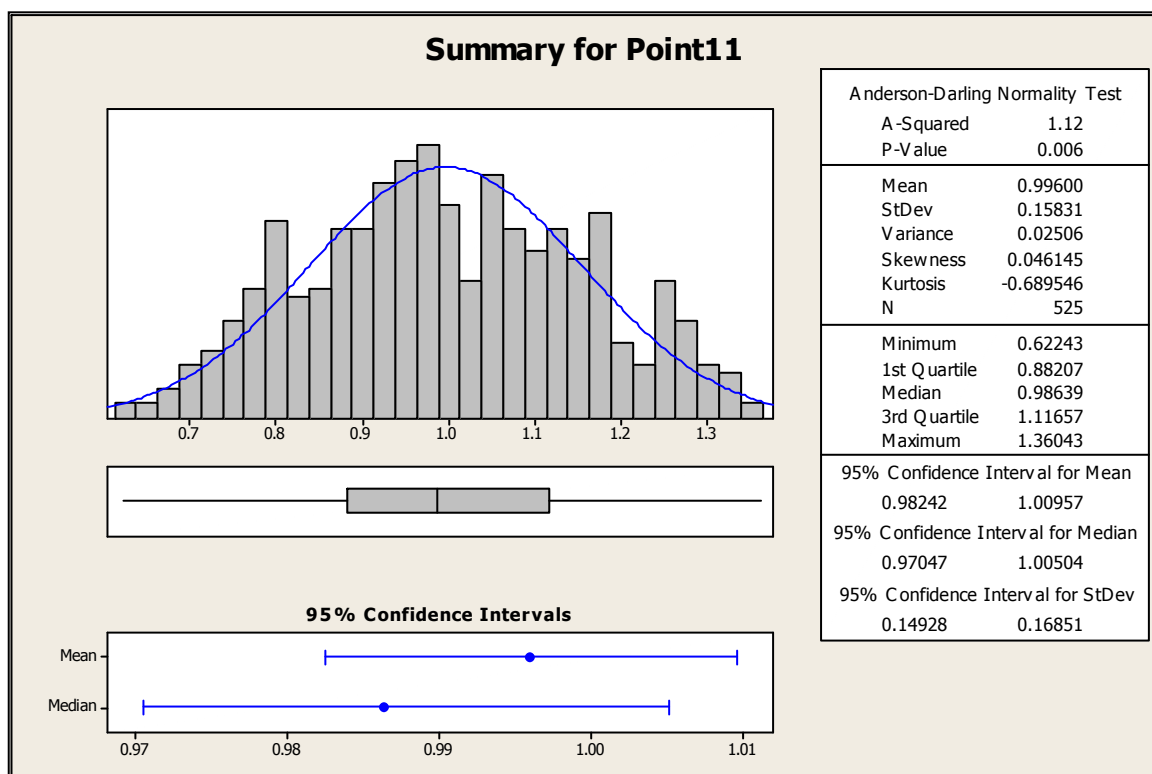
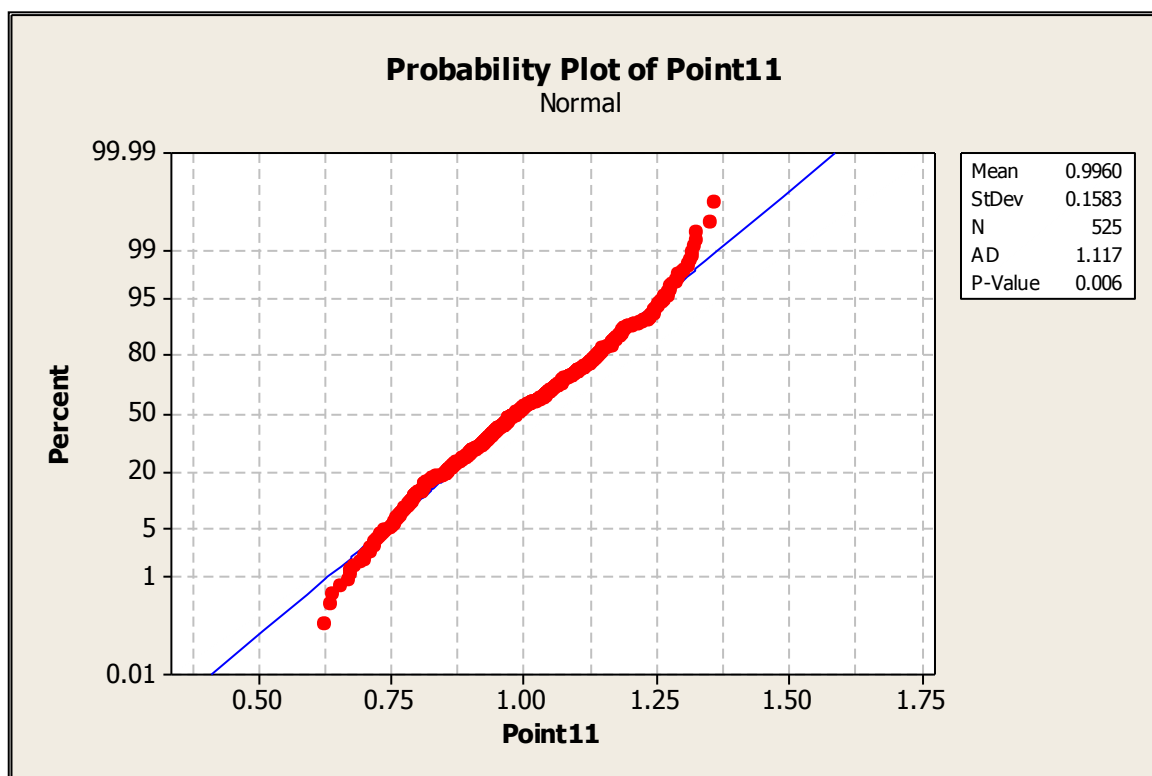


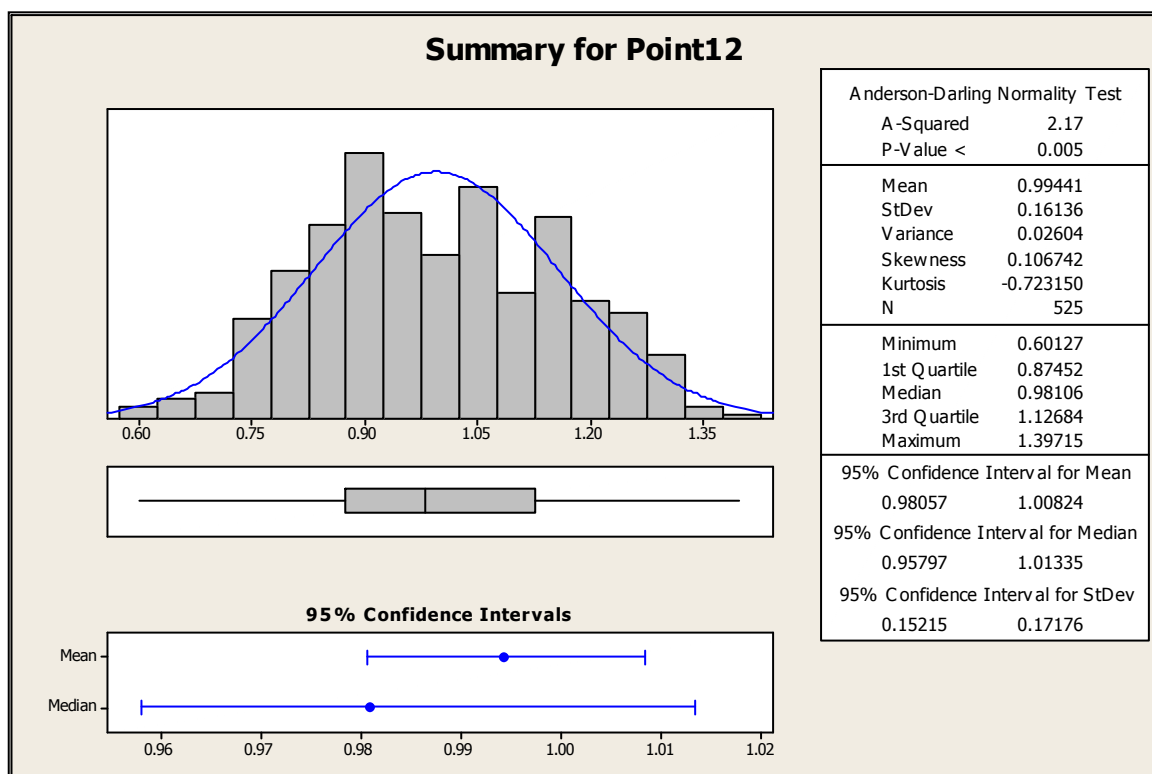
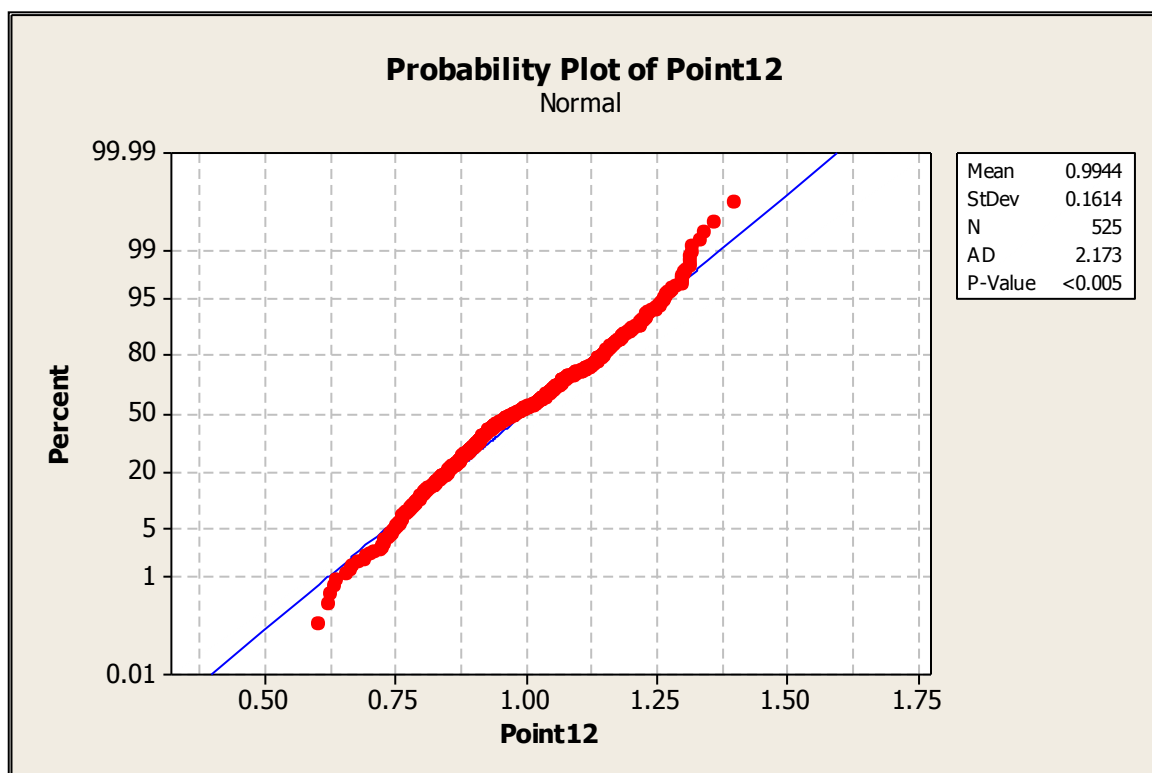


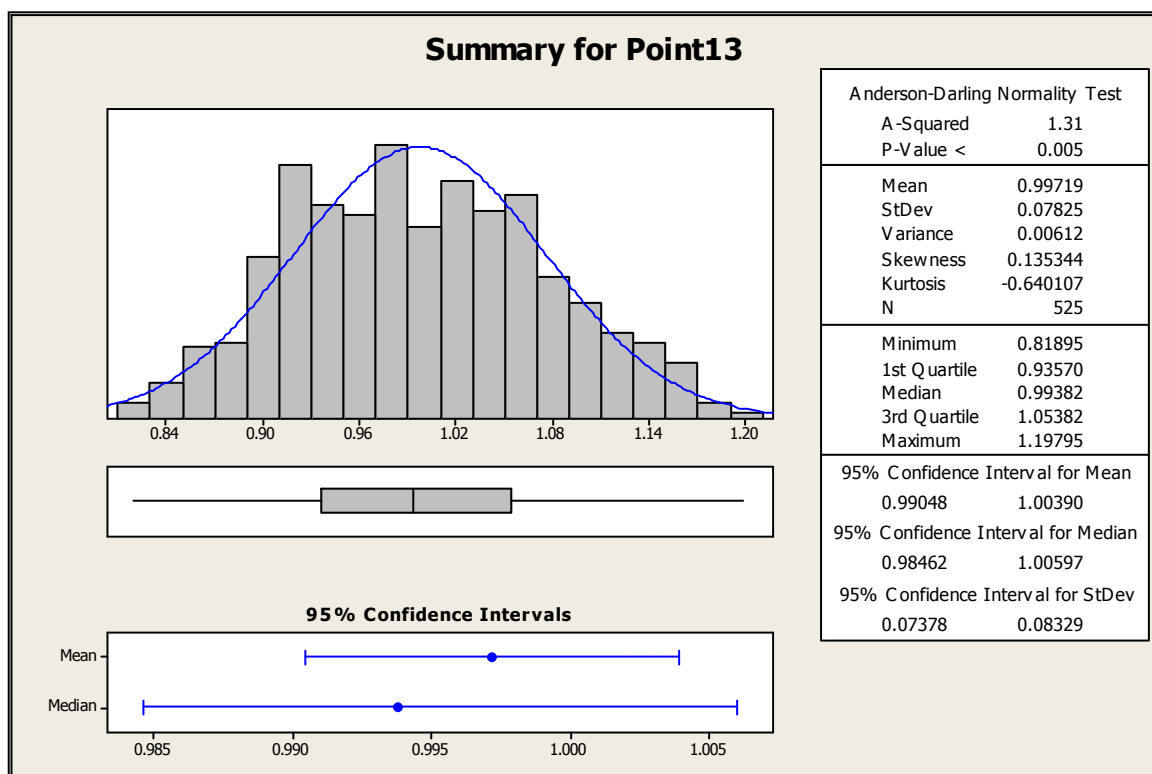
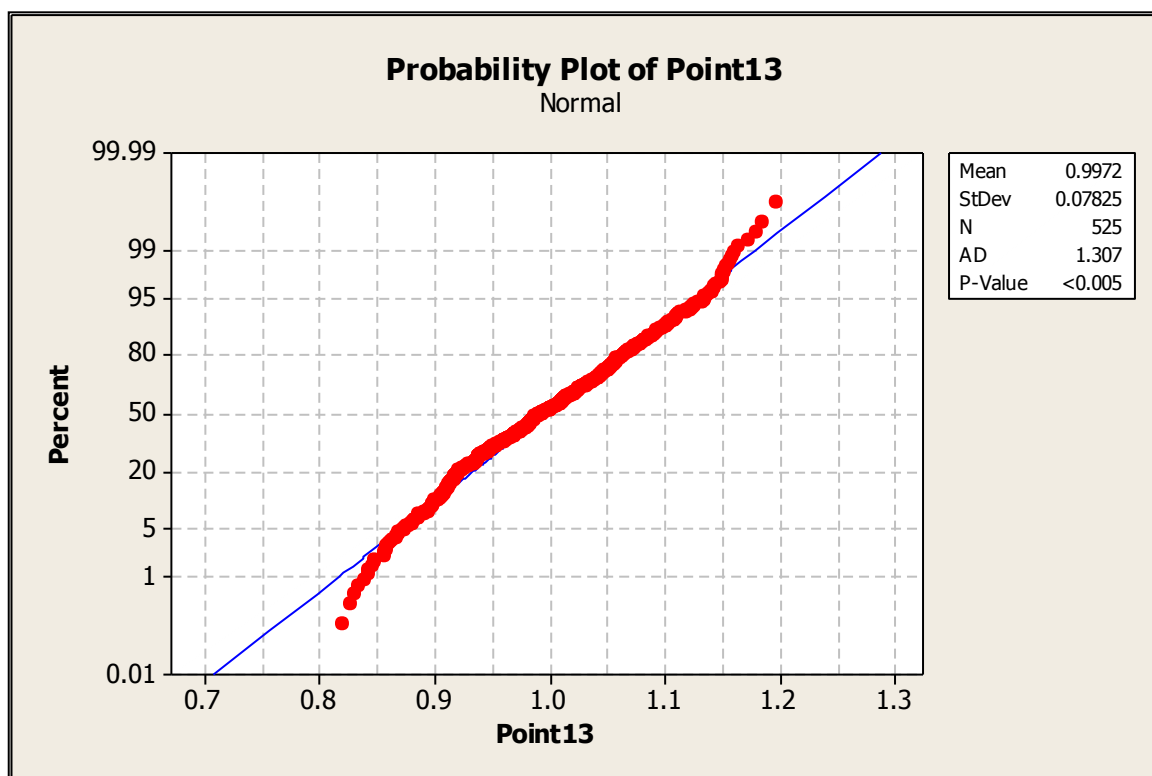


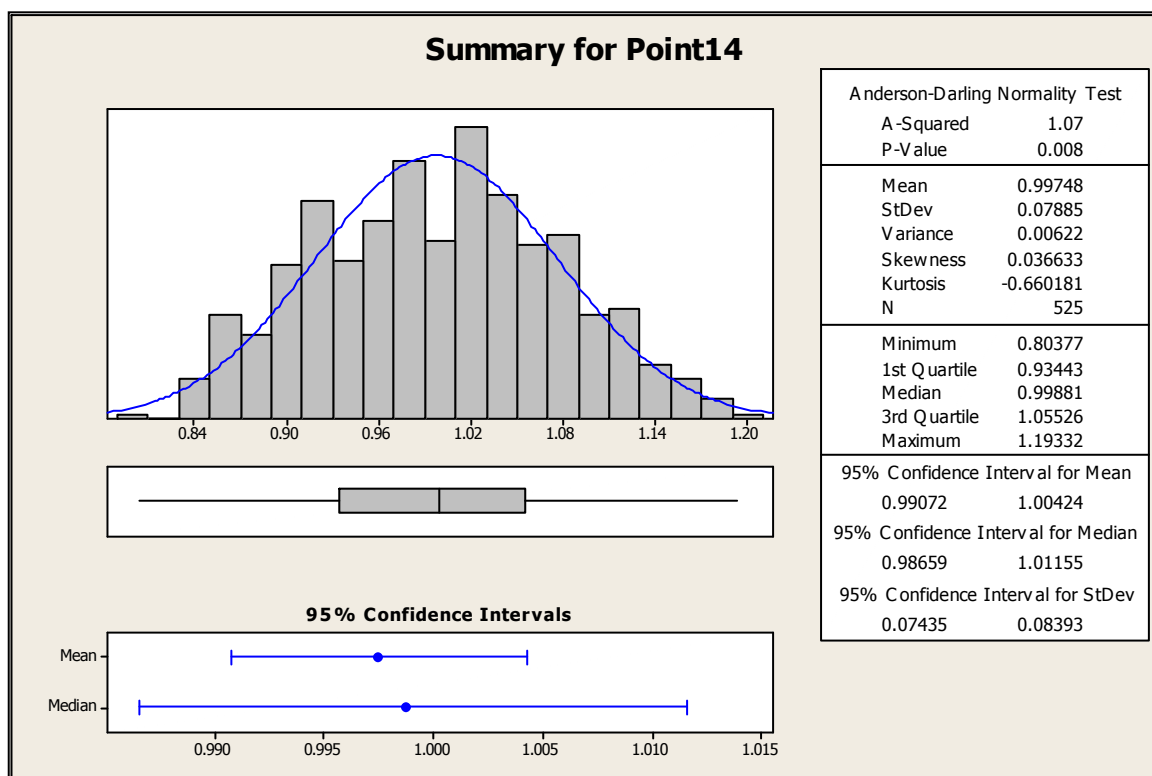
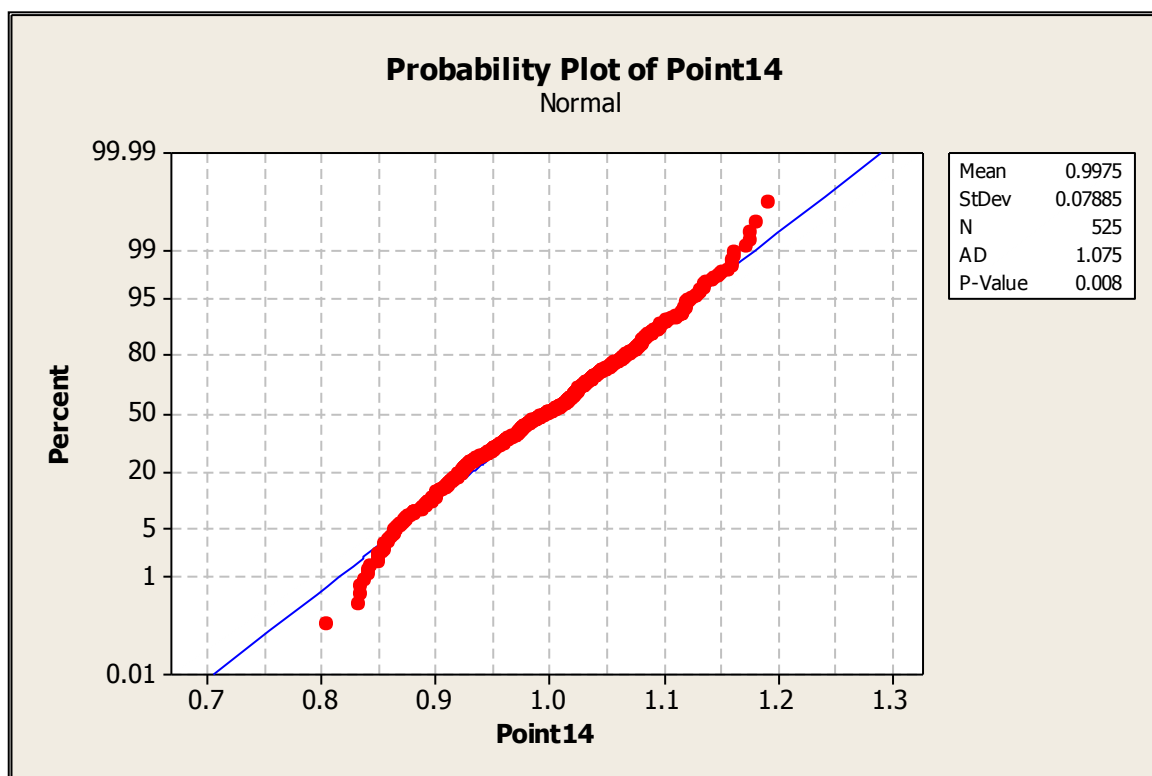


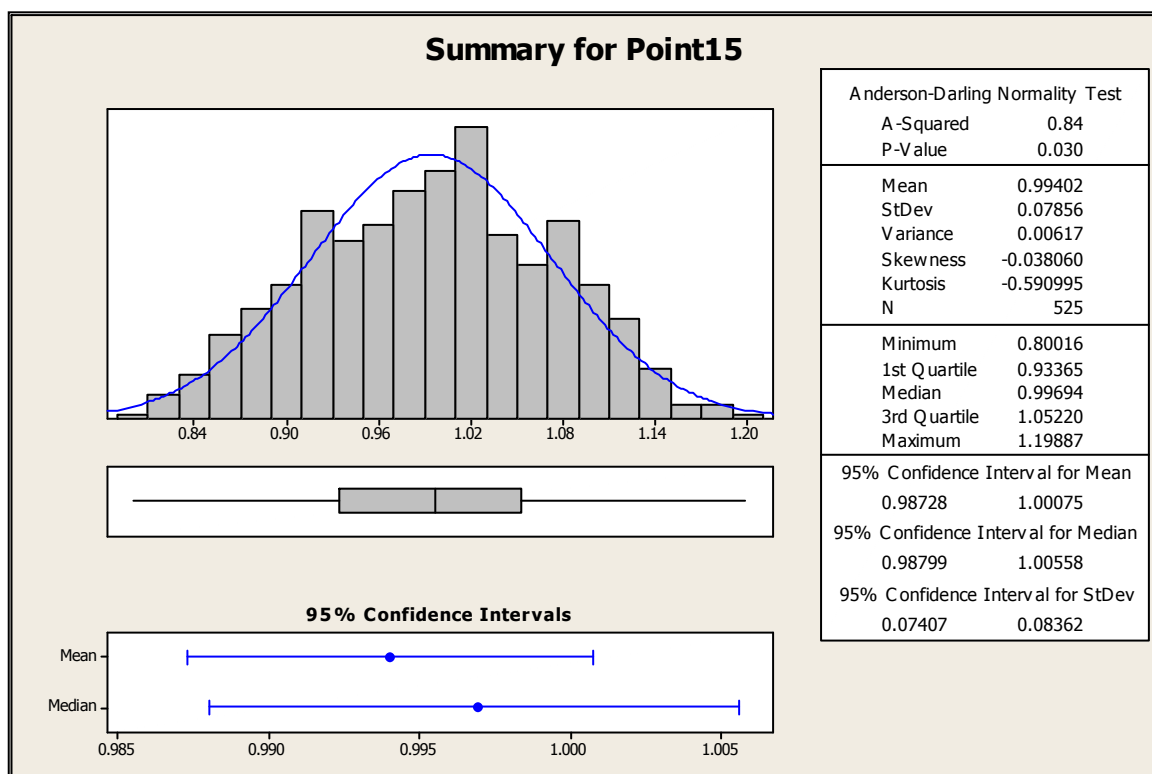
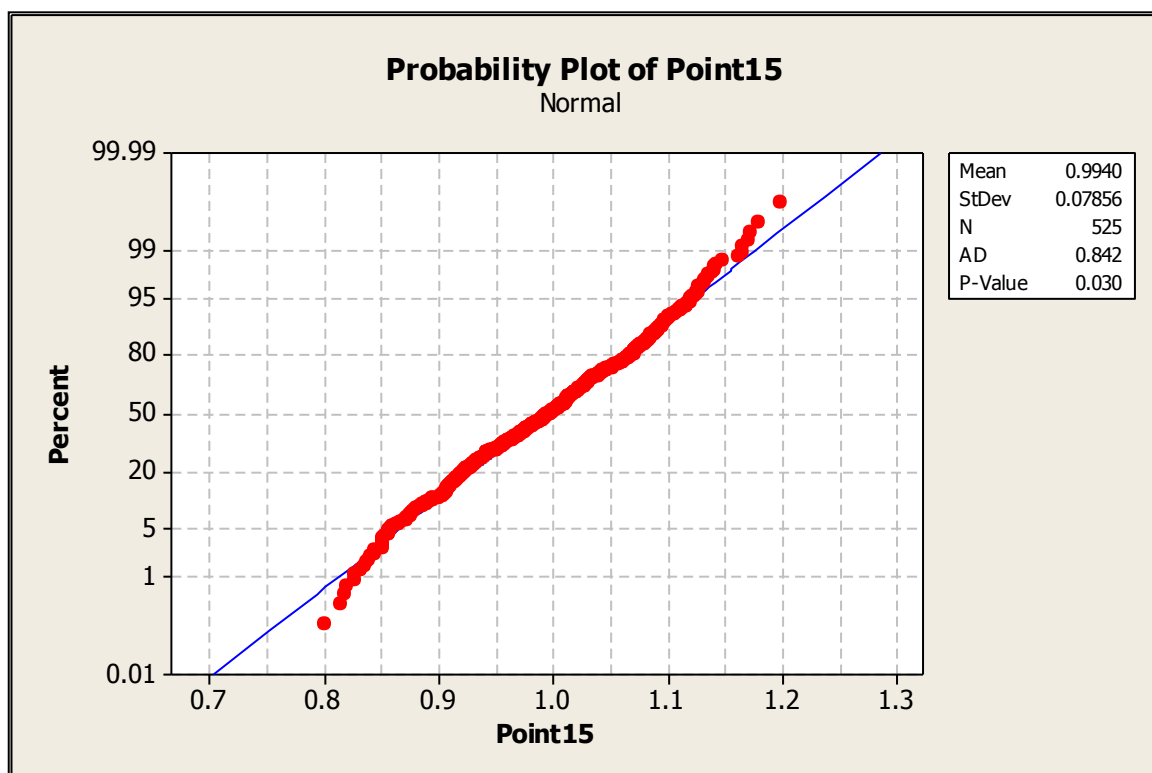


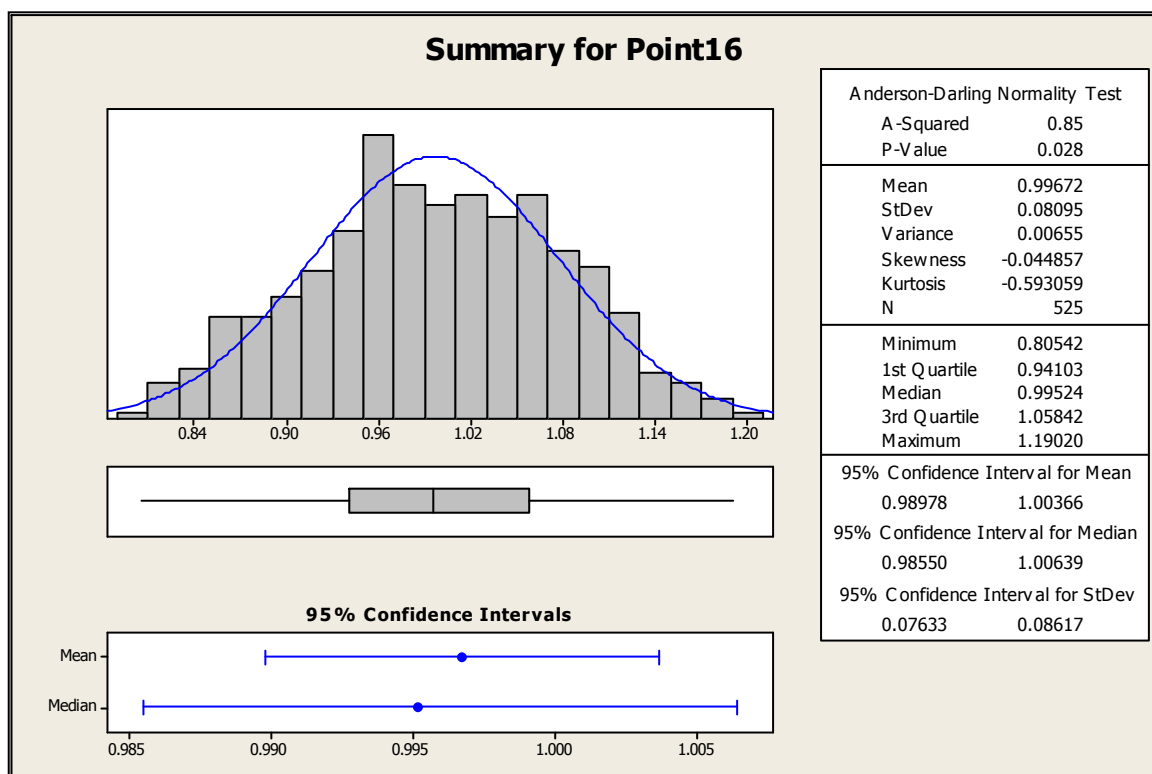
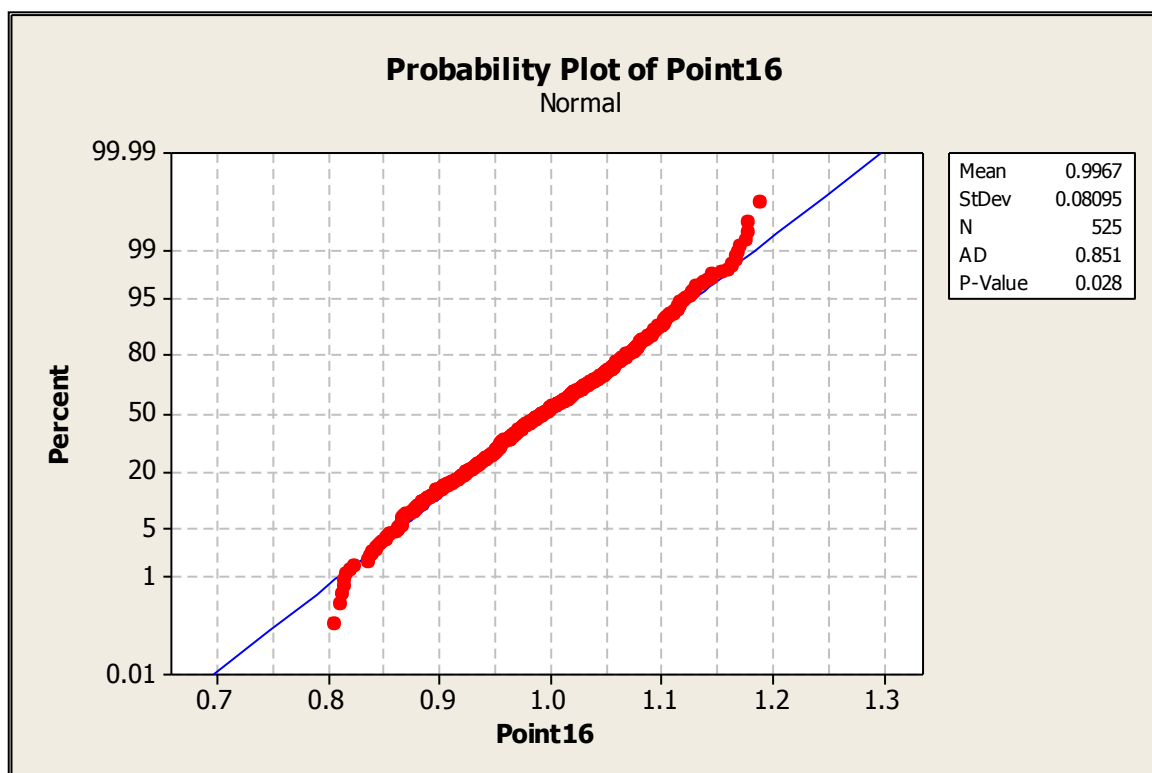


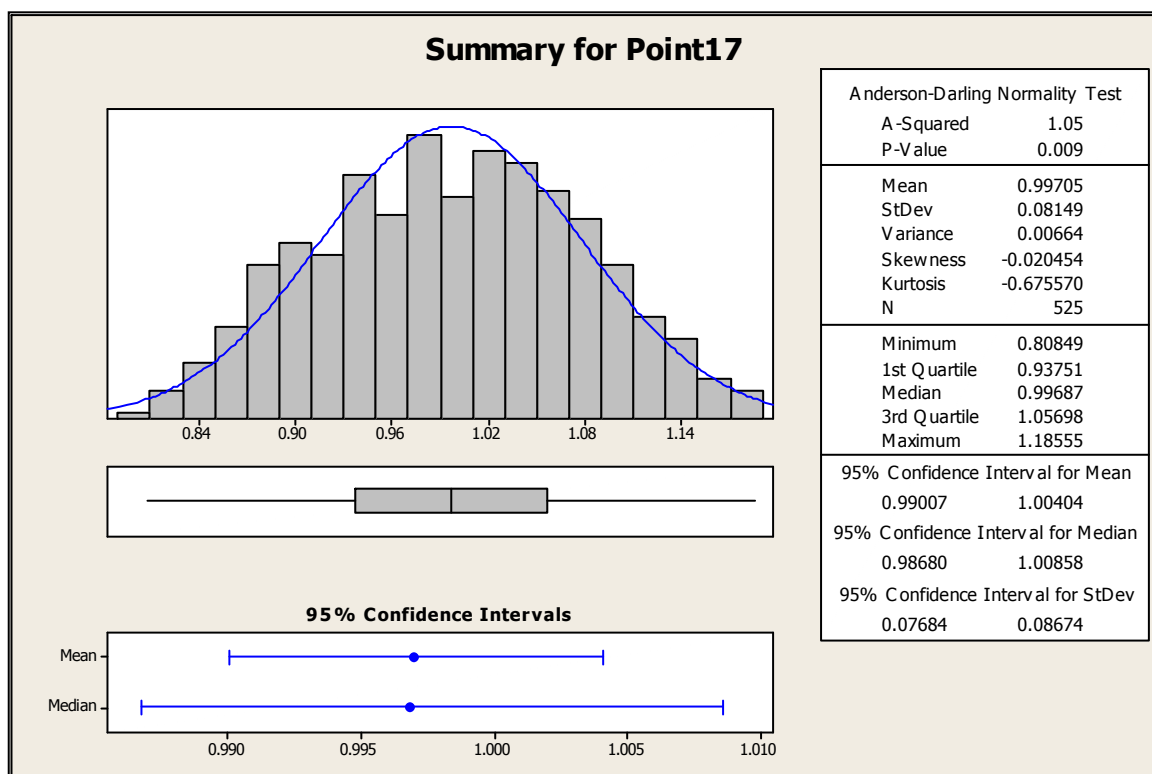
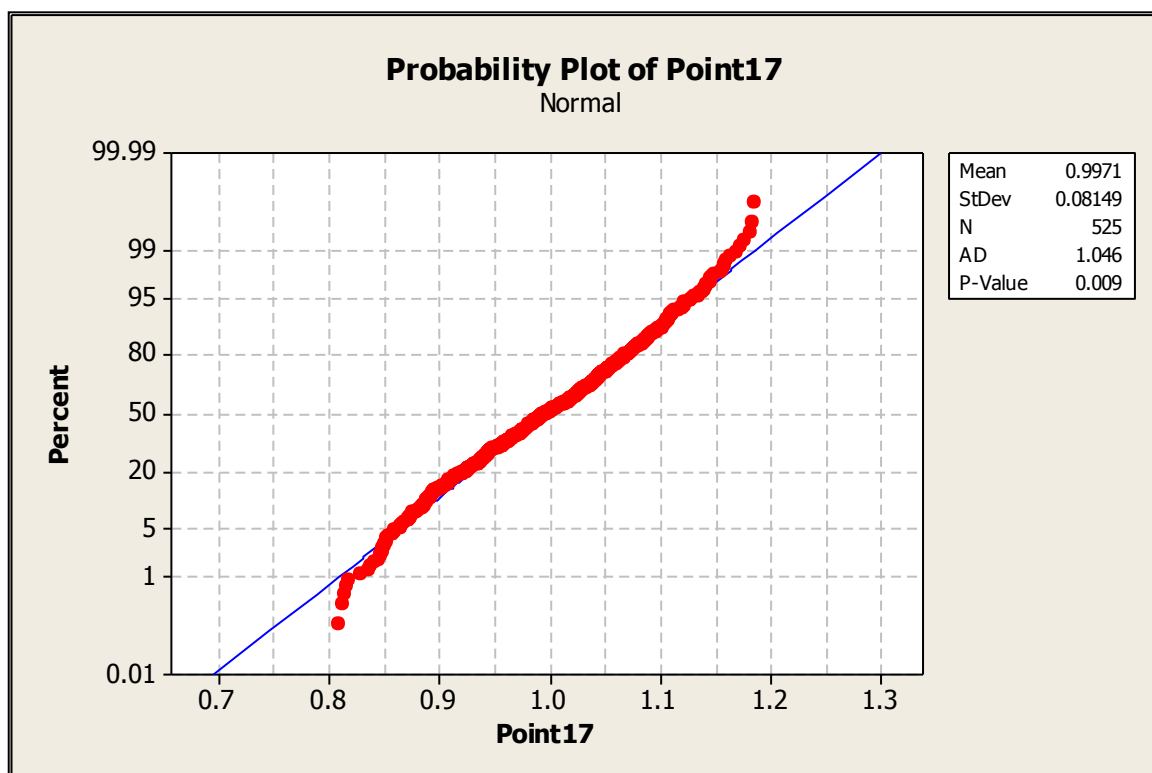


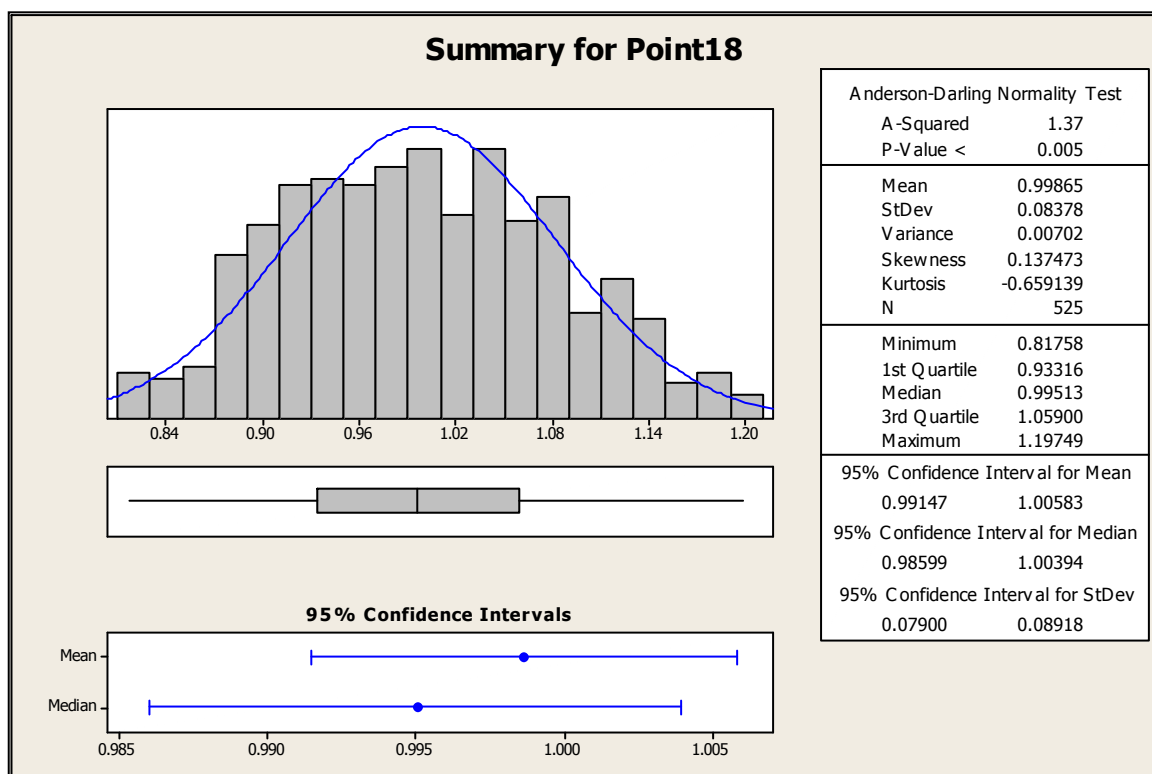
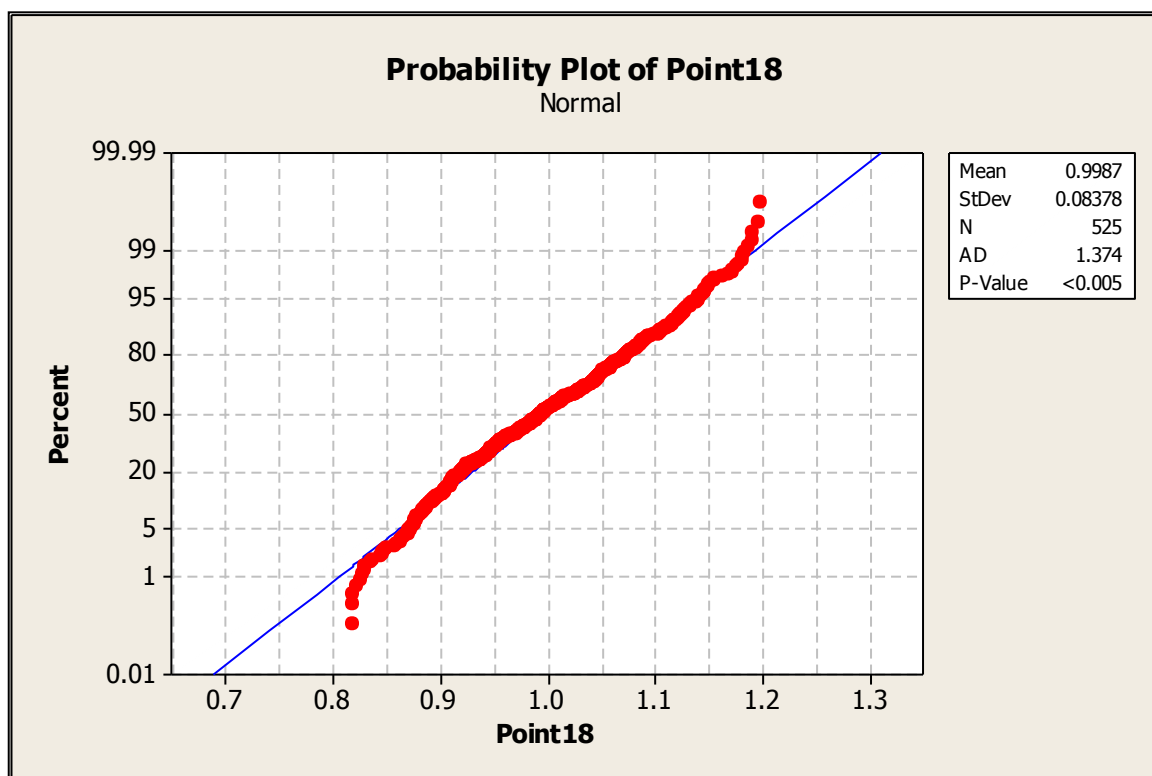


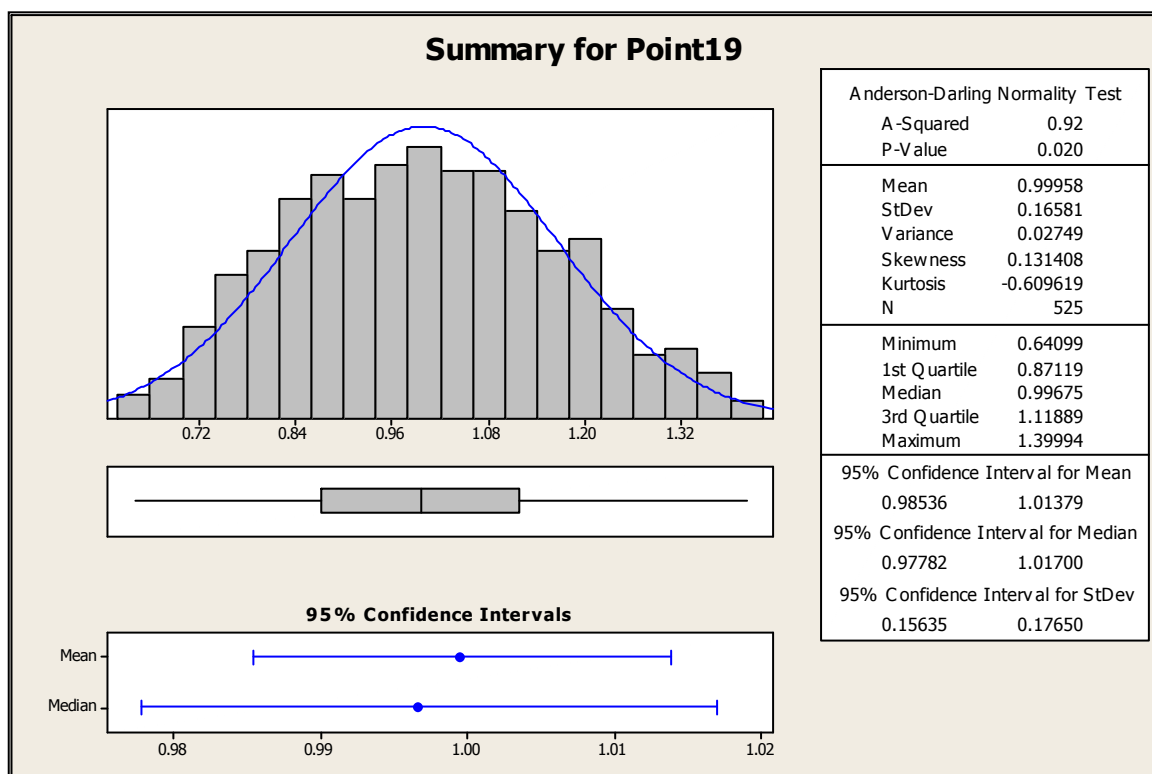
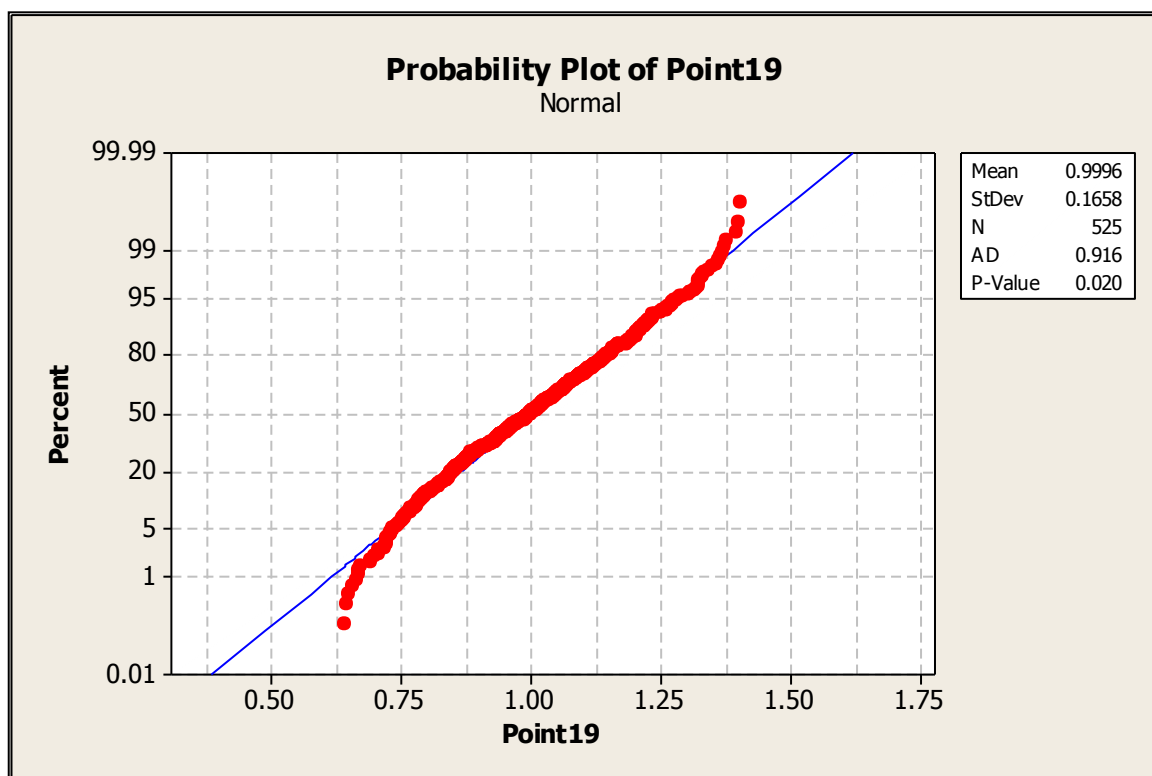


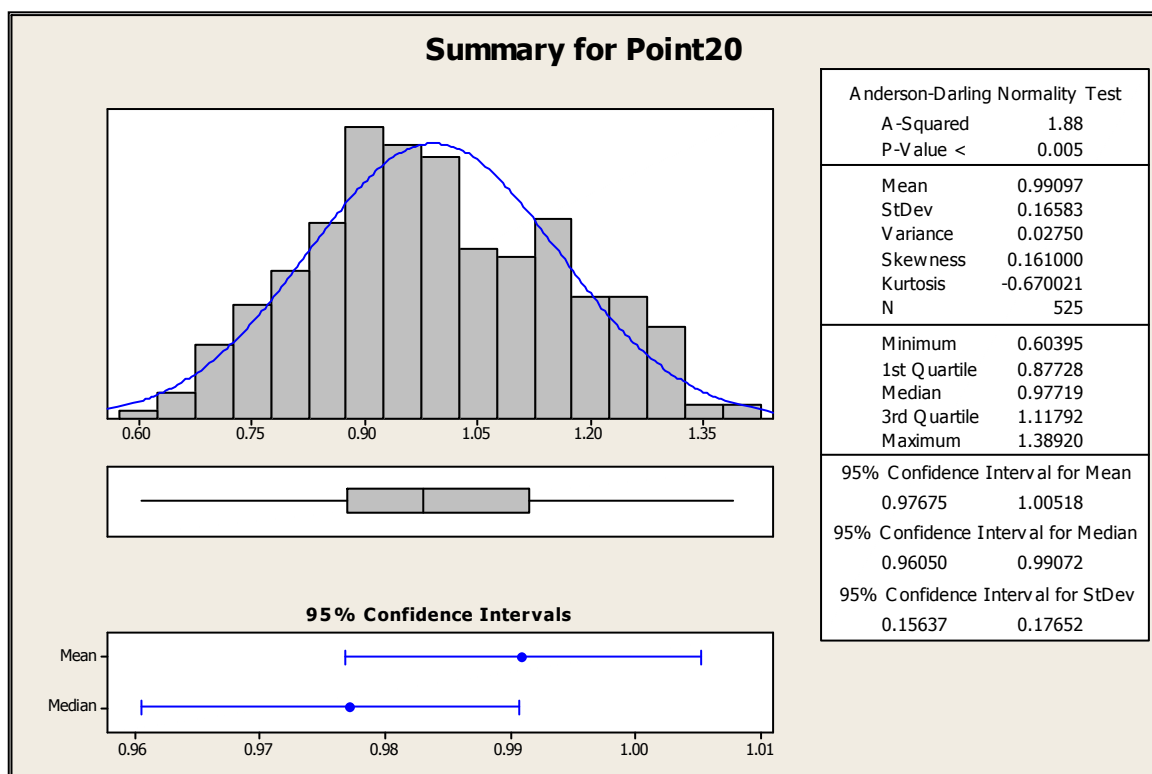
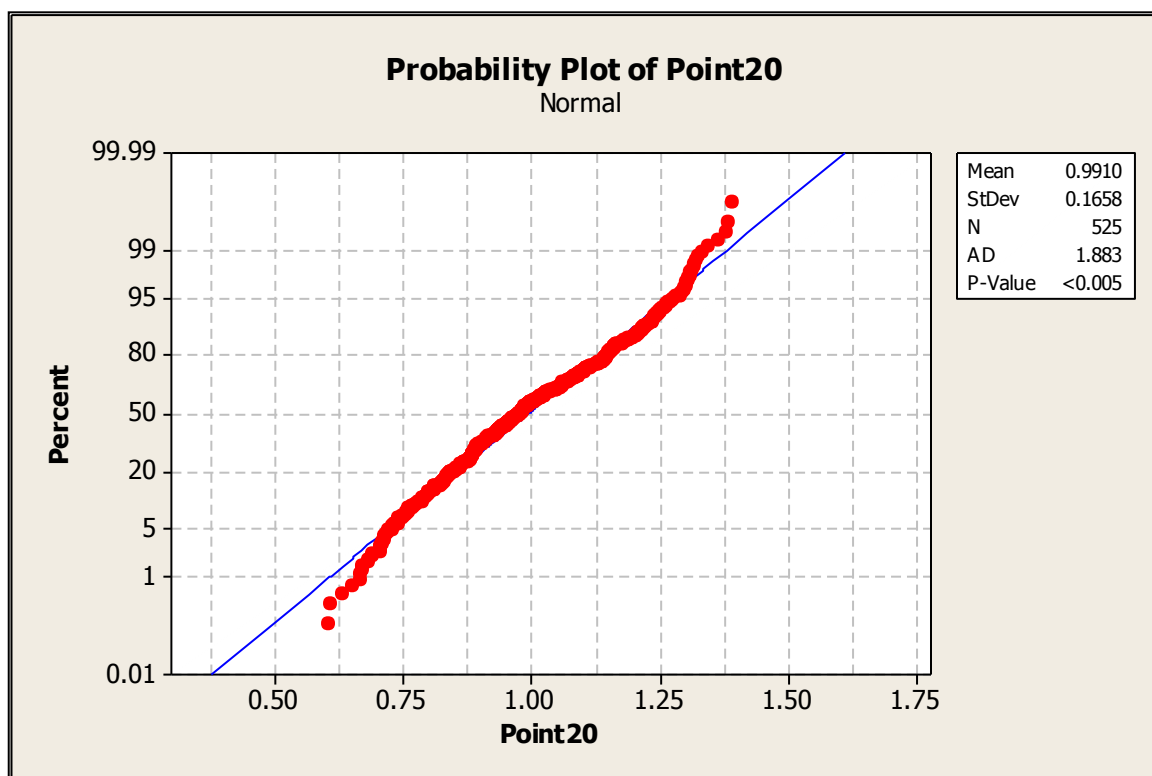


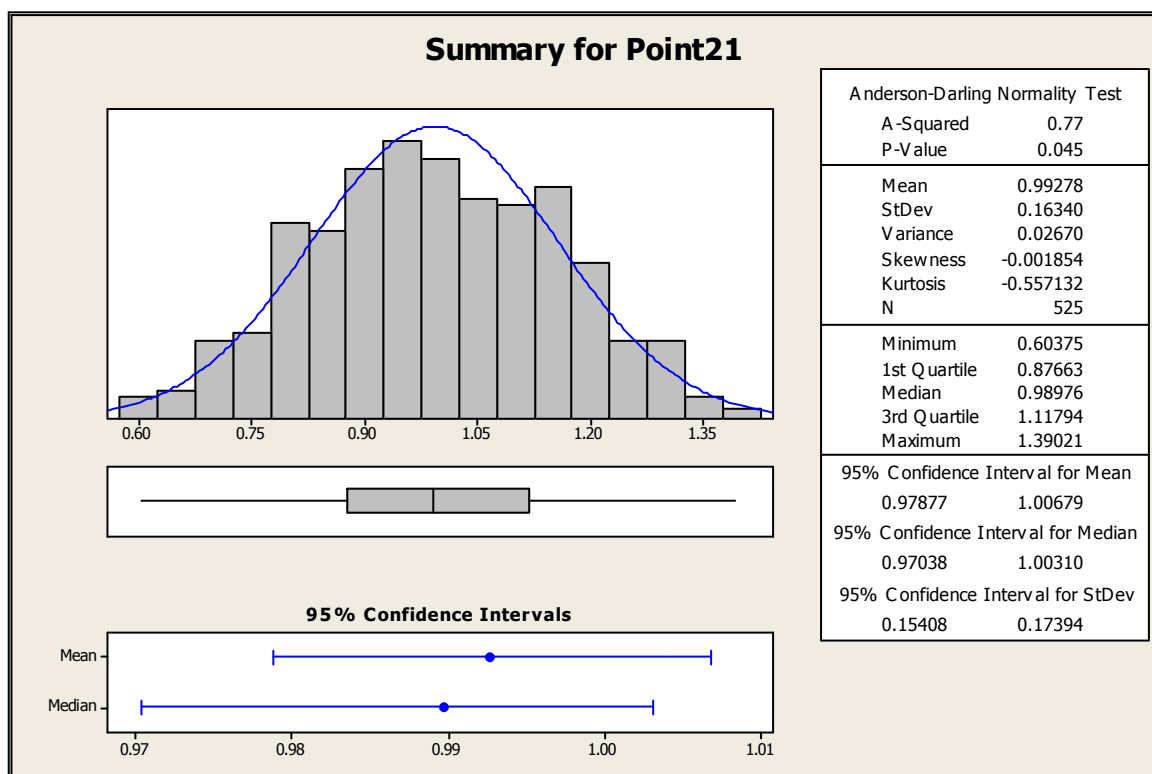
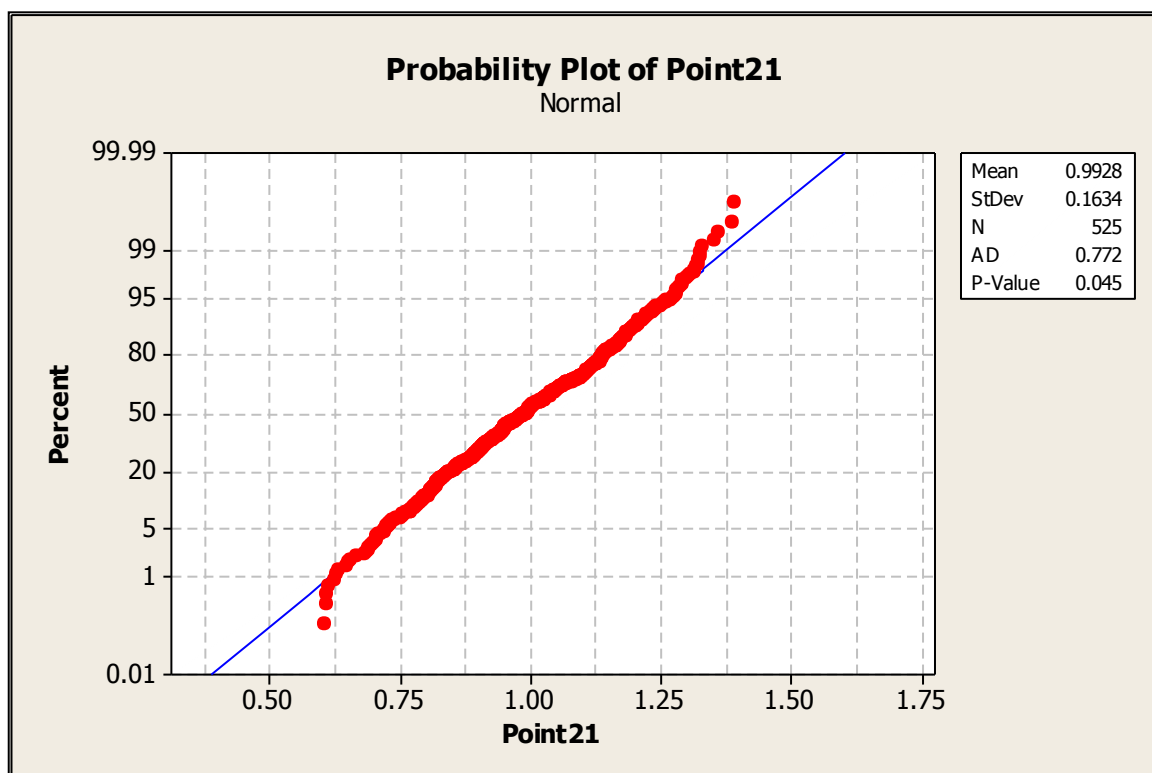


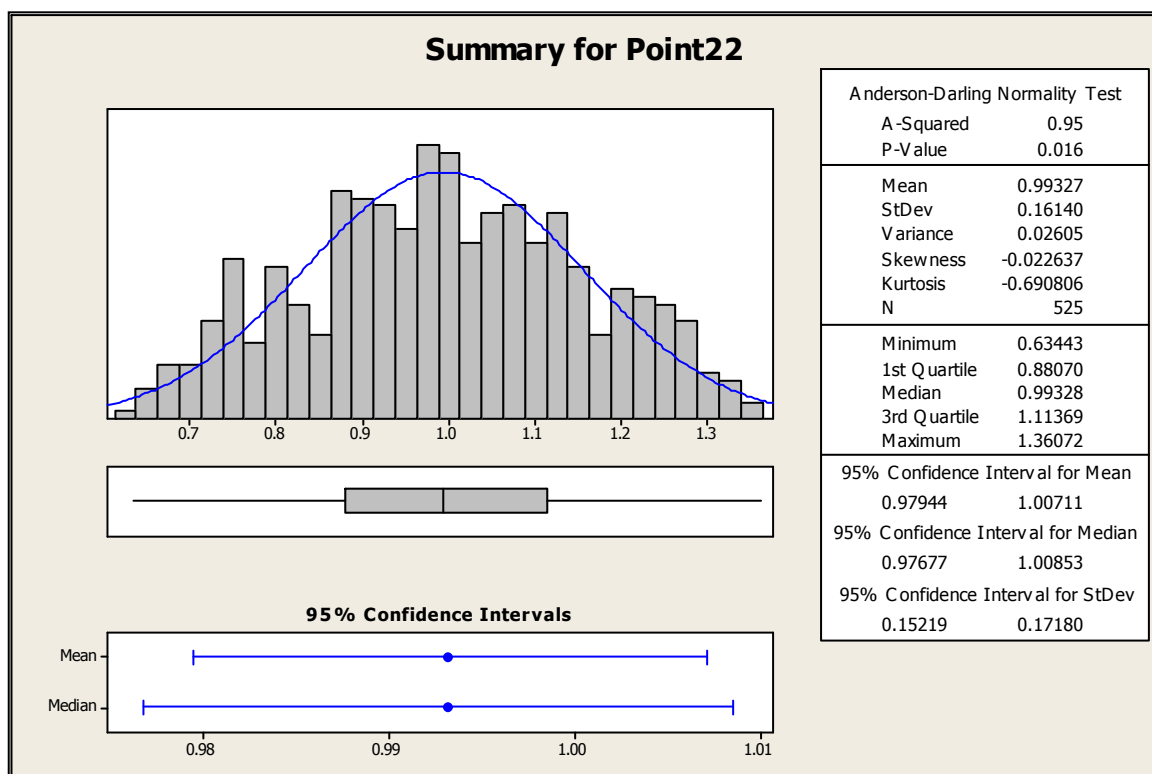
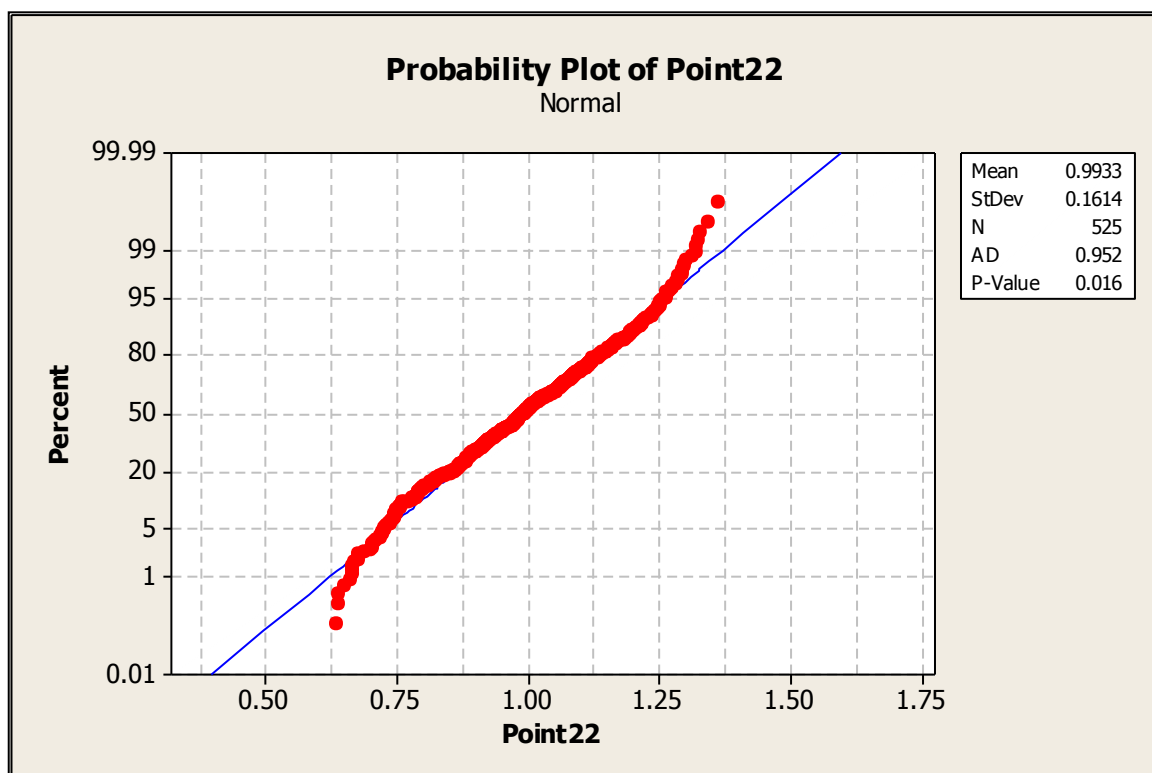


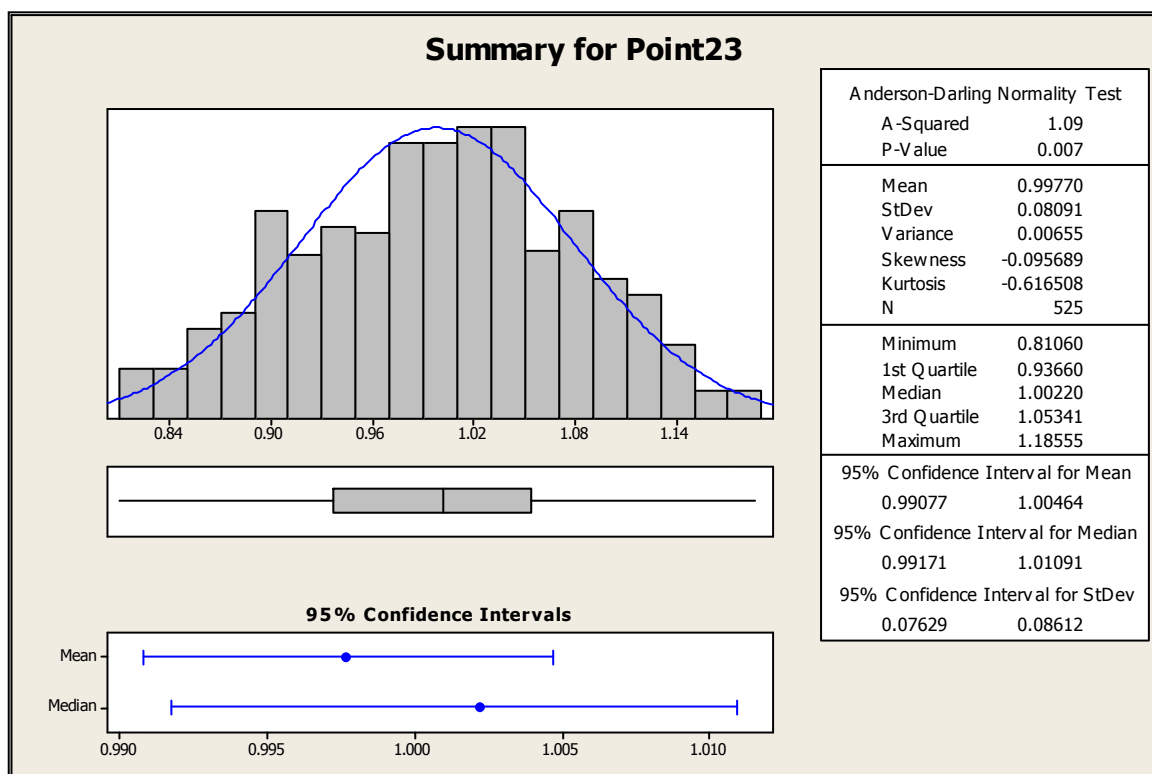
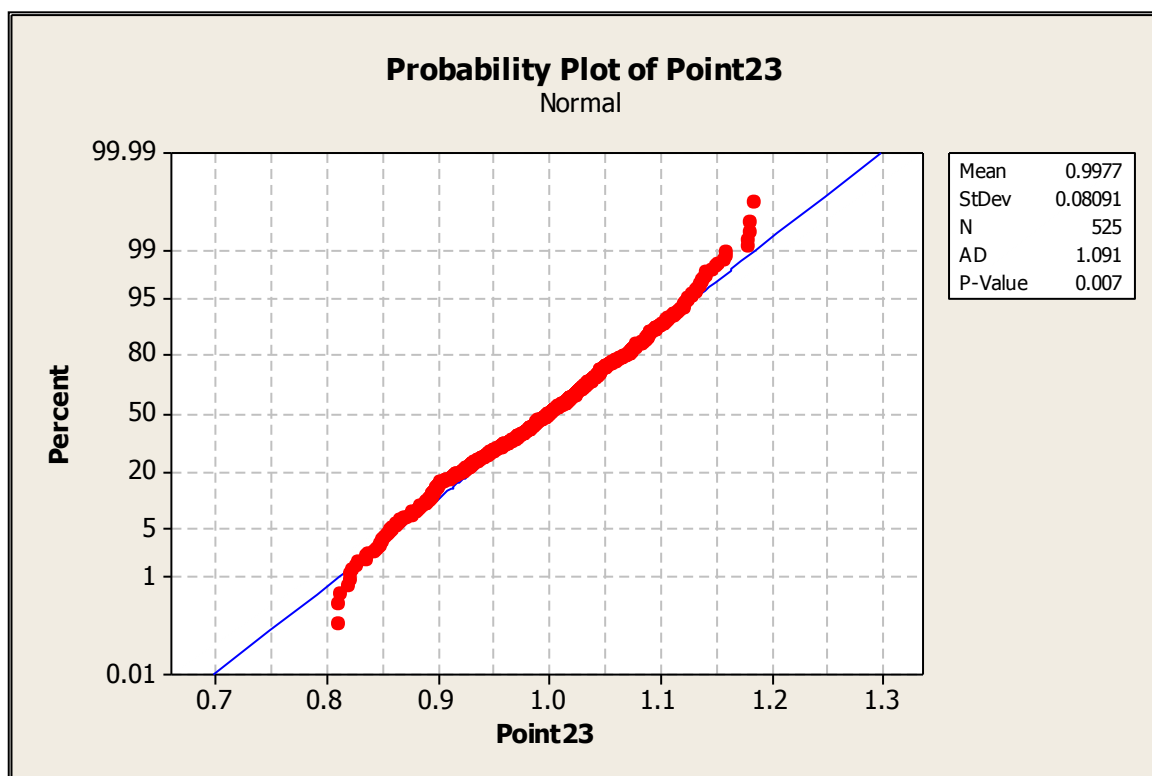


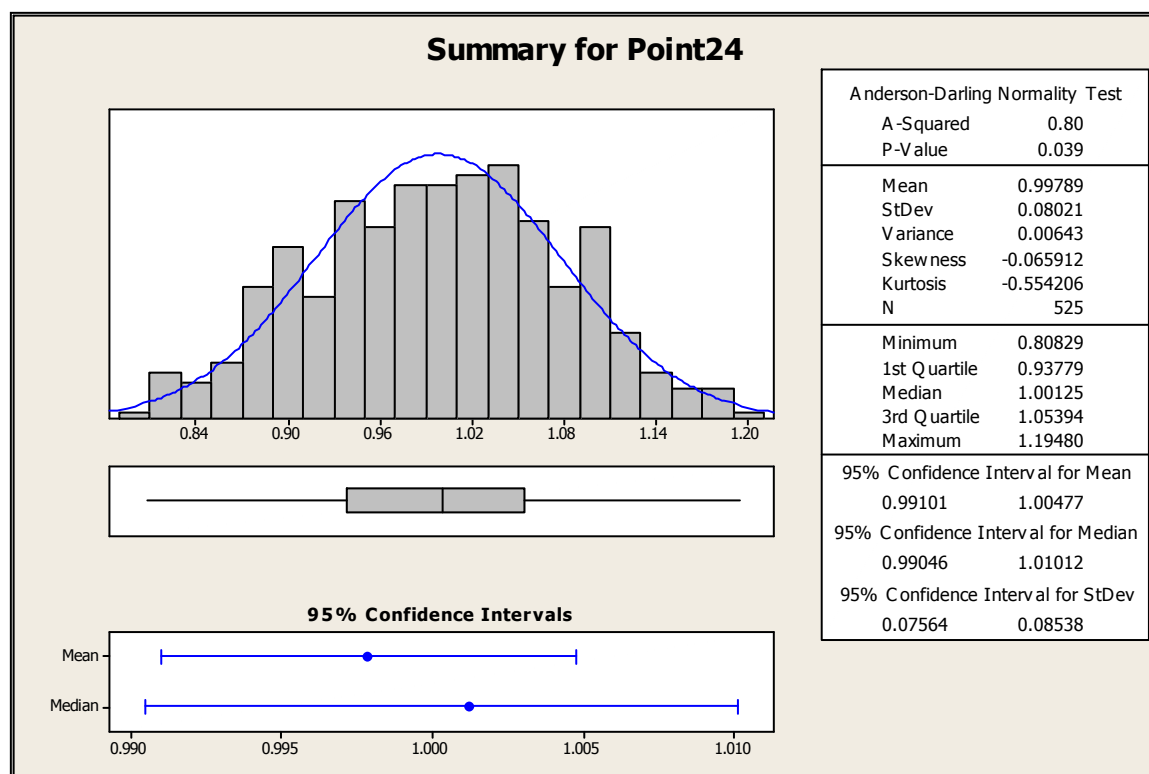
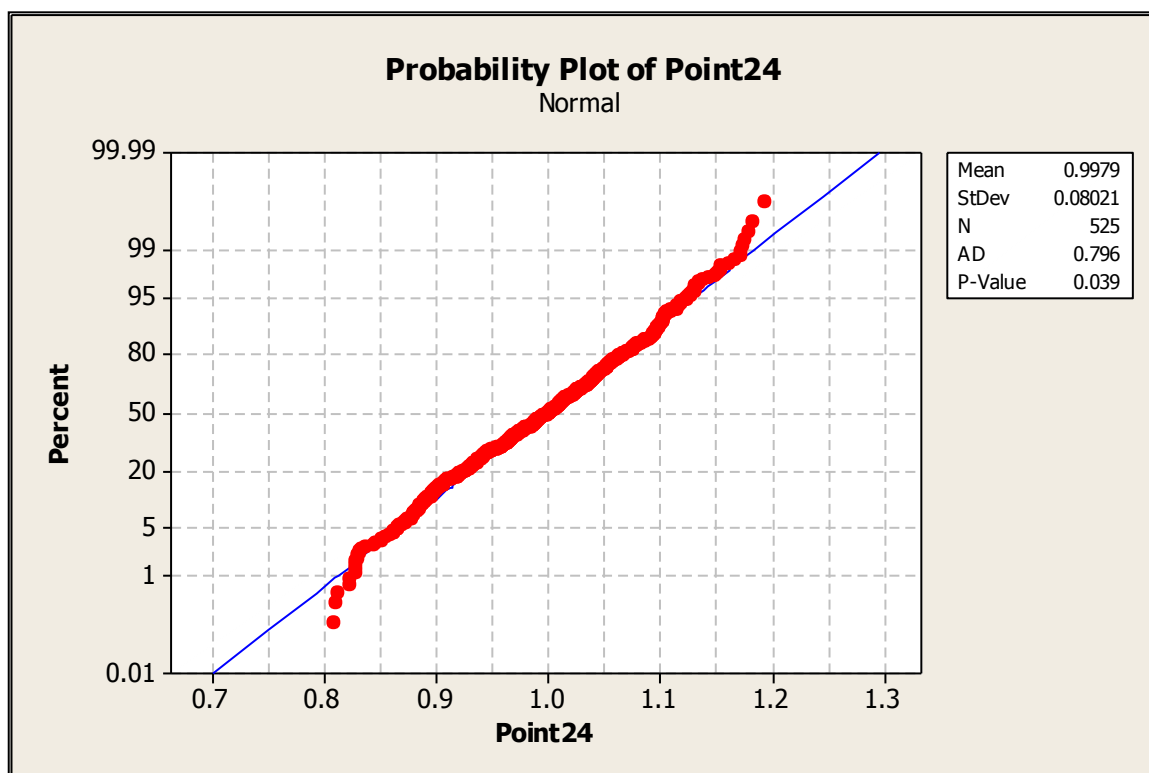


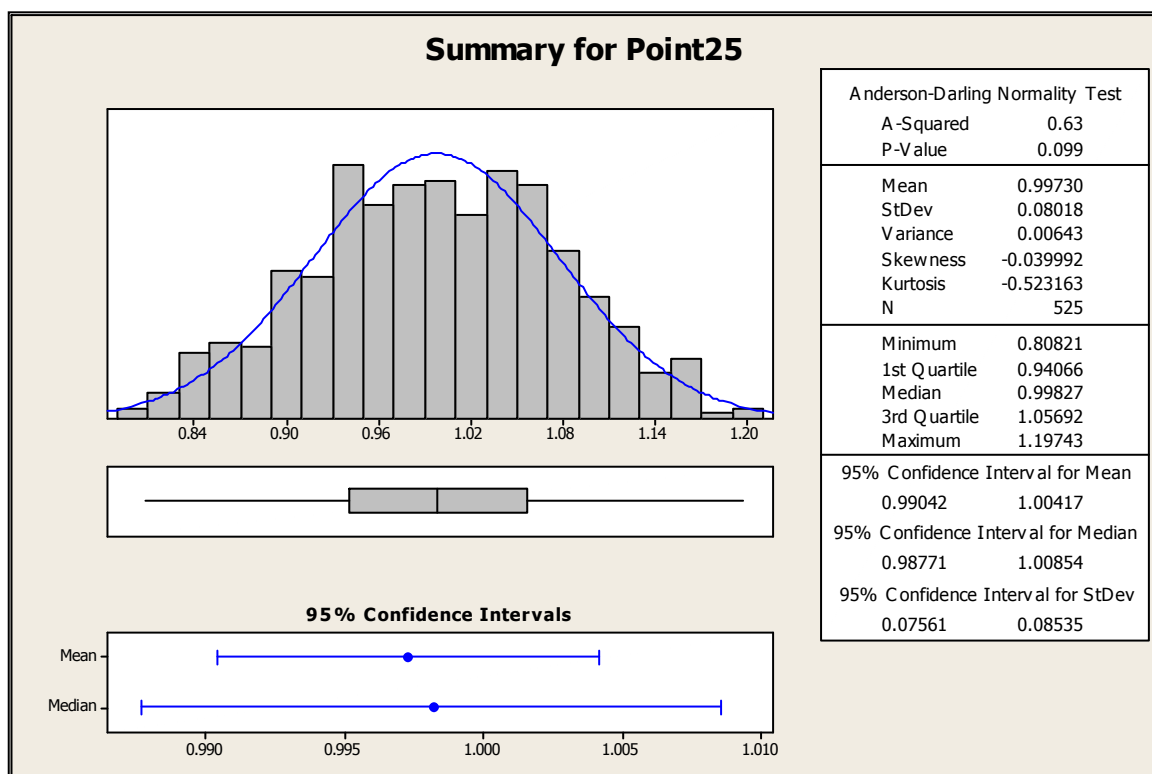
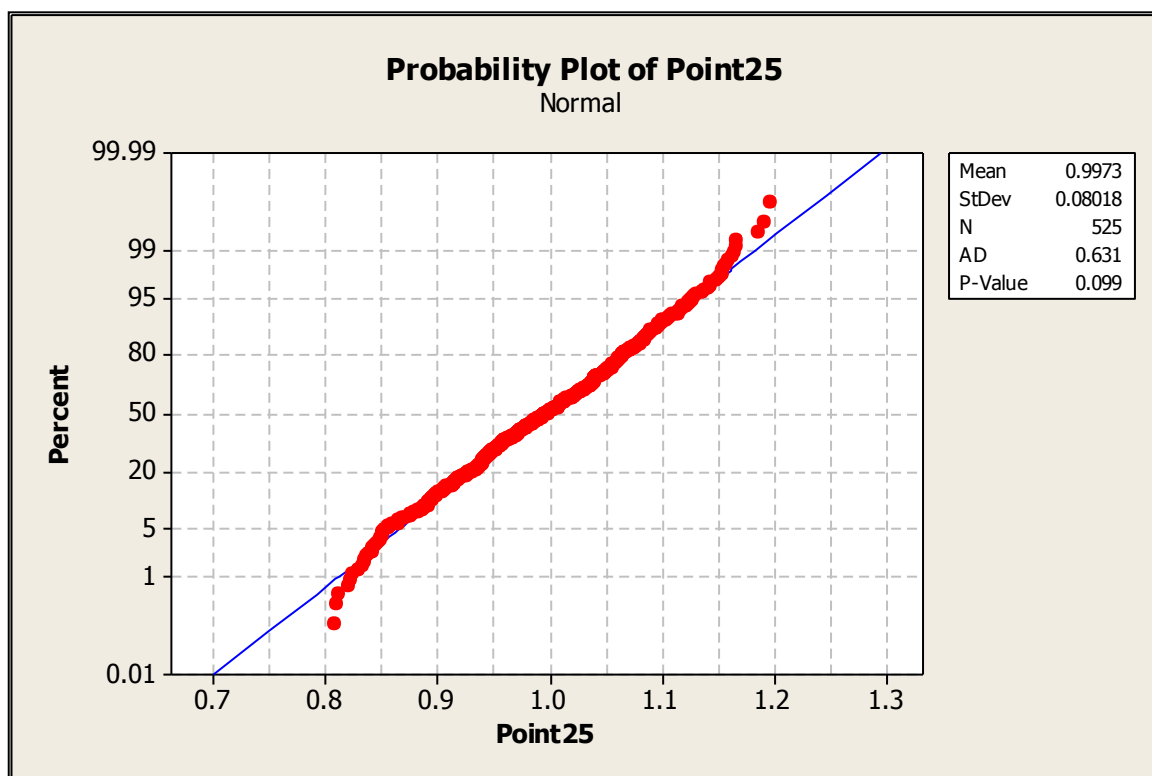


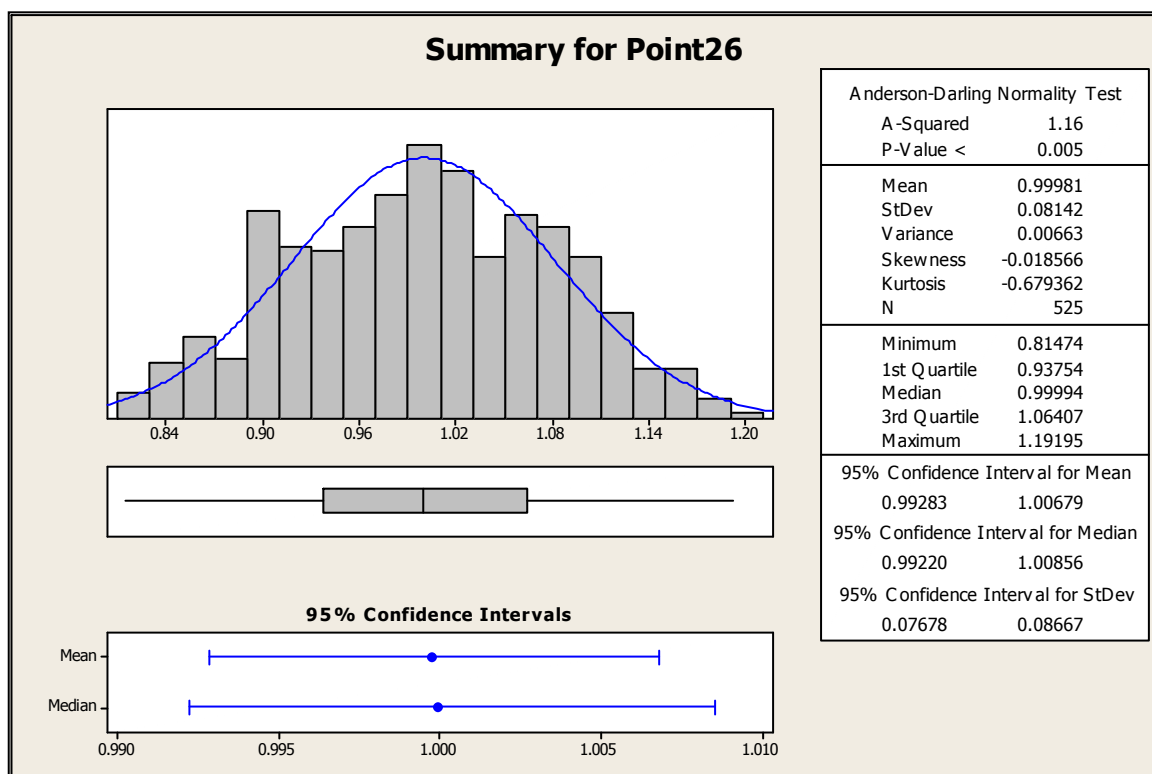
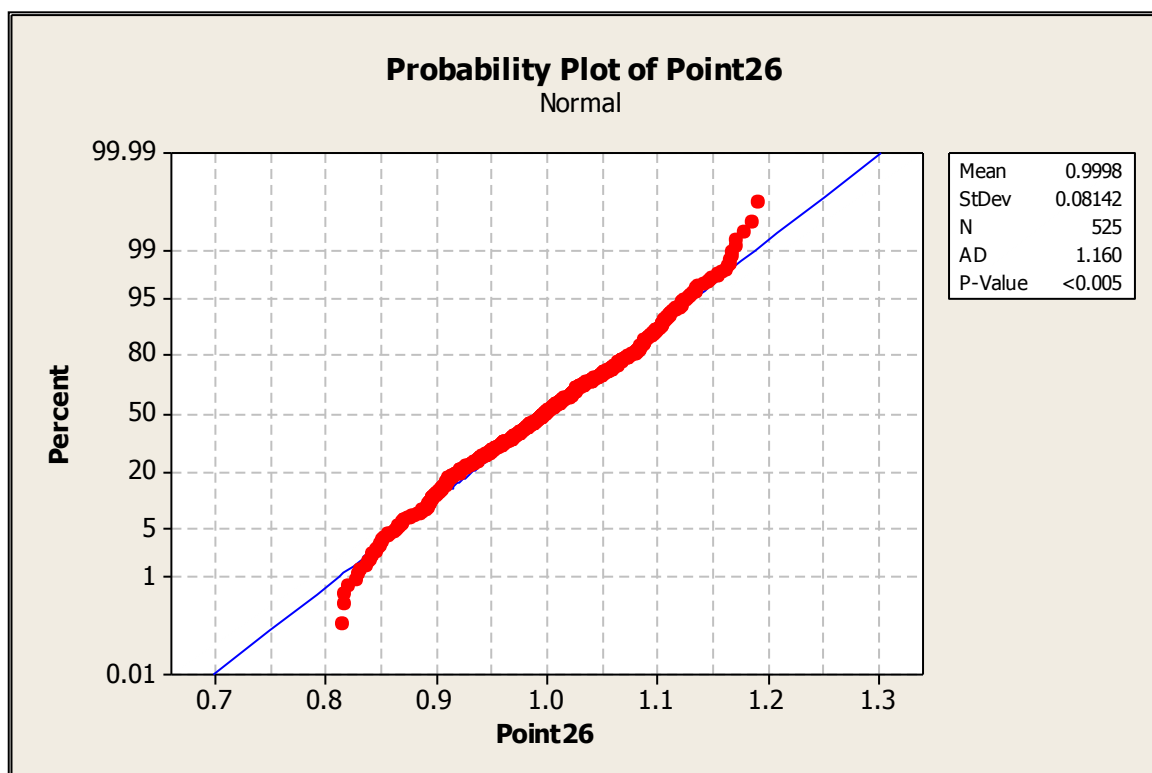


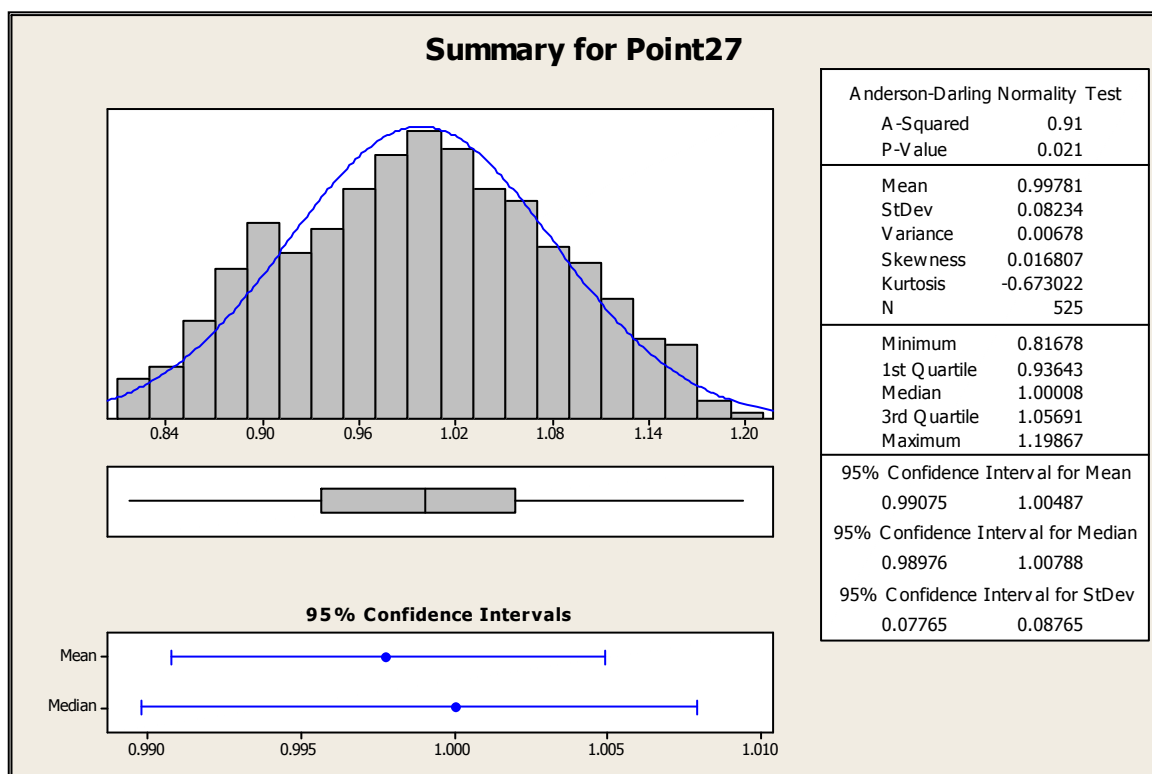
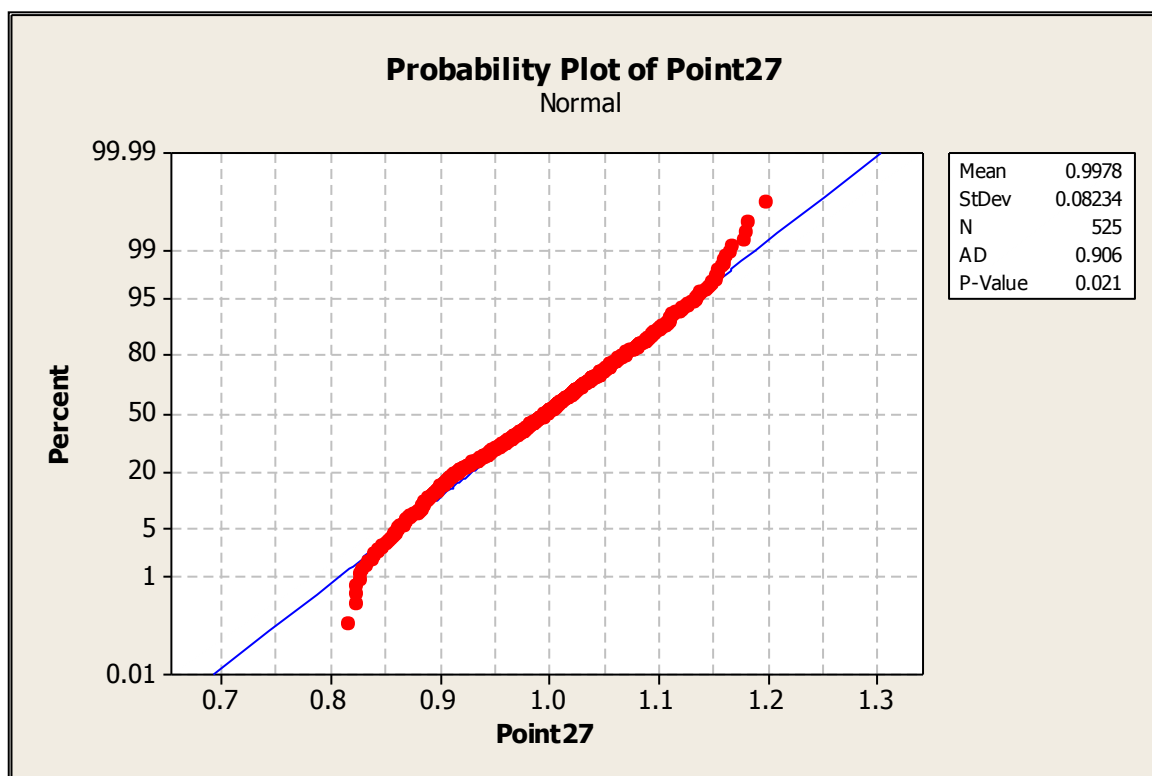


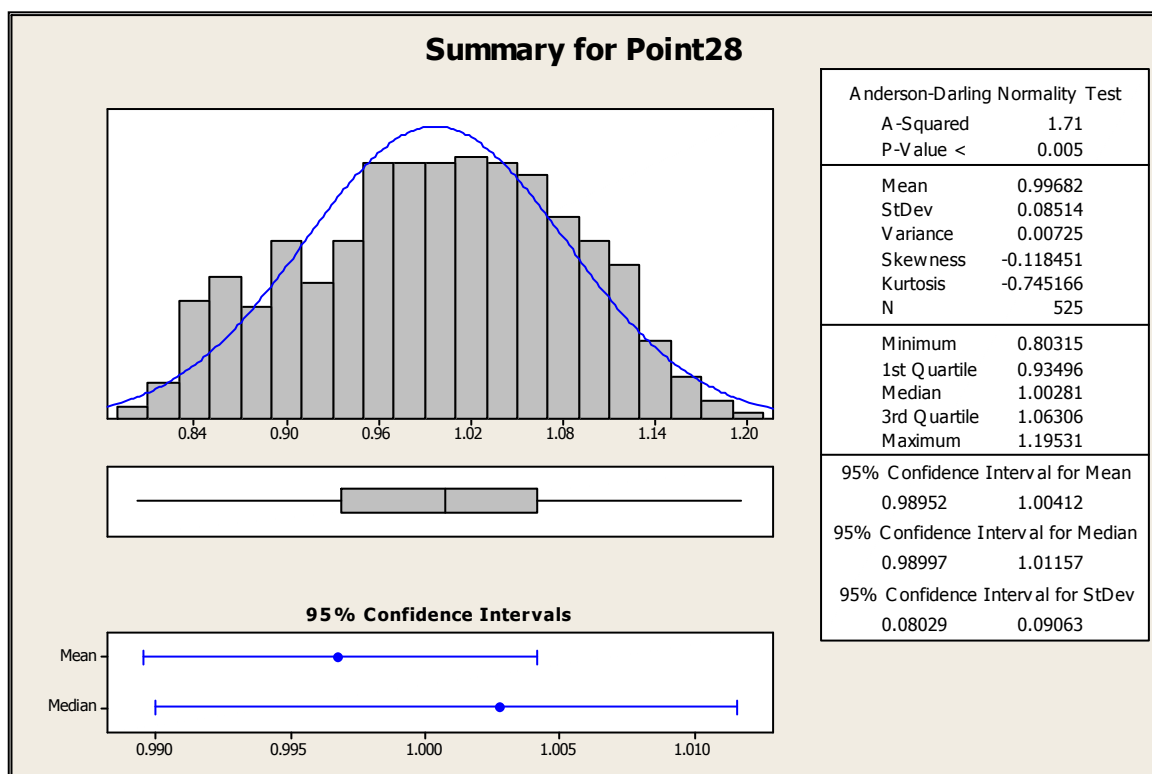
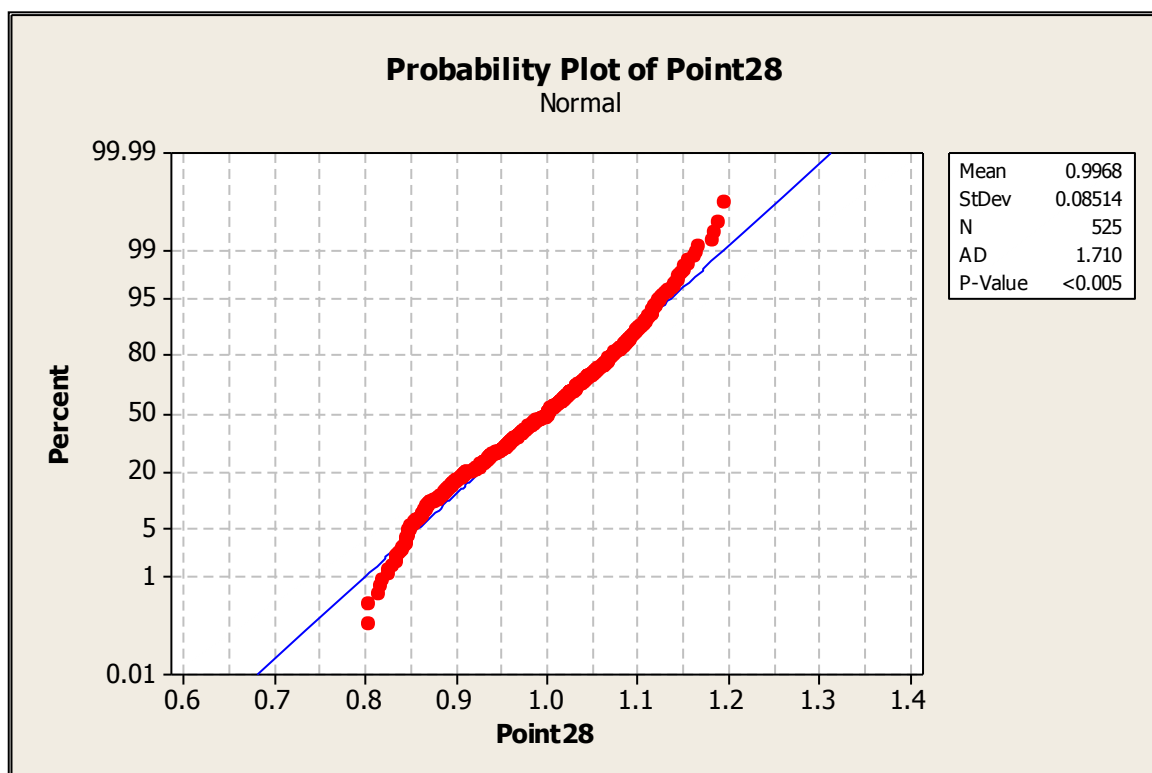


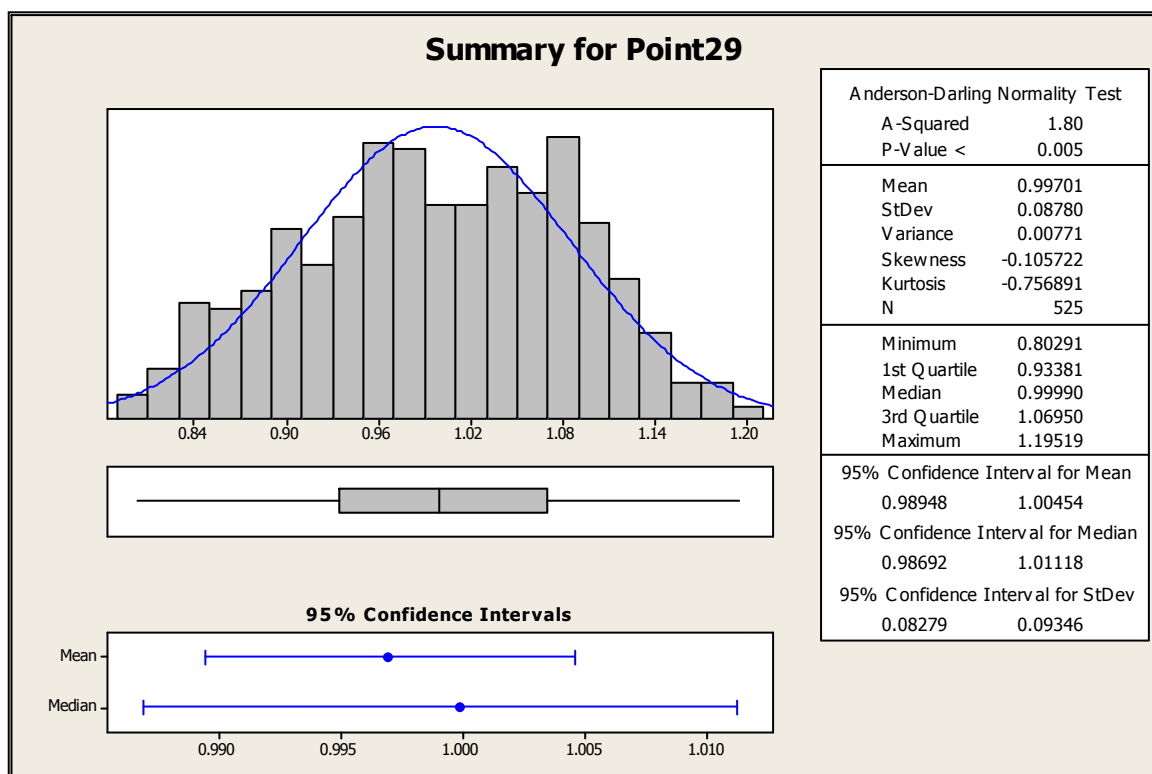
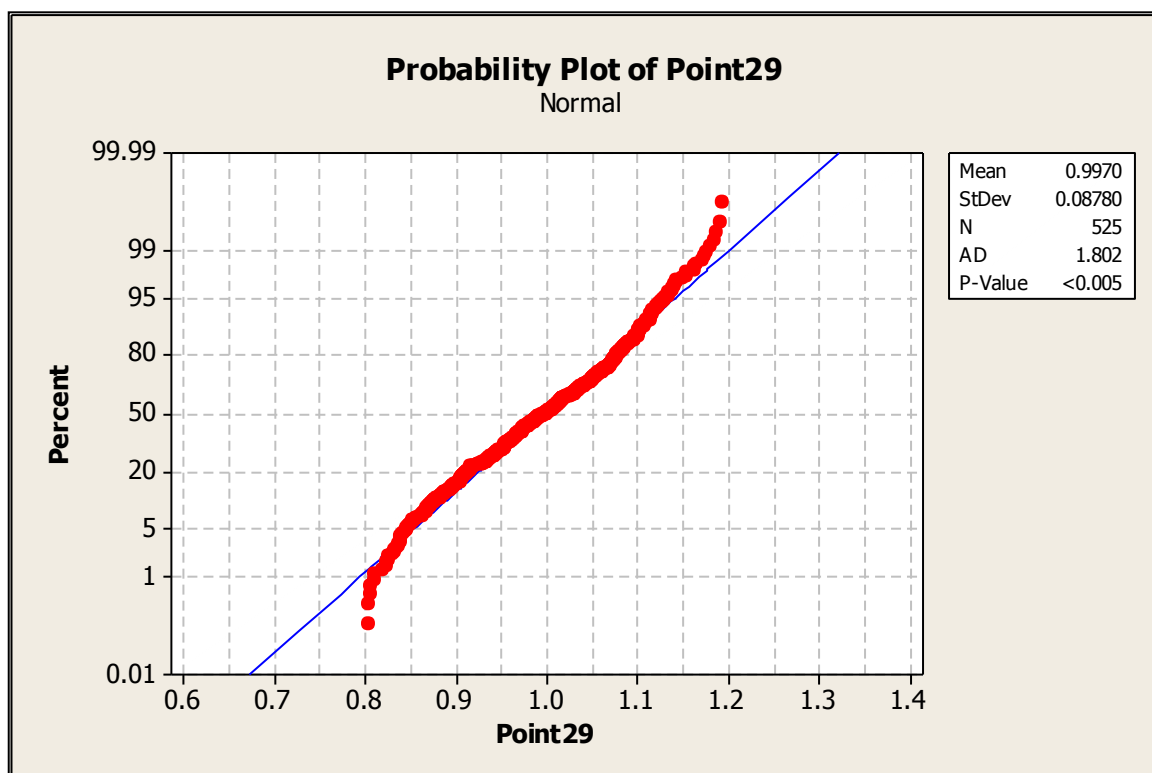


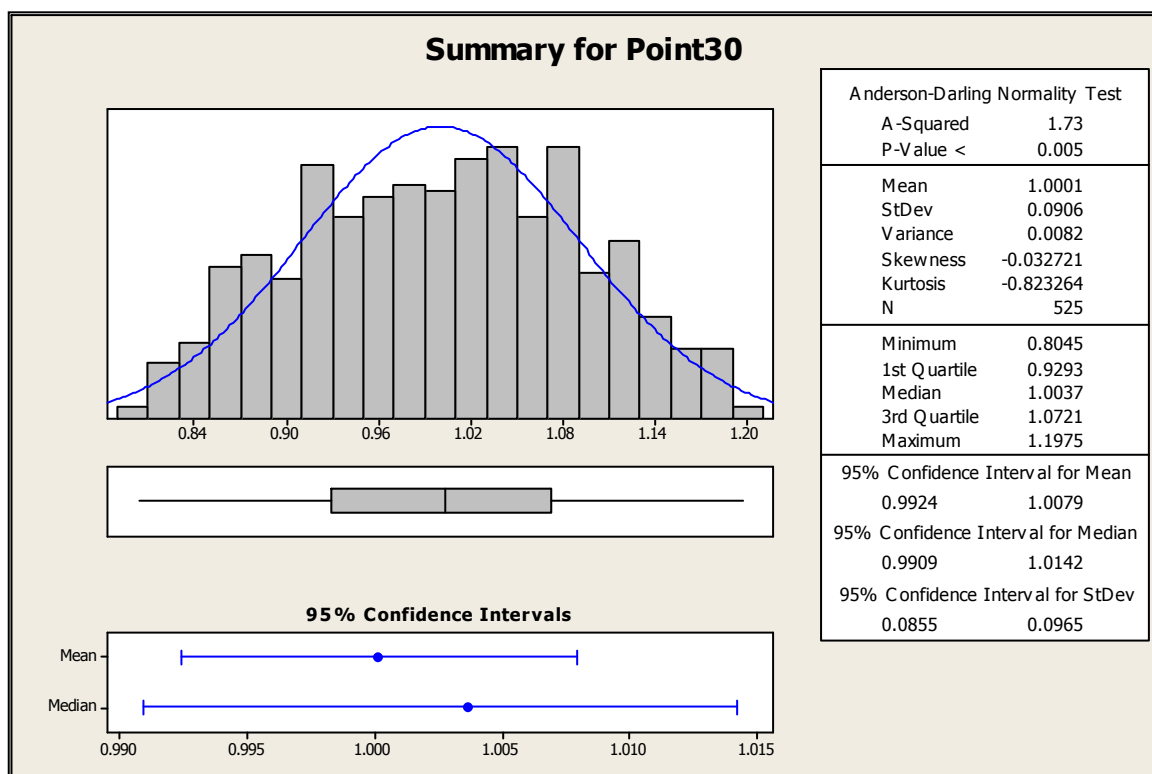
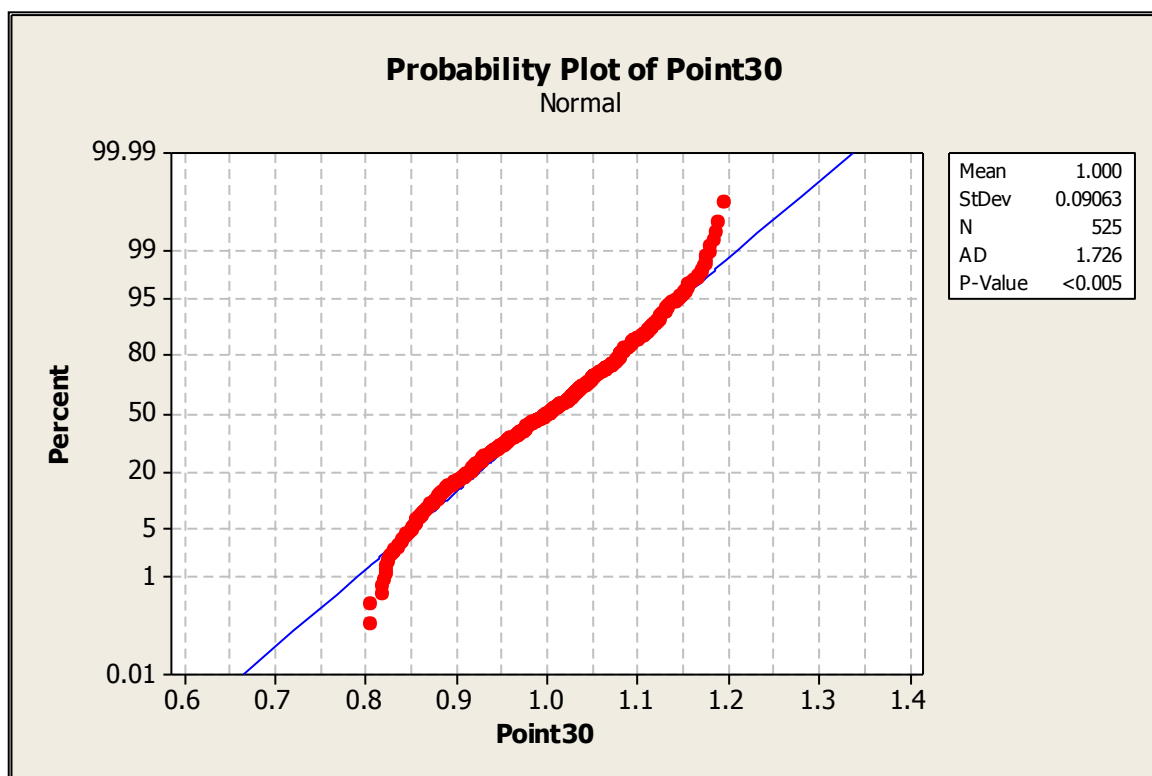












APPENDIX D: ANSYS MACRO

```

/CWD,./
FINISH
/FILNAME,Thesis_thermal_rev15_run,0
/PREP7
RESUME,Thesis_thermal_rev15,db,,,
/input,Input_isight,inp
! /UIS,MSGPOP,2
/NERR,0,10000,
!*
/prep7
shpp, off
allsel, all
!*
/PSF,DEFA, ,1,0,1
/PBF,TEMP, ,1
/PIC,DEFA, ,1
/PSYMB,CS,0
/PSYMB,NDIR,0
/PSYMB,ESYS,0
/PSYMB,LDIV,0
/PSYMB,LDIR,0
/PSYMB,ADIR,0
/PSYMB,ECON,0
/PSYMB,XNODE,0
/PSYMB,DOT,1
/PSYMB,PCONV,
/PSYMB,LAYR,0
/PSYMB,FBCS,0
!*
/PBC,ALL, ,1
/REP
!*

cmsel,s,e_five
nsle,s,1
sf,all,conv,%H_SIDE6%

cmsel,s,e_four
nsle,s,1
sf,all,conv,%H_SIDE5%

!*

```

!fist pass channel

!*
!

set,H_SIDE3(1,1,1),1.5(fact_one)
set,H_SIDE3(2,1,1),1.7(fact_one)
set,H_SIDE3(3,1,1),1.9(fact_one)
set,H_SIDE3(4,1,1),3.3245(fact_two)
set,H_SIDE3(5,1,1),3.442(fact_three)
set,H_SIDE3(6,1,1),3.5685(fact_four)
set,H_SIDE3(7,1,1),3.7085(fact_five)
set,H_SIDE3(8,1,1),3.8585(fact_six)
set,H_SIDE3(9,1,1),4.0165(fact_seven)
set,H_SIDE3(10,1,1),4.186(fact_eight)

!*
!

!tip turn

!*
!

set,H_SIDE3(11,1,1),4.372(fact_nine)
set,H_SIDE3(12,1,1),4.5672(fact_ten)
set,H_SIDE6(9,1,1),3.5965(fact_twelve)
set,H_SIDE6(10,1,1),3.54(fact_eleven)

!*
!

!second pass channel

!*
!

set,H_SIDE6(3,1,1),3.567(fact_eighteen)
set,H_SIDE6(4,1,1),3.581(fact_seventeen)
set,H_SIDE6(5,1,1),3.593(fact_sixteen)
set,H_SIDE6(6,1,1),3.6025(fact_fifteen)
set,H_SIDE6(7,1,1),3.608(fact_fourteen)
set,H_SIDE6(8,1,1),3.3075(fact_thirteen)

!*
!

!hub turn

!*
!

set,H_SIDE6(1,1,1),3.5295(fact_twenty)
set,H_SIDE6(2,1,1),3.549(fact_nineteen)
set,H_SIDE5(1,1,1),3.2135(fact_twentyone)
set,H_SIDE5(2,1,1),3.1565(fact_twentytwo)


```

!*
!third pass channel
!*

*set,H_SIDE5(3,1,1),3.1015*(fact_twentythree)
*set,H_SIDE5(4,1,1),3.051*(fact_twentyfour)
*set,H_SIDE5(5,1,1),2.999*(fact_twentyfive)
*set,H_SIDE5(6,1,1),2.949*(fact_twentysix)
*set,H_SIDE5(7,1,1),2.9025*(fact_twentyseven)
*set,H_SIDE5(8,1,1),2.855*(fact_twentyeight)
*set,H_SIDE5(9,1,1),2.809*(fact_twentynine)
*set,H_SIDE5(10,1,1),2.767*(fact_thirty)


allsel, all
/replot
/solu
solve


FINISH
/FILNAME,Thesis_structural_rev15_run,0
/PREP7
RESUME,Thesis_structural_rev15,db,,,
/NERR,0,10000,


allsel, all
lread,temp,1,,,,Thesis_thermal_rev15_run,rth


allsel, all
/solu
solve


allsel, all
nsel,r,loc,y,333.82,335.88
esln
nsle,s,corner

!Run lifing tool

```

```
allsel, all  
nsel,r,loc,y,343.09,345.15  
esln  
nsle,s,corner
```

```
!Run lifing tool
```

```
allsel, all  
nsel,r,loc,y,353.3,355.3  
esln  
nsle,s,corner
```

```
!Run lifing tool
```

```
!save,test,,,
```

APPENDIX E: AIRFOIL COORDINATES

Radius: 12.731 inches	
x	y
-5.140494	-0.136228
-5.235531	0.004528
-5.288572	0.147248
-5.314007	0.291261
-5.318106	0.436272
-5.316315	0.478823
-5.313033	0.521443
-5.308261	0.564133
-5.301997	0.606092
-5.294261	0.649721
-5.285771	0.692584
-5.273041	0.735506
-5.26507	0.778486
-5.252059	0.821524
-5.239587	0.861611
-5.225306	0.907746
-5.209908	0.950933
-5.193394	0.994172
-4.88343	1.611906
-4.577465	2.045373
-4.269501	2.387461
-3.961536	2.668682
-3.745957	2.83036
-3.530378	2.987761
-3.314799	3.115315
-3.09922	3.22798
-2.883641	3.32492
-2.668062	3.404873
-2.452383	3.47135
-2.236904	3.52315
-2.021325	3.560004
-1.805746	3.582818
-1.590167	3.591323
-1.374568	3.585334
-1.153	3.564828
-0.94343	3.529704
-0.727851	3.479757
-0.512272	3.415095
-0.296693	3.335719
-0.081114	3.239758
0.134465	3.127555
0.350044	2.999538
0.565623	2.85571
0.781202	2.696068
0.993781	2.512958

Radius: 12.731 inches	
x	y
-5.258417	0.595922
-5.362502	0.732609
-5.424432	0.875621
-5.45353	1.023049
-5.461378	1.173464
-5.461378	1.202943
-5.459219	1.232332
-5.456966	1.262232
-5.453931	1.292041
-5.450113	1.32196
-5.445526	1.351988
-5.440407	1.38209
-5.434587	1.412291
-5.42804	1.442593
-5.420768	1.472998
-5.412774	1.503505
-5.404057	1.534113
-5.394617	1.564822
-5.071709	2.263659
-4.748802	2.699115
-4.425895	3.016525
-4.102988	3.265797
-3.807256	3.410319
-3.671723	3.520609
-3.45609	3.622144
-3.246458	3.704931
-3.024825	3.768971
-2.809193	3.814263
-2.59356	3.849164
-2.377928	3.868733
-2.162295	3.87886
-1.946663	3.861696
-1.73103	3.837266
-1.515398	3.798313
-1.293765	3.744836
-1.094132	3.676836
-0.8695	3.593346
-0.652867	3.494012
-0.437235	3.379467
-0.221602	3.249708
-0.00597	3.104737
0.209663	2.944553
0.425295	2.762122
0.640928	2.56231
0.85656	2.345131

Radius: 14.410 inches	
x	y
-5.376126	1.735771
-5.419189	1.819716
-5.444962	1.903916
-5.457868	1.988395
-5.458617	2.072871
-5.457612	2.09856
-5.455537	2.124262
-5.45259	2.149977
-5.448772	2.175704
-5.444083	2.201445
-5.438816	2.227194
-5.433217	2.252948
-5.42697	2.278711
-5.420077	2.304484
-5.412536	2.330267
-5.404347	2.356059
-5.395511	2.38186
-5.386028	2.407671
-5.06551	3.003115
-4.744171	3.364969
-4.423243	3.625078
-4.102314	3.816893
-3.806745	3.91613
-3.671178	3.993459
-3.455609	4.047932
-3.240041	4.087191
-3.024473	4.107821
-2.808905	4.112199
-2.593336	4.100611
-2.377768	4.074163
-2.1622	4.032432
-1.946632	3.975567
-1.731063	3.903895
-1.515495	3.81724
-1.299827	3.715301
-1.084359	3.597863
-0.86879	3.484687
-0.653222	3.315428
-0.437634	3.150271
-0.222086	2.968748
-0.006517	2.770965
0.209051	2.557211
0.424619	2.327819
0.640187	2.002685
0.855758	1.822852

Radius: 12.731 inches	
x	y
1.21236	2.311299
1.427939	2.091152
1.643518	1.852515
1.859097	1.590063
2.074676	1.305524
2.290255	0.999871
2.505834	0.672754
2.721413	0.323088
2.930992	-0.046462
3.15257	-0.438297
3.368149	-0.84757
3.583728	-1.274374
3.799307	-1.720078
4.014886	-2.184684
4.230465	-2.657628
4.446044	-3.142337
4.661623	-3.640508
4.877202	-4.147542
5.092781	-4.652588
5.30336	-5.180191
5.419168	-5.450656
5.523975	-5.722041
5.640783	-5.984918
5.731591	-6.209482
5.892398	-6.545557
5.973206	-6.823128
5.980948	-6.847085
5.985454	-6.871856
5.986646	-6.897006
5.984302	-6.922092
5.978059	-6.946674
5.970414	-6.970321
5.956719	-6.992617
5.944178	-7.013171
5.927047	-7.031622
5.907628	-7.047646
5.886258	-7.060961
5.863318	-7.071335
5.839205	-7.078583
5.814346	-7.08258
5.789176	-7.083255
5.764141	-7.080596
5.739676	-7.07465
5.716211	-7.065322
5.69416	-7.053371

Radius: 12.731 inches	
x	y
1.072193	2.110587
1.287826	1.857761
1.503458	1.583543
1.719091	1.290372
1.934723	0.978248
2.150356	0.647106
2.365988	0.296878
2.581621	-0.072373
2.797253	-0.460647
3.012886	-0.867944
3.220518	-1.292444
3.444151	-1.7338
3.659784	-2.193045
3.875416	-2.670177
4.091048	-3.161523
4.306681	-3.665605
4.522314	-4.184704
4.737946	-4.71862
4.953579	-5.264592
5.169212	-5.81952
5.280407	-6.110355
5.391602	-6.404372
5.502797	-6.701495
5.613993	-7.000143
5.725188	-7.301449
5.836383	-7.605278
5.843391	-7.629331
5.847174	-7.634097
5.847665	-7.679146
5.844856	-7.704042
5.838795	-7.728351
5.829589	-7.751652
5.817397	-7.773539
5.802432	-7.793632
5.784953	-7.811581
5.765264	-7.827074
5.743708	-7.839841
5.720659	-7.849662
5.699519	-7.856364
5.671706	-7.859832
5.646653	-7.860006
5.621795	-7.856381
5.597565	-7.850513
5.574382	-7.841012
5.552652	-7.828543

Radius: 14.410 inches	
x	y
1.071324	1.547876
1.286892	1.257761
1.50246	0.954075
1.718028	0.636371
1.933597	0.30443
2.149165	-0.040164
2.364733	-0.3981
2.580301	-0.76942
2.79587	-1.153866
3.011438	-1.551531
3.227006	-1.952401
3.442574	-2.3865
3.658143	-2.822582
3.873711	-3.271117
4.089279	-3.732268
4.304647	-4.204363
4.520416	-4.695158
4.735984	-5.17644
4.951552	-5.67519
5.16712	-6.170046
5.277646	-6.438441
5.388171	-6.700576
5.498696	-6.961215
5.609221	-7.222268
5.719746	-7.483594
5.830272	-7.744029
5.838549	-7.767797
5.843612	-7.792451
5.845372	-7.817558
5.843798	-7.842677
5.838916	-7.867368
5.830817	-7.891197
5.819638	-7.913748
5.805577	-7.93462
5.768879	-7.953452
5.769839	-7.969912
5.748791	-7.983711
5.726103	-7.994607
5.702175	-8.002408
5.677425	-8.006078
5.652288	-8.006238
5.627205	-8.006163
5.602617	-8.000792
5.573954	-7.992217
5.556632	-7.98059

Radius: 12.731 inches	
x	y
5.655813	-7.020905
5.673909	-7.038411
5.640192	-7.001159
5.584886	-6.920846
5.529581	-6.840478
5.474278	-6.760055
5.418971	-6.679577
5.363668	-6.599045
5.30836	-6.518458
5.092781	-6.203495
4.877202	-5.88572
4.661623	-5.571445
4.446044	-5.257657
4.230465	-4.952578
4.014289	-4.654459
3.799307	-4.368324
3.583728	-4.096248
3.368149	-3.835775
3.15257	-3.590719
2.936992	-3.35808
2.721413	-3.141272
2.505834	-2.936096
2.290255	-2.742198
2.074676	-2.561894
1.859097	-2.393143
1.643518	-2.233014
1.427939	-2.081508
1.21236	-1.940656
0.986781	-1.808611
0.781202	-1.693253
0.565623	-1.564582
0.350044	-1.452951
0.134465	-1.34919
-0.081114	-1.251061
-0.296693	-1.158565
-0.512272	-1.071701
-0.727851	-0.991252
-0.94343	-0.916014
-1.159009	-0.845899
-1.374588	-0.780907
-1.590167	-0.721426
-1.805746	-0.666977
-2.021325	-0.617297
-2.236904	-0.572388
-2.452483	-0.532193

Radius: 12.731 inches	
x	y
5.515025	-7.795619
5.532751	-7.813324
5.499783	-7.775735
5.444688	-7.695087
5.389593	-7.614277
5.334497	-7.533303
5.270942	-7.452166
5.224307	-7.370865
5.169212	-7.289402
4.953579	-6.969002
4.737945	-6.639338
4.522314	-6.311225
4.306681	-5.996125
4.091049	-5.662287
3.875416	-5.334372
3.659784	-5.014036
3.444151	-4.701281
3.228518	-4.396105
3.012686	-4.09651
2.797253	-3.808307
2.581621	-3.518913
2.365988	-3.243968
2.150356	-2.97903
1.984723	-2.72404
1.719091	-2.47852
1.50345	-2.243226
1.297826	-2.01808
1.072193	-1.803116
0.85656	-1.598334
0.640928	-1.404283
0.425295	-1.220625
0.209663	-1.046615
-0.00597	-0.882253
-0.221602	-0.727541
-0.437235	-0.583097
-0.652867	-0.448236
-0.8685	-0.322566
-1.084132	-0.206086
-1.299765	-0.098786
-1.515398	-0.000636
-1.73103	0.068297
-1.946663	0.167995
-2.162295	0.238459
-2.377928	0.300747
-2.59356	0.35302

Radius: 14.410 inches	
x	y
5.517548	-7.949046
5.536043	-7.966115
5.501471	-7.920031
5.445746	-7.85354
5.390021	-7.777167
5.334298	-7.700564
5.276571	-7.623728
5.222845	-7.546904
5.16712	-7.469235
4.951552	-7.167141
4.733864	-6.863098
4.520416	-6.533766
4.304847	-6.247874
4.089279	-5.939367
3.873711	-5.63076
3.658143	-5.324074
3.442574	-5.020116
3.227003	-4.718708
3.011438	-4.421555
2.79587	-4.128118
2.580301	-3.839238
2.364733	-3.554675
2.149165	-3.274924
1.933597	-2.909237
1.718028	-2.728444
1.50246	-2.464199
1.266892	-2.205724
1.071324	-1.952504
0.855756	-1.708065
0.640187	-1.472408
0.424619	-1.244237
0.209051	-1.026171
-0.006517	-0.818394
-0.222088	-0.620959
-0.437654	-0.433645
-0.653222	-0.257197
-0.86679	-0.090481
-1.084358	0.067171
-1.209927	0.215036
-1.515495	0.354287
-1.731063	0.485353
-1.946632	0.608181
-2.1522	0.722075
-2.377768	0.823832
-2.593336	0.928746

Radius: 12.731 inches	
x	y
-2.883641	-0.466239
-3.09922	-0.440101
-2.668062	-0.496796
-3.314799	-0.419018
-3.530378	-0.403847
-3.745957	-0.395535
-3.961536	-0.390059
-4.110301	-0.388217
-4.259065	-0.38694
-4.40783	-0.387548
-4.556594	-0.383828
-4.596512	-0.382221
-4.68575	-0.379212
-4.674309	-0.374801
-4.712189	-0.368388
-4.74939	-0.360569
-4.785912	-0.351149
-4.821755	-0.340126
-4.857102	-0.327934
-4.891843	-0.314311
-4.925771	-0.298769
-4.958086	-0.281308
-4.991187	-0.261926
-5.022676	-0.240626
-5.05335	-0.217405
-5.083212	-0.192266
-5.11226	-0.165206

Radius: 12.731 inches	
x	y
-3.024825	0.428958
-3.240458	0.448204
-2.809193	0.395269
-3.45609	0.460653
-3.671723	0.462461
-3.887356	0.44974
-4.102988	0.441592
-4.25477	0.43042
-4.406552	0.419302
-4.558334	0.411257
-4.710117	0.411722
-4.746189	0.411187
-4.781807	0.412007
-4.816969	0.414182
-4.851677	0.417711
-4.865929	0.422595
-4.919728	0.428833
-4.953143	0.436204
-4.988322	0.444283
-5.018912	0.454115
-5.050912	0.465702
-5.082324	0.479043
-5.113146	0.494138
-5.143378	0.510937
-5.173022	0.52959
-5.202076	0.549947
-5.230541	0.572057

Radius: 14.410 inches	
x	y
-3.024473	1.1002
-3.240041	1.171868
-2.808805	1.018618
-3.455609	1.233337
-3.671178	1.264537
-3.808746	1.324955
-4.102314	1.356271
-4.307968	1.378318
-4.513621	1.397185
-4.719275	1.419802
-4.924928	1.456071
-4.957138	1.4633
-4.988385	1.471757
-5.019571	1.481201
-5.049795	1.491714
-5.079358	1.503295
-5.108256	1.515943
-5.136781	1.529198
-5.164559	1.543652
-5.191521	1.559427
-5.217665	1.57652
-5.242983	1.594931
-5.26771	1.614327
-5.29157	1.635104
-5.314342	1.657637
-5.336026	1.661928
-5.358621	1.707971

REFERENCES

- Aliaga, D.A, Lamb, J.P., and Klein, D.E., 1994. "Convection Heat Transfer Distributions over Plates with Square Ribs from Infrared Thermography Measurements." *International Journal of Heat and Mass Transfer*, Vol. 37, Issue 3, pp. 363-374.
- Al-Hadhrami, L., Griffith, T.S., and Han, J.C., 2002. "Heat Transfer in Two-Pass Rotating Rectangular Channels (AR=2) with Parallel and Crossed 45° V-shaped Turbulators." *AIAA Paper No. 2002-0789; ASME Journal of Heat Transfer*, April 2003, Vol. 125, No. 2.
- Al-Qahtani M., Jang, Y.J., and Chen, H.C., 2002. "Flow and Heat Transfer in Rotating Two-Pass Rectangular Channels (AR = 2) by Reynolds Stress Turbulence Model." *International Journal of Heat and Mass Transfer*, Vol. 45, pp. 1823-1838.
- Azad, G.S., Uddin, J.M., Han, J.C., and Moon H.K., 2001. "Heat Transfer in a Two-Pass Rectangular Rotating Channel with 45-degree Angled Rib Turbulators." *ASME Paper No. 2001-GT-186; ASME Journal of Turbomachinery*, April 2002, Vol. 124, pp. 251-259.
- Boyce, M.P.. Gas Turbine Engineering Handbook. Gulf Professional Publishing, 3rd edition, 2006
- Brown, M.W., and Miller, K.J., "Two Decades of Progress in the Assessment of Multiaxial Low Cycle Fatigue Life," in Low-Cycle Fatigue and Life Prediction edited by Amzallag, Leis, and Rabbe, American Society for Testing and Materials, Baltimore, 1982.
- Bunker, R.S., 2007, "Gas Turbine Heat Transfer: Ten Remaining Hot Gas Path Challenges." *Journal of Turbomachinery*, April, Vol. 129, pp. 193-201.
- Chandra, P.R., and Han, J.C., 1989. "Pressure Drop and Mass Transfer in Two-Pass Ribbed Channels." *Journal of Thermophysics*, Vol. 3, Issue 3, pp. 315-320.
- Chang, S.W., and Morris, W.D., 2003. "Heat Transfer in a Radially Rotating Square Duct Fitted with In-Line Transverse Ribs." *International Journal of Therm. Science*, Vol. 42, pp. 267-282.
- Chen, X., Gao, Q., and Sun, X.F., "Low-Cycle Fatigue under Non-Proportional Loading," *Fatigue & Fracture of Engineering Materials & Structures*, Vol. 19, Issue 7, pp 839-854, 1996.

- Chen, X., Xu, S., and Huang, D., "A Critical Plane-Strain Energy Density Criterion for Multiaxial Low-Cycle Fatigue Life under Non-Proportional Loading," *Fatigue & Fracture of Engineering Materials & Structures*, Vol. 22, Issue 8, pp 679-686, 1999.
- Cho, H.H., Wu, S.J., and Kwon, H.J., 2000. "Local Heat/Mass Transfer Measurements in a Rectangular Duct with Discrete Ribs." *Journal of Turbomachinery*, Vol. 122, pp. 579-586.
- Cho, H.H., Kim, Y.Y., Rhee, D.H., Lee, S.Y., Wu, S.J., and Choi, C., 2003a. "The Effects of Gap Position in Discrete Ribs on Local Heat/Mass Transfer in a Square Duct." *Journal of Enhanced Heat Transfer*, Vol. 10, Issue 3, pp. 287-300.
- Chyu, M.K., Siw, S., Karaivanov, V., Slaughter, W., and Alvin, M., 2009, "Aerothermal Challenges in Syngas, Hydrogen—Fired, and Oxyfuel Turbines- Part II: Effects of Internal Heat Transfer." *Journal of Thermal Science and Engineering Applications*, March, Vol. 1, pp. 1-10.
- Clifford, R.J., 1985. "Rotating Heat Transfer Investigations on a Multipass Cooling Geometry." AGARD CP 390.
- Coffin, L.F., "A Study of the Effects of Cyclic Thermal Stresses on a Ductile Metal," *Trans. ASME* 76:931-950, 1954.
- Coffin, L.F., and Sidey, D., "Low-Cycle Fatigue Damage Mechanisms at High Temperature," *Fatigue Mechanisms*. (A81-10726 -01-26) Philadelphia, Pa., American Society for Testing and Materials, 1979, pp. 528-544; Discussion, pp. 554-568.
- Deserno, M., 2002. "How to Generate Exponentially Correlated Gaussian Random Numbers." Department of Chemistry and Biochemistry UCLA, USA.
- Dowling, N.E. Mechanical Behavior of Materials: Engineering Methods for Deformation, Fracture and Fatigue, 2nd Edition. Upper Saddle River, New Jersey: Prentice Hall, 1999.
- Downs, James P., and Landis, Kenneth K., 2009, "Turbine Cooling Systems Design- Past, Present and Future." *Proceedings of ASME Turbo Expo 2009*, June 8-12, 2009, GT2009-59991.

- Gladden, H.J., and Simoneau, R.J., 1988. "Review and Assessment of the Database and Numerical Modeling for Turbine Heat Transfer." In *Toward Improved Durability in Advanced Aircraft Engine Hot Sections*; Proceedings of the Thirty-third ASME International Gas Turbine and Aeroengine Congress and Exposition, Amsterdam, Netherlands; UNITED STATES; 5-9 June 1988. pp. 39-55, 1988.
- Halila, E.E., Lenaben, D.T., and Thomas, T.T., 1982, "Energy Efficient Engine High Pressure Turbine Test Hardware Detailed Design Report," NASA-Lewis Research Center, CR-167955.
- Hammersley, J.M., and Handscomb, D.C.. Monte Carlo Methods. Chapman and Hall, London, 1964.
- Han, J.C., Glicksman, L.R., and Rohsenow, W.M., 1978. "An Investigation of Heat Transfer and Friction for Rib-Roughened Surfaces." *International Journal of Heat and Mass Transfer*, Vol. 21, pp. 1143-1156.
- Han, J.C., Park, J.S., and Lei, C.K., 1985. "Heat Transfer Enhancements in Channels with Turbulence Promoters." *ASME Journal of Engineering for Gas Turbines and Power*, Vol. 107, No. 1, pp. 628-635.
- Han, J.C., and Park, J.S., 1988. "Developing Heat Transfer in Rectangular Channels with Rib Turbulators." *International Journal of Heat and Mass Transfer*, Vol. 31, No. 1, pp. 183-195.
- Han, J.C., 1988. "Heat Transfer and Friction Characteristics in Rectangular Channels with Rib Turbulators." *ASME Journal of Heat Transfer*, Vol. 110, May, pp. 321-328
- Han, J.C., Ou, S., Park, J.S., and Lei, C.K., 1989. "Augmented Heat Transfer in Rectangular Channels of Narrow Aspect Ratios with Rib Turbulators." *International Journal of Heat and Mass Transfer*, Vol. 32, No. 9, pp. 1619-1630
- Han, J.C., and Zhang, P., 1991. "Effect of Rib Angle Orientation on Local Mass Transfer Distribution in a Three-Pass Rib-Roughened Channel." *ASME Journal of Turbomachinery*, Vol. 113, pp. 123-130.
- Han, J.C., and Zhang, Y.M., 1992. "High Performance Heat Transfer Ducts with Parallel and V-Shaped Broken Ribs." *International Journal of Heat and Mass Transfer*, Vol. 35, No. 2, pp. 513-523.
- Han, J.C., Zhang, Y.H., and Kalkuehler, K., 1993. "Uneven Wall Temperature Effect on Local Heat Transfer in a Rotating Two-Pass Square Channel with Smooth Walls." *Journal of Heat Transfer*, Vol. 115, pp. 912-920.

- Han, J. C., S. Dutta., and S. Ekkad. Gas Turbine Heat Transfer and Cooling Technology. Great Britain: Taylor & Francis, 2000.
- Han, J.C., 2004. "Recent Studies in Turbine Blade Cooling." *International Journal of Rotating Machinery*, Vol. 10, Issue 6, pp. 443-457.
- Hwang, J.J., and Lai, D.Y., 2000. "Buoyancy-Driven Flow Reversal Phenomena in Radially Rotating Serpentine Ducts." *Journal of Heat Transfer*, Vol. 122, pp. 179-183.
- Iacovides, H., and Launder, B.E., 2007. "Internal blade cooling: the Cinderella of computational and experimental fluid dynamics research in gas turbines." *Proc. IMechE Part:A J. Power and Energy*, Vol. 221, pp. 265-290.
- Incropera, F.P., and DeWitt, D. P.. Fundamentals of Heat and Mass Transfer. New Jersey: John Wiley & Sons Inc., 2002.
- Kim, K.M., Kim, Y.Y., Lee, D.H., Rhee, D.H., and Hyung, H.C., 2006. "Influence of duct aspect ratio on heat/mass transfer in coolant passages with rotation." *International Journal of Heat and Fluid Flow*, Vol. 28, pp. 357-373.
- Koch, N.P., 2002 "Probabilistic Design: Optimizing for Six Sigma Quality" AIAA Paper No. 2002-1471.
- Lin, Y.L., Stephens, M.A., and Chyu, M.K., 2001. "A Numerical Study of Flow and Heat Transfer in a Smooth and Ribbed U-Duct with and without Rotation." *Journal of Heat Transfer*, Vol. 123, pp. 219-232.
- Manson, S.S., "Behavior of Materials under Conditions of Thermal Stress," NACA TR 1170, 1954.
- Manson S.S., "Thermal Stress in Design - Part 19, Cyclic Life of Ductile Materials," Machine Design 139, 1960.
- Metropolis, N., and Ulam, S., "The Monte Carlo Method." *Journal of the American Statistical Association*, Vol. 44, No. 247, 1949.
- Metropolis, N., "The Beginning of the Monte Carlo Method." Los Alamos Science Special Issue, 1987.
- Mochizuki, S., Murata, A., Shibata, R., and Yang, W.J., 1999. "Detailed Measurements of Local Heat Transfer Coefficients in Turbulent Flow Through Smooth and Rib-Roughened Serpentine Passages with a 180° Sharp Turn." *International Journal of Heat and Mass Transfer*, Vol. 42, Issue 11, pp. 1925-1934.

- Moran, M.J., and Shapir, H.N.. Fundamentals of Engineering Thermodynamics 5th Edition. United States: John Wiley & Sons Inc., 2004.
- Moustapha, H., Zelesky M., Baines N., and Japikse D.. Axial and Radial Turbines. United States: Concepts NREC, 2003.
- Murata, A., and Mochizuki, S., 1999. "Effect of Cross-Sectional Aspect Ratio on Turbulent Heat Transfer in an Orthogonally Rotating Rectangular Smooth Duct." *International Journal of Heat and Mass Transfer*, Vol. 42, pp. 3814-3830.
- Otomo, F., Nakata, Y., Kubo, R., and Suga, T., 1997. "Pressure Loss Characteristics of Gas Turbine Nozzle Blade Row and Individual Film Cooling Injection Rows." *Proceedings of the 25th Annual Gas Turbine Conference*, JSME.
- Park, C.W., Lau, S.C., and Kukreja, R.T., 1998. "Heat/Mass Transfer in a Rotating Two-Pass Square Channel with Transverse Ribs." *AIAA, journal of Thermophysics. Heat Transfer*, Vol. 12, pp. 80-86.
- Parsons, J.A., Hand J.C., and Zhang, Y., 1994. "Wall Heating Effect on Local Heat Transfer in a Rotating Two-Pass Square Channel with 90° Rib Turbulators." *International Journal of Heat and Mass Transfer*, Vol. 37, Issue 9, pp. 1411-1420.
- Ricklick, M., 2009. "Characterization of an Inline Row Impingement Channel for Turbine Blade Cooling Applications." Ph.D. Dissertation, University of Central Florida, Orlando, Florida.
- Sautner, M., Clouser, S., and Han, J.C., 1992. "Determinations of Surface Heat Transfer and Film Cooling Effectiveness in Unsteady Wake Flow Conditions." AGARD Conference Proceedings 527, pp. 6-1 to 6-12.
- Siddall, J.N.. Probabilistic Engineering Design: Principles and Applications. New York: Marcel Dekker, Inc., 1983.
- Taslim, M.E., Bondi, L.A., and Kercher, D.M., 1991. "An Experimental Investigation of Heat Transfer in an Orthogonally Rotating Channel Roughed with 45 Deg. Criss-Cross Ribs on Two Opposite Walls." *Journal of Turbomachinery*, Vol. 113, pp. 346-353.
- Timko, L.P., 1990, "Energy Efficient Engine High Pressure Turbine Component Test Performance Report," NASA-Lewis Research Center, CR-168289.
- Willett, F.T., and Bergles, A.E., 2000. "Heat Transfer in rotating narrow rectangular ducts with heated sides oriented at 60-degree to the R-Z plane." *ASME Paper No. 2000-GT-224*.

- Williams, M.M.R., 2010. "A probabilistic study of the influence of parameter uncertainty on thermal radiation heat transfer." *International Journal of Heat and Mass Transfer*, Vol. 53, pp. 1461-1472.
- Zhang, Y.M., Han, J.C., Parsons, J.A., and Lee, C.P., 1995. "Surface Heating Effect on Local Heat Transfer in a Rotating Two-Pass Square Channel with 60-Degree Angled Rib Turbulators." *ASME Journal of Turbomachinery*, Vol. 117, Issue 2, pp. 272-278.